Robustness assessment in electro-nuclear scenario studies : evaluate the capacity of Sodium-cooled Fast Reactor deployment strategies to adapt to changes of objectives

Jiali Liang

Thèse de doctorat

NNT: 2021UPASP055

université PARIS-SACLAY

Robustness assessment in electro-nuclear scenario studies

Evaluate the capacity of Sodium-cooled Fast Reactor deployment strategies to adapt to changes of objectives

Etude de robustesse des scénarios électro-nucléaires

évaluation de la capacité des stratégies de déploiement de réacteur à neutron rapide refroidi au sodium à s'adapter aux changements des objectifs

Thèse de doctorat de l'université Paris-Saclay

École doctorale n° 576, Particules, Hadrons, Énergie, Noyau, Instrumentation, Imagerie, Cosmos et Simulation (PHENIICS)
Spécialité de doctorat: Energie nucléaire
Unité de recherche: Université Paris-Saclay, CNRS, IJCLab, 91405, Orsay, France
Référent: Faculté des sciences d'Orsay

Thèse présentée et soutenue à Orsay, le 7 juillet 2021, par

Jiali LIANG

Composition du jury :

Frederico GARRIDO Professeur, Université Paris-Saclay	Président
Guillaume MARTIN Ingénieur chercheur (HDR), CEA Cadarache	Rapporteur & Examinateur
Paul P.H. WILSON Professor, University of Wisconsin-Madison	Rapporteur & Examinateur
Gerald SENENTZ Directeur R&D, Orano	Examinateur
Barbara VEZZONI Ingénieur R&D, Framatome	Examinatrice

Direction de la thèse :

Sylvain DAVID Directeur de Recherche, IJCLab, CNRS/IN2P3, Université Paris-Saclay	Directeur de Thèse
Marc ERNOULT Chargé de recherche, IJCLab, CNRS/IN2P3, Université Paris-Saclay	Co-encadrant de Thèse

université PARIS-SACLAY

ÉCOLE DOCTORALE
Particules, hadrons, énergie et noyau : instrumentation, imagerie, cosmos et simulation (PHENIICS)

Titre :

Etude de robustesse des scénarios électro-nucléaires : évaluation de la capacité des stratégies de déploiement de réacteur à neutron rapide refroidi au sodium à s'adapter aux changements des objectifs

Mots clés :

étude de robustesse, scénario électro-nucléaire, disrupton de l'objectif, incertitude profonde, réacteur à neutron rapide refroidi au sodium

Résumé :

Au cours des dernières années, l'attitude mondiale envers l'énergie nucléaire a considérablement changé, notamment en ce qui concerne le déploiement des réacteurs à neutron rapide refroidi au sodium (RNR-Na) de IV^{e} génération. Cette évolution révèle l'incertitude substantielle des perspectives nucléaires, soumises à des décisions politiques et des estimations économiques variables. Dans ce contexte d'incertitude profonde, l'objectif actuellement adopté pour l'avenir du nucléaire sera possiblement disrupté brutalement. Les changements d'objectifs peuvent alors créer des regrets sur la stratégie mise en place au préalable.

Dans ce contexte, cette thèse définit la robustesse comme la capacité des stratégies à s'adapter aux changements d'objectifs et développe une méthodologie pour évaluer la robustesse des stratégies vis-à-vis des futurs incertains de l'énergie nucléaire. La disruption des objectifs est utilisée comme une approche à intégrer l'incertitude des objectifs dans ces études de scénario. Deux types de robustesse de stratégie sont analysés. Le premier est la robustesse statique, étudiée dans le contexte où la disruption est toujours incertaine, et les performances pour tous les objectifs possibles sont évaluées pour chaque stratégie. L'autre est la robustesse adaptative, étudiée dans un scénario d'adaptation post-disruption à partir de la trajectoire primaire induite par une stratégie pré-disruption. La comparaison de ces deux types de robustesse donne une vision globale sur les performances de stratégie, en ce qui concerne la dynamique de la disruption incertaine.

Avec le code de simulation dynamique du cycle CLASS, cette méthodologie d'évaluation de robustesse est mise en œuvre dans deux études de scénarios, basées sur les transitions exploratoire hypothétique du parc français. Dans la première, les stratégies sont évaluées à un moment prédéterminé, qui dépend de l'horizon temporel du scénario. Dans la seconde, l'évalation s'affranchit de cette dépendence pour renforcer la consistence inter-temporelle de l'évaluation. Enfin, la méthodologie est appliquée à une étude de scénario inspirée de la stratégie nationale française, qui envisage deux perspectives possibles et les disruptions respectives de l'une vers l'autre : le multi-recyclage de plutonium dans les réacteurs à eau préssurisée, et le déploiement des RNR-Na.

université PARIS-SACLAY
ÉCOLE DOCTORALE
Particules, hadrons, énergie et noyau: instrumentation, imagerie, cosmos et simulation (PHENIICS)

Title:

Robustness assessment in electro-nuclear scenario studies: evaluate the capacity of Sodium-cooled Fast Reactor deployment strategies to adapt to changes of objectives

Keywords:

robustness assessment, electro-nuclear scenario study, disruption of objective, deep uncertainty, Sodium-cooled Fast Reactor

Abstract:

During the recent years, the global attitude towards the nuclear energy has considerably changed, in particular in relation to the deployment of the 4^{th}-generation Sodium-cooled Fast Reactor (SFR). These changes reveal the substantial uncertainty in nuclear perspectives, subject to variable political decisions and economic estimations. Under these deep uncertainties, the adopted objective for the nuclear future may be abruptly disrupted. These objective changes may then create regrets on the strategy implemented beforehand.

In this context, this thesis defines the robustness as the capacity of strategies to adapt to objective changes and develops a methodology about the robustness assessment of strategies regarding the uncertain nuclear future. The objective disruption is used as an approach to integrate the uncertainty of objective in the scenario studies. Two types of robustness are analyzed. The first one is static robustness, under the assumption that the disruption is still uncertain and the performances for all possible objectives are evaluated for each strategy. The other one is adaptive robustness, studied in the post-disruption adaptation scenarios from the prior trajectory of a given pre-disruption strategy. The comparison of these two types of robustness provide a global insight on strategy performances regarding the dynamics of uncertain disruption.

With the dynamic fuel cycle simulator CLASS, this methodology of robustness assessment is implemented within two electro-nuclear scenario studies, based on hypothetical exploratory transitions of the French fleet. In the first one, strategies are evaluated at a predetermined time, which depends on the time horizon of scenario. In the second one, the evaluations are liberated from this dependency to encompass the inter-temporal consistency of assessments. Finally, this methodology is applied to a scenario study inspired from a French national strategy, which consider two possible options and the respective disruption from one to another: the plutonium multi-recycling in Pressurized Water Reactors, and the SFR deployment.

Acknowledgement

While this study focuses on the impact of deep uncertainty on the decisions, the progress of the study has also suffered from a series of disruptions subject to deep uncertainties, dramatically and ironically. Unlike the scenario analyses in this work, the life is a non-stop real-time game without a second-time simulation. It is evident that I cannot go through these difficulties without the help of others.

First, I would like to say respect and salute a thousand times to my supervisor Marc. At the beginning of this Ph.D study I asked you for help and for discussion every day, and you were always patient and kind. Your rich skills and thoughts, from numeric methods to angles of scenario analysis, provided me a broad vision on the thorough study. Without your help, I must be lost in the jungle of complicated scenarios, with two empty hands facing the danger of meaningless calculations, data overloading, over-interpretation...

I want to express my great appreciation to chef Xavier as well. Thanks for pulling me out each time when I got into a dead end of analyses. The interpretations of results with the error bars in a much larger order of magnitude, and a significant and specific focus on an "insect of no importance", are both ridiculous. And thanks to your red alerts just in time, I can minimize the occurrence of such kind of stupidity along my study and in this dissertation.

Huge gratitude to Sylvain! Each time you attended the meeting you had plenty of ideas and useful remarks. Your share of experience and vision about the industry complement a lot my knowledge on the electro-nuclear scenarios in different scales. Ah yea also thanks for your calls for "Conseil Scientifique" (CS)... there is no doubt that this special experience also broadened the spectrum of my study life!

Certainly, I should say thanks to other members of my examination board: Guillaume Martin, Paul Wilson, Barbara Vezzoni, Frederico Garrido, and Gerald Senentz, for spending lots of time on the examination of my dissertation. It is sometimes difficult to formulate the analysis processes in scenario studies due to the precision and assumptions; when I am not a native speaker, it can be worst. Your revision in detail helped me a lot about the improvement and made me more confident.

Special thanks to Fanny, Nicolas and Stéphanie. It was Fanny's Ph.D work (supervised by Nicolas) that provided me the first impression on electro-nuclear scenario study in a complete sense. The discussions with you updated my understanding of the roles and the notions of scenario studies, from different angles involving physical, industrial, economic and sociological factors.

I feel deeply grateful to the whole team RAPHYNEE of IJCLab who have made me very welcome during all my Ph.D study life: Sandra, Laurent, Claire, Melody, and young students Yang, Meng and Carolina. I am very grateful to Léa as well, who has set an excellent model of a third-year Ph.D student during my first year.

I have passed more than a year of research of tele-working. Indubitably I must thank Meiqi who has taken care of me since the first lockdown in March 2020. Great thanks to my family for their important support as well. Special gratitude to the Jiali 2020 and the Jiali 2021 who did not give up, so that the Jiali today can

write this acknowledgement in a peaceful way.

Last but not least, I should express my gratitude to the RER B, who has taught me to be tolerant, resistant, resilient, robust, flexible and adaptable to a series of unexpected and brutal changes. Dedicated to this, I would like to mark down the only one (relatively) successful joke that I have made in French, about RER B, to finish this section of acknowledgement, which can also prove that I did some research of reactor physics, in French and in Paris/Orsay:

“La solution triviale/zéro de l’équation Boltzmann doit être nommée « RER B », car elle est toujours nulle presque partout en tant qu’une solution de transport.”

Contents

Introduction

Nuclear power accounts currently for more than 70% of electricity generation in France. Given this dependency, strong efforts in French industry and academy are devoted to deep and advanced researches on innovative systems and fuel cycle managements. Based on the Act of radioactive materials and wastes management published in 2006 [1], the project of Advanced Sodium Technological Reactor for Industrial Demonstration (ASTRID) was launched in 2010. It was supposed to be a technical demonstrator for a future commercial Sodium-cooled Fast Reactor (SFR), improving the plutonium management and possible transmutation of Minor Actinide (MA) [2]. In parallel, a large number of scenario studies were carried out to shed the light on the possible prospects and consequences of SFR deployment.

During recent 10 years, the relevant actors' estimation on the global nuclear power future changed a lot. The delays and the rising cost of European Pressurized Reactor project in Flamanville starting in 2007 lead to more conservative attitudes of stakeholders on such kind of advanced nuclear mega projects, and the Fukushima nuclear accident had a global impacts on the worldwide deployment planning, lightening the burden on natural uranium and thus reducing the demand of SFR technology. For the ongoing ASTRID project, misalignments were progressively revealed on temporal scale, social scale and physical scale of the project infrastructure [3]. These factors lead to the abortion of ASTRID project as an SFR prototype, and the SFR deployment in France is out of consideration for near term. The alternative to improve spent fuel management without SFR becomes the plutonium multi-recycling in Pressurized Water Reactor (PWR). This option is considered in the governmental report Programmations Pluriannuelles de l'Energie.

This change of nuclear future pathway may seem contradictory to the perspectives and scenario studies made in the past. In the current French fuel cycle, plutonium accounts for the major part of transuranium inventory. In the prospect of SFR deployment, plutonium is valorized as the main resource for fuel fabrication and is supposed accumulated in the cycle. But in the fleet dominated by PWRs, plutonium is supposed to be stabilized at a minimum level. As a key component in the spent fuel and nuclear waste management, plutonium status may switch within this change. One may doubt then whether the efforts devoted before the change, in case plutonium inventory had been accumulated, might bring regrets for the options adopted afterwards.

Learning from this change, we may position ourselves on the trajectory of French fuel cycle and reevaluate the future of nuclear power a-posteriori. Problematically, the change subject to a considerable number of uncertain factors might not be well anticipated in the past, and lead us to analyze these sorts of uncertainties for the prospective studies. As shown by the halting of SFR-related studies, the uncertainty on the future of nuclear power can be so deep that no one can guarantee the use of one technology or fuel cycle transition in the future, despite existing projects or strategies being implemented. As a result, it

may be wise to consider for further adaptation, instead of sticking to only one single pathway. One issue raised by relevant scenario studies is the definition of optimization criteria that may evolve during the time horizon of the study. In other words, analysts may ask if seeking optimal trajectories should take into account, from the beginning, all possible futures or if they should consider possible adaptations to a dramatic changes of stakeholder's interest within the time horizon.

This work is performed based on this general principle. It aims to develop a methodology of strategy assessments incorporating the deep uncertainty of nuclear future for electro-nuclear scenario studies. This work takes the current French fuel cycle as example, under the context of SFR deployment planning but keeping the possibility of objective change for the future fleet in consideration. To describe the capacity of strategy to adapt to different uncertain changes, the notion of robustness is introduced. The robustness assessment investigates the existence of strategies that can be adapted to different futures.

To give a general understanding on the study context, Chapter 1 starts from the important role that the application of nuclear power may play in the global issues of climate change, then focuses quickly on the spent fuel and nuclear waste management in nuclear technology. The French trajectory and national strategy is then presented to introduce the scenario as an analysis approach and the deep uncertainty of nuclear future.

Chapter 2 sets the base of methodology development by presenting three principal elements. The first one is the simulator Core Library for Advance Scenario Simulation (CLASS) for the dynamic nuclear fuel cycle simulation. The electro-nuclear scenario studies allow the physical comprehension on the behavior of fuel cycle under the variation of parameters. The framework of robustness assessment is then presented, introducing the concepts of static robustness and adaptive robustness. The robustness is defined here as a strategy capacity to fulfill other objectives than the one it has been designed for. The robustness can be defined as static if no further readjustments are needed, and adaptive otherwise.

The strategy assessment at a predetermined time is a common assumption in lots of project evaluation. Chapter 3 develops the methodology of robustness assessment within a preset time horizon, evaluating strategy performances at the end of scenario. A pre-disruption scenario and a post-disruption adaptation scenario are studied, giving a primary insight on the static and adaptive robustness of different sets of strategies under respective scenario assumptions. In the pre-disruption scenario, SFR deployment is pre-selected as the primary objective, while the change to the minimization of nuclear wastes without SFR is deeply uncertain. The adaptation scenario supposes that this change happens and readjustments for the new objective are allowed. This adaptation scenario starts from one single prior trajectory. A complementary study is also carried out to investigate the influence of problem formulation on the strategy assessment.

The dependency on predetermined time of strategy evaluations may lead to assessment inconsistency under different time horizon of scenario. Chapter 4 introduces new assumptions in order to disconnect the assessment from predetermined time. Using a similar framework of scenario study as in Chapter 3, two additional studies are carried out for a more comprehensive analysis. The first one adapts a set of prior trajectories. We propose a definition for the notion of adaptability and some indicators are analyzed, which help complete the robustness assessment without the need of exhaustive runs of simulations. The second one unlocks a new option during adaptation which was supposed to be unavailable in the past: the plutonium multi-recycling in PWRs. This new option will intuitively lead to a broader adaptability of pre-disruption strategies regarding

the objective changes.

Finally, Chapter 5 applies this methodology to a concrete though academic case inspired from the French national strategy. Following a series of practical constraints, two main strategies and their respective changes are analyzed: one considers the plutonium multi-cycling in PWRs, and the other in SFRs. The analyses take a set of output metrics into account, aiming to assess these two strategies from various angles.

Chapter 1

Context of study

1.1 Nuclear power and concerns of wastes

Climate change is currently one of the most significant challenges in the world. Great efforts, involving collaborations and protocols of hundreds of countries and regions, have been and will probably be devoted to reducing greenhouse gases emissions. These efforts pursue the ambition of limiting the increase of average global temperature. Nevertheless, fossil fuels are still the world's primary source of energy. Emission increases are then driven by increasing energy demands for regional developments and energy policies. The dilemma between the development and the mitigation of climate change leads to consider low-carbon or decarbonized energy, particularly on the electricity generation.

Some experts reckon that nuclear power has helped reduce substantially the gases emissions from electricity generation over the past few decades [4]. They estimate that nuclear power has the potential to create very low-carbon mixes when used in synergy with renewable energy sources. A number of scenario studies have been carried out to investigate the role of nuclear power in the future goal of climate change [4, 5]. A rising importance of nuclear power were found in many pathways of these scenarios. Accordingly, the expansion of the use of nuclear energy is compatible with, and can be in favor of lower gases emissions.

Despite the high potential to produce low-carbon energy, nuclear power have faced many resistances from general public and several governmental and non-governmental organisations. Some resistances can be overwhelming in certain regions of the world, and have led some previously nuclear-dependent countries to choose phase-out strategy to be independent from the nuclear energy [6]. One of the concerns is the nuclear waste management. The irradiation of nuclear fuels creates a considerable amount of radioactive inventories that should be disposed, remaining highly radioactive in a long run. In particular, the strong toxicity of heavy metals like actinide elements may last from thousands to millions of years .

In general, two approaches may be considered to manage spent fuels. One is to limit the production of wastes and burn them as much as possible during irradiation. The other is to valorize a certain part of spent fuels in order to avoid conditioning all of them. In the latter case, only materials without future use will be sent to waste disposals. The other parts, like uranium and plutonium, are reused for new fresh fuels. Thus, the quantity of waste depends on the valorization of materials in spent fuels. This valorization strategy is, for instance, the one currently followed in France.

To handle the heavy metals, new designs and technologies were developed

for Minor Actinide (MA) transmutation and plutonium multi-recycling. Lots of efforts are devoted to plutonium management because it is the primary radioactive heavy metal in spent fuels in long term [7, 8]. In this section, the principles of reactor technologies regarding the plutonium multi-recycling are briefly presented, giving a basic understanding on the possibilities for the future of nuclear power. We will focus on the French case which allows a practical analysis without loss of generality.

1.1.1 Once-through cycle and plutonium mono-recycling in a fleet of PWR: the French fuel cycle as example

The first grid-connection of commercial nuclear reactors dated back to the 1960s. In 2021, 444 reactors are in service operation around the world, corresponding to a net total installed capacity of 394.1 MWe. During these decades of in-service operation, the technology of Pressurized Water Reactor (PWR) has been developed and progressively deployed worldwide. In the current global fleet, 303 PWRs are in operation, accounting for 73% of the total installed capacity. Depending on different national policies, either once-through or mono-recycling strategy is adopted.

For once-through strategy, the fissile element of fresh fuels comes from the uranium extracted in the mines, and the corresponding spent fuels after discharge and cooling are directly conditioned as wastes, without any reprocessing. Due to the considerable quantity and relatively long half-life of its isotopes, the plutonium accounts for the major part of long-term radio-toxicity among the radio-active components in these spent fuels [7, 8].

Some countries have implemented the mono-recycling strategy. They recycle the uranium and plutonium from spent Uranium OXide (UOX) fuels, in order to valorize the fissile components. The plutonium is mainly used for Mixed OXide (MOX) fuel fabrication. In spite of the incineration of plutonium during irradiation, there is still a large quantity of plutonium left in spent MOX fuels. UOX and MOX fuels will be presented in the next subsections. Because of nuclear safety concerns, plutonium from spent MOX fuels is currently not recycled. But if no further use is considered for this plutonium, it must be included into the waste. The gain on the radio-toxicity of total inventories relative to once-through fuel cycle is then limited [9, 10].

In this work, the nuclear fuel cycle in France is taken as a reference to describe and analyze fuel cycle strategies. A full detailed description of this nuclear fuel cycle is presented in [11, 12, 13]. A brief summary of the most important aspects is given in the following to allow a better understanding of the studies presented in this manuscript.

The installed capacity of nuclear power in France is around 63 GWe contributed by 58 PWRs, and the effective electricity production was around 420 TWh in 2016, contributing to 75% of the total electricity generation. Two PWRs in Fessenheim were shut down in 2020 [14]. 20 reactors among the 900MW-class PWRs are loaded with MOX fuels in 30% of the core. The fraction of power produced by MOX fuel in the whole French fleet is about 10%. The other 90% is produced by UOX fuels. The physical properties of those two fuels and the relevant operation of facilities in fuel cycle are extremely different. Subsequent descriptions of key processes and relevant nuclear facilities, summarized graphically in Figure 1.1 from [15], are specified for each fuel type.

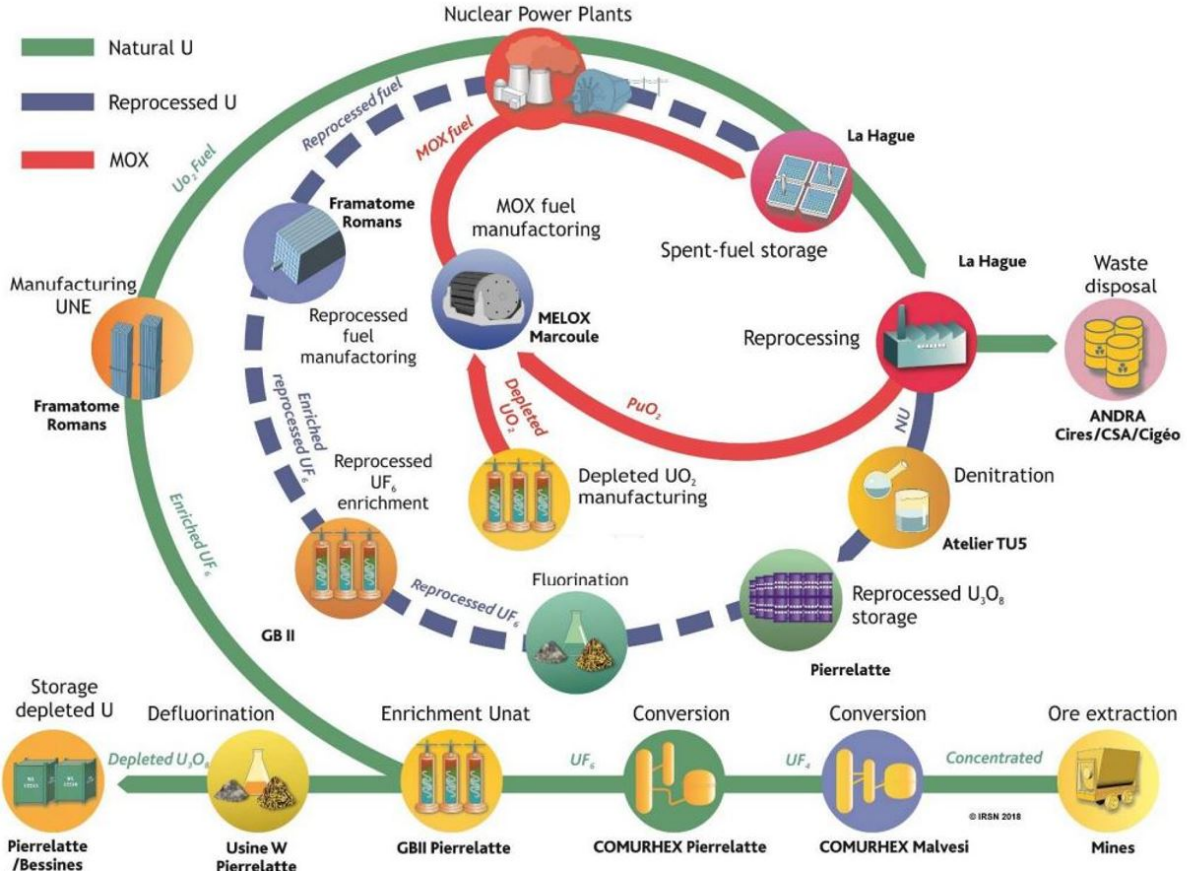

Figure 1.1: Current nuclear fuel cycle in France [15]

1.1.1.1 From mines to UOX fabrication

The uranium needed for fresh UOX fuels is first extracted by ore mining and milling, and converted through series of chemical process to UF_6. The natural uranium coming from the mines is mainly composed of the isotope ^{238}U whose abundance is about 99.27%, and ^{235}U accounts for 0.72%. Because only ^{235}U is fissile, this natural isotopic composition can not satisfy the core criticality in PWR (here denotes specifically the light water reactors). The uranium is thus enriched in ^{235}U for UOX fuel fabrication. In France, ^{235}U is enriched by gaseous centrifugation, up to the range of [3%, 5%] depending on the requirement of burn-up between 30 and 60 GWd/t. Afterwards, the UOX fuel is fabricated in the dedicated fabrication plant of Framatome. Meanwhile, large quantities of depleted UF_6 after the enrichment process, in which the isotopic fraction of ^{235}U is about 0.25%, are converted to U_3O_8 and stored in specific depleted uranium stocks. Fresh UOX fuels are then transported to power plants.

1.1.1.2 UOX reprocessing

After depletion in reactors, spent UOX fuels are discharged and moved to water-filled pools in nuclear power plants for several years of cooling. During the cooling, both residual heat and dose rate decrease due to the decay of short-lived nuclei. After years of cooling, the level of residual heat and dose rate of spent UOX fuels are low enough for transportation and reprocessing if demanded. Spent UOX fuels still contain a large amount of fissile materials. Mono-recycling strategies can recycle the plutonium from spent UOX fuels leading to some resource saving. Spent UOX fuels are thus transported to reprocessing plants, like La Hague in France. During reprocessing, the reusable part, uranium and plutonium, are separated from the high-level wastes (Minor Actinide (MA) and Fission

Product (FP)). Cladding and structural material of assemblies, are conditioned for storage as long-lived intermediate activity wastes. The reprocessed uranium from the spent UOX fuels is stored in specific reprocessed uranium stocks under the form of U_3O_8. The exact use of reprocessed uranium is not considered in this work.

1.1.1.3 MOX fabrication

MOX fuels are fabricated by mixing both plutonium oxide and depleted uranium oxide. MOX fuels are fabricated in dedicated plants like MELOX in France. The use of MOX fuel presents mainly two advantages [16]: the reduction of natural uranium resource consumption, and the reduction of volume as well as the long-term radio-toxicity of waste packages if the further use of plutonium after MOX irradiation is determined.

Plutonium content introduced in fresh MOX fuels depends mainly on the expected burn-up. Similar to the enrichment of ^{235}U in UOX fuel, high burn-up of MOX requires high plutonium content in fresh fuels. For industrial irradiation, plutonium content in MOX fuel cannot exceed 12% [17], due to nuclear safety constraints, notably on void effect.

1.1.1.4 Spent fuel management

Similar to spent UOX fuels, spent MOX fuels are moved to cooling pools after discharge, so the decay heat and dose rate of spent fuels can decrease. In the current fuel cycle in France, spent MOX fuels are stored in the pools of interim storage and not yet reprocessed. During the depletion in PWRs, the quality of plutonium decreases, preventing it to be recycled again in PWRs. In consideration of void effect with low plutonium quality, the multi-recycling of plutonium in PWR after MOX requires new design of fuels, which are not yet deployed in France. Plutonium is therefore recycled only once currently. The reprocessing of spent MOX fuels for the multi-recycling of plutonium is considered for the future advanced fuel design, in fast reactors but also in PWRs suggested in the French official strategy, written in the report Programmations Pluriannuelles de l'Energie (PPE) [18].

1.1.2 Plutonium multi-recycling in fast reactor

The multi-recycling of plutonium can be realized in fast reactors. Actually, the European-design uses plutonium as the principal fissile element [19]. In fast reactors, neutrons are not, or only marginally, moderated in the reactor core, leading to a fast neutron spectrum. The plutonium loaded in the core is burned for the energy production, while the fertile isotope ^{238}U is mainly converted to plutonium. The radio-toxicity of spent fuels of fast reactor is similar or even higher than those of PWR, due to a higher production of medium or long-lived Minor Actinide (MA) and a considerable quantity of plutonium [20], but the plutonium is recycled for the use of next irradiation. Based on this conception, plutonium in the cycle is valorized instead of being considered wastes, and thus the volume and the radio-toxicity of waste canisters are significantly reduced. Despite a slightly higher inventory accumulated of MA in total cycle, the increase of plutonium in total cycle within a fleet of fast reactor is far smaller than a fleet of thermal reactor in which the plutonium is constantly produced [21].

Depending on the core design, fast reactor can decrease, stabilize or increase the plutonium content during its irradiation. These designs are respectively called

burner, break-even or breeder. Some further conceptions of innovative system are developed for the recycling of americium, or even other MA, aiming to transmute them and reduce significantly the quantity of nuclear wastes as well as the relevant radio-toxicity [20, 22, 23, 24]. Given the potential of far smaller burden on the environment, these innovative systems may mobilize research efforts in the future. Nevertheless, they are still draft designs and need further examinations and analyses.

One should note that the first driving force of fast reactor deployment is the independence of energy supply from the uranium resource (more precisely, from the fissile $^{235}\mathrm{U}$). The current fleet worldwide relies on the use of $^{235}\mathrm{U}$, which accounts for 0.72% of the available uranium. With an expansion of nuclear power using the same types of nuclear fuels, we might encounter a risk of $^{235}\mathrm{U}$ shortage in decades or in a century, depending on the degree of expansion [25]. The use of plutonium-based fuel in fast reactor is able to free nuclear energy from such dependence.

Under these considerations and designs, the deployment of a number of fast reactor requires actually a considerable inventory of plutonium in the cycle. And, despite the existence of advanced burner or transmuter configurations, the original incentive of fast reactor deployment does not necessarily imply the net incineration of plutonium or transuranium (TRU) inventories in the cycle, especially in comparison to the current level of inventories. As a result, the fast reactor deployment planning should start from a certain level of plutonium accumulation in the cycle, even though it may reduce or stabilize it after the fleet transition.

1.1.3 Plutonium multi-recycling in PWR

The studies of plutonium multi-recycling in PWRs have been carried out since the 1990s [26, 27]. They aimed to stabilize the plutonium inventory, under the assumption that PWRs would dominate the nuclear fleet during most of the century. After decades of operation of PWR-fleet with UOX and MOX, spent MOX fuels pile up significantly. If PWR is still the major reactor type of fleet, advanced fuel designs are required to facilitate the spent fuel management. Four concepts have been mainly developed: MIX, COmbustible Recycling A ILot (CORAIL), Advanced Plutonium Assembly (APA) and DUPLEX [28, 29, 30].

MIX and CORAIL are advanced MOX fuels designed for near-term multi-recycling. These two types of fuel rely on different assembly configurations, but based on the similar principle of using enriched $^{235}\mathrm{U}$ to compensate the deterioration of plutonium quality after the recycling and relevant depletion in PWR. MIX mixes enriched $^{235}\mathrm{U}$ with plutonium homogeneously in the same oxide fuel pellet. In a CORAIL assembly, the MOX fuel rods containing multi-recycled plutonium and $^{235}\mathrm{U}$-enriched UOX fuel rods are arranged in different layers. The impacts of industrialization concerning the use of these two fuel designs in the PWR-fleet are analyzed in detail, setting a firm base for near-term industrial application [31, 32, 33]. In short, within a reasonable pace of transition, a PWR-fleet of near 100% CORAIL, or a PWR-fleet of near 30% MIX depending on the set plutonium content in the fresh MIX fuels, is able to stabilize the inventory of spent fuels and plutonium in the cycle.

The last two fuels, APA and DUPLEX, are studied as future technologies. Inert matrices of uranium-free fuels are used to avoid too many neutron captures by $^{238}\mathrm{U}$ and achieve a reasonable moderation in a hardened spectrum under high plutonium content. Above all, the industry-scale use of these four types of fuels requires more investigation.

In spite of the diverse fuel features and neutronics behaviors of these advanced fuels, MIX fuel is used in this work to present possible pathways of plutonium multi-recycling in PWRs. The systematic physics and neutronics analyses on the impacts of using all these advanced fuels on the cycle are out of scope.

1.1.4 French near-term strategy

This work uses the French nuclear fuel cycle as an example and reference for the analyses concerning the ambiguous status of plutonium. The evaluation of French-based strategy can be informative.

For the future low-carbon development regarding the fight against climate change, a series of governmental planning and assessments on the near-term transition of energy mix are established in the multi-year report PPE [18]. Besides the reduction of dependency on fossil fuels, this document highlights a rising share of renewables in the coming decades in the future structure of energy mix, with a certain decrease of the nuclear power in electricity supply following the shut-down of old-generation PWRs.

Regarding the nuclear power, PPE provides the guidelines on these aspects: the research on dismantling and decommissioning of facilities as well as the relevant disposition of very-low and low level wastes, the project of small modular reactor, the continuous research on the multi-recycling in PWR and fast reactor, the sustainable management of nuclear wastes according to the categories, and possible trajectories of nuclear fleet transition in France.

In the near term, the dynamic transition of nuclear fleet is determined in this report. The total installed capacity and the share of different adopted technology depict the fleet configuration and the actions anticipated for the next decades. As a direct result, this fleet transition will also influence the management of spent fuels and nuclear wastes in the near term. In this report PPE, the uranium resource is estimated to be sufficiently abundant and the market price is estimated to remain low. Under this estimation, the fast reactor technology which is dedicated to avoiding uranium resource shortages, is considered not economically competitive during at least the first half of 21st century. It can be an important technology by the end of century, and thus the accumulation of relevant knowledge and experimental feed-back should be maintained in the academic research and development. But from the viewpoint of national application, it is the multi-recycling of plutonium in PWRs that will be considered for the coming decades.

Respecting the life time of nuclear facilities, the current generation of PWRs will be replaced progressively by EPRs. Following the pace of decommissioning of reactors, the government pursues an objective that reduces the share of electricity production of nuclear power from the current 70% to 50% by year 2035. This share level can be maintained until year 2050. The mono-recycling strategy is regarded as an intermediate phase of the transition towards the plutonium multi-recycling. It will be kept during the share transition, requiring the MOX licensing of reactors following the shut-down of current MOXed PWRs. In year 2040, the facilities concerning the reprocessing of spent fuels, La Hague, and the fabrication of fresh fuels of recycled plutonium, MELOX, will have to be replaced or renewed. Beyond that, the strategy of multi-recycling of plutonium in PWRs should be determined based on the relevant research and development, linked to the replacement with new plants of fabrication and reprocessing. Designs of new facilities depend directly on the decision about the configuration of fuel cycle.

The outcomes of these actions are also related to the nuclear wastes management. Not only does the technology deployed, but the scale of fleet also control the quantities of wastes produced in each category defined in [34]. In particu-

lar, the production of intermediate and high level wastes during the operation of facilities of fleet are the focal points of concern which requires deep geological repository. The relevant projects and sites need specific assessment, which should match well the estimation of waste disposition related to the fleet and be well planned in advance.

1.2 Scenario study: a way to assess strategy conception

With respect to a set of strategy conceptions for possible fuel cycle transitions, the performance and possible outcomes should be evaluated through scenario study. Simply speaking, a scenario depicts specific future states and the possible associated pathways, according to the conceptions and interests of analysts. Based on the parameters and assumptions related to the strategy, the simulation of the system of inquiry (here, the nuclear fuel cycle) provides the outputs that can indicate the relevant consequences.

Scenario study is not only a simulation of a coherent future, but more importantly, it is a thought experiment to generate and observe the orientations of the possible futures of interest with specific interpretations of outcomes. Scenario studies should be carefully distinguished from the determined prognosis or forecast [35]. Some scenarios may take extreme hypotheses to indicate qualitatively the orientation of interest, even though they are unrealistic. Despite some confusing points on the distinction of techniques in the corresponding narratives [36], one may consider two principal categories of scenario studies [10, 35]. One is exploratory scenario, which reveals the diversity of consequences for a given wide range of possible hypotheses of trajectories. It starts from the parametric features of strategies and investigates their future outcomes. The other is normative scenario, which aims to provide some instructive norms towards desirable futures. It constrains the phase of outcomes and characterizes retroactively the strategies fulfilling the normative criteria. Depending on the purpose of study, both types of scenario study can be useful tools for the study of nuclear fleet strategy, because of the complexity of system and temporal limits of knowledge. This scenario categorization indicates the functionality of scenario study concerning the upper-level strategy, which comes from the decision-making and communications among the political, economic and industrial actors and stakeholders.

The time horizon is an important parameter of scenario, depending on the purpose of study. One may focus on several minutes for accident scenarios, while others think about millions of years for the deep geological repository. In the frame of this work, several lines of temporality bring to light the role of scenario study in the strategy assessment from nuclear industry.

First, the disposition of nuclear wastes, particularly the high level wastes, may last generations of human activities. Such long term surpasses evidently the supervision and management time length of an organization, and the possible consequences can only be projected in a scenario study. This long time horizon is out of the scope of this work, because the relevant outcomes of interest can be actually deduced from the deployment of reactors for the coming decades.

The facility operation lifetime is an important time characteristic for the use of scenario to assess transition strategies. The lifespan of nuclear facility, such as nuclear reactor, reprocessing plant, or fabrication plant, is around 50 years, with some deviations depending on the nature of facility, the operation parameters and economic factors. The facilities built during transition will continue their operation after. The influences of these facilities will be maintained or accumulated during and even after the remaining operation. If a much shorter horizon

is considered, like 10 years, it means that the possibility of facilities temporally stopping afterwards or being permanently shut down is not taken into account in the assessment. This seems not necessarily profitable for industry and thus not realistic, unless some other positive outcomes are able to compensate it. In other words, the construction of each new facility, implied by a transition strategy, requires a series of careful inquiries, investigations and assessments. Once implemented, the modification of the transition strategy can be hard within decades, or it should respect the operation life time and be coherent with the interests of stakeholders. In consideration of this temporality, a scenario study can then present the impacts of strategy on the fuel cycle under a temporal-consistent framework.

Last but not least, the time gap between the decision and implementation may also play a role on the strategy assessment. To give an example, the decision of using MOX fuels in some 900-MWe PWR was made in 1985, and the MOX was first loaded in 1987 in the reactors of St. Laurent [37]. In contrast, the construction of first EPR in France was authorized in 2007, and the connection to grid was first estimated in 2012 [38]. But following the identification of anomalies in the pressure vessel and in the welding of principal steam pipes, the in-service operation of EPR suffered several adjournments, and the current estimation postpones it to the year 2022 [38, 39]. This timeline of implementation varies from project to project, depending on the technical difficulties, and the order of magnitude can vary from months to decades. Consequently, its influence should be well anticipated by scenario studies.

In summary, the strategy concerning the future fleet transition involves essentially the deployment of facilities. This implies thus a time horizon of several decades in a coherent scenario study of nuclear fleet and the assessment of relevant transition strategies.

1.3 Deep uncertainty in the future of nuclear energy

1.3.1 Historical development of nuclear power in France

Even though the assessment of a transition strategy can be carried out with all details of hypotheses, the result of assessment is not necessarily constant over time during the temporality aforementioned. In fact, this time length is so long that some uncertainties non-anticipated may change the interest of actors in an inter-temporally incompatible way.

The historical trajectory of nuclear power in France gives a concrete example about how the nuclear development interacted with uncertain factors. The current reactors of French nuclear fleet, most of which were built and started operation during the 1980s, is principally a consequence of the oil crisis in the 1970s [40]. This sharp expansion of nuclear deployment, involving national policies based on the consideration of independent national energy generation, led to a strong dependence of nuclear electricity in France.

Motivated by the challenge against climate change, more countries become interested in nuclear deployment. In the past, the perspective of a rapid nuclear expansion worldwide brought the concerns of uranium resource shortage. The project ASTRID was then launched as a commercial fast reactor prototype for the deployment of coming decades in France [41, 42]. A large number of scenario studies of fast reactor deployment were in parallel with the theoretical and engineering research, aiming to explore possible pathways of diverse deployment designs and provide some instructive indications about the future transition of

fast reactor deployment [25, 21, 43, 42, 44]. Some optimistic studies supposed that a phase of demonstration should start from the middle of century, and a first phase of large-scale deployment would replace some of next-generation EPRs during the last 20 years of the century.

Despite purposeful endeavors devoted to this project, the current attitude to the option of fast reactor changed significantly during the recent ten years. The Fukushima accident has an evident impact on the energy-related policies and programs all around the world, especially on the projection of future [45]. France, as indicated in [18], decides to reduce the nuclear share in energy mix. The phase-out planning in some European countries are accelerated. China, which accounted a large part for future nuclear expansion in those estimations prior to the accident, stops the projects of inland sites and old-generation reactors, and slows down the pace of future expansion [46]. Even though [45] estimates that the ultimate change of global energy policies attributed to the Fukushima accident is quantitatively limited, lots of nuclear-dependent regions take more conservative attitude and strategies than before. The change of expectation is reflected in the estimation of future availability of uranium resources and the market price. These knock-on effects alter indirectly the evaluation of the transition strategy concerning fast reactor deployment in France. The fast reactor deployment planning made at the beginning of the 2000s was to some extent disrupted.

No matter the oil crisis in 1970s or the Fukushima nuclear accident in 2011, the influence of external shocks on future predictions and the adopted energy strategy cannot be well anticipated. Changes before and after the shock can be sometimes brutal and radical. This kind of change is called disruption in this work. It is hardly possible to quantify the probability of disruptions and their impacts on parameters by statistical distributions. The notion of deep uncertainty introduced in the following subsections is used to study such extreme situations. Given the highlighted time constraints of transition strategy and the inertia of nuclear fleet, it is important to recognize the deep uncertainty of nuclear future concerning the relevant transition pathways.

1.3.2 Uncertainty categorization in electro-nuclear scenario study

To consider the uncertainty in the assessment of transition strategies, the uncertainties should be first well categorized.

From the parametric point of view, [47] classifies uncertainties into five levels, depending on the precision on the uncertainty quantification, described by the density function of probability and the clearness of the outcome estimation. Level 1 corresponds to the clearest description of uncertainty, needing a single system, point estimates with sensitivity and single estimate with weights. Level 5, on the contrary, stands for those uncertainties that cannot be described by estimate or probability: no "parameter" in the description of uncertainty is known. Due to the comprehensive lack of parametric description, it is called "deep uncertainty". The foregoing example of external factors that pushed forward or slowed down the expansion of nuclear power can be reckoned as deep uncertainty. Even if these events can be imagined and listed, no one could foresee them with a degree of certainty before they take place.

From the angle of source in electro-nuclear scenario studies, [48, 49] consider principally six families of uncertainties:

- Nuclear data;
- Physics modeling;

- Historical data;
- The choice of parameter values for the future strategy;
- Formulation of criteria to satisfy, allowing to figure out the relevant trajectories and strategies of interest;
- Hypotheses in the political, economic, industrial and societal decisions that may impact the nuclear fleet.

The uncertainties of nuclear data can be, for the major part of nuclides and nuclear reactions in electro-nuclear scenario studies, represented by the relevant correlation matrices. The propagation of these uncertainties is analyzed in detail in [48].

The uncertainties of physics modeling may involve the essential simplifications or approximations in the resolutions of equations and the choices of physics parameters. To achieve an acceptable computational cost and a comprehensible analysis, the biases from this kind of approximations are usually unavoidable. This part will be discussed in Section 2.1.

Every single scenario study starts from a given point, usually the current situation that requires the simulation of the historical trajectory. In this case, the uncertainties of historical data lead to a confusing zone of the starting point, and it may influence the final assessment of scenario study. The impact of these uncertainties is well discussed in [50].

Overall, the uncertainties in these three families can be well controlled and quantified by relevant experimental and industrial feed-backs. It is sometimes problematic for innovative systems; in this case, the benchmark studies with validated codes can help estimate quantitatively the deviations. However, the last three families of uncertainties concerning the external factors of future can be deep and hard to describe accurately with appropriate parameters. At the same time, they are mutually dependent. The policy-making based on the political, economic and societal compromises determines the normative objective that infers the range or the set of fleet composition of interest. As shown by the foregoing French case, it is almost impossible to predict well those external factors a-priori, while they can disrupt the prior strategy or relevant estimation. If the updated perspective is contradictory to the prior one, the previous efforts devoted may lead to crucial vulnerabilities or regrets after disruption. Depending on the constraints imposed, it can be still possible or too late to heal these vulnerabilities.

It is worth noting that the uncertainty may not only originate in the lack of information or limited knowledge, but may also come from the increase or the abundance of information but without sufficient goodness of quality, clear agreement or interpretation [51, 52]. The progress of knowledge is conducive to recognition and understanding of domains that were not well known previously; but as the spectrum of knowledge is broadened, new uncertainties appear on the boundaries. Even if the system and outcomes are presented without confusion, individual or organizational preferences and interests may render different evaluation and options of strategy.

1.3.3 Integration of deep uncertainty in electro-nuclear scenario studies

Diverse options of nuclear energy development are still open. As indicated, scenario studies allow investigations on the outcomes of trajectories of interest, and

help identify the advantages and drawbacks of these strategies.

Even though some studies consider the influence of uncertainties of nuclear data and physics modeling, most of the physical analyses in electro-nuclear scenario studies start from justified but unchanged basic hypotheses of future tendency, such as a preset perspective of installed capacity and the technology applied. The results of analyses are implicitly constrained by these hypotheses. The result in one work may not be adaptable to another with different hypotheses. The deep uncertainty of perspective of nuclear energy, taking different possibilities of these basic hypotheses into account, is rarely considered in these physical analyses.

1.4 Outline of the thesis

The objective is the fruit of high-level strategies, implying the desirable shape of future. But as introduced above, this desirable shape may be sometimes deeply uncertain and may change abruptly. This work aims to integrate the deep uncertainty in electro-nuclear scenario studies, involving several sorts of uncertainties. The primary uncertainty concerns the choice of objective that can impact directly the fuel cycle. At the beginning of the 2000s, fast reactor was supposed to be deployed from the 2040s and this objective put forward a number of relevant studies. Following a series of changes, one may currently prefer the options that minimize nuclear wastes without the consideration of fast reactor. Nevertheless, one still lacks a clear vision about which choice is pertinent.

Even if the nuclear future is well oriented by the determination of objective, there is still an ambiguity on the criterion used to assess the strategy. This ambiguity comes from the transformation from language formulation to mathematical expressions. In this transformation process, additional assumptions are needed, which reflects delicate differences of strategy assessments. Last but not least, some fuel cycle parameters regarding the near-term transitions, such as the total installed capacity of fleet, may be also explicitly linked to the shape of future, and may meet some levels of uncertainty.

To analyze their impacts on the strategy assessment, the uncertain disruption of objective, which points out the global orientation of nuclear future, is considered for the subsequent scenario studies. We focus first on the situation when the disruption has not yet taken place. In this pre-disruption scenario, strategies are explored in consideration of the possibility of disruption. Then in an adaptation scenario, the disruption of objective is supposed at a given time, and adaptive strategies based on a given prior trajectory of the pre-disruption strategy are evaluated.

Based on this general framework, the notion of strategy robustness is introduced. In this work, the robustness is used to quantify the capacity of a strategy to adapt to the disruption of objective. For example, a strategy is implemented for a given objective before any disruption. In case of a disruption, the trajectory may be easily adapted to the new objective with or without readjustments. If it is the case, the strategy originally implemented or complemented with an appropriate adaptive planning is considered robust.

To set the base of robustness assessment in electro-nuclear scenario studies, the notions and the paradigm developed for this work are presented in Chapter 2. First of all, the simulator Core Library for Advance Scenario Simulation (CLASS) is presented in Section 2.1, the tool for the dynamic simulation of fuel cycle in this work. With the use of CLASS, the methodology of Global Sensitivity Analysis (GSA) for electro-nuclear scenarios studies is presented in Section 2.2, taking the

screening method of Morris [53] as an example. The GSA of scenario provides a fundamental understanding on the behavior of fuel cycle subject to large variations of parameters. After that, Section 2.3 details the framework of strategy robustness assessment. This framework clarifies the relation between strategy assessment and the deep uncertainty of disruption in scenario studies. It provides a solid frame for robustness study to adapt to various context and scenario hypotheses.

To present the methodology, the French fleet is studied, and two contradictory objectives based on its historical trajectory are considered. The SFR deployment is regarded as the pre-selected objective. In case of disruption, the new objective can be the minimization of potential wastes without SFR.

The strategy assessment at a predetermined time is often an assumption of scenario study, giving an intuitive vision on the performance of strategy (e.g. analyze the output values at the end of scenario). Through an exploratory scenario study in Chapter 3, the methodology is first developed based on this assumption within a preset time horizon of scenario. In Section 3.1, the problem is formulated into mathematical expressions and numeric criteria, in order to perform the assessment with determined values. The robustness assessment is divided into two phases. The first one focuses on the pre-disruption scenario in Section 3.2. In this scenario, the analyses give a primary view on the consequences of possible strategies based on limited information before any disruption. The second one in Section 3.3 considers the adaptation from the prior trajectory a pre-disruption strategy, supposing that the pre-selected objective is disrupted. Robust adaptive strategies for the new objective of minimizing the wastes are identified. In these two scenario studies, the assessments start from two distinct principles and scenario assumptions, and thus reveal the outcomes of strategies under different context. To highlight the influence of problem formulation and criteria used on the assessment, the minimization of normalized wastes instead of the absolute quantity is considered for post-disruption adaptation in Section 3.4. Given the normalization by the cumulative nuclear electricity production, the analysis gives an insight on the assessment much less sensitive to the uncertainty of installed capacity. Therefore, this choice of problem formulation can be interpreted as an optional management of uncertainty for scenario studies.

The assessment at a predetermined time in Chapter 3 implies the consideration of the same preset time horizon in all studied scenarios. Despite the common use of this assumption in a large number of scenario studies, the assessment results are likely to be inconsistent in another time horizon. For instance, a given strategy is robust under the evaluation at a predetermined time; but if it is assessed at a later time or in an extended horizon, it may be no longer robust. To address the possible inter-temporal inconsistencies, the framework of robustness assessment is adapted in Chapter 4 to the independence from the need of predetermined time. The problem and criteria are reformulated in Section 4.1 by introducing new assessment assumptions. Using the same framework of scenario study as in Chapter 3, Section 4.2 analyzes the pre-disruption scenario, and 4.3 analyzes the post-disruption adaptation scenario from one prior trajectory. The following two sections complement then the strategy assessment from different angles. Section 4.4 considers the adaptation from a set of prior trajectories. It gives a much broader vision on a large set of pre-disruption choices connected with the outcomes under necessary adaptations. Section 4.5 unlocks a new post-disruption doorway that is not available before disruption, e.g. the plutonium multi-recycling in PWRs. This change may bring potentially a large difference on the strategy assessment.

Chapter 3 and 4 build the methodology from different basic scenario assump-

tions. In these GSA-based studies, a relatively high variability of fleet leads to the statistical analyses of a large-size set of strategies. Chapter 5 focuses finally on the practical cases, applying the framework of robustness assessment to possible transitions inspired from the French national strategy presented in PPE.

Chapter 2

Dynamic Simulation of Nuclear Fuel Cycle and Methodology of Electro-nuclear Scenario Analysis

Introduction

Scenario studies are often performed to evaluate different futures for nuclear energy. Those futures may involve the deployment of new technologies, the choice of different options for fuel reprocessing and the selection of different parameters for fuel cycle and reactors. With simulations, the trajectories and outputs of interest can be calculated, and the strategies are then assessed. The scenario study is often a key point for every decision-making process related to nuclear energy.

When it involves the material irradiation in nuclear reactors, the simulation in scenario studies can be problematic due to the complexity of nuclear reactor modeling, demanding heavy computational time and high requirement of data storage. Moreover, the time-consuming depletion computation only calculates material evolution of several years. When the scenario considers the recycling of materials, dynamic fuel cycle simulations need numerous depletion calculations in a row to complete decades or even hundreds of years of simulation time period. Meanwhile, the mass flows in the fuel cycle also concerns the ones in other facilities than reactors as well as the transportation between them, according to different management strategies and fuel cycle parameters. To achieve an acceptable precision of simulation with reasonable simulation time, specific simulators rather than depletion codes should be developed. In this work, the dynamic simulation of nuclear fuel cycle is performed by Core Library for Advance Scenario Simulation (CLASS) [54, 55].

With the simulator CLASS, a large number of transition strategies characterized by different fuel cycle parameters can be investigated within acceptable computational time. To understand the general behavior of the nuclear fuel cycle, the Wide Parametric Sweeping (WPS) technique for Global Sensitivity Analysis (GSA) is used to reveal the intrinsic relations between parameters and the responses of the system. In consideration of the large variability of input variables, extreme cases can be taken into account in the fuel cycle analyses. The basic understanding on the behaviors and the responses of fuel cycles help interpret strategies performances and robustness assessment subject to uncertainty.

In this chapter, Section 2.1 presents the physics of nuclear fuel cycle and the difficulties on the related dynamic simulations, in particular the material irradiation in reactors. Differences between depletion codes for reactor modeling and

fuel cycle simulators are highlighted. CLASS, the fuel cycle simulator in this work, is then presented. Section 2.2 presents an analysis method of electro-nuclear scenario. A simple cycle defined by a PWR loaded with 30% MOX, demonstrates how CLASS simulates the fuel cycle dynamics. An exploratory scenario of fuel cycle transition is then given to illustrate the WPS technique applied to the GSA of fuel cycle. The Morris method [53], a derivative-based screening method, is used to investigate the responses of fuel cycles, and to rank the input parameters of fuel cycles according to their importance on several outputs. Then Section 2.3 introduces the general framework of robustness assessment of strategy under disruption of objectives in electro-nuclear scenario. Section 2.4 concludes the preliminary analysis results and the general presentations of analysis methods employed in this work.

2.1 Dynamic simulation of nuclear fuel cycle

The fuel cycle in France is described in Section 1.1. This fuel cycle is taken as example in this work. Before introducing CLASS for the dynamic simulation of fuel cycle, important concepts on reactor physics and depletion codes for reactor modeling are presented to help understand the material irradiation processes. It justifies why such codes are not directly usable for fleet transitions in electro-nuclear scenario studies. In fact, fuel cycle simulators may not be required for steady-state scenario studies. In this work, we focus on dynamic transitions that need a dynamic fuel cycle simulator. To end this section, the simulator CLASS used in this work is presented in detail.

2.1.1 Modeling of reactor depletion and other processes for fuel cycle simulation

2.1.1.1 Principal concepts and reactor physics notions

To calculate the time-dependent material inventories in a nuclear fuel cycle, the first major step is the fuel depletion in reactors. The numeric resolution of material depletion by reactor modeling codes requires the resolution of two equations: Boltzmann equation and Bateman equation.

Boltzmann equation describes the neutron transport in reactor. Its resolution gives neutron reaction rates as a function of the space for a specific time. The numerical methods to resolve Boltzmann equation is out of the scope and not presented here.

Bateman equation describes the evolution of materials under neutron irradiation. For a given nuclide i, the evolution of its quantity N_i can be written under a general form:

$$\frac{dN_i}{dt} = Prod_i - Disap_i \tag{2.1}$$

where $Prod_i$ denotes the production rate of nuclide i and $Disap_i$ denotes the disappearance rate. Production and disappearance of nuclides result from nuclear reactions, such as radioactive decay, neutron capture and fission. If the nuclide i is not a fission product, the creation term $Prod_i$ can be written as

$$Prod_i = \sum_j N_j(\lambda_{j\to i} + \int_E \sigma_{j\to i}(\varepsilon)\Phi(\varepsilon)d\varepsilon) \tag{2.2}$$

where $\lambda_{j\to i}$ denotes the decay constant from nuclide j to i, $\sigma_{j\to i}$ denotes the microscopic cross-section of the nuclear reaction on nuclide j that generates i, and

Φ denotes the energy-dependent neutron flux. If the nuclide is a fission product, a term of production by fission should be added. Similarly, the term $Disap$ can be written as

$$Disap_i = N_i(\lambda_i + \int_E \sigma_i(\varepsilon)\Phi(\varepsilon)d\varepsilon) \tag{2.3}$$

where λ_i denotes the total decay constant of nuclide i, and σ_i denotes the total microscopic cross-section excluding the scattering.

In this work, we focus particularly on the transmutation of heavy metal nuclides. Figure 2.1 shows a part of important reaction chain of heavy nuclides during the depletion in reactor. Note that the fission and some other reactions are not shown in this figure; it helps to understand how these heavy nuclides transmute from one to another through nuclear reactions. The production and the disappearance of these nuclides are, evidently, the results of Bateman equation.

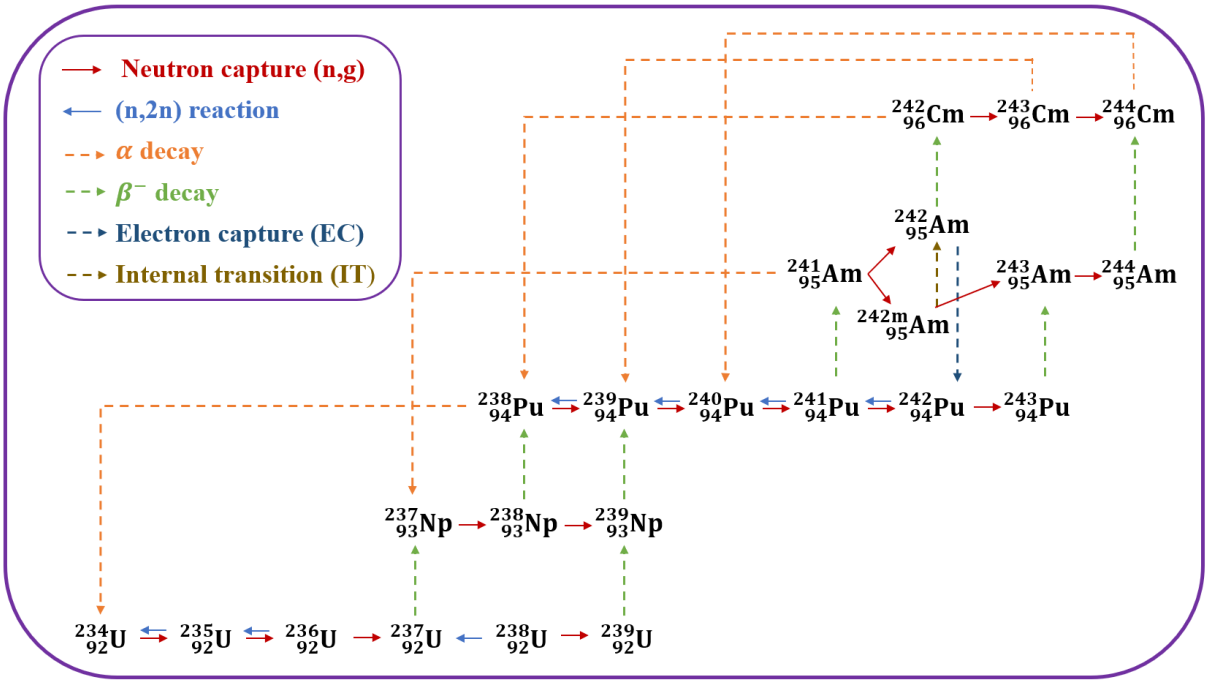

Figure 2.1: Extract of transmutation chain of heavy nuclides during depletion in nuclear reactor

2.1.1.2 Composition of typical spent fuels after depletion

The prediction of spent fuel composition is complicated because it depends on the fuel nature and the operation history. Spent UOX fuels are still principally composed of ^{238}U (about 95%). They also contain the fission products (3%), other uranium isotopes (1% to 2%; 0.8% to 1% for ^{235}U), plutonium (1%) and minor actinides (order of 0.1%) [8]. More than half of plutonium is ^{239}Pu. Meanwhile, the half-life of abundant plutonium isotopes are relatively long (e.g. 2.4×10^4 years for ^{239}Pu, 6561 years for ^{240}Pu). If these plutonium inventories are disposed as wastes, this significant amount of radioactive inventories maintains an extreme high level of radio-toxicity and dose rate during a long time.

The composition of spent MOX fuels depends on the initial plutonium content and isotopic composition of plutonium in the fresh fuels. The simulation of MOX depletion in the study of [56] gives several typical isotopic compositions of plutonium in spent MOX fuels. In general, the plutonium content decreases over irradiation, particularly the isotope ^{239}Pu. Even though ^{241}Pu is a short-lived fissile nuclide, its quantity during irradiation in PWR may reach equilibrium, principally

due to the neutron capture reaction of $^{240}\mathrm{Pu}$ which is also abundant in MOX fuels. Meanwhile, the plutonium quality in MOX fuels decreases over the irradiation. Here the quality can be defined as the fraction of odd-number isotopes in the isotopic composition of plutonium (or equivalently, the ratio between the quantity of odd-number isotopes and the quantity of even-number isotopes [57, 42]). Given the burn-up, low quality of plutonium needs a high content in the fresh fuel. The plutonium in spent MOX fuels are not currently recycled.

Other advanced fuels e.g. MIX fuel for PWR and MOX fuels for SFR, have more complicated physical properties under irradiation. Even though they may be employed in this work, the study of material evolution of these fuels are complete studies in themselves in dedicated chapters and will not be detailed in this chapter.

2.1.1.3 Why dynamic simulations of fuel cycle need more than a depletion code

One challenge of reactor modeling for depletion calculation is the long computational time and the significant computational memory [58]. This computational cost depends strongly on the requirement of precision, the objective of studies and simplification methods. Lots of efforts have been devoted to simplifying and accelerating the simulations. For example, multi-threading parallelization is a typical option to speed up the program. Simplifications specific to algorithm characteristics, such as the cut-off methods of nucleus tree suggested in the depletion code SMURE [59], also reduce parts of computational time [60]. Instead of total core simulation with fine details, simulation of representative assemblies also reduce the complexity without generating unacceptable deviations [61]. However, even with such methods, the computational time is still too expensive to simulate tens of different irradiation cycles for a specific transition.

Another problem of complexity involves the necessity of iterations to determine reasonable isotopic composition for fresh fuels. In depletion codes, compositions of fresh fuel is predetermined and the criticality over burn-up is an output of calculation. Depending on the fresh fuel composition and the burn-up, the core can be over- or sub-critical. In electro-nuclear scenario studies, the criticality of reactors needs to be ensured. The composition of fresh fuel that ensures the criticality is a-priori unknown, and can only be found through iterations of depletion computation. If a depletion code is used for these iterations, even if one computation can be relatively fast, the corresponding iteration may increase significantly the time cost [56].

Last but not least, depletion codes focus on the material evolution in reactor, whereas a scenario study investigates the behavior within the entirety of fuel cycle. Not only the material evolution in all facilities, but also the "events", e.g. the start of operation or decommissioning of facilities and the material transportation are taken into account. Meanwhile, the mass flows are constrained by the operation capacities of facilities, possibly playing important roles on the justification of validity. In consideration of these needs, a dedicated module to organizing and handling these threads is essential.

Given different needs of computation cost and parameters of interest, dedicated simulator of nuclear fuel cycle to electro-nuclear scenario studies should be developed.

2.1.1.4 Current simulators of nuclear fuel cycle

Several tools dedicated to the dynamic simulations of nuclear fuel cycle have been developed in the last few decades to answer the demands of studies possi-

ble nuclear futures. The purposes of these studies can be:

- Relation between the reactor systems and the evolution of mass flows;
- Impact of introduction of new concepts or technologies on the fuel cycle;
- Demand of resources and waste management;
- Adaptation of the nuclear fleet to uncertainties;
- Economic estimates.

Meeting different purposes of analyses, diverse simulators of nuclear fuel cycle have their own characteristics, simulation hypotheses and specialties. Because of the timescale and the size of facilities considered, it is extremely difficult to validate the fuel cycle simulators by real-life experiments. Regardless, several efforts have been done to increase the confidence of these simulators. An international study of benchmarking has been coordinated to compare five codes of reference developed by different institutions all over the world [62], including COSI [63] by CEA in France, DESAE [64] by the Russian Kurchatov Institute, EVOL-CODE/TR_EVOL [65] by CIEMAT in Spain, FAMILY21 by JAEA in Japan and VISION [66] by the Idaho National Laboratory in the US. This benchmark puts into light the importance of conceptions on the capabilities of these simulators. Three simple scenarios concerning respectively PWR UOX, PWR MOX and fast reactor are used to demonstrate their consistency in global tendency of outputs and disagreements in complex system analysis. Some of these codes also participated in a collaborative analysis of uncertainties of input parameters in the fuel cycle [67] which includes two other codes: COSAC used by ex-AREVA in France and SITON developed by EK in Hungary [68]. The investigation on several outputs of interest reveals not only the sensitivity of some specific outputs on the input parameters, but also the nuances of mass flow management due to implicit hypotheses of conception in different codes.

Not only the code conceptions, but also the common physics modeling shared by the codes should be investigated, which help indicate the confidence level of simulation concerning the physics modeling. In conventional studies, experimental and industrial data can calibrate and benchmark the modeling. For the validation of physics modeling conceptions, there is always a lack of industrial feedback due to the inaccessibility of industrial data, preventing any validation and qualification program. It is even worse for innovative systems that have never been deployed. To quantify the necessary level of confidence concerning the conception of physics models, Functionality Isolation Test (FIT) project has been launched [69], involving the simulator ANICCA [70], CLASS [55], COSI6 [63], Cyclus [71], JOSSETE [72] and TR_EVOL [65]. This project aims to perform the intra-comparison of physics modeling of simulators by specific test exercises, with a focus on the discrepancies between the preset fraction model and the specific loading model adapting for material physical properties (called Fuel Loading Model (FLM) in FIT). The agreements and particularities of results among the participant codes help estimate and quantify the potential biases of loading models, especially the preset fraction that has been used.

2.1.2 CLASS: simulator for dynamic nuclear fuel cycles

2.1.2.1 Introduction of CLASS

Since 2012, CLASS is developed by Centre National de la Recherche Scientifique ([EN.] French National Center for Scientific Research) (CNRS) with initial support

of Institut de Radioprotection et de Sûreté Nucléaire ([EN.] Institute for Radiological Protection and Nuclear Safety) (IRSN). It is a package with libraries written in C++, in which the instances of facilities and other physics models can be created and plugged together to simulate different fuel cycle transitions. The facilities to be simulated include fabrication plant, reactor, cooling pool, separation plant and interim storage [54]:

Fabrication plant

The complicated chemical processes in the front-end of cycle are yet not simulated in CLASS. Fabrication plant provides directly the fresh fuel with fissile fraction depending on the operation parameters of depletion. Each fabrication plant can be customized by choosing the fabrication time, the stocks from which the fresh materials as resources are extracted in which sequence. The fabrication time represents the time needed inside the fabrication plant to prepare the fresh fuel. In CLASS the model is doing the fabrication process instantaneously. If the resource includes the recovered materials from spent fuels, an instant separation of spent fuels is supposed at the start of fabrication period. The target materials are then recovered, while non-reusable materials are sent to the block WASTE. This block represents the conditioning and repository of waste canisters. After waiting for the given fabrication time inside the fabrication plant, the fresh fuels are transported instantly to the associated reactor.

Reactor

Reactors are the facilities where the materials evolve under irradiation producing electricity. They can be customized by choosing physics model, operation parameters e.g. heavy metal mass loaded in core, burn-up, power level, effective loading factor, operation/shut-down time and associated back-end facilities to which the spent fuels are instantly transported after discharge. Through years of development and specific analyses, many reactor models and relevant modules have been developed, including PWR UOX and MOX [55], PWR MOXEUS [73, 74, 50], PWR mono-Am [75], ESFR [76], flexible ESFR-like model [77], ASTRID-like model [78, 42] and ADS [79]. The MOXEUS can be used for MIX fuel simulation, and it is also used in this work.

Pool

Pools represent the cooling pools located nearby reactors where spent fuels are stored just after discharge, and wait for the decrease of decay heat and dose rate during a set time of cooling. During this period, materials are not available for reprocessing. After the time of cooling determined by user, the spent fuels are transported instantly to the associated back-end facility.

Separation plant

Separation plants are used for the separation of elements for given flow of spent fuels, corresponding to the spent fuel reprocessing. Not only the materials to be separated, but also the corresponding separation efficiency can be customized. The separation is supposed to be immediate, and then the selected part of materials are transported instantly to the associated back-end facility, while the rest is sent to the WASTE.

Storage

Storage represents the interim stocks of spent fuels after the cooling in pools or after the separation by separation plant. Radioactive nuclei continue their decay in the stocks, and they can be recovered at any time if needed by another facility.

In the previous paragraphs, instant transportation of materials is emphasized, responding to the demand of resource in front-end and to the parameters of spent fuel management in back-end. For instance, a given quantity of plutonium from the spent fuels in an interim storage is needed for MOX fabrication. The spent fuels in the stock with respect to the required quantity of plutonium is then reprocessed instantly. As mentioned, the plutonium inventory is then transported instantly to the fabrication plant of MOX and stays in the plant during a given time of fabrication. The remaining elements from the spent fuel assemblies where plutonium have been extracted are sent immediately to the WASTE. The level of mass flow in the separation and fabrication plants are driven by the demand and a-priori no limit is given. This demand of separation and fabrication leads to a large variation of mass flow in the facilities from one year to another with peak at the starting of new irradiation cycles. This does not represent a really realistic industrial process; it comes from the CLASS conception and does not seem worse than other options for our studies.

2.1.2.2 Mass flow management in CLASS

A specific module, called *time vector* in CLASS, is dedicated to the automatic creation of the time schedule as well as the designation of material transportation.

The progression of simulations is driven by this time vector. First, the time of fresh fuels loading and spent fuels discharge can be deduced from the start time of reactors and the time of each irradiation cycle. The times of fresh fuel transportation can then be decided by considering the time of fresh fuel loading and the time of fabrication; the times that move spent fuels from the pools to interim storage can be decided by considering the time of discharge and the time of cooling. With iteration, the time vector can be pre-built to manage the mass flows in simulation.

One should note that any modification of operational parameters for a reactor, e.g. the power level and the burn-up of fuels, respects the irradiation cycle. In other words, if the parameters of a reactor need to be modified when the fuel depletion is not yet finished, the modifications will only be applied at the start of next irradiation phase. This hypothesis makes sense in reality, but it also desynchronizes some timing of interest. In the analyses of subsequent chapters, this desynchronization will be frequently highlighted when the results of robustness assessment are interpreted.

2.1.2.3 Physics modeling in CLASS

The simplest method to consider fuel loading and depletion calculation in scenario study is the use of recipes. This method uses one or several representative fuel evolutions that have been pre-calculated by reactor simulations. Each depletion in the scenario is then only a re-normalization of the recipe to match the installed capacity of reactors. This method does not need complex calculations of depletion or criticality verification during the scenario simulation, and thus the simulation can be very fast. Nonetheless, the number of recipe is usually limited and cannot be sufficiently representative when the variability of fuel cycle parameters or recycled plutonium isotopy is relatively large [69].

In CLASS, the physics modeling of irradiation consists of two parts: the FLM, and the irradiation model which includes a cross-section model and a solver of Bateman equations. Once the time-dependent cross-sections are known, the Bateman equations are solved by the Runge-Kutta fourth-order method [80]. The prediction of fresh fuels is far more complex, and CLASS uses Artificial Neural Network (ANN) in order to achieve reasonable computational cost with acceptable precision.

Fuel Loading Model in CLASS

FLM predicts the composition of fresh fuel, depending on a given determination criterion. The resources for the fissile components of fresh fuel can be simply classified into two categories. The first one is $^{235}\mathrm{U}$ coming from natural resources, and in this case the enrichment should be determined. The other concerns the components recovered from spent fuels, e.g. the plutonium. In this case the isotopic composition is determined by the history of material evolution, and thus the composition prediction for plutonium-based fuel focuses on the plutonium content.

The determination of fresh fuel by the FLM should guarantee the criticality during irradiation. As an important indicator of criticality, the evolution of effective multiplication factor k_{eff} is used as a criterion parameter, and the k_{eff} predictor as a function of time and the fresh fuel composition are built by ANN from a database of reactor simulations. The database used for training cover a high variability of fresh fuel composition to guarantee that all conditions encountered during the scenario simulation stay within the boundaries.

The database of PWRs for ANN training are based on the simulations of infinite assemblies, without considering control rod nor variable boron control. Therefore, the effective multiplication factor k_{eff} decreases strictly over the burn-up in PWR simulation data. To ensure the criticality until the end of depletion, the multiplication factor at the End Of Cycle (EOC), denoted as $k_{eff,EOC}$, should be larger than 1 with a reactivity margin defined by a customized threshold. To maximize the use of the fissile components of fuel, the $k_{eff,EOC}$ should be as closed as possible to the threshold. Given the burn-up, the $k_{eff,EOC}$ is strongly correlated to the fissile fraction, e.g. the $^{235}\mathrm{U}$ enrichment in UOX fuel, or plutonium content in MOX fuel. Under these hypotheses, the fissile fraction of fresh fuel can be determined using an iterative dichotomy algorithm.

To take into account the core fractioning, the global k_{eff} can be approximated by the mean value of k_∞ of different batches [55]:

$$k_{eff}(t) = \frac{1}{N}\sum_{i=1}^{N} k_\infty(t + \frac{iT}{N}) \tag{2.4}$$

where N is the number of fractioning, T is the total irradiation time for a given burn-up, and k_∞ denotes the evolution of infinite multiplication factor over the burn-up without core fractioning.

For SFR, the evolution of k_{eff} depends strongly on the isotopic composition of fresh fuel and reactor design, and it is not necessarily monotonic over time, especially for break-even configurations. In consideration of the criticality, the multiplication factor at the Beginning Of Cycle (BOC), denoted as $k_{eff,BOC}$, can be an option of criterion. Actually, given an isotopic vector of plutonium, the plutonium content in the fresh fuel of SFR is strongly correlated with $k_{eff,BOC}$, and thus it can be determined by dichotomy [76].

For other more complex reactors and fuels, e.g. PWR MIX, flexible ESFR-like reactors and ASTRID reactors, more parameters should be taken into account, but the general idea remains the same.

Irradiation model in CLASS

To calculate the material evolution, time-dependent one-group cross-sections are predicted. They depend on the burn-up and can be defined at each time step by:

$$< \sigma >= \frac{\int_E \sigma(\varepsilon)\Phi(\varepsilon)d\varepsilon}{\int_E \Phi(\varepsilon)d\varepsilon} \tag{2.5}$$

The level of neutron flux is then normalized by the effective power level:

$$\Phi(t) = \frac{P}{\sum_i N_i < \sigma_{i,f} > \epsilon_i} \tag{2.6}$$

where $< \sigma_{i,f} >$ is the one-group fission cross-section of nuclide i and ϵ_i is the energy released by one fission. For each time step, cross-sections are accessible by ANN predictors of time-dependent cross-sections. With these hypotheses, the reaction rate $R_{i,r}$ of a given reaction r of nuclide i at the time t can be deduced:

$$R_{i,r}(t) = N_i < \sigma_{i,r} > \Phi(t) \tag{2.7}$$

and then the Bateman equation previously presented can be resolved by Runge-Kutta fourth-order method.

In other facilities, nuclides only decay without neutron flux to cause nuclear reaction. The evolution is calculated by other numeric method.

2.1.2.4 Discussion: trade-offs between computation cost, precision and approximations

With the foregoing predictors constructed by ANN, reasonable computation time can be achieved for a simulation of tens of irradiation cycles. Compared to the reference calculations by standard depletion simulations, the deviations from ANN predictors on the inventories of important nuclides after one irradiation cycle are limited [55, 76, 77, 74, 78]. Concerning PWR UOX and MOX, deviations between CLASS predictions and databases are smaller than 1% for plutonium and uranium, and smaller than 5% for MA.

Some measurable biases may come from the assumptions of reactor modeling for each evolution in databases. E.g. the estimation of k_{eff} by equation 2.4 can induce percentages of deviation on the prediction of fissile content, in comparison with the simulation of core fractioning in PWR [56]. These biases are mainly introduced by the FLM. Nevertheless, owing to the high precision of cross-section predictors, the bias of global inventories in the cycle are still acceptable.

Moreover, the PWR loaded with 30% core of MOX are simulated by two separate reactors in CLASS: a PWR UOX and a PWR MOX, because the predictors of PWR MOX (resp. PWR UOX) are built by the simulations of an infinite MOX (resp. UOX) assembly. This approximation neglects the neutronic communication between UOX and MOX assemblies and can lead to some biases on the material evolution compared with the depletion in reality.

Considering fast reactors, each evolution of databases are based on full-core calculations supposing fewer approximations of k_{eff} calculations. However, the heterogeneity of material in the core brings new challenges as illustrated in

[78, 42] for the case of the ASTRID modeling. Actually, most of cross-section predictors in CLASS are homogenized by conserving the respective total reaction rate in the total core. It is shown that a highly heterogeneous core as ASTRID requires multi-zone modeling to reduce the bias on the material evolution.

In this work, we focus on PWR UOX and PWR MOX which are well described in the literature. More innovative concepts like PWR MIX and SFR are studied only in Chapter 5.

In conclusion, an electro-nuclear scenario study about fleet transitions requires a specific tool for the dynamic simulation of nuclear fuel cycle. CLASS is used in this work, which employs ANN to build predictors for physics models and can achieve a good trade-off between computation time and precision. Although some systematic bias resulting from the modeling assumptions still exist, their impacts on the strategy assessment are low enough for the studies made in this work.

2.2 Methodology of analysis of nuclear fuel cycle and electro-nuclear scenario

With the simulator CLASS, a wide range of nuclear fuel cycles can be simulated taking into account various parameters, like reactor burn-ups, cooling time, and fabrication time. In this section, the simulation of fuel cycle by CLASS is presented. Implicit hypotheses and limitation of the code are explained. After that, a scenario study is carried out to demonstrate the method of GSA employed in this work and to clarify relevant hypotheses of use.

2.2.1 Presentation of CLASS simulation

2.2.1.1 Simulation of two simple trajectories

To illustrate the simulation process of CLASS, this section studies a simple fuel cycle concerning the operation of PWR UOX and MOX. The Figure 2.2 describes the simulated facilities and the material flows between them.

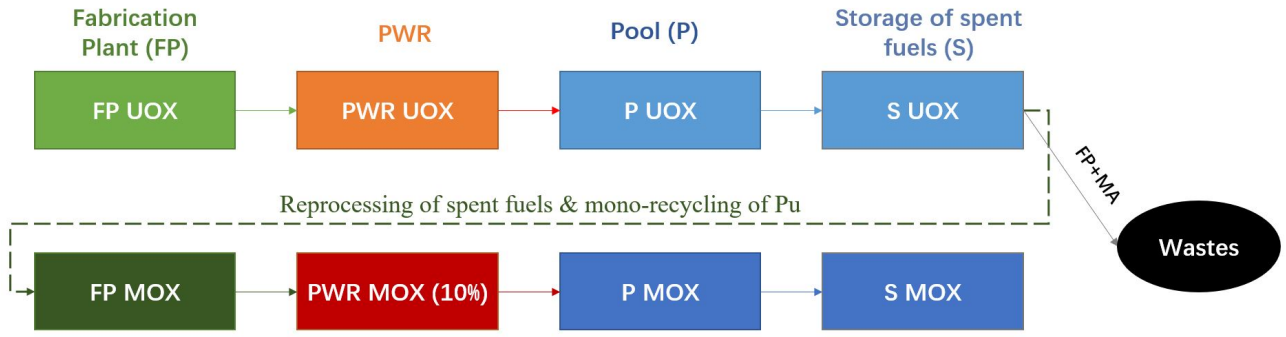

Figure 2.2: Graphical representation of the simulated fuel cycle

A fabrication plant dedicated to the UOX fuel fabrication is simulated, where the FLM of PWR UOX is used to predict the composition of fresh UOX fuels. After that, the UOX fuels are depleted in the PWR UOX, where the PWR UOX irradiation model is used. Then, the spent UOX fuels are cooled in the pool and then disposed in the interim storage. When the MOX fuel fabrication is demanded, the spent UOX fuels in the interim storage are reprocessed; the plutonium is recovered while the fission products and minor actinides are sent to the waste. Similarly, the

fabrication of MOX fuels requires the FLM of PWR MOX, and its depletion requires the irradiation model of PWR MOX. Finally, the spent MOX fuels are cooled in the pool and disposed in the interim storage of spent MOX fuels.

As a first illustrative study, two trajectories are simulated, as shown in Figure 2.3. Trajectory 1, shown in figure 2.3a, considers a PWR UOX with a thermal power of 2785 MWth, a 900 MWe-class PWR operated for 100 years. The initial mass of heavy metal of fresh fuel in total core is 72.3 tons. Trajectory 2 differs from trajectory 1 from year 40, when 30% of the core starts to be loaded by MOX fuel. The thermal power level instead of the electric power or the annual electricity production is simulated in CLASS.

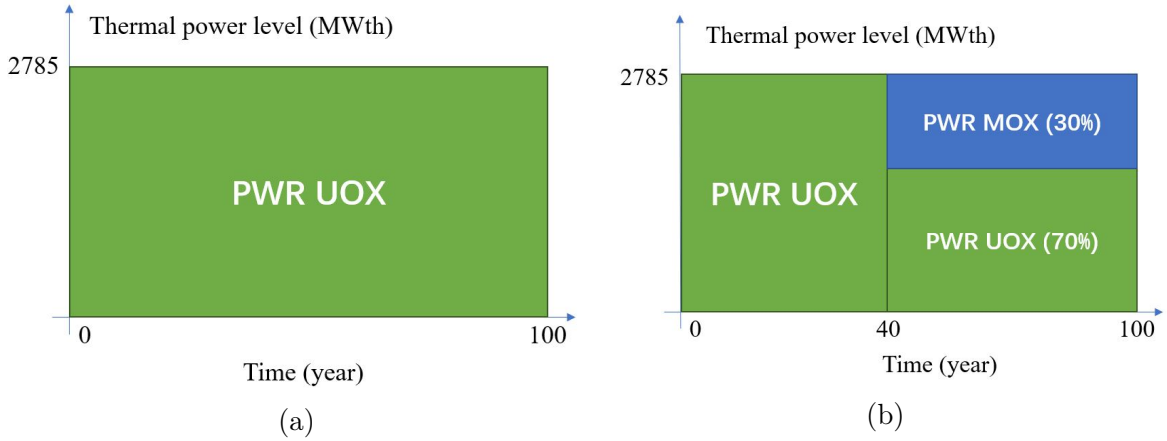

Figure 2.3: Two trajectories of demonstration: (a) Trajectory 1 - operation of PWR UOX for 100 years; (b) Trajectory 2 - disruption of trajectory 1 in year 40 - loading of MOX

The power evolution of these two trajectories are a-priori the same, a constant power of 2785 MWth. After the simulations, we can see in Figure 2.4a that the power evolution of Trajectory 2 is not constant over time. Indeed, a peak occurs in year 40 when the MOX is loaded for the first time, reaching 3620.5 MWth; and then, from year 56, the stopping of energy production from MOX leads to discontinuities in the power level. As introduced previously, the depletion of UOX and of MOX are separate in the simulation of CLASS, and thus the peak results from the desychronization between the loading of UOX and of MOX . The absence of energy production from MOX is due to missed loading, called *missload* in this work. They are the consequences of the lack of plutonium for the MOX fabrication, as shown by the plutonium inventory in the interim stock of spent UOX fuels in Figure 2.4b. After several times of MOX loading, the plutonium inventory in spent UOX fuels decreases until it is not sufficient for the next irradiation cycle of MOX. This happens in year 54, two years for fabrication before the next loading time of MOX. CLASS skips automatically this irradiation cycle of MOX, and waits for the next cycles until when the plutonium inventory is sufficient. Due to two missloads, plutonium in the interim stock of spent UOX fuels re-increases (being accumulated without being used). In year 62, such accumulation leads again to sufficient inventory of plutonium for the fuel fabrication of PWR MOX. The loading of MOX and missloads alternate this way depending on the plutonium availability.

The comparison of inventory evolution in the two trajectories shows the effects of using MOX fuels. Figure 2.5 shows the material evolution in two fuels during the depletion in the reactor. Evolution before year 40 shows the evolution in a PWR loaded with full UOX. Around 3.10 tons of ^{235}U are used to create the fresh fuel corresponding to 4.3% of enrichment. After depletion, 0.73 tons of ^{235}U is left in spent fuels, corresponding to 1.0%, while 0.80 tons of plutonium and

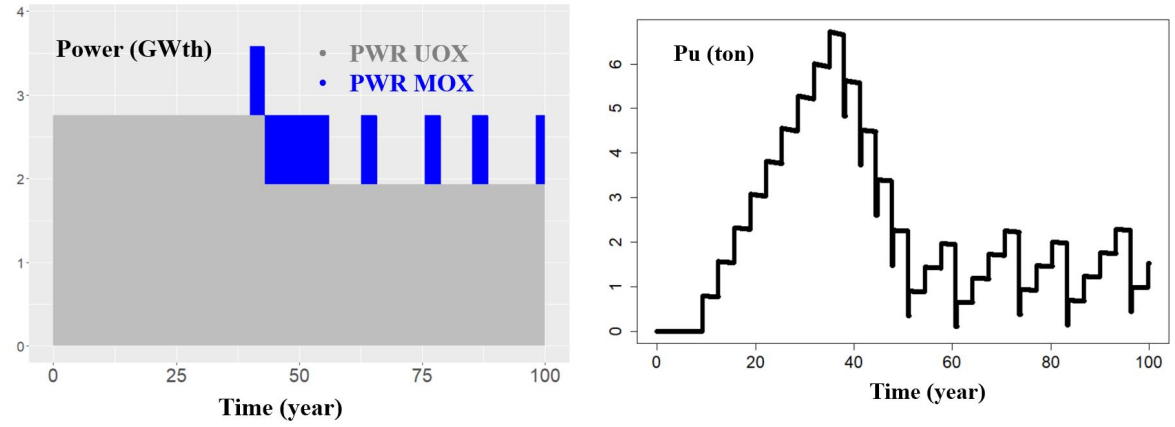

(a) (b)

Figure 2.4: Results of Trajectory 2: (a) power evolution; (b) Pu inventory in the interim stock of spent UOX fuels

0.071 tons of MA are created, corresponding to 1.1% and 0.1% of spent fuels. After year 40, the size of PWR UOX decreases 30% and a PWR MOX is started to replace the missing part of the PWR. 1.8 tons of plutonium is used to create the fresh MOX fuel, corresponding to a plutonium content of 8.3%. 0.016 tons of ^{241}Am is also loaded in the fresh fuel. It was created from the decay of ^{241}Pu during the fabrication. After the depletion of MOX, around 0.45 tons of plutonium are incinerated, corresponding to 25% of initial quantity, and 0.087-0.016=0.071 tons of MA is created. The absence of plutonium and the MA for several irradiation cycles of MOX is a result of the plutonium shortage MOX fabrication leading to missload.

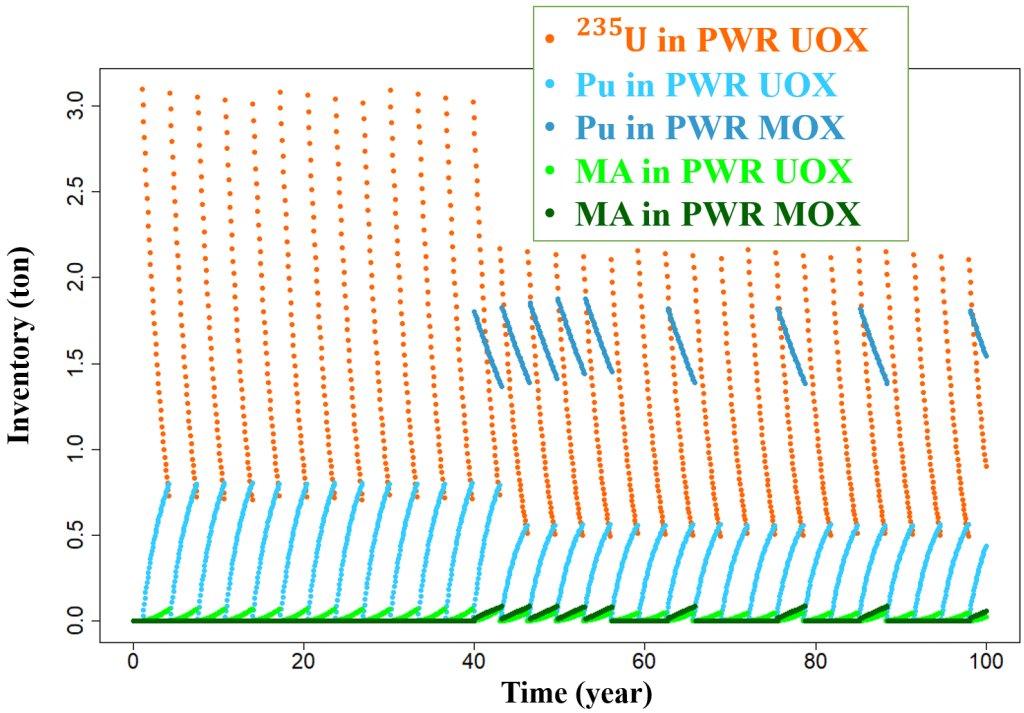

Figure 2.5: Material evolution in the reactor of trajectory 2: evolution of ^{235}U in UOX, plutonium and MA in both UOX and MOX

Figure 2.6 shows in detail the evolution of important nuclides in MOX fuels during depletion. Figure 2.6a allows to understand the incineration of plutonium in these fuels, mainly leading to the decrease of ^{239}Pu, while ^{241}Pu still increases

from the neutron capture reaction of ^{240}Pu. Inventories of ^{238}Pu and ^{242}Pu are nearly constant. Figure 2.6b shows the evolution of MA nuclides. Some ^{241}Am at BOC is loaded, coming from ^{241}Pu decay during MOX fabrication. ^{243}Am and ^{244}Cm increases much faster than ^{241}Am. The inventory of ^{243}Am is higher than ^{241}Am at discharge. But if spent fuels stay enough long time in cooling pools and interim stockpiles, ^{241}Am may be dominant in MA in the cycle due to the ^{241}Pu decay.

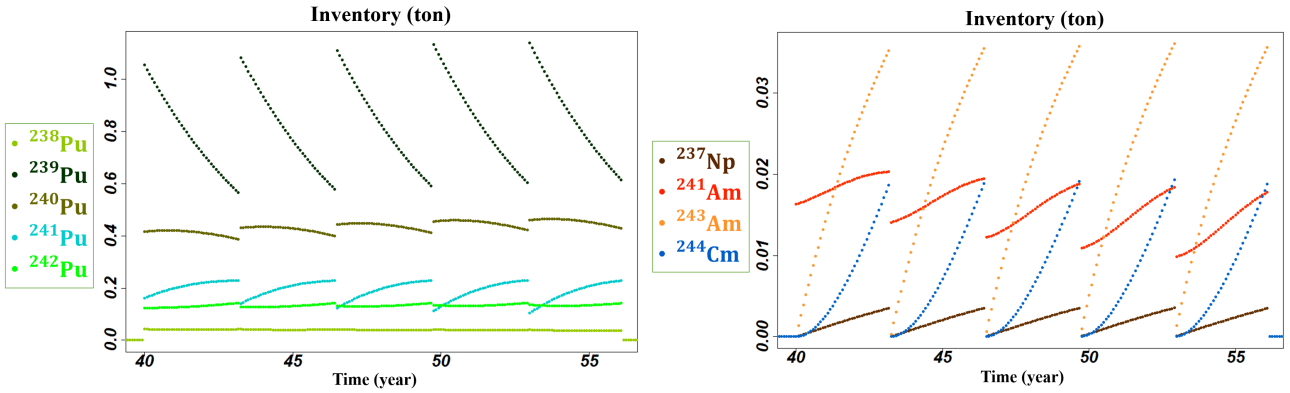

(a) (b)

Figure 2.6: Evolution of important isotopes in MOX fuels during depletion: (a) Isotopes of plutonium $^{238\sim242}$Pu; (b) MA isotopes ^{237}Np, ^{241}Am, ^{243}Am, ^{244}Cm,

Figure 2.7a compares the total-cycle plutonium in trajectory 2 with the one of the 100% PWR UOX in trajectory 1. At the beginning of reactor operation, total-cycle plutonium in both trajectories increase at the same speed. Then, between year 40 to 56, the one in trajectory 2 flattens; after that, it re-increases but with a smaller slope than the 100% PWR UOX trajectory. Actually, year 40 is when MOX fuels are loaded for the first time. It shows that the loading of MOX in 30% of the core can immediately stabilize the inventory of plutonium in the total cycle but for a limited time period. Due to successive missloads, the plutonium inventory still increases slowly. The smaller slope of plutonium inventory evolution in trajectory 2 than the one in trajectory 1 is a combined effect of the incineration of plutonium by MOX and the lower production rate of plutonium due to lower quantity of UOX fuels.

Figure 2.7b shows that the use of MOX can lighten the consumption of uranium resources. Evidently, with the use of MOX fuels, 30% fewer UOX fuels are used.

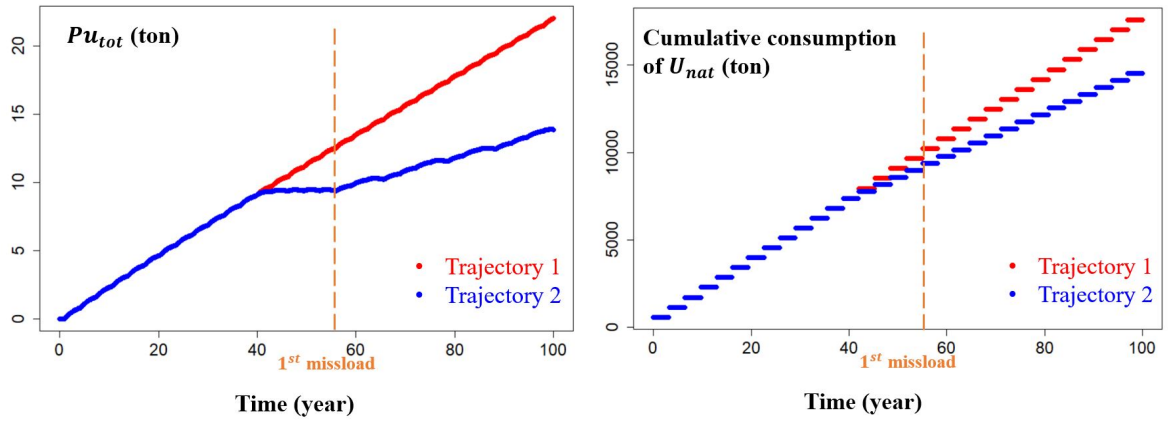

(a) (b)

Figure 2.7: Comparison of two trajectories of demonstration: (a) Pu inventory in the total cycle; (b) Cumulative consumption of natural uranium

2.2.1.2 Simulation of the historical nuclear fleet in France

Since this work focuses on the French fuel cycle, CLASS is used to simulate the French historical trajectory in order to set the starting point of work. The historical data of operation parameters are accessible in [14] and also summarized in [50, 42]. According to these data, 58 PWRs started operation successively from year 1977, when Fessenheim-1 was connected to the grid for the first time.

Figure 2.8 shows the French fleet power evolution simulated by CLASS. It started in the 1970s when the first power plants were installed. A rapid increase of installed capacity between 1980 and 1990 can be observed. Following the new in-operation PWRs, some old ones got the license for MOX loading and started using it from 1990. The latest PWR began its operation in 2000. Since 2015, the two reactors of Fessenheim have been shut down; for the sake of simplicity, we have not considered any power reduction and those two units are then supposed to be operated in our following simulations. Under this assumption, the effective thermal power of the whole fleet is 138 GWth (the nominal total power is 188.1 GWth). The effective fraction of power contributed by MOX fuels in the fleet is around 10%.

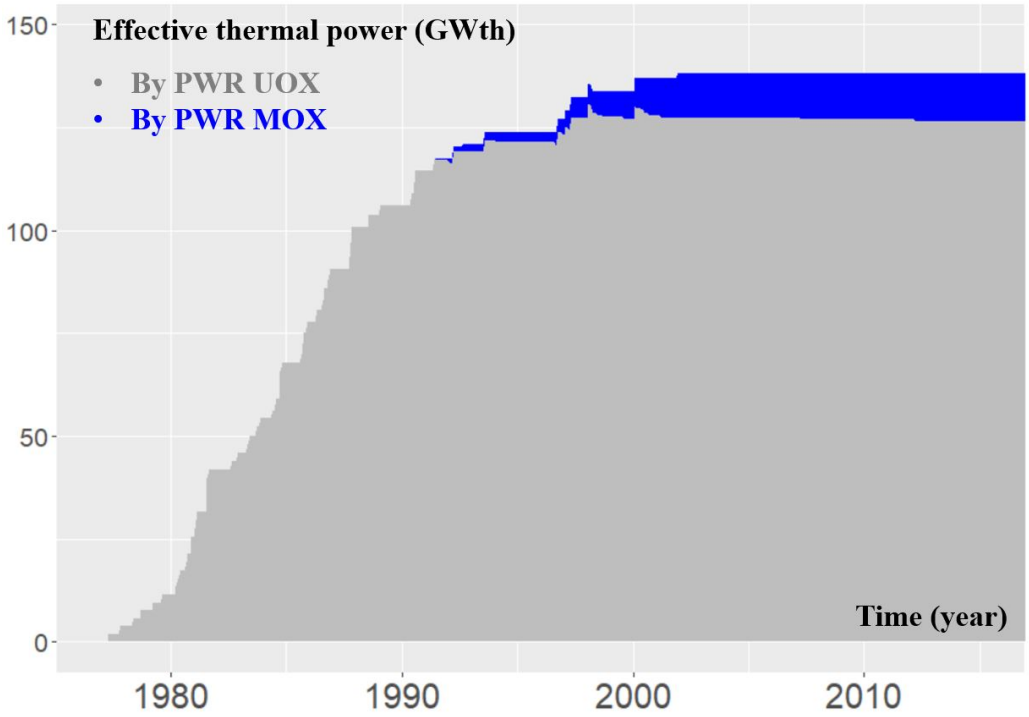

Figure 2.8: Evolution of the effective thermal power of the French fleet until 2015

The inventories of transuranium (TRU) in the total cycle are presented in Figure 2.9. Due to the particular status linked to non-proliferation and industrial valorisation potential, any data about real plutonium inventory is hardly accessible [50] and the uncertainty is relatively significant (between 274 and 411 tons according to the estimation in [50]). Our calculation gives 318.5 tons of plutonium in the total cycle in 2015, compatible with the estimated range.

For MA, it is mainly composed of neptunium, americium and curium, presented in Figure 2.9b. By 2015, 19.3 tons of neptunium, 30.4 tons of americium and 2.2 tons of curium are accumulated in 2015 according to our calculation. It shows that the americium inventory increases much faster since the use of MOX than before, mainly from the $^{241}\mathrm{Pu}$ decay with 14.3 years of half-life which is more produced in MOX than in UOX per unit of energy produced. Compared to americium and neptunium, curium is much less produced, but the quantity is not negligible,

especially in regards to its dose rate.

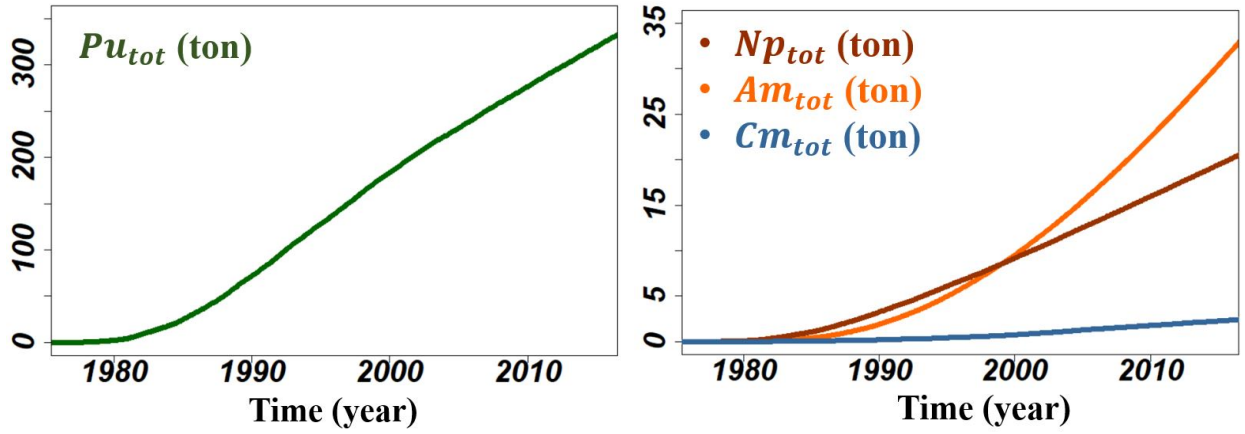

(a) (b)

Figure 2.9: Evolution of transuranium inventories in the total cycle of the French fleet until 2015: (a) plutonium inventory; (b) MA inventory

The simulation of the French fuel cycle is used as an appropriate starting point for all further simulation of this work. As CLASS is deterministic, it is not necessary to re-simulate the history for each run if several trajectories of different futures are simulated. Moreover, this simulation of 38-year history of individual reactors takes more than 5 minutes and requires more than 100 MB of memory storage. The repetitions of this identical part of run would only result in a waste of time and memory; the study can therefore start from the year 2015, based on the results of this computation.

Some exploratory or statistical studies may involve tens of individual reactors. The specific management of each of them implies hundreds or even thousands of operational parameters [81, 49]. Following such high number of parameters would be overwhelming for sensitivity analysis and the basic understanding of system behavior. Moreover, it may increase output variability. In the subsequent analyses, we will see that the simulation of thousands of trajectories are considered, and thus necessary simplifications should be taken.

2.2.1.3 Macro-reactor simplification

To reduce the computational cost, the simplification of macro-reactor is employed in this work [82]. Macro-reactor simplifications consist in the creation of a single macro reactor through the grouping of all similar individual reactors. The parameters of the same type of reactors are considered identical, and the nuances of individual reactors are neglected. Under this simplification, the number of input parameters for simulations decreases by an order of magnitude. However, it may lead to some timing effects, e.g. synchronization of reactor behavior and relevant missloads [82].

In our work, the gain by macro-reactor simplification is considered to be much larger than the loss of precision. The French PWR fleet is grouped into two macro-reactors: one is macro PWR UOX and the other is macro PWR MOX. These two macro-reactors contribute to 188.1 GWth of nominal power and a normalized loading factor of 72.8%. The effective MOX fraction is normalized to match the number of spent MOX assemblies in 2014 from our simulations to the data coming from [83]. This lead to an effective MOX fraction of about 7.6%. Burn-ups of each reactor should be averaged over the global fleet for the calculation of the burn-ups of the macro reactors UOX and MOX. To respect the energy produced by each

type of fuel in the fleet, each burn-up are weighted by the heavy metal mass of each reactor according to the expression:

$$BU_R = \frac{\sum_i BU_{R,i} \times HM_{R,i}}{\sum_i HM_{R,i}} \tag{2.8}$$

where R denotes the fuel type UOX or MOX, and HM denotes the initial heavy metal mass of the i-th reactor. Final burn-ups for macro reactors UOX and MOX are respectively 45.3 and 45 GWd/t.

As other simplifications, some other parameters of fuel cycles with little influence on the results are considered unchanging. For instance, five years of cooling is supposed for spent UOX and spent MOX fuels. The fabrication of UOX needs one year and the MOX needs two years. LiFo is supposed to be the reprocessing management of spent UOX fuels for the MOX fuel fabrication.

With the assumption of macro-reactor, the complex reactor fleet characterized by a huge number of parameters can be reduced to two reactors, and the relevant management of material flows is facilitated by the module of time vector in CLASS. The analysis becomes achievable regarding both the computational cost and the system management.

2.2.2 Global sensitivity analysis of nuclear fuel cycle

CLASS can simulate fuel cycles with various parameters. In this work, a strategy is defined by a specific combination of parameter options. Under the uncertain future of nuclear plans, the variability of strategies can be large, and the impact on the fuel cycle from the variation can be difficult to interpret. To investigate the response of fuel cycles to a given strategy variations, global sensitivity analysis is required, and the method of WPS is employed: first, the ranges of variation of those parameters of interest are determined, and then a Design of Experiment (DoE) is used to sample the strategies. The trajectories defined by the sampled strategies are simulated, and the impacts are evaluated by calculating different outputs of interest. The method of GSA reveals the intrinsic relation between the input variables of strategy and the outputs of interest, and thus gives a global understanding on the behavior of the system studied.

To illustrate the GSA of nuclear fuel cycle and check that the parameters considered are the relevant ones, an academic scenario inspired from possible French fleet transitions is studied. As justified previously, macro-reactors are simulated instead of individual reactors. The scenario starts from year 2015 to year 2140, a long time scope that can reveal even the more subtle effects of strategies. In this study, the transition, which will start from an unknown time, is supposed to last more than 10 years and to end before year 2140. After the start of the transition, the burn-ups of UOX and MOX fuels and the cooling time of two types of spent fuels are modified. The management of spent UOX fuel for MOX fabrication can be changed as well; it is either LiFo or FiFo. During the transition, the total thermal power of fleet and the power contributed by MOX fuel (using the shorter locution "MOX fraction" in the subsequent analysis) change linearly. After the transition, the final total power and the final MOX fraction are constant until the end of scenario. To summarize, 9 input variables are taken into account, characterizing the strategy space. These inputs and their ranges of variation are shown in Table 2.1.

The ranges of variation of inputs presented in Table 2.1 are chosen to be as wide as possible. Year 2025 is considered to be the earliest possible transition time t_{start}. First, because the normalization of fleet by macro-reactors requires

Input var.	Init. value	Min.	Max.	Unit	Explanation
t_{start}	-	2025	2140	-	Starting time of transition
D	-	10	130	year	Duration of transition
$P_{tot,f}$	188.1	18.8	282.2	GWth	Total thermal power of the fleet after transition
$FrMOX_f$	7.6	0	30	%	MOX fraction after transition
BU_{UOX}	45.3	30	60	GWd/t	Modified burn-up of UOX fuels
BU_{MOX}	45	30	60	GWd/t	Modified burn-up of MOX fuels
TC_{UOX}	5	3	10	year	Modified cooling time of spent UOX fuels
TC_{MOX}	5	3	10	year	Modified cooling time of spent MOX fuels
MPu	1/LiFo	1/LiFo	2/FiFo	-	Modified management of spent UOX fuels

Table 2.1: Strategy space of the exploratory scenario for the demonstration of GSA

several irradiation cycles to re-build an appropriate material flow and to reduce the impacts of normalization; but also year 2025 is close to the estimated of the grid-connection time of the first EPR in France. The duration D should be longer than 10 years so that the fuel cycle has enough time to adapt for the changes. The variability of $P_{tot,f}$ corresponds to the interval of [10%, 150%] of the initial level (188.1 GWth). This range indicates the wide options of future installed capacity in this exploratory study, including larger deployment of nuclear reactors than the current level and approximate phase-out strategies. The maximal $FrMOX_f$ is set to respect the current limit that only up to 30% of the core of MOXed PWRs can be loaded with MOX fuels. The assumptions of ranges of burn-up involve both historical value and economic factors, as justified in [25]. Variability of TC_{UOX}, TC_{MOX} and MPu cover the respective ranges of industrial application.

As mentioned in Chapter 1, the decisions guiding the fleet transition are driven by the future nuclear plans, e.g. the deployment of SFR or phase-out. With respect to the future interest, outputs of interest are calculated to evaluate the impacts of transition strategies. In this study, three outputs are considered:

- Number of deployable SFR N_{SFR}
- Ratio of substitution of the PWR-fleet with deployable SFRs R_{Subs}
- MA inventory in the total cycle MA_{tot}, including those in the waste canisters.

No SFR is simulated in the studied scenario. According to the design of ESFR [19], the operation of each SFR in France requires a large quantity of plutonium, and thus the availability of plutonium inventory can be seen as the primary constraint of SFR deployment. The plutonium quantity for each SFR is unknown because the design of SFR is still under investigation. However, uncertainties on plutonium inventories needed for the deployment of N_{SFR} can be seen as systematic errors and are tackled by margins on the considered outputs N_{SFR} and R_{Subs}.

In this study, the large-size oxide core (MOX 3600 GWth) in [19] is considered. Under these assumptions, N_{SFR} is proportional to the available inventory of plutonium to the first degree of approximation:

$$N_{SFR}(t) = \frac{Pu_{in}(t)}{HM_{SFR} \times c_{Pu}} \times f_{eff} \tag{2.9}$$

where Pu_{in} denotes the plutonium inventory in the cycle, HM_{SFR} denotes the heavy metal mass of fresh fuels in the active core of SFR, and c_{Pu} denotes the

average plutonium content in these fresh fuels. According to the design in [19], HM_{SFR} is 75 tons and c_{Pu} is about 17%. f_{eff} denotes the effective factor in consideration of the necessary recycling time of plutonium in the fleet of break-even SFR, calculated as:

$$f_{eff} = \frac{T_{irrad}}{T_{fab} + T_{irrad} + T_{cool}} \tag{2.10}$$

The irradiation time T_{irrad} of SFR corresponds to the burn-up of 100 GWd/t with a normalized loading factor, and thus equals to 7.8 years; 2 years of fresh fuel fabrication and 5 years of spent fuel cooling are supposed. Hence, $f_{eff} = 0.53$ in this study.

According to its definition, N_{SFR} measures the material availability of immediate deployment of N_{SFR} SFRs; the available plutonium includes the ones in reactors, in cooling pools and in interim storage. These assumptions are certainly not realistic; in reality, the SFR deployment involves the schedule as well as other strategy details of management. But in this work, we aim to focus on the contradiction of different objectives, and we choose to avoid making detailed hypotheses for precise scenario simulations that can add uncontrolled biases.

Last but not least, the given plutonium content c_{Pu} neglects the effects of isotopic composition on the plutonium content of SFR fresh fuel. The fluctuation of c_{Pu} due to the isotopic composition results from the fuel cycle parameters suggested by strategies, but a precise content is hard to predict, requiring iterations of SFR simulations. It also depends on the reactor design and the core behavior. Nevertheless, the variation is to some degree under control, potentially much smaller than the uncertainties of SFR deployment schedule and relevant strategies that are not considered.

Besides the absolute capacity of SFR deployment measured by N_{SFR}, the proportion of the total fleet installed capacity that may be replaced by SFRs is also important. It can be represented by the substitution ratio R_{Subs}, defined as

$$R_{Subs}(t) = \frac{N_{SFR}(t) \times 3.6\,GWth \times Y_{SFR}}{P_{tot}(t) \times Y_{PWR}} \tag{2.11}$$

where the value of 3.6 GWth denotes the nominal thermal power of ESFR design in [19], P_{tot} denotes the total nominal thermal power of the PWR fleet, Y_{SFR} and Y_{PWR} denotes the energy conversion efficiency of SFR and PWR, being 40% and 33% respectively. The efficiency of a reactor may vary depending on the power plant design. The relevant deviations owing to the uncertainty of yield are systematic and therefore neglected in this study.

Whether SFR will be deployed or not, it is always important to estimate the MA inventory which contributes to a large part of nuclear wastes. In this study, the output MA_{tot} considers mainly the total inventory of neptunium, americium and curium in the total cycle, including those in conditioned wastes.

In addition to these physics quantities, the effect of observation time should be also considered. Actually, the time when strategy performances are evaluated plays an important role in both uncertainties and strategy assessments. In this sensitivity analysis, three observation times are considered: year 2050, 2095 and 2140, representing short-term, mid-term and long-term effects. Therefore, 9 outputs of interest are taken into account.

2.2.3 Introduction of Morris method: ranking and screening of input variables

Dedicated methods and designs of experiments are needed for sensitivity analysis. Sobol indices [84, 85] calculations are widely used for GSA. As a variance-

based method, it focuses on the decomposition of output variance, into the contributions of inputs and their interactions. The importance of an input and the strength of interaction are indicated by corresponding indices, which are the ratios between conditional variances and the total variance of output. The indices of each input can be simply classified into these categories:

- Total index: indicates the contribution of a given input, including its variation and the interaction with other inputs
- First-order index: indicates the contribution by the independent variation of a given input, without consideration of its interaction with others
- Higher order indices: indicates the contribution by the interaction of a given input with others

Sobol indices are used in electro-nuclear scenario studies to assess the importance of tens of fuel cycle parameters on a given output [86, 87, 88]. The application of Sobol analysis have been proven very insightful for electro-nuclear scenario studies.

In this study, we choose to test another GSA method, the Morris method [53], which is a derivative-based screening method. The introduction of Morris method in this preliminary analysis is mainly based on two considerations: the first one is to test the Morris method in the sensitivity analysis of electro-nuclear studies; the second and the main objective is to rank the inputs in order to reduce the exploratory phase space of parameters in the subsequent analyses if possible. Results of this analysis allows to find the minimal number of parameters to take into account for the scenario studies in Chapter 3 and 4. Even though the validity of method is not a-priori guaranteed, its introduction into preliminary analysis can still give some useful information on the relation between outputs and inputs of interest.

For a given output, the Morris method evaluates the contributions of input variables by the estimation of output partial derivatives regarding each input One At a Time (OAT). With a given number of repetition, the statistical properties of partial derivative approximations with respect to input variables reveal their importance on the output. The general idea of the DoE of the Morris method can be presented by an example in Figure 2.10. The space of 2-dimension input variables (X_a, X_b) is divided into a grid of 6×6 levels. The first point $(x_a^{l_1}, x_b^{l_1})$ is randomly chosen (for the so-called "repetition 1" in the figure). From this point, two others are determined in order to define an elementary pattern able to estimate first order derivative for each dimension. Here a random choice of variation indicates a jump along the input X_a followed by another jump along the input X_b, and thus $(x_a^{l_3}, x_b^{l_1})$ and $(x_a^{l_3}, x_b^{l_3})$ are selected respectively. For all these points, the output $Y = f(X_a, X_b)$ is calculated, where f denotes the system's response function. It gives then y_1, y_2 and y_3, the values of the output for each point defined by the elementary pattern. To investigate the elementary effects of input variations, partial derivatives of the output Y with respect to inputs X_a and X_b are approximated by

$$d_a^y = \frac{y_2 - y_1}{x_{a,l_3} - x_{a,l_1}}$$

$$d_b^y = \frac{y_3 - y_2}{x_{b,l_3} - x_{b,l_1}}$$

These calculations are then repeated, such as the "repetition 2" shown in Figure 2.10. A number of repetition creates the estimations of elementary effect of each input on the output of interest. Statistical metrics are finally considered to

evaluate the randomly sampled derivatives. The mean as well as the standard deviation of partial derivative with respect to each input is calculated, denoted respectively as $\mu(d_i^o)$ and $\sigma(d_i^o)$ where i and o denotes the input and output.

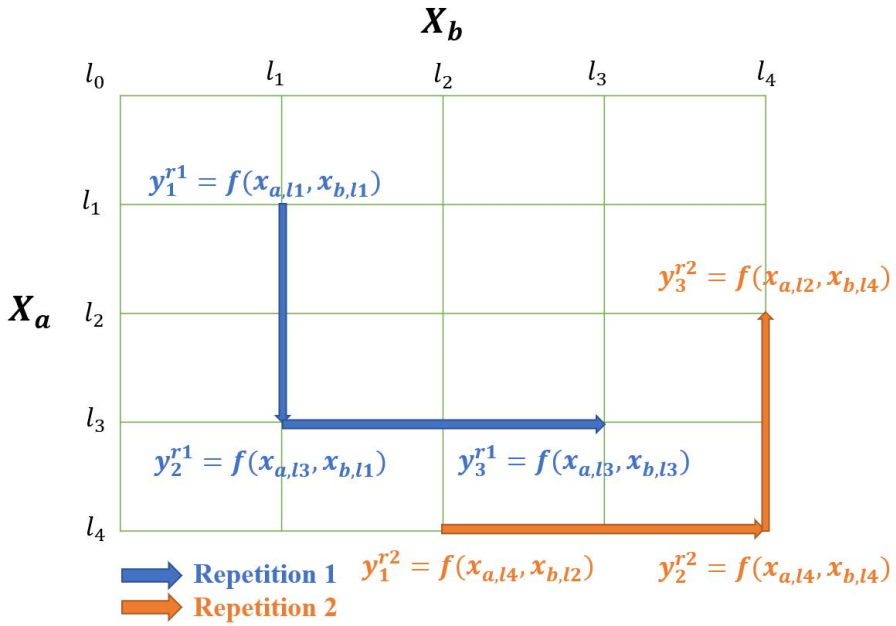

Figure 2.10: Graphical representation of Morris method

In this exercise, among all possible variations for Morris customization, the number of repetition is calibrated. r times of repetition for a p-dimension input space requires then $r(p+1)$ calculations of system response. According to the mean μ and standard deviation σ of partial derivative, inputs can be qualitatively classified into four categories:

- Small $\mu(d_i)$ and small $\sigma(d_i)$: effect non-measurable;
- Large $\mu(d_i)$ and small $\sigma(d_i)$: strong linear effect;
- Small $\mu(d_i)$ and large $\sigma(d_i)$: highly non-linear effect on output or strong interaction with other inputs;
- Large $\mu(d_i)$ and large $\sigma(d_i)$: strong linear effect on output as well as strong interaction with other inputs.

Input variables are then ranked according to $\mu(d_i^o)$ and $\sigma(d_i^o)$ regarding the derivative observations of output o with respect to input i.

2.2.4 Ranking of inputs by Morris method

2.2.4.1 Calibration of repetitions: taking year 2095 for an example analysis

Three physics quantities (N_{SFR}, R_{Subs} and MA_{tot}) for three observation times (2050, 2095 and 2140) are considered. One should note that a transition starting after the observation time does not give any useful information. The transition starting time t_{start} should be therefore earlier than the observation time. Meanwhile, Morris method supposes the independence of input variables. Since the observation time is set for each output while t_{start} varies, the transition may finish after the observation time, questioning the needed independence of inputs. D is then still in the range of [10, 130] years.

The derivatives introduced in section 2.2.3 have different units with respect to the input variables. One may think that the comparison of results in different units does not make sense. E.g. the variation of an output per 1 GWth and per 1 MWth may differ a factor of 1000 if the output is linear function of power level. Even though they have the identical physical meaning, the values for comparison are not the same. In local sensitivity analysis, the derivatives are usually normalized by reference levels of the OAT design, which represents the percentage of change of output resulted from a given percentage of relative input variation. But in GSA, reference levels can be of very different size, and the meaning of "reference" becomes much weaker. One may use the initial levels of investigated parameters for normalization, but two problems should be tackled here: one involves the normalization with respect to the inputs whose "initial value" does not exist, e.g. t_{start} and D; the other is linked to the variability of input. Initial levels of variables are not strongly related to the variability of inputs in the scenario, whereas the latter is an important assumption of the study and may impact the results and relevant interpretation. As a result, the derivatives of output y with respect to given inputs are normalized as

$$\tilde{d}_i^y = \frac{y_{k+1} - y_k}{(x_{i,k+1} - x_{i,k})/L_i} = L_i \times d_i \tag{2.12}$$

where L_i denotes the length of range of the i-th input. It can be interpreted as the approximate variation of output under a maximum-allowed variation of the given input, estimated by a given fraction of such maximum-allowed variation. The mean value and standard deviation of $\tilde{d}_i$ are denoted as $\mu(\tilde{d}_i^o)$ and $\sigma(\tilde{d}_i^o)$. This is specifically true for MPu since it only has two discrete values, whereas not necessarily realistic for other parameters. This option of normalization is not arbitrary, because the variability of inputs is also an important assumption of the study for the interpretation of scenario analysis. One may interpret the variation ranges in the study as the controllability on the parameters, or even coupled with the uncertainties; nevertheless, this discussion is out of the scope in this work, and this normalization step should be kept in mind along the analysis.

Before ranking the input variables, the number of repetition should be determined: if there is not sufficient statistical information with low number of repetition, results can be biased, whereas a high number requires too many calculations and it can be time-consuming. In this preliminary step, the number of 10, 15, 20, 30, 50, 100, 200, 300 and 500 are investigated, and the observation time of 2095 is taken as an example.

The rankings of input variables over the number of repetition are shown in Figure 2.11. The higher is the value of metric (μ and σ respectively), the higher is the rank. From this figure, we conclude that at least 200 repetitions need to be performed. Even though ranking may change even after 200 repetitions, we are still able to group these input parameters regarding their importance on the output value. The fluctuation of rank of BU_{MOX} in $\sigma(\tilde{d}^{R_{Subs}})$ can be explained by the fact that the corresponding standard deviation of derivatives with respect to $FrMOX_f$, BU_{UOX} and BU_{MOX} are close. In all cases, TC_{MOX} has always the lowest ranks, because spent MOX fuels are not reprocessed and its cooling does not affect in any way these three outputs of interest.

For the three outputs of interest, t_{start}, D and $P_{tot,f}$ have inherently high ranks on both the mean value and the standard deviation, regardless the number of repetition. It means that these three inputs impact strongly the three outputs and also have strong interactions with each other not in a linear way. t_{start} and D describe the transition timing, on which the impacts of other parameter variations depend strongly. Most of the interactions involve those various options

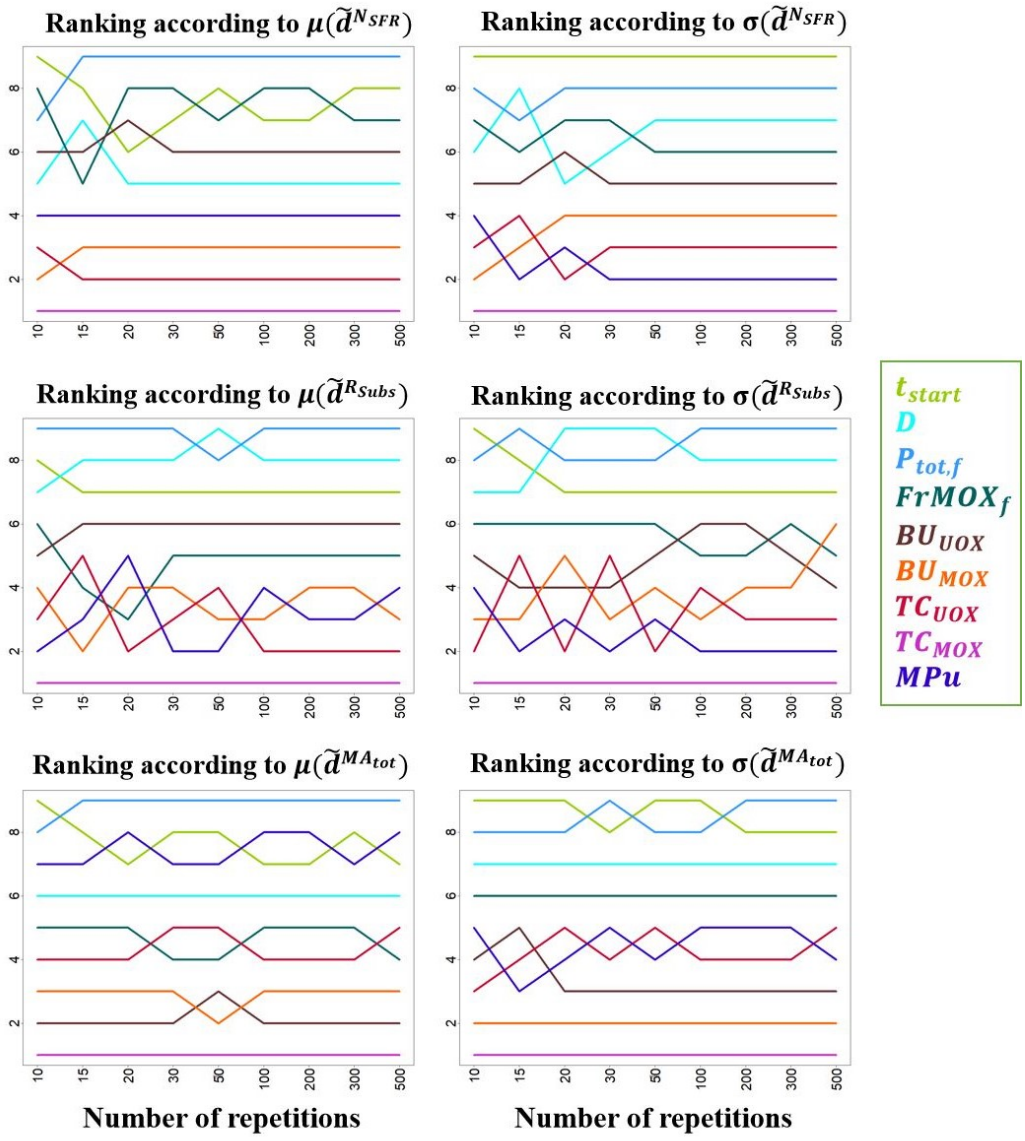

Figure 2.11: Ranking of input variables according to the mean value and standard deviation of corresponding outputs observed in 2095

of t_{start} and D. $P_{tot,f}$ dominates the final scale of fleet after transition and thus impact all extensive quantities, e.g. N_{SFR} which is proportional to in-cycle plutonium inventory, and MA_{tot}. Dependence of R_{Subs} on $P_{tot,f}$ is more subtle, which is the result of competition between the effect of $P_{tot,f}$ on N_{SFR} and the effect on the power level at the time of observation. Meanwhile, the effects of $P_{tot,f}$ is always subject to the transition schedule controlled by t_{start} and D, and thus the standard deviation of derivatives with respect to $P_{tot,f}$ are all at high level. $FrMOX_f$ and BU_{UOX} have measurable impacts on N_{SFR} and R_{Subs}. Both of them have strong correlation with in-cycle plutonium inventory [86] and therefore with N_{SFR} and R_{Subs}. Regarding MA_{tot}, the effects of $FrMOX_f$ and BU_{UOX} are much smaller than MPu. In fact, the major part of MA in the total cycle is $^{241}\mathrm{Am}$ which comes from the $^{241}\mathrm{Pu}$ decay. Since $^{241}\mathrm{Pu}$ is relatively short-lived compared with the recycling time, LiFo strategy can use more efficiently the $^{241}\mathrm{Pu}$ in new spent fuels, while the $^{241}\mathrm{Pu}$ decay in old spent fuels remains at a limited level. FiFo strategy leads to significant $^{241}\mathrm{Pu}$ decays into $^{241}\mathrm{Am}$ for each new arrival of spent fuels during the wait for reprocessing; this part of $^{241}\mathrm{Am}$, which contributes a large part of MA in spent fuels, are sent to the wastes when the assemblies are reprocessed. As a result, much more quantities of MA are accumulated by FiFo than by LiFo. TC_{UOX}

affects MA_{tot} in a similar way that a long time of cooling leads to the decay of large amount of $^{241}\mathrm{Am}$.

As suggested in [53], the scatter plots of standard deviations $\sigma(\tilde{d})$ versus means $\mu(\tilde{d})$ of derivatives are shown in Figure 2.12a, taking 200 repetitions as example. One important information that the scatter plots convey is the signs of $\mu(\tilde{d})$s, which indicate the negative/positive correlation between outputs and inputs. In this step only the signs of relatively significant $\mu(\tilde{d})$s are analyzed.

In terms of $P_{tot,f}$, $\mu(\tilde{d}^{N_{SFR}}_{P_{tot,f}})$ and $\mu(\tilde{d}^{MA_{tot}}_{P_{tot,f}})$ are positive while $\mu(\tilde{d}^{R_{Subs}}_{P_{tot,f}})$ is negative. The behavior of the increase/burning of in-cycle plutonium depends mainly on the MOX fraction. Within the range of $FrMOX_f$ in this study, most of trajectories have a net production of plutonium and thus accumulates plutonium over time. A higher $P_{tot,f}$ with a low $FrMOX_f$ can amplify the net production of plutonium, and therefore N_{SFR}. In terms of R_{Subs}, it is mainly the power level that leads to a negative correlation according to its definition. For MA_{tot}, it is simply due to the extensive effect dominated by $P_{tot,f}$ as explained.

$FrMOX_f$ and BU_{UOX} have similar impacts on these three outputs of interest, because the plutonium contributes a lot on fission during the depletion of high BU_{UOX}, which is approximately similar to increasing the use of MOX fuel. $\mu(\tilde{d}^{N_{SFR}}_{FrMOX_f})$ and $\mu(\tilde{d}^{R_{Subs}}_{FrMOX_f})$ are negative because a larger use of MOX increases the incineration of plutonium. It is also the same explanation for the negative $\mu(\tilde{d}^{N_{SFR}}_{BU_{UOX}})$ and $\mu(\tilde{d}^{R_{Subs}}_{BU_{UOX}})$. The $\mu(\tilde{d}^{MA_{tot}}_{FrMOX_f})$ is positive, because the use of MOX increases the time-average production rate of $^{241}\mathrm{Pu}$, which will finally decay into $^{241}\mathrm{Am}$, one of the major components of MA. Actually, even though $^{241}\mathrm{Pu}$ is one of major fissile components in MOX irradiation, the production rate of $^{241}\mathrm{Pu}$ in MOX is much higher than in UOX, due to the higher fraction of other plutonium isotopes. Similarly, the higher is BU_{UOX}, the higher is the time-average production rate of $^{241}\mathrm{Pu}$. Thus, the $^{241}\mathrm{Am}$ production in spent UOX fuels is also dependent on BU_{UOX}.

t_{start} and D describe the transition timing and their corresponding μ of derivatives of a given output have the same sign. One should note that their signs depend strongly on the initial parameters values of fleet as well as the variation ranges of parameters. As a dominant parameter on the outputs, the initial power of fleet is at the high level of range. The random sampling of $P_{tot,f}$ tends averagely to select a lower level of power than the initial level. This leads to a lower inventory of plutonium, and thus a smaller N_{SFR}, a higher value of R_{Subs} and a smaller inventory of MA than sticking to the initial state. The MOX fraction may have an opposite effect but is weaker than the fleet power variation. High values of t_{start} and D delaying the transition then tends to increase the inertia of the initial fleet state, and thus mitigates the statistical responses of the system to other parameters. As a result, the increase of t_{start} and D tends to statistically increase N_{SFR} and MA_{tot}, and decrease R_{Subs}.

Last but not least, those derivatives of impactful inputs have a similar order for standard deviation σ as for the mean μ. As mentioned, they have strong interactions, mainly due to the time effects resulted from the inputs t_{start} and D.

2.2.4.2 Effect of missload on the grouping and ranking of inputs

Some trajectories may have some missloads due to plutonium shortages for MOX fabrication, leading to irregular evolution of power level. Missload of some trajectories should be emphasized in this sensitivity analysis. It may result from high consumption rate of plutonium, e.g. high power level and high MOX fraction, or low production rate of available plutonium such as high BU_{UOX}. Missload leads to unexpected fluctuations of power level and may be considered unrealistic depending on the purposes of study. In particular, the power level is not always

the same as the input parameters indicated in this case. The evolution of material inventories can be then deviated depending on the acceptation of missload in analyses and the definition of validity of strategy or trajectory. However, the verification of missload requires a complete computation and cannot be decided in the design of experiment. If missloads are considered unacceptable, one alternative is to add a back-up stock of plutonium for MOX fabrication to avoid the plutonium shortages. It is evident that the inclusion/exclusion of missload can change the results of calculation, and thus the ranking of input variables.

To quantify the effect of missload on the ranking, a new ranking have been performed with a new DoE that considers a huge initial stock of plutonium preventing any missload. The comparison between this new ranking and the previous where simulations may present some missloads is the subject to this paragraph, taking 200 repetitions and year 2095 as example and shown in Figure 2.12. The ranking with missloads and the one without missload present a small difference.

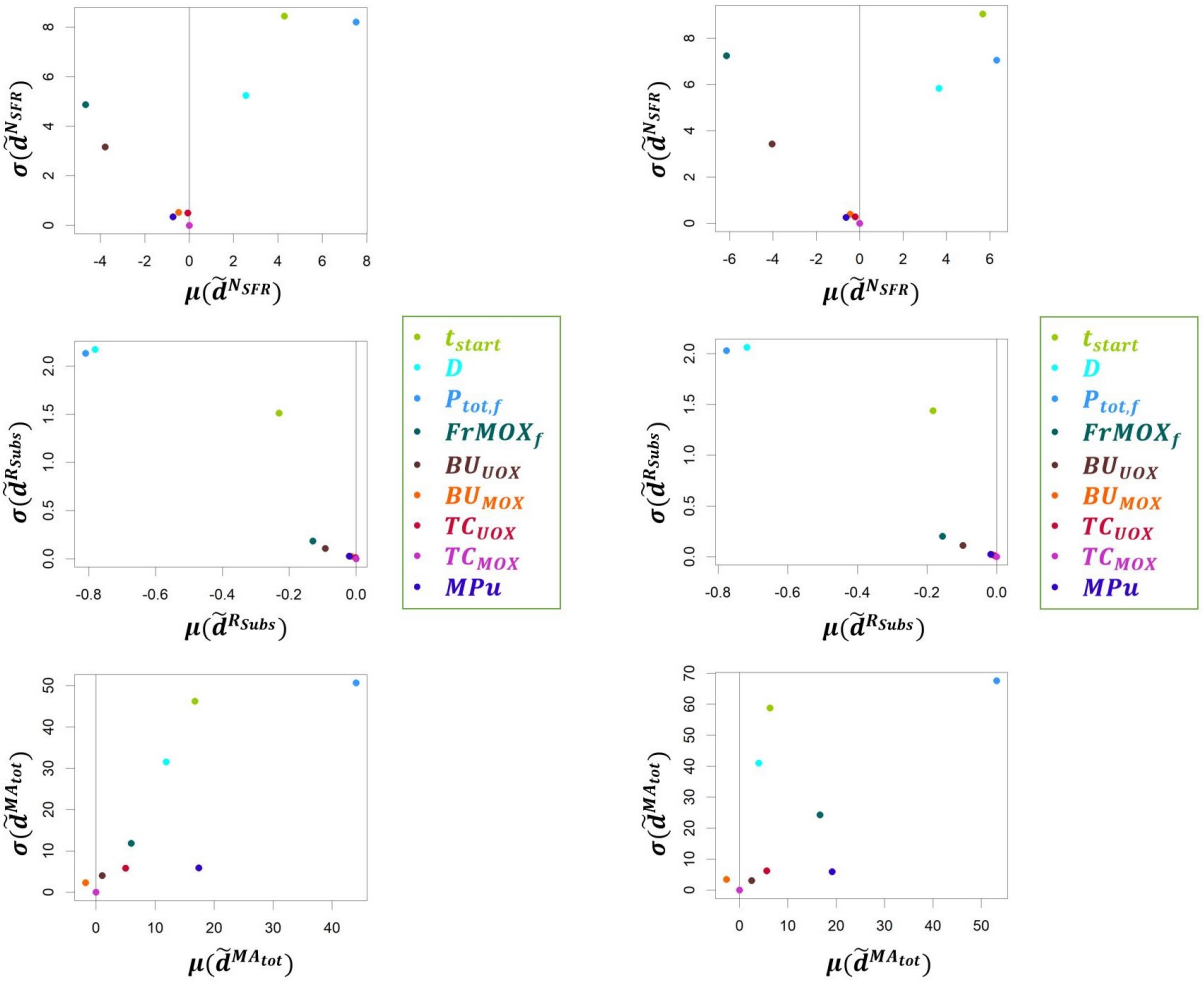

(a) σ vs μ of derivatives of outputs, in the case with missloads

(b) σ vs μ of derivatives of outputs, in the case without missload

Figure 2.12: σ vs μ of derivatives of outputs in 2095: comparison between the case with missloads and the one without missload

For N_{SFR}, the major difference of derivatives can be observed on those with respect to $FrMOX_f$ and to $P_{tot,f}$. The case with an additional stock of plutonium, in which missloads are avoided, presents larger $\mu(\tilde{d}^{N_{SFR}}_{FrMOX_f})$ (absolute value) and larger $\sigma(\tilde{d}^{N_{SFR}}_{FrMOX_f})$ than the case in which missloads cannot be excluded. In fact, when there is no missload, the high consumption rate of plutonium by some sampled trajectories can be realized and thus a stronger negative effect can be

perceived. For the same reason, the statistically positive effect contributed by $P_{tot,f}$ represented by $\mu(\tilde{d}^{N_{SFR}}_{P_{tot,f}})$ is weaker than the case with missloads. Also, the $\sigma(\tilde{d}^{N_{SFR}}_{P_{tot,f}})$ without missload is slightly smaller than the one with missloads because missloads over-estimate the change of N_{SFR} contributed by the variation of $P_{tot,f}$. Actually, missloads due to the increase of $P_{tot,f}$ result in an accumulation of plutonium inventory more rapidly without the incineration by MOX fuels.

Regarding R_{Subs}, the difference of μ and of σ of derivatives is not measurable.

In terms of MA_{tot}, σ and μ of derivatives with respect to the input t_{start}, D, $P_{tot,f}$ and $FrMOX_f$ increase a lot when the availability of plutonium is ensured. These 4 inputs are evidently important factors for the missload, and have globally positive correlation with MA_{tot}. Missloads owing to the variation of these four inputs lead to the stop of several irradiation cycles of MOX and thus reduce the production of MA.

Nevertheless, these two cases, with and without missloads, share a very similar pattern of $\sigma(\tilde{d})$-$\mu(\tilde{d})$. The ranking and grouping of inputs according to their importance on the given output does not change much regardless of missload. We can therefore suppose that the ranking of inputs with 200 repetitions is credible in the previous DoE of Morris method.

2.2.4.3 Ranking of inputs over observation times

For observations in 2050 and 2140, 200 repetitions are considered for the corresponding Morris analysis. One may note that this number is far higher than that is employed in the original design [53] or some other applications. In fact, a relatively low number is sufficient for a fast screening and to group variables with acceptable biases. In this study, this high number relies on the foregoing calibration results, which can be less biased. In order to simplify the visual comparison of the ranking of inputs over different times of observation, the normalized $\mu(\tilde{d})$ and normalized $\sigma(\tilde{d})$, denoted as $\mu_{norm}(\tilde{d})$ and $\sigma_{norm}(\tilde{d})$ and defined as

$$\mu_{norm}(\tilde{d}^o_i) = \frac{\mu(\tilde{d}^o_i)}{\max_j |\mu(\tilde{d}^o_j)|}$$

$$\sigma_{norm}(\tilde{d}^o_i) = \frac{\sigma(\tilde{d}^o_i)}{\max_j \sigma(\tilde{d}^o_j)}$$

are plotted separately in radar chart in Figure 2.13. This last normalization process is only used to simplify the comparisons between different observation times. Signs of mean values are noted beside the variable names. To give an order of absolute level of these metric values, the maximal ones used for normalization for each μ_{norm} and each σ_{norm} are listed in Table 2.2.

The rankings of inputs remains relatively stable over different observation times. For these three outputs of interest over three times of observation, inputs t_{start}, D, $P_{tot,f}$ and $FrMOX_f$ are always important factors. BU_{UOX}, TC_{UOX} and MPu have some measurable effects depending on the metrics of outputs. Effect of BU_{MOX} and TC_{MOX} are negligible.

The interpretation of ranking should be linked to the assumption of variation and variability of inputs. We could have shown that a variation range of $P_{tot,f}$ in [180, 200] GWth, which is a much more reduced range than that in this study, would have led it to a lower rank. As highlighted above, the variability of inputs is an important hypothesis of the analysis on which the assessment of inputs depends.

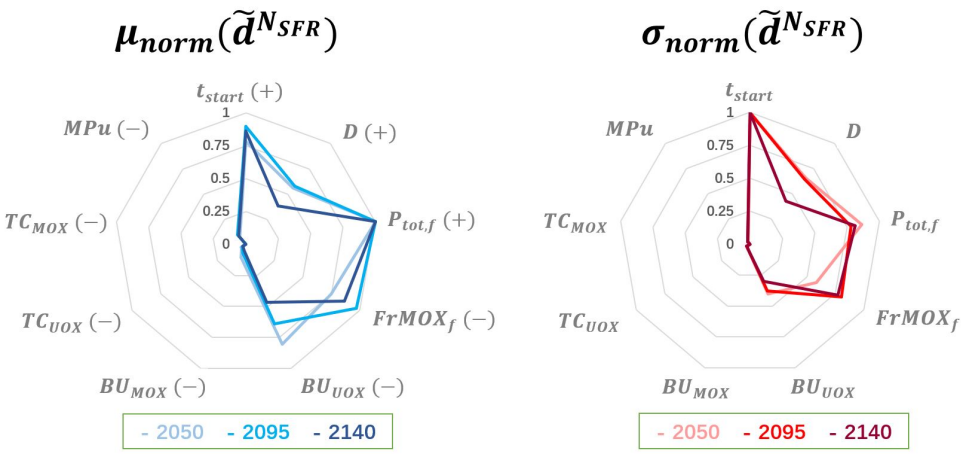

(a) $\mu_{norm}(\tilde{d})$ and $\sigma_{norm}(\tilde{d})$ of the output N_{SFR}

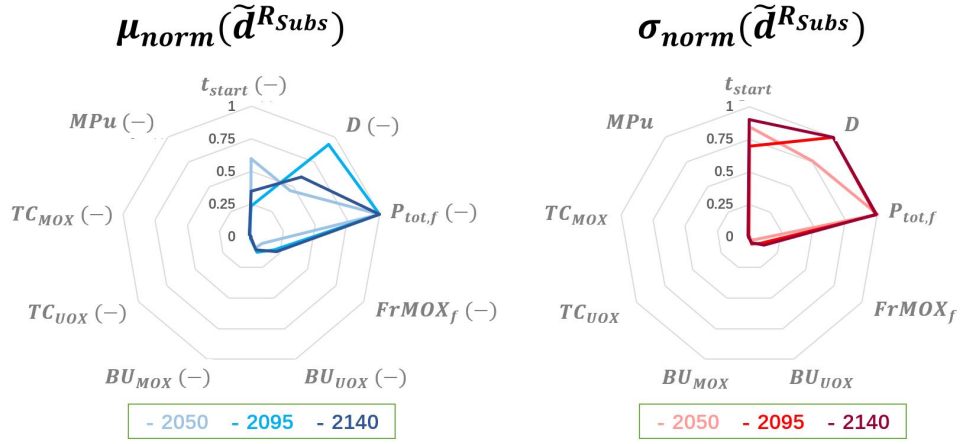

(b) $\mu_{norm}(\tilde{d})$ and $\sigma_{norm}(\tilde{d})$ of the output R_{Subs}

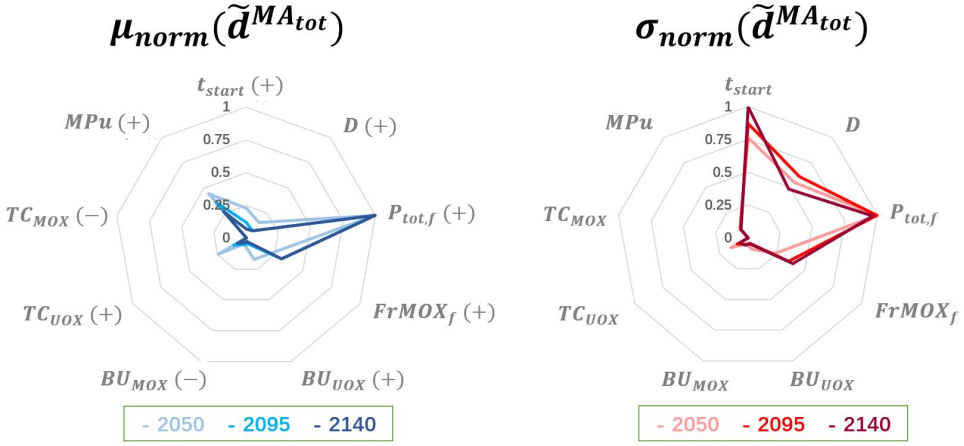

(c) $\mu_{norm}(\tilde{d})$ and $\sigma_{norm}(\tilde{d})$ of the output MA_{tot}

Figure 2.13: $\mu_{norm}(\tilde{d})$ and $\sigma_{norm}(\tilde{d})$ of three outputs of interest with respect to nine inputs over the times of observation

Obs. time	2050	2095	2140
$\boldsymbol{\mu_{norm}(\tilde{d}^{N_{SFR}})}$	$\mu(\tilde{d}^{N_{SFR}}_{P_{tot,f}}) = 1.38$	$\mu(\tilde{d}^{N_{SFR}}_{P_{tot,f}}) = 6.32$	$\mu(\tilde{d}^{N_{SFR}}_{P_{tot,f}}) = 14.26$
$\boldsymbol{\sigma_{norm}(\tilde{d}^{N_{SFR}})}$	$\sigma(\tilde{d}^{N_{SFR}}_{t_{start}}) = 2.58$	$\sigma(\tilde{d}^{N_{SFR}}_{t_{start}}) = 9.06$	$\sigma(\tilde{d}^{N_{SFR}}_{t_{start}}) = 18.30$
$\boldsymbol{\mu_{norm}(\tilde{d}^{R_{Subs}})}$	$\mu(\tilde{d}^{R_{Subs}}_{P_{tot,f}}) = -0.24$	$\mu(\tilde{d}^{R_{Subs}}_{P_{tot,f}}) = -0.78$	$\mu(\tilde{d}^{R_{Subs}}_{P_{tot,f}}) = -1.58$
$\boldsymbol{\sigma_{norm}(\tilde{d}^{R_{Subs}})}$	$\sigma(\tilde{d}^{R_{Subs}}_{P_{tot,f}}) = 0.99$	$\sigma(\tilde{d}^{R_{Subs}}_{D}) = 2.06$	$\sigma(\tilde{d}^{R_{Subs}}_{D}) = 3.10$
$\boldsymbol{\mu_{norm}(\tilde{d}^{MA_{tot}})}$	$\mu(\tilde{d}^{MA_{tot}}_{Ptot,f}) = 6.32$	$\mu(\tilde{d}^{MA_{tot}}_{Ptot,f}) = 53.17$	$\mu(\tilde{d}^{MA_{tot}}_{Ptot,f}) = 138.10$
$\boldsymbol{\sigma_{norm}(\tilde{d}^{MA_{tot}})}$	$\sigma(\tilde{d}^{MA_{tot}}_{P_{tot,f}}) = 11.08$	$\sigma(\tilde{d}^{MA_{tot}}_{P_{tot,f}}) = 67.56$	$\sigma(\tilde{d}^{MA_{tot}}_{t_{start}}) = 148.21$

Table 2.2: Maximum metric values of these output metrics with respect to different inputs over the observation times: $\mu(\tilde{d}^{N_{SFR}})$, $\sigma(\tilde{d}^{N_{SFR}})$, $\mu(\tilde{d}^{R_{Subs}})$, $\sigma(\tilde{d}^{R_{Subs}})$, $\mu(\tilde{d}^{MA_{tot}})$ and $\sigma(\tilde{d}^{MA_{tot}})$

Meanwhile, the change of absolute values of μ and σ over observation time should be noted, which can be deduced from Table 2.2 and Figure 2.13. It means that the absolute change of outputs of interest owing to the given change of parameters diverges over time. This simple fact can be a crucial factor for the assessment related to different time horizons of scenario studies.

2.2.5 Discussion and remarks on this preliminary sensitivity analysis of electro-nuclear studies using Morris method

Morris method is applied to the GSA of an example scenario study in this section. As a complement of other approaches such as variance-based Sobol indices, this derivative-based method is used to screen the important inputs for given outputs of interest. For these three outputs of interest N_{SFR}, R_{Subs} and MA_{tot}, inputs t_{start}, D, $P_{tot,f}$ and $FrMOX_f$ are very important factors; BU_{UOX}, TC_{UOX} and MPu have measurable effects on some outputs; while the effects of BU_{MOX} and TC_{MOX} are negligible. But as indicated, the validity of method is not mathematically proven in our case. The results should be taken with precaution.

The first factor that possibly affects the credibility of results can be the dependence of input variables. In this analysis, t_{start} and D are supposed independent. One may argue that these two inputs should be dependent because the transition should finish before the time of observation. Some advanced processing of Morris method [89] can employ dependent input variables to perform global sensitivity analysis. But in all, whether the time of observation is disconnected from the end of transition depends on the purpose and the interest of study.

More importantly, if missloads are not allowed, the results of evaluations may be biased and this could lead to invalid conclusions. The problem of plutonium shortages can be "solved" by several options, e.g. adjusting the capacity of fabrication as presented in [67], or adding a back-up stock of plutonium as done here if the adjustment is not satisfying. The unrealistic trajectories can then be turned to a feasible one in simulation. However, they are not definitive solutions: even if the missload can be avoided by back-up stocks, the corresponding strategy and trajectory is only virtually valid, because the combination of parameters is physically prohibited. The results that should not exist in reality may bias the analysis. For example, $P_{tot,f}$ is highly non-linear with N_{NSFR} or the in-cycle plutonium inventory in this exercise, due to strong interaction with $FrMOX_f$ and other time-related inputs. If missloads are considered invalid and those combinations of inputs are removed, a stronger correlation between $P_{tot,f}$ and in-cycle

plutonium inventory can be expected.

Another solution is to cut the trajectories with missloads, and to analyze directly the valid samples without missload after cut. This option creates implicitly dependence between input variables that cannot be predicted a-priori in the DoE, and thus the corresponding analysis method should allow sampling a-posteriori determined to rank inputs and to investigate input-output relation. When the fraction of missload in the input space is relatively small, cut-off of the results of DoE can be applied to Morris method. But in this exercise, the phase space of missload is measurable, and the number of valid repetitions for a given input is not ensured for Morris method.

The problem of missload can be generalized to other similar constraint problems that require post-simulation verification. For instance, the reprocessing of spent fuels in CLASS is immediate in response to the needs. Some strategies may lead to an unacceptably high level of reprocessing capacity, requiring calls of simulation to verify. Nevertheless, the constraints also depend on the interest of study. Also, the setting of scenario should be reasonable and "intelligent" so that the fraction of phase space that respects the constraints of interest can be sufficiently large.

The last remark made in this preliminary analysis is related to the observation time or the temporal horizon of scenario. It is intuitive that the output differences owing to different choices of important input parameters diverge over time, and so is the respect of constraints of the problem, which depends on the temporal horizon of scenario. In other words, both the absolute impacts of inputs and the validity of a strategy and a trajectory are temporal. As will be shown in subsequent analyses, the strategy assessment can be affected by the time horizon of scenario studies.

2.3 Methodology of strategy robustness assessment: notions and general framework

In additional to the method of sensitivity analysis applied to electro-nuclear scenario studies, specific framework for the robustness assessment should be built in this work. The concepts of robustness are defined in this section. As introduced in chapter 1, the uncertain context of nuclear planning implies various scenarios and strategies that are not directly comparable. In this section, the methodology allowing the inter-scenario comparison is presented, regarding the robustness of strategy subject to the deep uncertainty of objective.

2.3.1 Trajectory, strategy and the relation with objective

Several basic notions need first to be defined clearly. As frequently used in the preliminary sensitivity analysis, "trajectory" and "strategy" are distinct concepts. A trajectory denotes the single pathway defined by the total nuclear fleet evolution, and leads to one deterministic simulation. A strategy refers to a future planning summarizing a set of measures. In this work, a trajectory is the result of one unique simulation subject to a strategy represented by a group of input parameters. Even though they are conceptually distinct, a strategy and the corresponding trajectory can be bijectively matched and considered equivalent under the common hypotheses and constraints of scenario.

As introduced in [10], some scenario studies aim to investigate the outcomes with respect to a wide range of possibility of strategies. They are referred to as

exploratory scenario studies. The strategy performances regarding given objectives are quantified by specifying the outputs of interest and investigating the responses of outputs to a large diversity of strategies of interest. Meanwhile, some studies back-cast the dedicated choices of strategy to a given future objective. They are called normative scenario studies. In this kind of study, criteria describing the objective in quantitative manner are imposed on the output responses to given strategies. The phase space that satisfy the criteria can then be identified as the ones that achieve the given objective.

The studies in this work are rather exploratory scenario studies: a wide range of strategies are explored, and the performance of a given strategy are evaluated. Strategies that satisfy given criteria of interest are identified, and they are compared according to the objectives considered.

2.3.2 Deep uncertainty of objective and possible options to consider them

The decision-making processes for future fleet transitions are driven by different objectives that may evolve drastically. More than uncertainty this is even a deep uncertainty on the objective because both the probability and the time of change are unknown. Depending on the evolution of industry operation, economic estimation, political decision and public opinions, the change of objective can be abrupt for which it lacked clear anticipation in the past. This kind of change is called the *disruption* of objective in this work. Note that it is distinguished from the disruption of parameter in the study of resilience in [49, 81].

As introduced in Chapter 1, the evolution of policy changes regarding SFR deployment in France, can be viewed as an example of disruption of objective. The deployment of SFR is deeply uncertain given the insufficient competitiveness of economic estimation and technological challenges. Without the option of SFR, the minimization of TRU inventories with limited measures and limited need in new technologies can be crucial. To build a firm framework of methodology, objectives of two incompatible futures are taken as examples for this study:

- Obj. A: To allow the use of plutonium and the reprocessing of TRU in further design, deployment of SFRs in the whole French fleet is planned. This objective is considered pre-selected in this study.

- Obj. B: The future deployment of SFR is no longer a priority; in this perspective, the transuranic inventories in the total cycle should be minimized, without the need of SFR or any technology not yet proven. It is linked to the disruption of prior objective A.

The ambiguity on the plutonium status, whether it should be considered as a waste or a valuable matter, is the first consequence of the deep uncertainty on the SFR deployment. The operation of SFR of European design demands a large inventory of plutonium. If SFR deployment is considered, the plutonium produced in the cycle is a valuable resource for the start of future SFR. On the contrary, if SFR deployment is not considered, plutonium produced in the cycle can become the material which we aim to minimize. Since the major part of TRU inventories in the total cycle of PWR UOX and PWR MOX is contributed by the plutonium which can be potentially used for SFR operation, the relevant minimization may seem contradictory to the objective of SFR deployment, even though they are not entirely incompatible. In the following, we consider that these two objectives are completely independent.

Strategy assessments subject to uncertainties require dedicated methods, which have been developed since long time in decision-making studies. One intuitive option is to optimize the expected utility inside a random future state with probabilities, to be one or the other considered future through an estimated probability density function. However, there can be significant biases when the probability function is not well agreed upon. Particularly, under the context of deep uncertainty, the probability cannot be described precisely by definition, and it may lead to considerable vulnerabilities within the choice of strategy [51, 90]. Another option is to be as precautionary and conservative as possible for any change, constructing a strategy that is guaranteed to work in all possible future states. But this may lead in many cases to important sacrifices regarding the original objective [91].

To ensure acceptable strategy outcomes subject to deep uncertainty, robust decision-making is needed. Various robustness studies involve a large diversity of processes, designs and metrics of evaluation, employing diverse but conceptually similar notions and concepts [51, 90, 92]. [47] summarizes systematically four categories of strategies regarding the deep uncertainty of future evolution and possible disruptions: resistance, resilience, static robustness and adaptive robustness. Terminologies in [47] are mainly introduced in this work and the relevant concepts are adapted to the electro-nuclear scenario studies, as schematized in Figure 2.14.

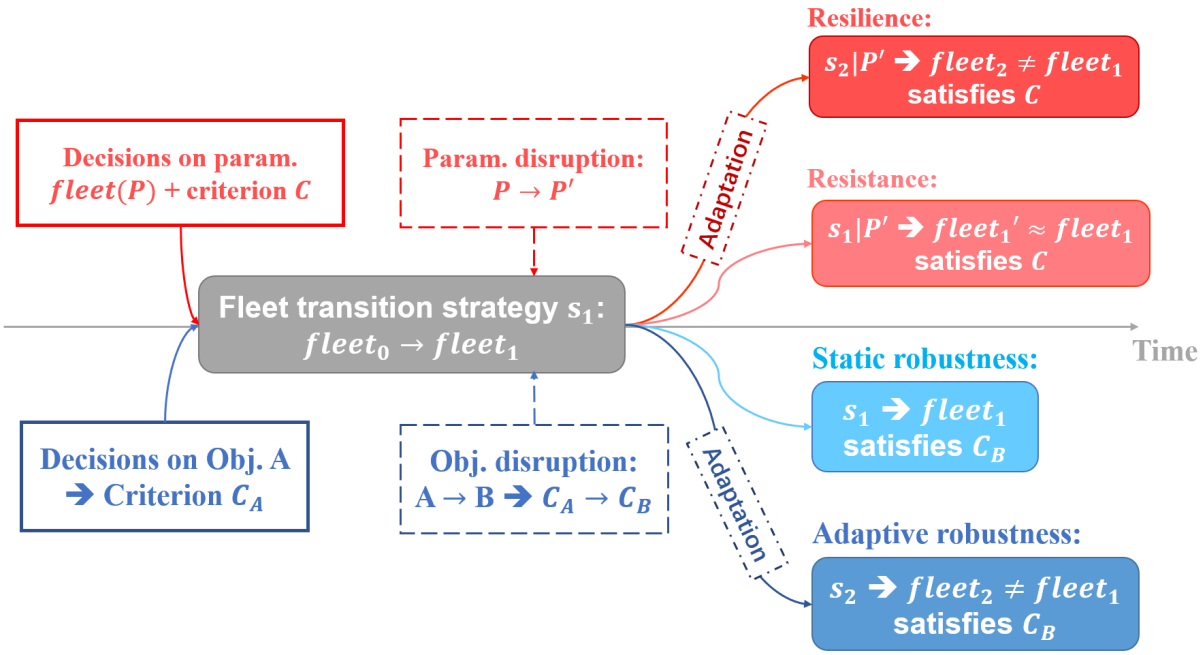

Figure 2.14: Schema of the concepts resistance, resilience, static robustness and adaptive robustness adapted to the electro-nuclear scenario studies

Resistance and resilience refer to the capacity of a given strategy to absorb the impacts of uncertainties of system parameters regarding the respect of given criteria or constraints. A resistant strategy is able to offset the effects of disrupted parameters by the endogenous adjustments by the system itself without any external adjustments. Precaution is usually considered in advance for uncertain disruptions in a resistant strategy. But in some cases the impacts of parameter disruption can be unbearable; exogenous readjustments outside the system are necessary to compensate the unacceptable results from disruption and to recover the system. If the respect of criteria is guaranteed by these exogenous adaptations, the strategy is then considered resilient. A concrete example of

strategy resilience assessment in electro-nuclear scenario study can be found in [49]. In this example the French nuclear fleet is studied, subject to the constraints in terms of reprocessing capacities, quantity of separated stockpiles, inventories of spent fuels and MOX fraction. The respect for these constraints is regarded as the criterion to identify the strategies of interest. Due to the deep uncertainty on the future installed capacity, the evolution of electricity supply is disrupted, and the resistance as well as the resilience of possible strategies are investigated regarding their performances on the constraints.

Static and adaptive robustness describe the capacity of strategy to adapt to uncertain disruptions of objectives. The objectives imply instructively the criteria to respect. Static robustness represents the acceptable goodness level of outcomes resulted from a given strategy for all possible conditions. Such strategy can fulfill any objective finally adopted without additional readjustments. Adaptive robustness quantifies the performance of reevaluation with adaptation in case of disruption of objective or constraint criteria.

The objective disruption is studied in this work, and correspondingly, the robustness of strategies of interest is assessed. The following sections present how the concepts and methods of robustness assessment are adapted to electro-nuclear scenarios in this study.

2.3.3 Static robustness: a precautionary approach

The study of static strategy is essential due to the nature of deep uncertainty. It highlights the performance boundaries of the strategies that are currently available. More precisely, a static strategy means that the time-dependent configuration of fuel cycle is determined in the beginning, and the parameters evolve as initially planned without further dynamic readjustments outside this pre-determined planning, even in case of disruption. The static robustness assessment investigates the performance of static strategies with respect to different objectives.

In our example, the SFR deployment is the pre-selected objective A, but there is always a doubt of changing this planning. If this objective is disrupted, the TRU inventories in the total cycle should be minimized at least within the currently available technology. A robust static strategy implies that by implementing this strategy, objective A can be achieved, while the TRU inventory in total cycle is sufficiently low if A is disrupted and B is considered. It is equivalent to an appropriate strategy with good performances for all possible objectives in a multi-objective problem.

The static robustness of strategy can be thus investigated by non-disrupted scenario studies. Under the context before any disruption, WPS is used for the analysis of scenario, and a strategy space can be created in terms of fuel cycle transitions to explore the possibilities to achieve given objectives. The outputs of interest to quantify the performance of strategies with respect to two objectives should be defined. After the simulations of sampled strategies, the analysis of outputs indicates the strategy performances regarding given objectives, with dedicated criteria to identifying robust static strategies. These criteria can be determined by specific thresholds, or as presented in the subsequent analyses, by deterministic calculation.

Due to the contradiction of two objectives, robust static strategy is supposed to be a precautionary option to avoid unacceptable consequences in any situation. Analysis of robust static strategy can reveal the necessary precautionary actions which should be considered before any disruption to counterbalance the uncertainty of objective.

One may interpret the implementation of static strategy as a hypothesis of

a scenario. In fact, the degree of liberty of fuel cycle readjustment in case of disruption is not obvious, and it is possible that the fuel cycle has to stick to the original planning of pre-disruption strategy. Static robustness assessment indicates then the performance of strategy under this hypothesis.

2.3.4 Adaptive robustness: a dynamic approach with post-disruption readjustments

The counterpart of static robustness is to look for appropriate adaptations in case of disruption. The relevant assessments of adaptive robustness of strategies requires a dedicated scenario of adaptation, which confirms the disruption and differs from the pre-disruption scenario context. This post-disruption scenario starts from a given prior trajectory, which may be the result of a pre-disruption strategy. At the first step, the trajectory of a representative pre-disruption strategy achieving objective A, or an optimal strategy for objective A, can be chosen to determine the prior trajectory. In fact, it is intuitive to employ the trajectory related to objective A because it is pre-selected before any disruption.

The trajectory can be adapted from different times because the disruption is deeply uncertain. After the disruption, objective B is adopted in an updated context. A new space of adaptive strategy can be created, different from the pre-disruption one. Employing the similar analysis method, the performance of available adaptive strategies is investigated to indicate which readjustments have to be made to adapt to objective B.

Adaptations can always improve the performance regarding objective B, in comparison to the prior trajectory, or at least keep it at the same level. To highlight the effects of adaptation and to carry out inter-scenario comparison between static and adaptive robustness, a threshold as criterion level deduced from the phase space of pre-disruption strategy can be used. The most conservative strategy for objective B among pre-disruption strategies that achieve objective A can be chosen, as in Chapter 3; it is called robust static optimum in this work. Note that this conditional optimum is different from the global optimum for objective B, due to the priority of objective A before any disruption. The robust static optimum, leading to minimal TRU inventories among those achieving objective A, indicates the best achievable level among historical available choices. The difference between the results of prior trajectory and the outcomes of this optimum implies the regret from the implemented pre-disruption strategy under the disruption of objective; readjustments are thus explored to countervail this regret. The trajectories with adaptation are then compared with the robust static optimum. If the adaptive strategy performs better than the robust static optimum, the concatenation of that implemented pre-disruption strategy and this adaptive one is considered adaptively robust, and this adaptation is called robust adaptive strategy.

The choice of the criterion level for comparison is not unique. Similar to the criteria related to static robustness, it can be decided by meaningful thresholds from the estimation of industry or political decisions; but as presented in the following chapters, the validity of threshold is sometimes difficult to justify, whereas the assessment can be highly sensitive to the choice of value. Therefore, criteria from deterministic runs, such as the robust static optimum, can be more useful.

The main objective of this Ph.D thesis is to build a methodology for robustness assessment for electro-nuclear scenario studies. Chapter 3 adapts this framework to offer a first glance for the robustness assessment dependent on a predetermined time or a preset time horizon. Chapter 4 aims to free the assessment

from these temporal hypotheses.

2.3.5 Remarks on the methodology of robustness assessment

The framework of robustness assessment previously illustrated is still narrative, since the assumptions or other implicit hypotheses of scenario study are not completely defined. To perform effectively the study, the assessment process can be translated into mathematical operations; but it means that the relevant hypotheses should be explicitly highlighted for the interpretation of results.

Actually, even the given examples of objectives are also all narrative, indicating the strategic orientation without sufficient accuracy. The relevant interpretation of these objectives into mathematical criteria and the choice of relevant output metrics can be diverse depending on the interest of analysts or stakeholders [92]. The strategic orientation of objective, the numeric interpretation of objective, and the choice of threshold related to a given objective, may correspond respectively to three different levels of deep uncertainties of objective.

Another factor that can affect the assessment is the exploratory space of strategy in both pre-disruption and adaptation scenario studies, which indicates the variability of inputs and richness of options, depending on the context, hypotheses of scenario, and the interest of analysts or stakeholders [91]. As an example, the resilience study in [49] shows the significant impact of different preferences on input values of strategy on the resilience assessment. It also indicates the necessary modifications of the fuel cycle for robust adaptations, which motivates the discussion among stakeholders.

2.4 Conclusion of this chapter

In this chapter, the fuel cycle simulator CLASS and relevant physics models have been introduced. A simulation of the historical French fleet by CLASS has also been presented to set an appropriate starting point for subsequent scenario studies.

To analyze the fuel cycle responses to the variation of fuel cycle parameters, Morris method [53] was used for the GSA. An exploratory scenario inspired from the French fleet of PWR UOX and MOX from 2015 to 2140 was considered, focusing on the variations of nine input parameters and the responses of three outputs. This exploratory study provides an example of an electro-nuclear scenario study and allows to clarify the choices made for the more complicated studies in the subsequent chapters. For all three outputs N_{SFR}, R_{Subs} and MA_{tot}, the input $P_{tot,f}$ standing for the final power level of fleet after transition has a dominant influence. Its interaction with other inputs like t_{start} and D characterizing the timing of transition, and the final MOX fraction $FrMOX_f$ and the burn-up of UOX BU_{UOX}, also have measurable effects on these outputs, in particular N_{SFR}. The cooling time for spent UOX fuels TC_{UOX} and the reprocessing order MPu account for some variation of MA_{tot}. MOX-related parameters, BU_{MOX} and TC_{MOX}, however, have limited influence on these three outputs of interest.

To take the deep uncertainty of objective for nuclear future into account, the framework for strategy robustness assessment was introduced. Two types of scenarios of interest have been described. One is the pre-disruption scenario, which identifies the reference strategy optimized for the single pre-selected objective, and also the set of robust static strategies which trade the performance on the pre-selected objective for the one linked to the disruption. Before any disruption, robust static strategies can be interpreted as taking precautionary action

with conservative attitude, and in case of disruption it may lead to acceptable outcomes even without post-disruption readjustment. The other is adaptation scenario, which allows post-disruption readjustments. The performance of adaptive strategies based on a given prior trajectory will be compared with an optimal level deduced from the pre-disruption scenario. If this adaptive strategy has a better outcome than this level, it means the adaptation is able to adapt the situation to the best level that could be chosen before disruption, and thus can be considered robust.

However, the framework defined this way needs more precise characterization to be practically applicable. In the following chapters, the methodology to assess robustness are presented. Chapter 3 and 4 differ in the additional assumptions and the definition of numerical criteria concerning the dependency on the time horizon of scenarios.

Chapter 3

Robustness assessment with a preset time horizon of scenario

Introduction

The methodology of scenario analysis and robustness assessment presented in Chapter 2 needs a very precise and clear formulation of each problem of interest. One way to determine if a given objective is fulfilled is to estimate and evaluate the relevant outputs of interest at a given time. In this chapter, two objectives, one related to SFR deployment and the other linked to the minimization of TRU inventories without SFR, are redefined as mathematical expressions that focus on observations at the end of scenario, with deterministic criteria and relevant outputs of interest.

This formulation of the problem implies that the robustness assessment of strategies depends strongly on the temporal horizon of the scenario. As revealed in the example scenario of Section 2.2, the observation time can be a key factor in assessment, since the absolute values of outputs evolve over the time. Nevertheless, an objective defined with a given point of time is quite common in lots of projects and perspectives, which set a clear and explicit reference point to evaluate the results and performance of implemented strategies. This point of view with a set time horizon is a common way for strategy assessment. For instance, this is how the French strategy is discussed in different national institutions.

Within a set time horizon and at a predetermined observation time, the performance of strategies can be well-defined and strategies of interest can be assessed depending on the chosen objectives. Using Wide Parametric Sweeping techniques to investigate the statistical behaviors of fuel cycle in a huge phase space of parameters, a large sized sampling of strategies is performed. As indicated in Section 2.1, thousands of simulations of individual reactors require a heavy management of fuel cycle parameters and computational cost. Simplification of macro reactor is thus applied. Note that under the assumption of macro reactor, parameters of same type of reactor are uniform and their behaviors are synchronized.

To perform the strategy assessment, numerical formulation of problem and the criteria for the assessment are determined in Section 3.1, introducing new assumptions to clarify all numerical criteria. The pre-disruption scenario study is performed in Section 3.2, using Principal Component Analysis (PCA) to evaluate the importance of inputs on two possible outputs of interest. The physical analysis of all simulated trajectories considers both objectives equally. However, the selection of different particular strategies relies on the choice of the primary (or pre-selected) objective which is here the deployment of SFR. Using the criteria of

static robustness assessment, two strategies are identified. The first one is reference strategy, which is optimal for the single pre-selected objective without any regard on the secondary. And the second one is the robust static optimum. These two strategies represents two extreme cases in the Pareto front. The Pareto front standing for the zone of trade-offs between two contradictory objectives is also analyzed.

In Section 3.3, adaptive strategies are studied, based on the prior trajectory of reference strategy. According to the criteria defined in Section 3.1, the temporality of adaptive robustness is determined. Finally, Section 3.4 considers a different numerical formulation of the secondary objective. The new numerical criteria is built to decouple the objective from the uncertainty on the total fleet power evolution. Furthermore, this new reformulation allows to study the influence of problem formulation on the strategy assessment.

3.1 Problem formulation

3.1.1 Determination of numeric criteria

The problem considers the deeply uncertain disruption of objective. Based on the French fuel cycle, two possible objectives with respect to two different future states are taken as examples: one is the substitution for PWR-fleet with SFRs, and the other is to minimize TRU inventories in total cycle without SFR.

The time horizon of the scenarios studied in this chapter should be defined before anything. Time horizon represents primarily the time of interest in the study. The results beyond horizon are not of interest. In this chapter, the scenario starts in year 2015 and ends in year 2090. This choice of horizon matches possible reactor fleet transitions. According to the start time of PWRs and the estimation of reactor life limit ranging from 40 to 60 years, the generation of current PWRs will start their decommissioning from year 2020, and the fleet will be progressively replaced with EPRs [39]. Year 2090 corresponds then to the end of this generation of EPRs and to the time period for next replacement of fleet with new generation reactors after EPRs, possibly SFRs. Two objectives of interest are connected with the end, year 2090, which means that the strategy performances are directly quantified by the corresponding results in year 2090. It represents a natural choice of perspective, setting a time point to evaluate strategies.

The preset time horizon of scenario implies that the trajectories with missloads before 2090 are not acceptable, and thus unfeasible in practise. The replacement with UOX in case of plutonium shortages for MOX is not modeled because it hides the real MOX fraction which is different from the value indicated by input parameters of strategy. Trajectories and the relevant strategies with missloads are considered invalid in this study, and are then discarded before any strategy assessment.

In this time frame, only PWRs UOX and PWRs MOX similar to what exist in the French fuel cycle, are simulated. In the following illustration, the objective A denotes the pre-selected objective related to SFR deployment, and objective B denotes the TRU minimization. Even though both objectives are considered, no innovative system nor advanced fuel is modeled. This absence of simulation of SFR or multi-recycling of plutonium only allows for a rough estimation on the strategy performance for objective A. For a more precise evaluation of strategies in regards to objective A, several other hypotheses would be needed, but it would greatly complexify the study. This choice of a simplified evaluation keeps the physical analysis clear without the loss of generality: only the effects

of depletion of PWR UOX and PWR MOX are involved, and it avoids complicated technical details concerning the behaviors of innovative systems and transition details during the substitution phase.

Trajectories and strategies related to SFR deployment have been widely analyzed in various studies with various purposes, such as the consequences of final system configuration of fleet on fuel cycle [93, 21], the back-end reprocessing mode of spent fuels [93], the impact of deployment schedule on uranium consumption and wastes [43]. In this work, these technological issues and related consequences are not detailed and we focus on the valorization of plutonium and relevant constraints on material availability. To quantify the performance in regards to objective A, the substitution ratio R_{Subs} defined by Equation 2.11 in Chapter 2 is used. As a reminder, R_{Subs} measures the plutonium availability to replace the whole PWR-fleet with SFRs, with the hypotheses of given plutonium content in the fresh fuel (17%), the default specific power of future SFR (48 W/gHM), the necessary recycling time of plutonium (seven years including the fabrication of fresh fuel and cooling of spent fuel), etc. As assessments are connected with the end of scenario, $R_{Subs}(t = 2090)$ of trajectories resulting from possible strategies are calculated.

Objective A represents the goal of the substitution of fleet with SFRs. Under the assumption of time-set evaluation in year 2090 and the relevant connection with output R_{Subs}, objective A demands strategies achieving $R_{Subs}(t = 2090) = 1$. This implies that the material availability in 2090 allows the entire substitution of PWR-fleet with SFRs. However, due to the assumptions on the estimation of R_{Subs}, margins should be taken to ensure the entire replacement. Objective A is then recast in criterion A as:

- $C_A^{t\text{-}set}$: Giving priority to $R_{Subs}(t = 2090) > 1$, maximization of $R_{Subs}(t = 2090)$.

where *t-set* means that criterion A and objective A studied in this chapter depend on the evaluation in year 2090. The larger the margin, the more at ease the substitution of PWRs with SFRs is.

One may argue that the plutonium inventories should not be in excess even if SFRs are deployed. For example, $R_{Subs}(t = 2090) = 10$ may be an inappropriate choice because too much plutonium is out of use even after the full fleet substitution. Since ranges of $R_{Subs}(t = 2090)$ of possible strategies in the given strategy space cannot be anticipated, an acceptable range indicated by two boundary thresholds can be an alternative. Under different context of future states in robustness study, a criterion determining a so-called optimal or representative strategy is a better choice. Choosing the representative with average input values among target ones [94] or using clustering methods as suggested in [95] is then possible, but requires additional hypotheses and relevant interpretations. In this study, as will be shown in the following analyses, the use of $C_A^{t\text{-}set}$ is a-posteriori justified because $R_{Subs}(t = 2090)$ never reach extremely high values. Because of that, this criterion can determine directly a so-called optimal strategy of objective A and simplify the analysis.

One may also note that $R_{Subs}(2090) > 1$ implies the complete replacement of fleet with SFRs by 2090 (from the angle of plutonium availability), which is a deployment schedule much faster than most planned deployment [21, 43]. In this work, an accelerated deployment is considered which amplifies the contrast between the two future states and objectives, and thus emphasizes the impact of disruption.

Similarly, objective B can be recast in criterion B as:

- $C_B^{t\text{-}set}$: Minimization of TRU inventory in total cycle including that in the wastes in 2090, $TRU_{tot}(t = 2090)$.

TRU considered in this work mainly consists of neptunium, plutonium, americium and curium.

When the future state and objective are uncertain in the pre-disruption scenario, taking precautionary actions can be a good choice. To determine such strategy, a conditional criterion $C_{B|A}$ can be useful:

- $C_{B|A}^{t\text{-}set}$: Minimization of $TRU_{tot}(t = 2090)$ among all valid strategies achieving $R_{Subs}(2090) > 1$.

The notation of $B|A$ means that objective B is considered but only in condition objective A is fulfilled. $C_{B|A}^{t\text{-}set}$ is therefore a criterion different from $C_{A}^{t\text{-}set}$ which pursues purely objective A without consideration of disruption. $C_{B|A}^{t\text{-}set}$ will be used to determine the so-called robust static optimum in the analysis of static robustness in pre-disruption scenario. On the contrary, if the objective is disrupted, the SFR deployment is no longer of interest, and $C_{B}^{t\text{-}set}$ should be used to search for optimal readjustments in adaptation scenario.

3.1.2 Possible source of bias affecting the assessment

Even after the reformulation of the problem in numeric criteria without ambiguity, several sources of bias may still be involved in the strategy assessment. First of all, there are the systematic errors in each CLASS simulation. Subject to the lack of industry and experimental feedback, simulation errors of CLASS can only be quantified by benchmarks with reference simulations. The errors induced by cross-section predictors of ANN can be compared with Monte Carlo depletion calculations, as quantified in [55].

For modeling errors, as indicated in Section 2.1 and in [56], the lack of fuel batches modelling in CLASS (even if approximation is made, see Section 2.1) leads to a bias on in-core inventories much larger than the depletion predictors. These errors are mainly reflected on "local" inventories, such as that in pools, stocks and fabrication plants, coming from the FLM. But thanks to the precision of cross-section predictors, biases may compensate themselves between the loaded inventories and the discharged ones. Thus, the outputs of interest defined in this study, R_{Subs} and TRU_{tot}, which depend on "global" inventories in the cycle, are not so biased as "local" inventories.

Another source of uncertainties comes from the hypotheses of scenario study. An impactful one is the respect of irradiation cycle and synchronization effect due to the use of macro reactors. The timing of fuel cycle transitions respects the irradiation cycles of those macro reactors. The use of macro reactor assumption synchronizes all reactors of the same type. The change of parameters of all PWR UOXs may take place only one irradiation cycle after the beginning of transition. A typical irradiation cycle of UOX and MOX last around four years. Consequently, there is a maximal bias on the beginning of transition around four years in this study.

As an indirect results of this timing shift due to the respect of irradiation cycle, the inventories of plutonium and MA at a given time is also deviated. In the current fleet, 169.3 GWth at nominal state is contributed by PWR UOX and 18.8 GWth is contributed by PWR MOX. Normalized by the power level and based on the simulation of a 900-MWe reactor (2785 MWth of thermal power in nominal state) in Section 2.2.1, the production of plutonium and MA in one irradiation cycle of all UOX fuels are respectively 49 tons and 4.3 tons. For MOX fuels, those productions are respectively -10 tons and 1.6 tons. Hence, if the irradiation cycles are not respected, the deviation on the estimation of plutonium inventory in one

cycle may range between -10 and 49 tons. The deviation in terms of MA can reach around 6 tons. These ranges of bias are deduced from the extreme cases with synchronization of reactors, and they are therefore the most conservative estimations.

As for hypotheses on scenario outputs, the most impactful are probably the assumptions on the estimation of R_{Subs}. Because of this importance we will explicit them more clearly than what was presented in Section 2.2. As mentioned therein, the plutonium content in the fresh fuels of future SFR is supposed to be 17%, and the value of R_{Subs} is proportional to plutonium content in fresh SFR fuels. However, this content may fluctuate due to the variation of isotopic composition of plutonium in stocks. This dependency is systematically studied in [57, 42], based on ASTRID-like reactor. The plutonium content in fresh fuel is highly correlated with the plutonium quality, which is defined as the ratio between the quantity of odd-number isotopes and the quantity of even-number isotopes of plutonium, denoted as Pu^o/Pu^e in [57, 42]. Extrapolating the results in [42], the maximum uncertainty of Pu^o/Pu^e in the spent fuels of French fleet leads to at most 6.5% of relative bias on the estimation of R_{Subs} in this study.

3.2 pre-disruption scenario and static robustness analysis

Numeric criteria with respect to uncertain objectives allow us to analyze quantitatively the impact of a disruption. In this section, the pre-disruption scenario, in which the disruption is still uncertain, is studied. Strategies of interest in this scenario are analyzed and their static robustness can be assessed. Before all, a basic analysis on the behavior of fuel cycle in response to diverse options of parameters should be performed.

Eight inputs and two outputs are considered (three outputs in the case of plutonium shortage study). Conventional graphical techniques can be exhaustive but give limited information if it lacks quantitative analysis. Meanwhile, even though Morris method used in Section 2.2 gives a primary insight on the behavior of fuel cycle, it may be biased when valid observations do not match well the original DoE. To address these issues, Principal Component Analysis (PCA) is used to analyze the input-output relation and to figure out the importance of inputs with respect to given output. After that, inputs can be grouped, and graphical techniques can be used on different groups as a complement and verification of the analysis. From the analysis, specific strategies from the Pareto front are analyzed and compared, leading to the definition of robust static strategies which is clarified in the last part of section.

3.2.1 Description of pre-disruption scenario

The pre-disruption scenario, inspired from the French nuclear fuel cycle of PWR UOX and PWR MOX, starts from year 2015 and ends in year 2090. Similar to the scenario illustrated in Section 2.2, strategies of interest are linked to the transition of fleet according to the French national strategy, pursuing objective A and B, as shown in Figure 3.1. The transition starts from the time t_{start} and lasts a time period D. t_{start} ranges from year 2030 to 2050, a time interval related to the decommissioning of large number of old reactors and the start of new EPRs. These two time variables characterize the timing of transition. The transition is supposed to finish before year 2090, which means that $t_{start} + D < 2090$. After t_{start}, burn-ups BU_{UOX} and BU_{MOX}, cooling time of spent UOX fuels TC_{UOX} and the management of spent UOX fuels for reprocessing MPu change immediately. As

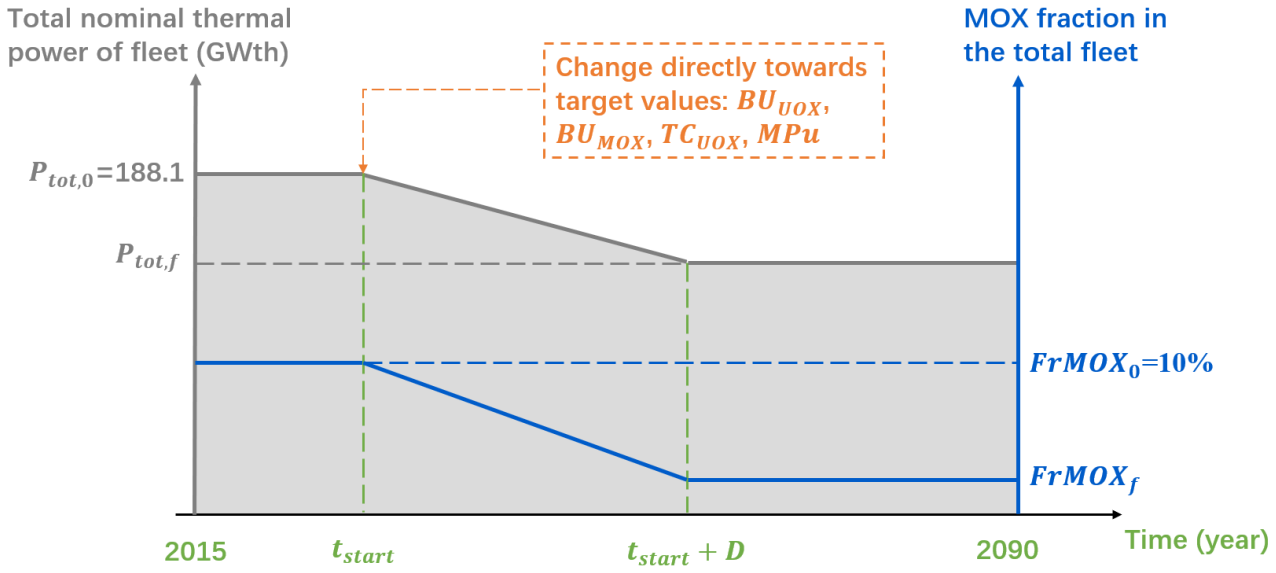

Figure 3.1: Graphical representation of the evolution of fleet in pre-disruption scenario

revealed by the analysis of Morris method in Section 2.2, the change of cooling time of spent MOX fuels does not have any effect on two outputs of interest R_{Subs} and TRU_{tot} and it is not considered here. In this study, it is set to five years. Even though the burn-up of MOX BU_{MOX} influences little these two outputs of interest, it may affect the mass of plutonium demanded for MOX and thus the plutonium shortage and the missloads. It is therefore considered in this study. During the transition, total thermal power of fleet and global MOX fraction change linearly, reaching their final values, $P_{tot,f}$ and $FrMOX_f$ respectively, at the end of transition and kept constant until year 2090.

Under the macro reactor assumption, only two reactors are simulated, representing respectively the global behaviors of PWR UOX and PWR MOX. In summary, a strategy in this pre-disruption scenario is characterized by eight input variables, presented in Table 3.1. Difference on $P_{tot,f}$ and $FrMOX_f$ from the ones in the preliminary analysis in Section 2.2 can be noted. In terms of $P_{tot,f}$, the lower bound of power level corresponds to 50% of current level instead of 10%. Because objective A targeting the SFR deployment in the future is pre-selected, a power level corresponding to phase-out in the fuel cycle is not of interest. The lower bound 50% of current level covers the envisaged decrease of nuclear installed capacity in [18] with reasonable margins. In terms of the MOX fraction, 10% as the initial level is chosen, different from 7.6% selected in Chapter 2.

Input var.	Init. value	Min.	Max.	Unit	Explanation
t_{start}	-	2030	2050	-	Starting time of transition
D	-	10	2090-t_{start}	year	Duration of transition
$P_{tot,f}$	188.1	94.1	282.2	GWth	Total thermal power of the fleet after transition
$FrMOX_f$	10	0	30	%	MOX fraction after transition
BU_{UOX}	45.3	30	60	GWd/t	Modified burnup of UOX fuels
BU_{MOX}	45	30	60	GWd/t	Modified burnup of MOX fuels
TC_{UOX}	5	3	10	year	Modified cooling time of spent UOX fuels
MPu	1/LiFo	1/LiFo	2/FiFo	-	Modified management of spent UOX fuels

Table 3.1: Strategy space of pre-disruption scenario

To achieve an efficient sampling in this 8-dimension variable space, Latin Hy-

percube Sampling (LHS) is used for the DoE [96, 97, 98]. To guarantee the dependence of D on t_{start}, a cut is done in the hypercube. A sampling with a size larger than 10000 is generated by software R [99], and 6401 are kept after the cut.

All these trajectories are simulated by CLASS. The results are graphically presented at the end of this section. Given the huge amount of data, we first try to extract statistically the important parameters for the outputs.

3.2.2 Introduction of principal component analysis: a flexible option to study the input-output relation of system of interest

As shown in Section 2.2, some methods of GSA , such as Morris method and Sobol indices, may be too complicated when the fraction of valid observations is uncertain or varies depending on the purpose of analysis. In this chapter, the method of Principal Component Analysis (PCA) is introduced, which is flexible regarding this complicated feature of validity.

PCA is a method of multivariate analysis, which can be applied directly to the valid samples selected by analyst. In principle, for a given variable vector of interest, PCA identifies the orthonormal linear transformations that can explain successively the maximal variances. Suppose a p-dimension original variable vector $\boldsymbol{X}$, whose correlation matrix is $\boldsymbol{C}$. PCA identifies the first variable Y_1, which is the normalized linear combination of these p original variables that maximizes the variance among all possible linear combinations. Then the second variable Y_2 of normalized linear combination is identified, which maximizes the variance among all possible linear combinations but subject to the orthonormality to Y_1. The iterative steps are carried out to identify one-by-one new variables as normalized linear combinations of original variables that maximize the variance, subject to the orthonormality to previously identified variables. p new variables, called Principal Component (PC), are then generated, denoted as Ys or a p-dimension variable vector $\boldsymbol{Y}$ in the subsequent analyses. The original variable vector $\boldsymbol{X}$ and the new variable vector of PCs $\boldsymbol{Y}$ can be written in a matrix form as

$$\boldsymbol{Y} = \boldsymbol{A}\boldsymbol{X}$$

or

$$\boldsymbol{X} = \boldsymbol{A}^{-1}\boldsymbol{Y} = \boldsymbol{A}^{t}\boldsymbol{Y}$$

where matrix $\boldsymbol{A}$ denotes the orthonormal transformation matrix, and its elements are denoted as α_{ij}. Because of the orthomormality, its inverse $\boldsymbol{A}^{-1}$ is its transposed $\boldsymbol{A}^{t}$.

It can be shown [100, 101] that under these criteria of variance maximization and the orthonormality, the variance of the j-th PC Y_j, is actually the j-th largest eigenvalue λ_j of the correlation matrix $\boldsymbol{C}$; the relevant linear combination is then the corresponding normalized eigenvector. Or equivalently,

$$\lambda_i = \max_{\boldsymbol{b}\perp\mathscr{P}_{i-1}} V(\boldsymbol{b}\boldsymbol{X}) = \boldsymbol{\alpha}_{i\cdot}\boldsymbol{X} \tag{3.1}$$

where $\mathscr{P}_{i-1}$ denotes the space created by $i-1$ previously identified PCs $(Y_1, Y_2, \ldots, Y_{i-1})$, V denotes the variance, and $\boldsymbol{\alpha}_{i\cdot} = (\alpha_{i1}, \alpha_{i2}, \ldots, \alpha_{ip})$ denotes the i-th row of $\boldsymbol{A}$. The correlation matrix of PCs $\boldsymbol{Y}$ is therefore a diagonal matrix $\boldsymbol{L} = diag(\lambda_1, \lambda_2, \ldots, \lambda_p)$.

Some analysts use covariance matrix instead of correlation matrix of $\boldsymbol{X}$ to deduce PCs. Numerical results can be quite different with respect to the choice, and so is the relevant interpretation of results. The huge difference of variability

of original variables in this work requires standardization according to their own variability, which implies the use of correlation matrix.

The total variance of original variables, denoted as V_{tot} in the following illustration, is usually used to represent the sum of variances of original variables. According to the definitions above, it is also the sum of variances of PCs:

$$V_{tot} = \sum_{i=1}^{p} V(X_i) = tr(\boldsymbol{C}) = \sum_{i=1}^{p} V(Y_i) = \sum_{i=1}^{p} \lambda_i = tr(\boldsymbol{L}) \tag{3.2}$$

where tr denotes the trace of matrix, and it equals to p in this work because PCs are deduced from correlation matrix $\boldsymbol{C}$. In some applications, the sum of few largest variances is quite approximate to V_{tot}. Those corresponding PCs can explain the major part of variability of $\boldsymbol{X}$. In this case, the original high-dimension of variable space can be reduced to a lower dimension space, so that the problem is simplified. But we will see it is never the case in our studies, showing that we do not have too many input parameters. Meanwhile, if the smallest variance of PCs λ_p is far smaller than V_{tot} (i.e. $\lambda_p << 1/p$), Y_p accounts for little variability of $\boldsymbol{X}$, implying a linear dependency among original variables [101]. In fact, the Y_p in this case can be regarded as a constant compared to global behavior of $\boldsymbol{X}$, which implies the correlation of original variables:

$$\sum_{i=1}^{p} \alpha_{pi} X_i = Y_p \approx \text{Constant} \tag{3.3}$$

Another feature of PC useful in our study, concerns the squared correlation of a given original variable X_i and a given PC Y_j, denoted as $\rho^2(X_i, Y_j)$. Evidently,

$$X_i = \sum_{j=1}^{p} \alpha_{ji} Y_j \tag{3.4}$$

According to the orthonormality of $\boldsymbol{A}$, the variance of X_i can be written as

$$V(X_i) = \sum_{j=1}^{p} \alpha_{ji}^2 V(Y_j) \tag{3.5}$$

and

$$\rho^2(X_i, Y_j) = \frac{\alpha_{ki}^2 V^2(Y_j)}{V(X_i)V(Y_j)} = \frac{\alpha_{ki}^2 V(Y_j)}{V(X_i)} \tag{3.6}$$

Equations 3.5 and 3.6 reveal together that $\rho^2(X_i, Y_j)$ can be interpreted as the fraction of variability of X_i explained by the variation of PC Y_j [100]. If it is near 1, X_i can be approximated by Y_j, which also means that a linear combination of original variables represented by Y_j shows a similar variation pattern as X_i. In this case, the coefficients of linear combination indicates the importance weight of original variables on Y_j as well as on X_i, because they share highly similar variation.

In this study, inputs and output are regarded as components of the original variable vector $\boldsymbol{X}$. According to the method above, $\rho^2(X_{out}, Y_j)$ (where X_{out} stands for the output variable) with respect to each PC Y_j is calculated, and the composition of the PC with the highest squared correlation coefficient is investigated.

3.2.3 Application of PCA to the analysis of pre-disruption scenario

3.2.3.1 Primary analysis on missload

Depending on the purpose of study, PCA can be applied to those observations determined after simulations. Before assessing strategies with respect to $R_{Subs}(t = 2090)$ and $TRU_{tot}(t = 2090)$, it is important to analyze the missloads of all sampled strategies.

All 6401 sample strategies are taken into account. The number of missloads in 2090, denoted as $N_{ML}(t = 2090)$ resulted from a strategy, is regarded as the output in this part of analysis. To simplify the notations, "year 2090" is omitted in this section; but it should be always noted that the observation of outputs of interest are always the one in the year 2090.

At the first glance on the histogram of N_{ML} in Figure 3.2, almost half of strategies meet plutonium shortages for MOX fabrication before 2090 ($N_{ML}(t = 2090) > 0$), while 3214 do not have missload.

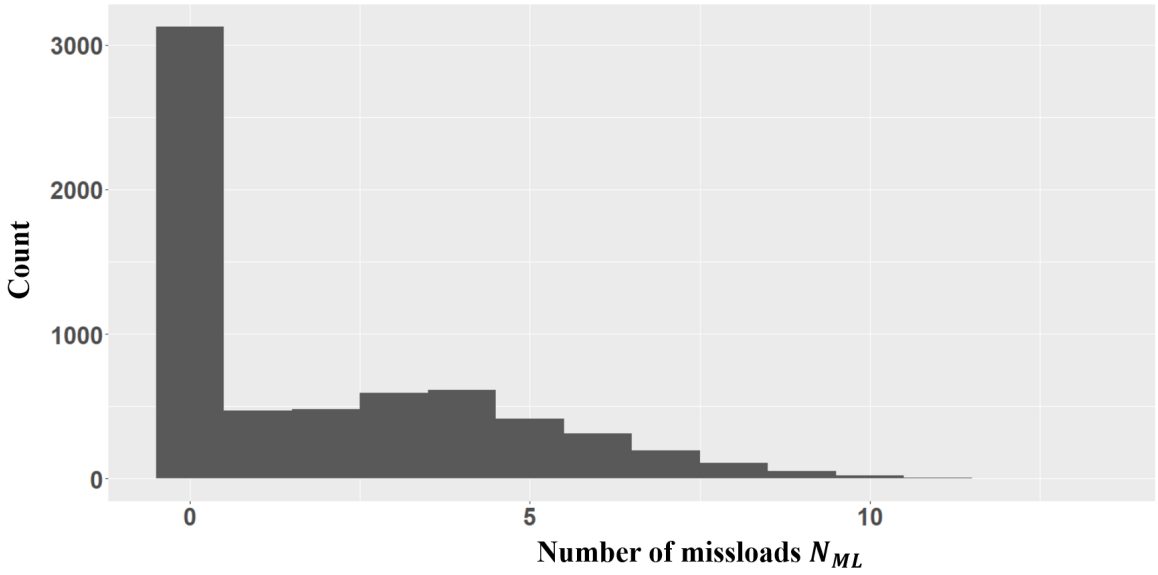

Figure 3.2: Histogram of number of missloads N_{ML} of static strategy samples

This proportion of missloaded strategies is measurable. Discarding the missloaded strategies is equivalent to remove a certain portion of input phase space. The dependencies of inputs can be shown by the correlation matrix of inputs before and after the cut of trajectories with missloads presented in Table 3.2. In this table, only the correlation coefficients larger than 0.1 are presented; the upper triangle contains the coefficients with respect to all 6401 samples, while the lower triangle corresponds to those 3124 samples without missload after the cut. When there is not cut of trajectories with missloads, only t_{start} and D presents a correlation coefficient larger than 0.1, which is created by the dependency of the preliminary cut that supposes $t_{start} + D < 2090$. Due to the use of LHS, other correlations are negligible, which are actually smaller than 0.03. The cut of trajectories with missloads mainly creates the correlation on the pair of $P_{tot,f}$-$FrMOX_f$, and the pair of $FrMOX_f$-BU_{UOX}, presented in lower triangle of Table 3.2. Subject to the plutonium availability, a relatively high $FrMOX_f$ requires a relatively low $P_{tot,f}$ to limit the consumption rate of plutonium in spent UOX fuels, and demands a relatively low BU_{UOX} so that plutonium in the stock of spent UOX can be accumulated efficiently. These correlations induced by the validity of trajectory are not surprising, but it shows the advantage of PCA relative to the Morris method presented in Chapter 2.

Cor. Coef.	t_{start}	D	$P_{tot,f}$	$FrMOX_f$	BU_{UOX}	BU_{MOX}	TC_{UOX}	MPu
t_{start}	1.	-0.24						
D	-0.23	1.						
$P_{tot,f}$			1.					
$FrMOX_f$			-0.24	1.				
BU_{UOX}				-0.21	1.			
BU_{MOX}						1.		
TC_{UOX}							1.	
MPu								1.

Table 3.2: Correlation matrix of input sampling: upper triangle considers all 6401 samples; lower triangle cuts off those with missloads and consider 3124 valid samples

To analyze the plutonium availability for MOX fabrication, the PCA is performed. The original variable vector $\boldsymbol{X}$ has nine components, including eight inputs and one output N_{ML}. Since PCA in this work depends on the correlation matrix of $\boldsymbol{X}$, it is useful to add the correlations between input and the output N_{ML}, as presented in Table 3.3. Only those (absolute value) larger than 0.1 are presented. PCs are then identified by calculating the eigenvalue-eigenvector pairs of the sampling correlation matrix of $\boldsymbol{X}$. Three metrics concerning PC are calculated:

- Individual fraction of total variance explained by Y_j: λ_j/V_{tot}
- Cumulative fraction of total variance explained by first j PCs: $\sum_k^j \lambda_k/V_{tot}$
- Squared correlation between the output N_{ML} and Y_j: $\rho^2(N_{ML}, Y_j)$

The results relevant to these metrics are presented in Table 3.4.

Input X_{in}	t_{start}	D	$P_{tot,f}$	$FrMOX_f$	BU_{UOX}	BU_{MOX}	TC_{UOX}	MPu
$\rho(X_{in}, N_{ML})$	-0.13	-0.11	0.19	0.79	0.19	-0.19		

Table 3.3: Correlation coefficients between input and the output N_{ML}

PC	Y_1	Y_2	Y_3	Y_4	Y_5	Y_6	Y_7	Y_8	Y_9
λ_j/V_{tot}	0.21	0.14	0.11	0.11	0.11	0.11	0.11	0.09	0.01
$\sum_k^j \lambda_k/V_{tot}$	0.21	0.35	0.46	0.57	0.68	0.79	0.90	0.99	1.00
$\rho^2(N_{ML}, Y_j)$	**0.94**	0.	0.	0.	0.	0.	0.	0.	0.05

Table 3.4: Statistical information of principal components in the PCA where $N_{ML}(t = 2090)$ one component of original variable vector

The rows of individual fraction λ_j/V_{tot} and cumulative fraction $\sum_k^j \lambda_k/V_{tot}$ indicate that at least eight PCs are necessary to account for most of the variability of original variable vector. It means that the correlations of original variables are globally weak. If a reduction of original variables is required, only one dimension can be removed. Y_9 explains extremely little the total variance. It indicates a potential linear dependency between the original variables in $\boldsymbol{X}$.

In regards to $\rho^2(N_{ML}, Y_j)$, Y_1 is sufficient to explain most of the variability of N_{ML}, as shown by $\boldsymbol{\rho^2(N_{ML}, Y_1)} = 0.94$ highlighted in red in the table.

According to these numeric results, Y_1 and Y_9 are two PCs of interest to investigate: Y_1 is strongly correlated with $X_{out} = N_{ML}$, while Y_9 has little variability that may imply linear dependency of original variables. The coefficients of original variables in the linear transformations Y_1 and Y_9 are shown in Table 3.5.

Coef. in Y_j	t_{start}	D	$P_{tot,f}$	$FrMOX_f$	BU_{UOX}	BU_{MOX}	TC_{UOX}	MPu	N_{ML}
Y_1	-0.09	-0.07	**0.16**	**0.64**	**0.16**	**-0.16**	0.09	-0.01	**0.71**
Y_9	**0.14**	**0.13**	**-0.16**	**-0.63**	**-0.15**	**0.15**	-0.07	-0.02	**0.70**

Table 3.5: Coefficients of original variables in the linear transformations of PCs Y_1 and Y_9, where $X_{out} = N_{ML}$

Table 3.5 shows that Y_1 is mainly composed of $FrMOX_f$ and N_{ML}, highlighted in bold in red. The variance of N_{ML} can be nearly explained by Y_1. The significant coefficient of $FrMOX_f$ implies that it affects strongly Y_1 and thus N_{ML}. This implication is coherent with the relatively strong correlation between $FrMOX_f$ and N_{ML} shown in Table 3.3. The composition of Y_9, which can be regarded as a constant, confirms the measurable effect of $FrMOX_f$ on N_{ML}. This effect is expected, because a high level of MOX fraction, requiring a huge inventory of plutonium, may keep stopping the loading of MOX until the end and provokes many missloads. The importance of other parameters such as $P_{tot,f}$, BU_{UOX} and BU_{MOX} are second order effect (highlighted in bold if the coefficient is larger than 0.1).

3.2.3.2 PCA on the outputs of interest with respect to the objectives

For the analyses of $R_{Subs}(t = 2090)$ and $TRU_{tot}(t = 2090)$, invalid strategies are cut off. Only the 3214 strategies without missload are considered valid. To simplify the notations, "year 2090" is omitted in this section for the evaluation of $R_{Subs}(t = 2090)$ and $TRU_{tot}(t = 2090)$. Histograms of these two outputs of interest for valid strategies are shown in Figure 3.3. For the explored valid strategies, R_{Subs} ranges from 0.58 to 1.68, and TRU_{tot} from 849 to 1666 tons. The range of R_{Subs} justifies the use of criterion $C_A^{t\text{-}set}$ to look for a maximal R_{Subs}: the upper bound of output space still indicates a reasonable margin for plutonium availability regarding objective A.

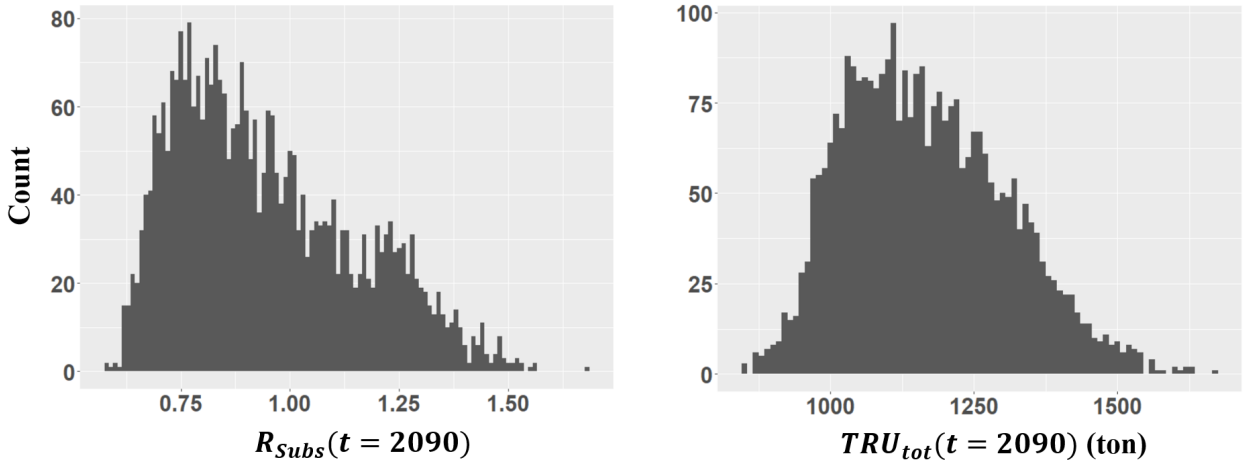

Figure 3.3: Histogram of $R_{Subs}(t = 2090)$ and $TRU_{tot}(t = 2090)$ resulted from valid trajectories without missloads. Bin width is 0.01 for $R_{Subs}(t = 2090)$ and 10 tons for $TRU_{tot}(t = 2090)$.

To investigate the relation of these output distributions to the inputs, PCA with respect to $X_{out} = R_{Subs}(t = 2090)$ and to $X_{out} = TRU_{tot}(t = 2090)$ are performed sepa-

rately. This separation allows focusing on the effect of inputs on one single output without the consideration of interaction between outputs. Before all, the correlation between input and the outputs R_{Subs} and TRU_{tot} are given in Table 3.6. Only those (absolute value) larger than 0.1 are presented. PCA are then performed on $\boldsymbol{X} = (t_{start}, \ldots, MPu, R_{Subs})$ and $\boldsymbol{X} = (t_{start}, \ldots, MPu, TRU_{tot})$ respectively.

Input $\boldsymbol{X_{in}}$	$\boldsymbol{t_{start}}$	$\boldsymbol{D}$	$\boldsymbol{P_{tot,f}}$	$\boldsymbol{FrMOX_f}$	$\boldsymbol{BU_{UOX}}$	$\boldsymbol{BU_{MOX}}$	$\boldsymbol{TC_{UOX}}$	$\boldsymbol{MPu}$
$\boldsymbol{\rho(X_{in}, R_{Subs})}$			-0.90		-0.18			
$\boldsymbol{\rho(X_{in}, TRU_{tot})}$			0.88	-0.45	-0.28			

Table 3.6: Correlation coefficients between input and the outputs R_{Subs} and TRU_{tot}

Similar to the analysis of missload, the overall variability of original variables explained by given PCs, represented by λ_i/V_{tot}, is not of interest, except the last one if it accounts little variation in comparison to the total variability. Instead, the variance of output of interest explained by PCs can give more information. In these two separate PCA, PCs are identified respectively. For each PC Y_j, λ_j/V_{tot} and $\rho^2(X_{out}, Y_j)$ are calculated for $X_{out} = R_{Subs}$ and $X_{out} = TRU_{tot}$ separately, presented in Table 3.7. Therefore, PCs in the PCA with respect to $X_{out} = R_{Subs}$ and those with respect to $X_{out} = TRU_{tot}$ are totally dissociate.

PC	$\boldsymbol{Y_1}$	$\boldsymbol{Y_2}$	$\boldsymbol{Y_3}$	$\boldsymbol{Y_4}$	$\boldsymbol{Y_5}$	$\boldsymbol{Y_6}$	$\boldsymbol{Y_7}$	$\boldsymbol{Y_8}$	$\boldsymbol{Y_9}$
$\boldsymbol{\lambda_j/V_{tot}|X_{out} = R_{Subs}}$	0.22	0.14	0.13	0.11	0.11	0.11	0.09	0.08	0.01
$\boldsymbol{\rho^2(R_{Subs}, Y_j)}$	**0.89**	0.02	0.04	0.	0.	0.	0.02	0.01	0.02
$\boldsymbol{\lambda_j/V_{tot}|X_{out} = TRU_{tot}}$	0.24	0.14	0.13	0.11	0.11	0.11	0.09	0.07	0.
$\boldsymbol{\rho^2(TRU_{tot}, Y_j)}$	**0.95**	0.01	0.02	0.	0.	0.	0.	0.	0.02

Table 3.7: Statistical information of PCs in separate PCA with valid observations

In both cases, their own first PC Y_1 can explain most of the variability of output, and last PC Y_9 has a relatively limited variability. The compositions of Y_1 and Y_9 in both PCAs are then investigated, and the coefficients are presented in Table 3.8.

Coef. in $\boldsymbol{Y_j}$	$\boldsymbol{t_{start}}$	$\boldsymbol{D}$	$\boldsymbol{P_{tot,f}}$	$\boldsymbol{FrMOX_f}$	$\boldsymbol{BU_{UOX}}$	$\boldsymbol{BU_{MOX}}$	$\boldsymbol{TC_{UOX}}$	$\boldsymbol{MPu}$	$\boldsymbol{X_{out}}$
$\boldsymbol{Y_1|X_{out} = R_{Subs}}$	0.02	0.05	**-0.68**	**0.23**	**-0.17**	-0.04	-0.03	0.	**0.67**
$\boldsymbol{Y_9|X_{out} = R_{Subs}}$	0.	0.	**0.69**	**0.19**	**0.18**	0.02	0.01	0.02	**0.68**
$\boldsymbol{Y_1|X_{out} = TRU_{tot}}$	-0.07	-0.07	**0.61**	**-0.39**	**-0.10**	-0.05	0.05	0.01	**0.67**
$\boldsymbol{Y_9|X_{out} = TRU_{tot}}$	0.02	0.01	**-0.59**	**0.24**	**0.25**	0.03	0.	0.	**0.72**

Table 3.8: Coefficients of original variables in the PCs of interest, with $X_{out} = R_{Subs}$ and $X_{out} = TRU_{tot}$ in separate PCA

For both outputs, coefficients of $P_{tot,f}$ and X_{out} are the most significant in the PCs of interest. In other words, $P_{tot,f}$ is the most important parameters on these two outputs of interest. As revealed in Section 2.2, the power level has a direct effect on R_{Subs} according to the definition, and TRU_{tot} is an extensive quantity. Therefore, $P_{tot,f}$, which determines the final magnitude of power level of fleet, has dominant impacts in terms of both the capacity of SFR substitution and the TRU inventory accumulated in the whole cycle. As Y_9 for two PCAs are nearly constant, the sign of coefficients of $P_{tot,f}$ and X_{out} imply that $P_{tot,f}$ has negative

correlation with R_{Subs} and positive correlation with TRU_{tot}, which are coherent with the previous analyses.

In addition, the coefficients of $FrMOX_f$ and BU_{UOX} are not negligible. As indicated, they have similar influence on the production of plutonium, and thus on R_{Subs} and TRU_{tot}. Similarly, the sign of coefficients in Y_9 for two PCAs indicate that these two inputs have statistically negative correlation with R_{Subs} and TRU_{tot}. Their non-negligible coefficients may also reveal the combined effects with $P_{tot,f}$ on the two outputs.

In summary, $FrMOX_f$ is the primary factor that induces the number of missloads, and other parameters including $P_{tot,f}$, BU_{UOX} and BU_{MOX}, as well as the timing factors of transition t_{start} and D, have a secondary effects on the missload. For both outputs of interest R_{Subs} and TRU_{tot}, $P_{tot,f}$ is always the most important input, while $FrMOX_f$ and BU_{UOX} may have some measurable effects. In these cases, the analysis of missload considers all simulated trajectories, while the studies with respect to R_{Subs} and TRU_{tot} focus on the ones without missloads.

3.2.3.3 Discussion on the use of PCA

As demonstrated in previous analyses, PCA is flexible regarding the determination of valid sampling. One should note the difference between the results with PCA and the ones in the analysis with Morris method in Section 2.2. Some can be explained by the differences in the phase space and the time horizon of scenarios. It may be also due to the rejection of invalid strategies. For example, the derivatives of outputs with respect to input $P_{tot,f}$ by Morris method are widely disperse, because the standard deviation is even larger than the mean in Figure 2.12. In this Morris analysis, the outputs do not follow the linear trend with $P_{tot,f}$, mainly due to the interaction with other inputs such as t_{start}, D and $FrMOX_f$. However, in the PCAs where missloaded trajectories are cut, a strong linearity can be observed between $P_{tot,f}$ and the outputs as presented in Table 3.6.

To perform PCA, the correlations between inputs and outputs are calculated. One may prefer using directly those correlation coefficients between input and outputs of interest, which are much more simple to interpret. In this study, PCA is also used because correlation coefficient does not consider the interaction with other inputs. For example, one may think that $FrMOX_f$ do not have any effect on R_{Subs} due to a correlation coefficient equal to 0.03. On the contrary, PCA reveals the symbiotic effects of inputs, including $FrMOX_f$, on the output R_{Subs}.

The main shortcoming of PCA is that it cannot deal with the non-linear relations, since it is based on the covariance/correlation matrix. For instance, an output Y is a square function of input X which is uniformly distributed in [-1,1]. Their correlation matrix is then an identity matrix. Evidently, Y and X are also PCs; in this case, PCA cannot reveal the dependency of Y on X. To complement, we use graphical techniques in the following analyses, in order to verify if some non-linear relations between outputs of interest and inputs have been missed.

3.2.4 Complement of analysis of input-output relation with graphical representations

PCA in this scenario study is able to regroup the input parameters according to their importance on the outputs of interest. In this exercise, graphical techniques are used, principally the pairs plots, to qualify the impacts of inputs on the outputs, and to verify the results of PCA. For N_{ML}, the most important input is $FrMOX_f$, while t_{start}, D, $P_{tot,f}$, BU_{UOX} and BU_{MOX} have measurable effects and

may interact with each other. For both R_{Subs} and TRU_{tot}, $P_{tot,f}$ is dominant, while $FrMOX_f$ and BU_{UOX} may have some non-negligible effects. With respect to the output, inputs leading to measurable changes are grouped and plotted by pairs, so that their effects on the output and the interaction with each other can be presented. Those negligible ones are plotted versus the outputs, so their limited contribution on the variation of output can be verified.

The plots concerning N_{ML} are shown in Figure 3.4. The color in the pairs plot of Figure 3.4a is blue-to-red depending on N_{ML}, which can be viewed in the columns and rows of N_{ML}. Near-blue points denote the strategies leading to small N_{ML}, while near-red points denote the strategies to high N_{ML}. To simplify the visualization, those without missload are in grey. In the pairs plot, the impacts of these six inputs on N_{ML} are verified and visualized. The boundaries between valid strategies ($N_{ML} = 0$) and invalid ones ($N_{ML} > 0$) are clearly shown, mainly characterized by $FrMOX_f$ and its correlation with other input variables. High-N_{ML} points are concentrated in the zone of early t_{start}, short D, high $FrMOX_f$, high BU_{UOX} and low BU_{MOX}. For $FrMOX_f$ and BU_{UOX} it is well explained in the relevant PCA. For time-related variables, early t_{start} and short D may emphasize the plutonium shortages when $FrMOX_f$ and BU_{UOX} are high. BU_{MOX} also influences N_{ML} because low BU_{MOX} implies a short irradiation cycle of MOX. When the plutonium from spent UOX fuels meets a long-term shortage, short irradiation cycle leads to higher number of missloads within the same time horizon. Figure 3.4b verifies the limited effect of TC_{UOX} and MPu on N_{ML}. Actually, TC_{UOX} still has some visible effects on N_{ML}, due to the fact that a long TC_{UOX} delays the supply of available plutonium for MOX fabrication and reduces the plutonium quality ($^{241}\mathrm{Pu}$ decays to $^{241}\mathrm{Am}$). But this influence is far lower than other important inputs. For MPu, the patterns of two colors of points are not distinguishable.

Plots for the outputs R_{Subs} and TRU_{tot} are shown in Figure 3.5 and 3.6 respectively. Similarly, the colors in the two pairs plots are blue-to-red depending on the values of respective output, which can be viewed by the columns and rows of the outputs. Figure 3.5a and 3.6a verify the dominance of $P_{tot,f}$ on these two outputs (clear correlations), those measurable effects of $FrMOX_f$ and BU_{UOX}, and the effects of their interactions. Figure 3.5b and 3.6b verify that the other five inputs have limited effects. A slight tendency of TRU_{tot} convergence over t_{start} and D can be observed in Figure 3.6b. It is due to the timing effect discussed in Section 2.2. Later t_{start} delays the transition and longer D mitigates the variations of transition. As the observation time is set, the later and the longer is the transition, the smaller is the output variability due to the transition. It converges to the state of current French fleet for very late and slow transitions. The time effect, which is not linear to the outputs, cannot be revealed by PCA. This is typically an area where scatter plots can be complementary.

One should note that the negligible effects of inputs shown in this section does not mean that the outputs of interest are independent on these inputs. In this global analysis, the variability of inputs, indicated by their ranges considered in the scenario, is crucial to relevant evaluations. For example, the change of two outputs of interest, R_{Subs} and TRU_{tot}, are mainly driven by input $P_{tot,f}$ in this pre-disruption scenario. One extreme case is that the variability of $P_{tot,f}$ is quite small in another study, even it can be seen as constant. It is evident that the change of outputs can be driven by other factors than the slight fluctuation of the power level. Therefore, the effects of inputs on the output depends also intrinsically on the hypotheses of scenario, especially the distribution of input parameters.

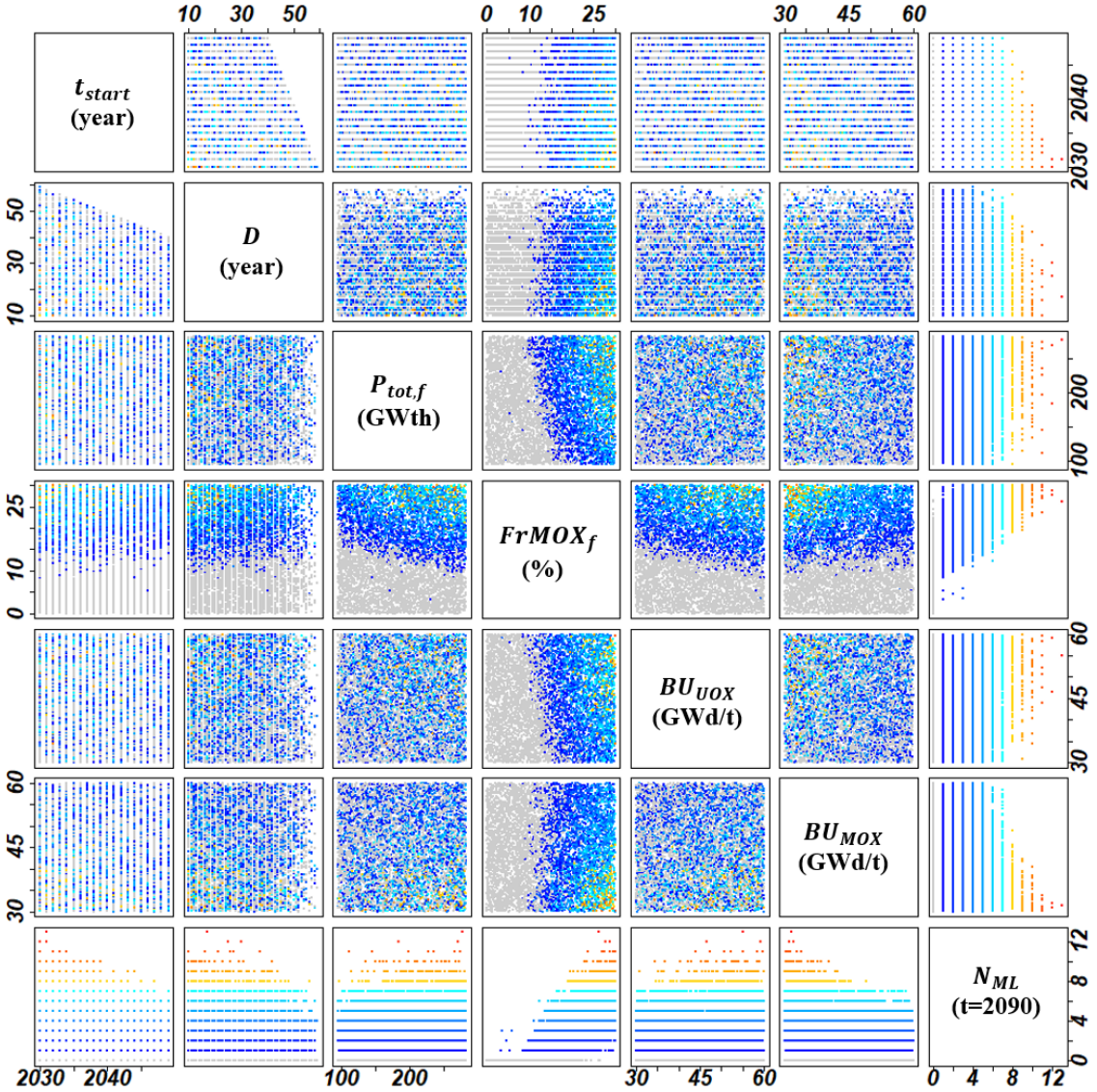

(a) Pairs plots of t_{start}, D, $P_{tot,f}$, $FrMOX_f$, BU_{UOX}, BU_{MOX} and N_{ML}, colored blue-to-red by N_{ML}; grey points represent the strategies without missload

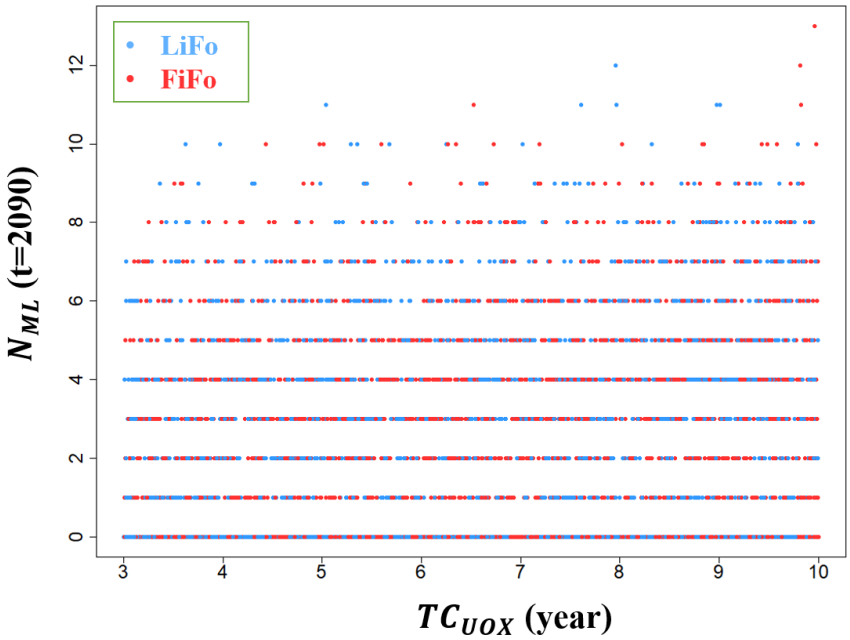

(b) N_{ML} vs TC_{UOX}, over MPu

Figure 3.4: N_{ML} vs input variables

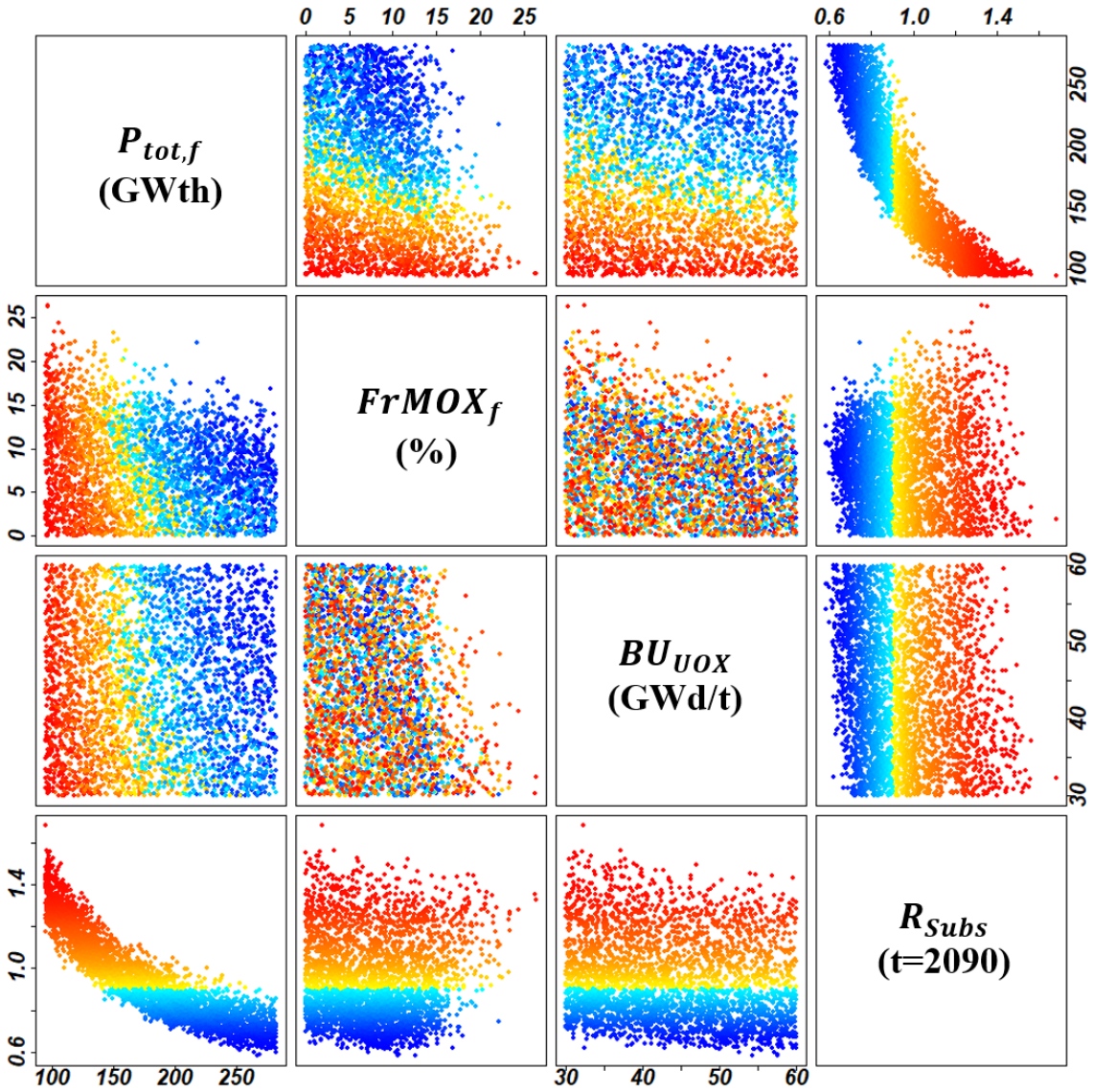

(a) Pairs plots of $P_{tot,f}$, $FrMOX_f$, BU_{UOX} and R_{Subs}, colored blud-to-red by R_{Subs}

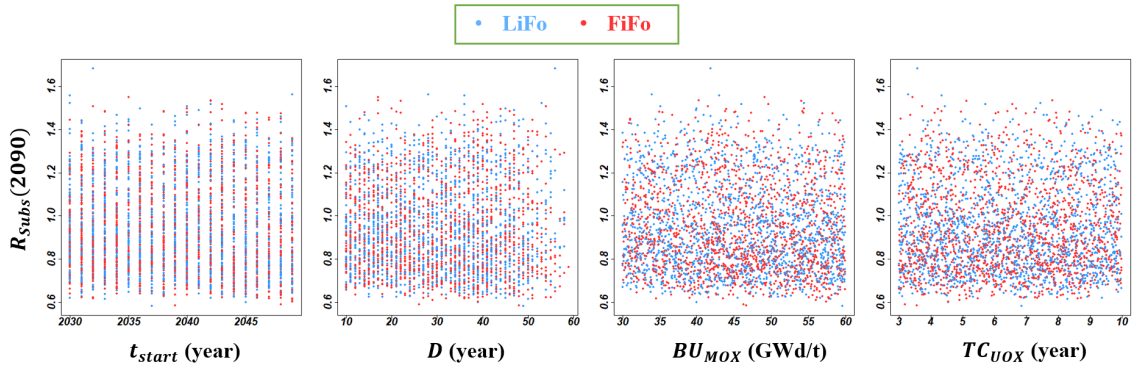

(b) R_{Subs} vs t_{start}, D, BU_{MOX} and TC_{UOX}, over MPu

Figure 3.5: R_{Subs} vs input variables

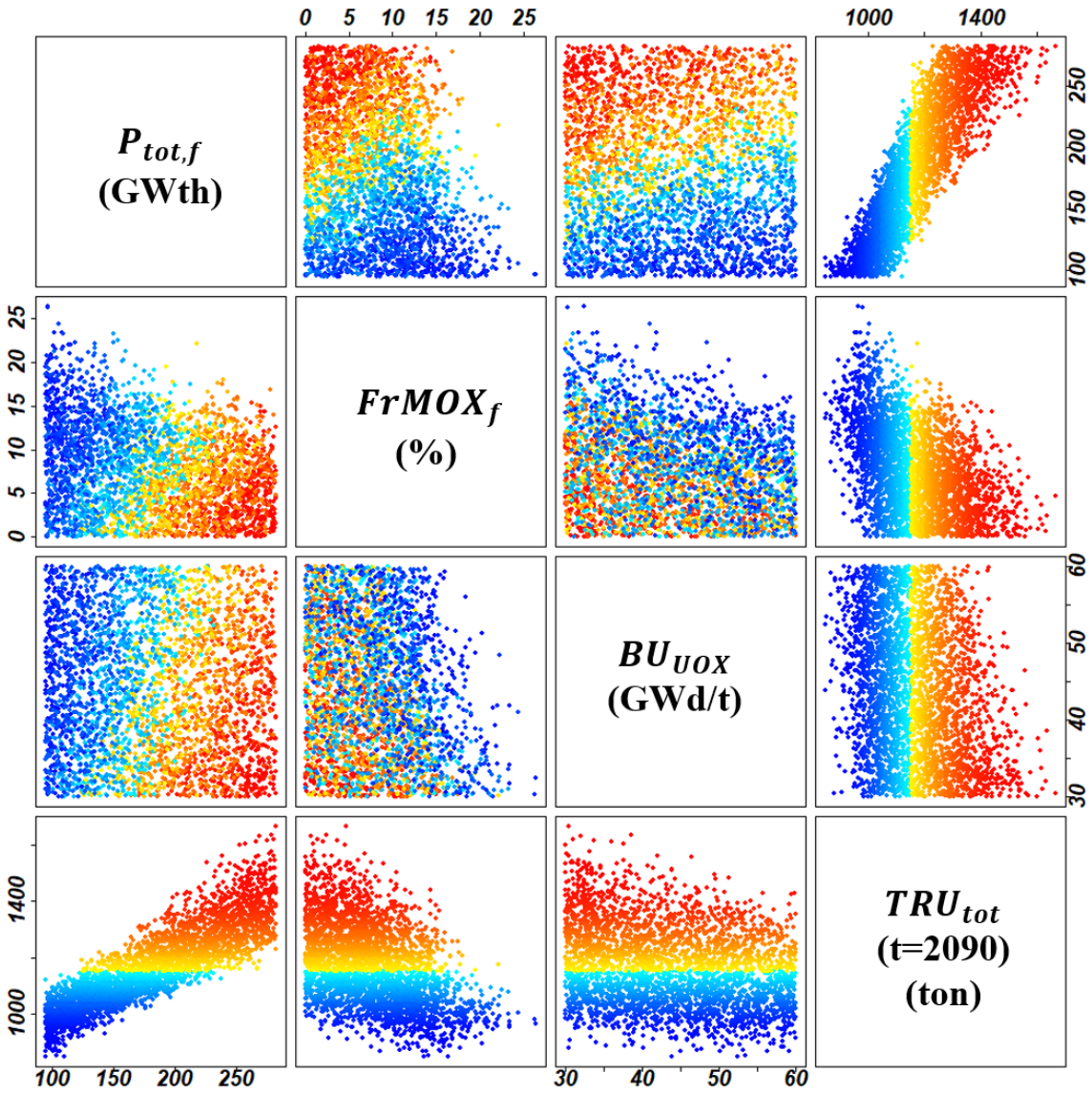

(a) Pairs plots of $P_{tot,f}$, $FrMOX_f$, BU_{UOX} and TRU_{tot}, colored blue-to-red by TRU_{tot}

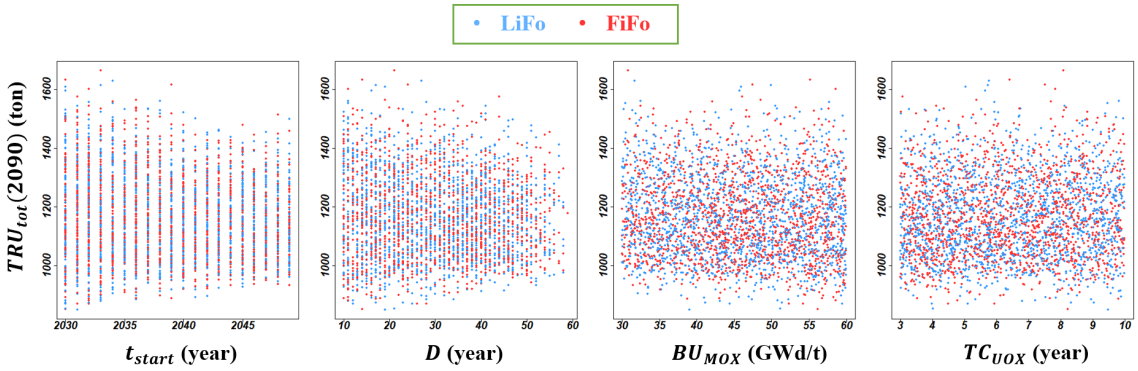

(b) TRU_{tot} vs t_{start}, D, BU_{MOX} and TC_{UOX}, over MPu

Figure 3.6: TRU_{tot} vs input variables

3.2.5 Static robustness assessment and focus on particular cases

As illustrated in Section 3.1, numeric criteria are used to determine strategies of interest, including the optimal static strategy and robust static strategies. Given the basic understanding of input-output relations in the last subsection, we can analyze the strategies of particular interest.

3.2.5.1 Static robustness: assessment of static strategies

The assessment of strategies depends on the evaluation of outputs of interest according to the criteria. For valid static strategies without missload sampled in the pre-disruption scenario, the substitution ratio R_{Subs} and the TRU inventories in the total cycle TRU_{tot} in 2090 are plotted in Figure 3.7. The point color represents the level of $P_{tot,f}$ of each corresponding strategy. The figure shows clearly the impact of $P_{tot,f}$ on these two outputs. It seems to show a linear relation between R_{Subs} and TRU_{tot} for each given level of $P_{tot,f}$. The slope of their linearity depends strongly on $P_{tot,f}$. Actually, if $P_{tot,f}$ is constant, R_{Subs} is proportional to in-cycle plutonium inventory in this case which accounts for the major part of TRU_{tot}.

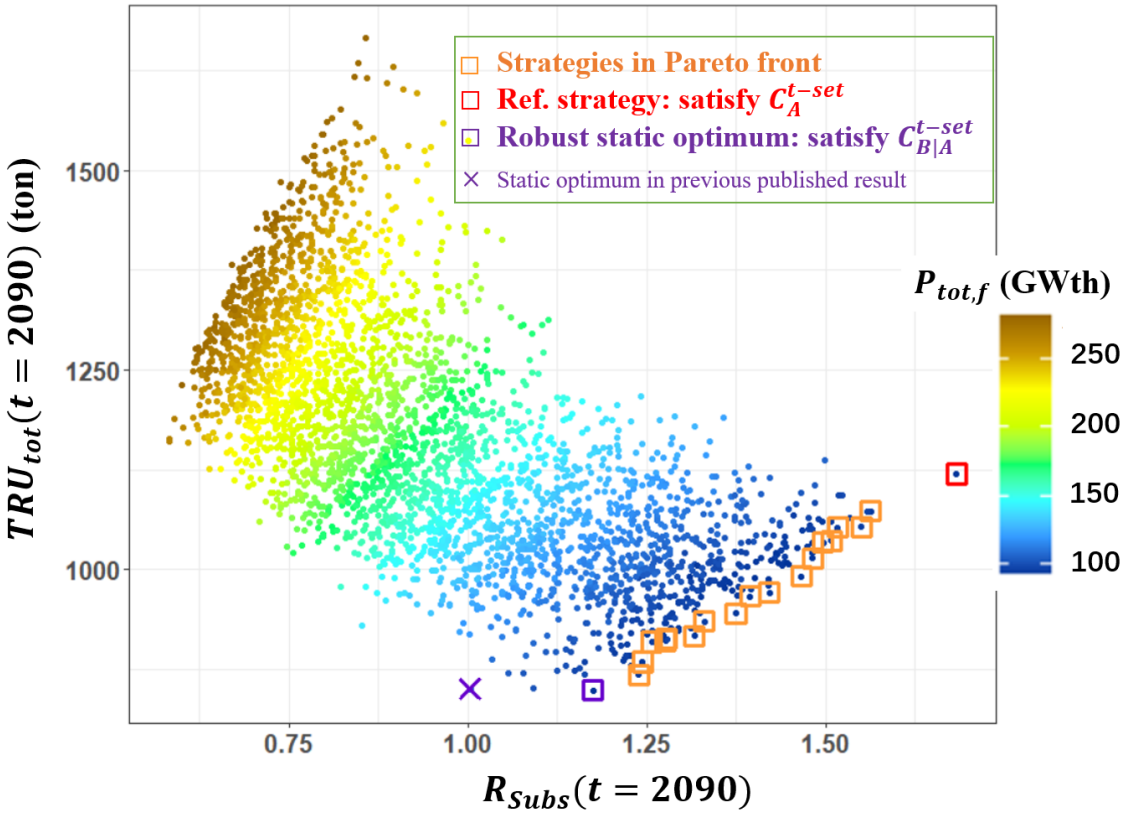

Figure 3.7: TRU_{tot} vs R_{Subs} by 2090 of valid static strategies, colored by input $P_{tot,f}$

To assess their robustness, the strategies are defined as "of interest" if a given numeric output satisfies a comparison to an arbitrary threshold which represent a goodness level of strategy performances [47]. In this study, a threshold for $R_{Subs} = 1$ makes sense, indicating that the strategy can complete substitution of PWR fleet with future SFRs. This threshold is employed in the criterion $C_{B|A}^{t\text{-}set}$. In contrast, the threshold for TRU_{tot} is somehow not well defined. It should depend on the evaluation of related geological wastes disposal projects and introduces many other constraints and uncertainties, which is out of the scope of this work.

Otherwise, we can use statistical metrics, such as percentiles [92] or optimization in the sampling to define values for the criteria in robustness assessments.

Here, the maximization of R_{Subs} and minimization of TRU_{tot} are employed respectively in criteria $C_A^{t\text{-}set}$ and $C_B^{t\text{-}set}$. Moreover, subject to the priority of objective A, it is reasonable to add a conditional constraint of $R_{Subs} > 1$. According to the criteria employed in this study and the priority given to objective A, strategies in the Pareto front under $R_{Subs} > 1$ can be assessed as robust strategies. In Figure 3.7, a Pareto front is shown in consideration of these two optimization criteria, represented by the points surrounded by squares. R_{Subs} of these strategies ranges in [1.18, 1.68] (satisfying the condition $R_{Subs} > 1$), while TRU_{tot} ranges in [849, 1120] tons. These results of Pareto front depend directly on the DoE in this scenario study.

The zone is bounded by two extreme cases. According to the criteria $C_{B|A}^{t\text{-}set}$ and $C_A^{t\text{-}set}$ defined previously, we define the robust static optimum as the strategy in purple square and the reference strategy in red square, which are discussed in the following subsection. One may note that the robust static optimum in this study is different from the one in previously published study in [102] which is represented by purple cross in Figure 3.7. This specific strategy is also discussed in the subsequent analysis to highlight the effects of different simulation hypotheses on the simulation results as well as the assessment.

Strategies in Pareto front reveal the trade-offs between two objectives: each of them cannot be improved for one objective if the performance on another objective is not sacrificed. In multi-objective problem, this zone corresponds to the set of optimal strategies. Each of them leads to the highest R_{Subs} among those leading to lower TRU_{tot}, and leads to the lowest TRU_{tot} among those leading to higher R_{Subs}. The Pareto front means that if the deep uncertainty of objective keeps till the end, the largest achieved R_{Subs} in our DoE equals to 1.68, implying a margin of plutonium availability for objective A among static strategies of 68%. At the same time, the lowest achieved TRU inventories in total cycle with the possibility of achieving objective A is 849 tons. This high R_{Subs} and low TRU_{tot} cannot be achieved simultaneously; instead, trade-offs should be made among the robust static strategies in the Pareto front.

Two outputs and the important inputs $P_{tot,f}$, $FrMOX_f$ and BU_{UOX} of these strategies are shown in the parallel plot of Figure 3.8. The axes of the three inputs are normalized by their sampling ranges. Each connected line characterizes the same strategy, which is colored by blue-to-red levels of outputs. Near-blue lines indicate the low values of R_{Subs}/TRU_{tot}, while near-red lines means the high values. We show again the near-constant low $P_{tot,f}$ in the Pareto front, which is a direct result of our DoE. Given the very similar power level, R_{Subs} and TRU_{tot} of strategies in this zone presents a strong correlation, principally affected by the in-cycle plutonium inventories by 2090. The trade-offs between the maximization of R_{Subs} and the minimization of TRU_{tot} can be realized by the control on $FrMOX_f$ and BU_{UOX}, both of which plays a similar role on the in-cycle plutonium inventories.

3.2.5.2 Focus on specific strategies

One may be interested in the result of the continuation of current French fleet. By 2090, 865 tons of plutonium are accumulated in the cycle, which correspond to $R_{Subs} = 0.83$ with respect to a $P_{tot,f} = 188.1$ GWth, and $TRU_{tot} = 1139$ tons are accumulated. Evidently, the continuation of the current fleet cannot achieve objective A, and the accumulation of TRU inventories in the total cycle is far higher than the lowest achieved in this DoE.

In the Pareto front, two particular strategies are of specific interest. One is the strategy that satisfies criterion $C_A^{t\text{-}set}$, which maximizes R_{Subs} by 2090 among all valid ones and represents one extreme case in the front. It is shown as the point

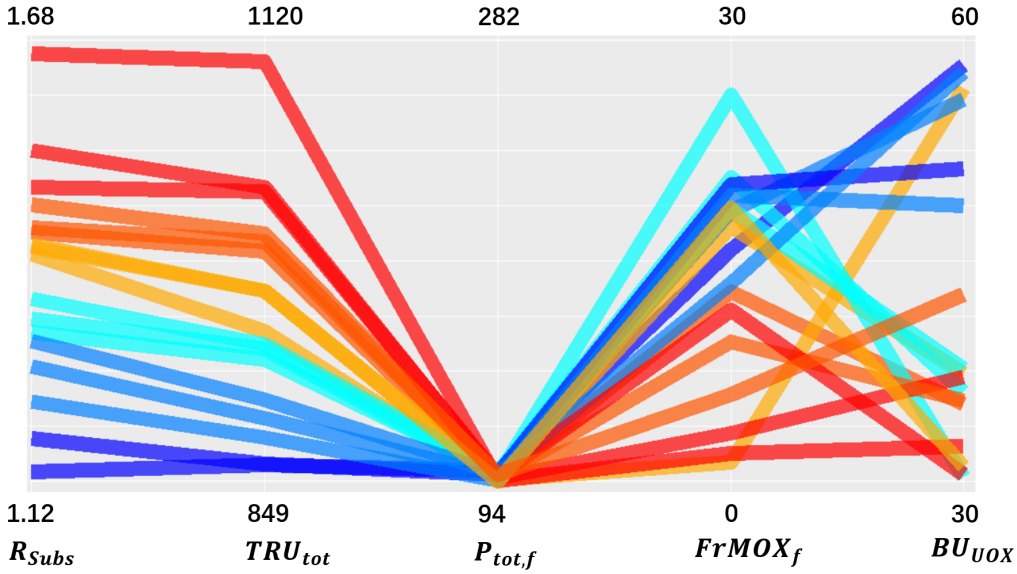

Figure 3.8: Parallel plot of important inputs $P_{tot,f}$, $FrMOX_f$ and BU_{UOX}, and the outputs R_{Subs} and TRU_{tot} of strategies in the Pareto front

surrounded by a red square in Figure 3.7. If the uncertainty of objective is not considered, it is the optimal strategy for objective A; in this case, this strategy is highly possible to be implemented for future SFR deployment. Hence, it is called *reference strategy* in the following of this chapter. It neglects objective B and accumulates high TRU_{tot} in 2090 compared to other strategies in the Pareto front.

The values of inputs and outputs are presented in Table 3.9. According to the reference strategy, $P_{tot,f}$, $FrMOX_f$ and BU_{UOX} are close to the lower bounds of variation ranges, maximizing R_{Subs} and accumulating efficiently plutonium. This confirms the results from [86] which shows that $FrMOX_f$ and BU_{UOX} are two main factors for plutonium production. This strategy also suggests an early transition from year 2032 and the long period of 56 years, so that the reduction of MOX fraction starts early and plutonium production by UOX can be kept relatively high during long time. This t_{start}-D pair implies that the transition lasts as long as possible, and thus it is also close to the bound in terms of these two input variables.

Strategy	t_{start}	D	$P_{tot,f}$	$FrMOX_f$	BU_{UOX}	BU_{MOX}	TC_{UOX}	MPu	R_{Subs}	TRU_{tot}
Ref.	2032	56	94.6	1.94%	32.4	41.9	3.6	LiFo	1.68	1120
Rob. stat. op.	2031	19	94.3	16.31%	43.9	39.0	9.5	LiFo	1.18	849
Prev. stat. op. in [102]	2030	14	109.4	13.58%	52.5	56.2	8.2	FiFo	1.00	851
Unit	year	year	GWth	%	GWd/t	GWd/t	year	-	-	ton

Table 3.9: Values of inputs and outputs of particular strategies, calculated in this study: reference strategy, robust static optimum, and the static optimum identified in the previous published study [102]

The other extreme case in Pareto front satisfies criterion $C_{B|A}^{t\text{-}set}$, and is shown as the point surrounded by a purple square. Among all valid strategies allowing $R_{Subs} > 1$, it minimizes TRU_{tot}. It means that this strategy takes the most precaution regarding the uncertain disruption of objective while it preserves the theoretical availability of plutonium for objective A. Therefore, it is called *robust static optimum* in the subsequent analysis, where "optimum" stands for the viewpoint of precaution to disruption. The values of inputs and outputs are presented in Table 3.9. $P_{tot,f}$ of this strategy is low and $FrMOX_f$ is relatively high, so that

a relatively high R_{Subs} can be achieved while large quantity of plutonium can be incinerated by MOX depletion, minimizing the plutonium inventory in 2090. The transition starts early from year 2031 and lasts for a short time, for 19 years. Limited production of plutonium by UOX and relatively high incineration by MOX can then be achieved as soon as possible. In 2090, 18% of margin is preserved for objective A and only 849 tons of TRU are accumulated in the total cycle. These input values indicate an optimal transition that minimizes the consequence of objective disruption. It can be regarded as an acceptable level even if no readjustment is taken. Note that the limit of validity is mainly driven by $FrMOX_f$ and its interaction with $P_{tot,f}$, as shown by the boundary between the zone of blue points and the grey points in pairs plots with output R_{Subs} and TRU_{tot} in Figure 3.4a. The $P_{tot,f}$-$FrMOX_f$ pair of this strategy is quite close to the border of validity. The high risk of plutonium shortage for MOX fabrication by 2090 is verified by the plutonium evolution in the interim stock of spent UOX in Figure 3.9. Due to the high MOX fraction, the inventory of available plutonium in the stock of spent UOX decreases progressively, reaching 4 tons by 2090. Here the importance of time horizon in simulation should be highlighted. If extended to 2100, it is highly possible that this strategy would have been rejected due to the missload between 2090 and 2100.

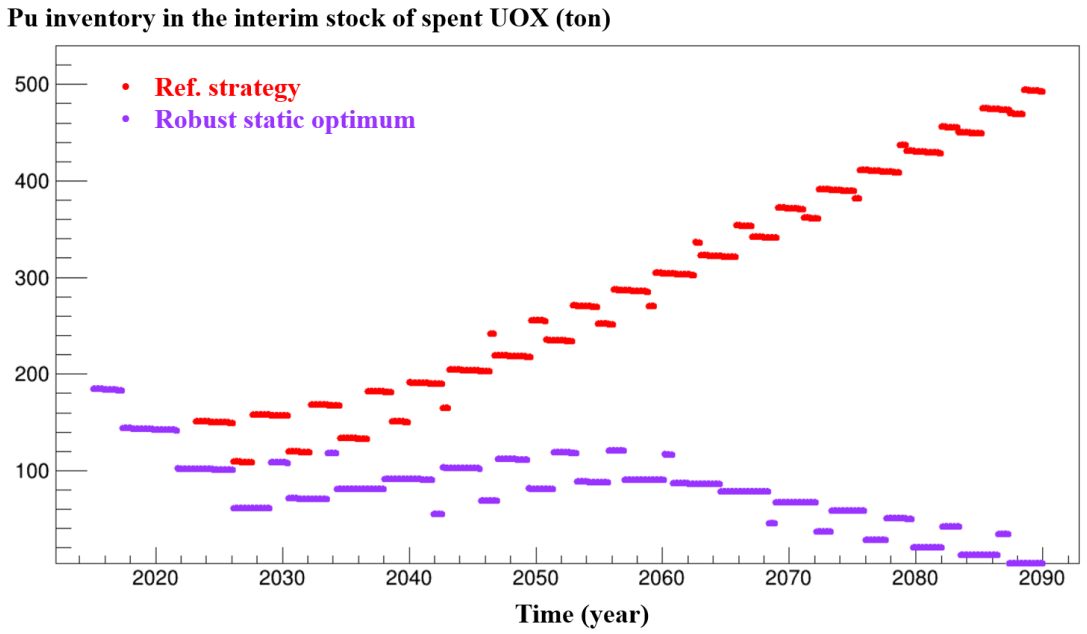

Figure 3.9: Evolution of plutonium inventory in the interim stock of spent UOX, resulted from the reference strategy and the robust static optimum

The relevant results of robust static optimum published in the previous study [102] is different from the one identified here. To distinguish those two strategies, the previous one is called *previous static optimum* in this comparison, represented as the point covered by a purple cross in Figure 3.7. Its inputs and outputs calculated in this study are shown in Table 3.9. Actually, the previous study employs slightly different hypotheses of depletion parameters in reactor modelling (mainly the specific power), which affects the length of irradiation cycle and thus the timing of transition. Due to the respect of irradiation cycle, a slight difference on the transition timing can lead to some discrepancies of output, such as TRU_{tot}. Nevertheless, these two strategies, the robust static optimum in this study and in the previous one, lead to an extremely similar TRU_{tot}, with a very small difference that is compatible with the errors mentioned in Section 3.1. More importantly, there seems to be a flat boundary of constant TRU_{tot}

over R_{Subs} in Figure 3.7, where the strategies nearby are quite close to the invalid zone. It may indicate additional trade-offs between significant risk of missloads and limited gain on TRU_{tot} but with a considerable change of R_{Subs}. One may therefore prefer a much higher R_{Subs} while sacrificing little gain on TRU_{tot}.

In respect with the numeric results in this study, the strategy of robust static optimum identified here is considered for the following analysis.

To complement, the evolution of R_{Subs} and TRU_{tot} over time of these three particular strategies (reference strategy, robust static optimum and the previous one) are shown in Figure 3.10. R_{Subs} of these three trajectories increases over time, mainly due to the reduction of power level during transition besides the accumulation of plutonium in cycle. Several jumps of discontinuities result from the changes of power level of macro reactors during transition, and thus justify the contribution of power reduction on the increase of R_{Subs}. On the contrary, calculations of our DoE not presented here but analyzed during my Ph.D show that strategies supposing measurable increase of power level lead to decreasing R_{Subs}, regardless the plutonium accumulation in cycle. Evolution of TRU_{tot} in Figure 3.10b verifies that TRU_{tot} of robust static optimum identified in this study and the old one in previous study are really close.

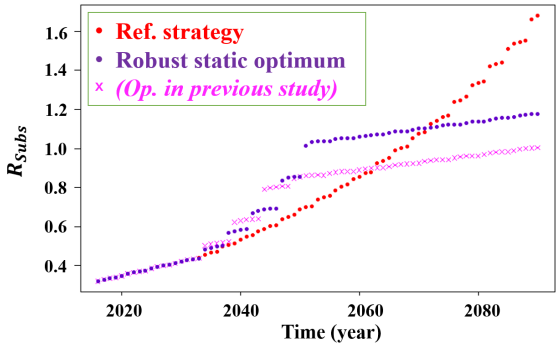

(a) Evolution of R_{Subs} of three particular strategies of interest

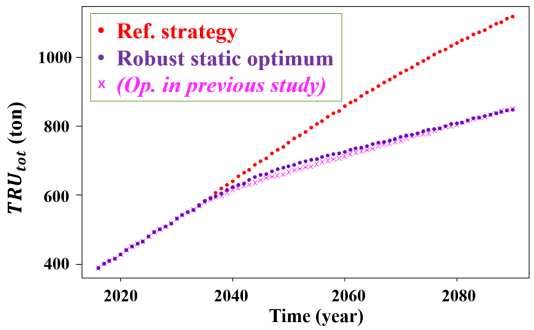

(b) Evolution of TRU_{tot} of three particular strategies of interest

Figure 3.10: Evolution of R_{Subs} and TRU_{tot} of three particular strategies of interest

3.2.6 Conclusion of the analysis of pre-disruption scenario and the static robustness assessment

In this section, a pre-disruption scenario which pre-selects the objective A and retains a doubt of disruption towards objective B is described. Possible strategies are explored, and they are viewed static because the disruption of objective is always deeply uncertain. This scenario sets the time horizon by 2090, the observation time on which the evaluation of outputs of strategies depends. Assessment of static strategies is therefore able to give an insight of possible consequences regarding two objectives under this context.

First, PCA is introduced to analyze the responses of missloads and outputs of interest with respect to the two objectives. It is shown that the number of missloads N_{ML} is quite sensitive to the final MOX fraction of fleet $FrMOX_f$.In terms of two outputs of interest R_{Subs} and TRU_{tot}, $P_{tot,f}$ is dominant while $FrMOX_f$ and BU_{UOX} have measurable effects.

With the understanding of this fuel cycle physics, static robustness is assessed for valid strategies. According to the optimization criteria, Pareto front of strategies is found, presenting trade-offs with respect to the contraction between two objectives. In this study, strategies in Pareto front are regarded as robust static

strategies. In the front, two particular cases are identified. One is the reference strategy that satisfies criterion $C_A^{t\text{-}set}$, maximizing R_{Subs} without consideration of performance regarding TRU_{tot}, which means that it is the optimal strategy in mono-objective problem concerning the future SFR deployment. The other one is the robust static optimum that satisfies criterion $C_{B|A}^{t\text{-}set}$, which minimizes TRU_{tot} among all strategies that allow $R_{Subs} > 1$. It means that by preserving the possibility to achieve objective A with a margin of 18%, it takes the most conservative action regarding the uncertain disruption of objective. These two cases mark the boundaries of possible consequences of uncertain disruption, and tradeoffs can be made among robust static strategies in the Pareto front according to the interests of stakeholders.

One important remark in this study is the role of the input variable $P_{tot,f}$: it is so dominant that R_{Subs} can be so different even the in-cycle plutonium inventories are similar in two strategies. One example is that the reference strategy leads to an accumulation of 879 tons of plutonium in the cycle, and $R_{Subs} = 1.68$ with $P_{tot,f} = 94.6$ GWth; whereas the continuation of current fleet will accumulate 865 tons but leads to $R_{Subs} = 0.83$ since $P_{tot,f} = 188.1$ GWth. One may doubt that the power level cannot be controlled in such a large variability to respond to the objective; instead, it should be adjusted, subject to the energy demand and political policies related to the deployment of other energetic technologies. Actually, the variability of controllable parameters are parts of hypotheses of this scenario. Results and interpretations of this study should be connected with these hypotheses. As highlighted in the study of system by PCA, importance of inputs depends on their variation ranges, and so is the assessment of strategies. Meanwhile, all stakeholders are supposed to be involved in this scenario, including scientific and economic analysts, industry sectors, politicians, public, etc. Since the objectives are simplified by dualization, the variability of $P_{tot,f}$ makes sense but subject to hypotheses aforementioned, and so is its effect on the outputs of interest in this study.

3.3 Adaptation scenario and adaptive robustness assessment

In the last section, strategies without any adaptation have been assessed in a pre-disruption scenario, where the deep uncertainty of objective is always present. In this section, adaptation scenarios are studied: the disruption of objective is supposed to happen, and parameter adaptations for objective B are allowed. In other words, the objective A is no longer a priority, and SFR deployment is out of consideration. Instead, after disruption, the minimization of TRU inventories in total cycle, objective B, becomes the only objective. Within the hypothesis of time-set horizon, the objective B is also connected with the time of evaluation, year 2090. In this context, adaptive robustness is assessed for adaptive strategies in comparison with the robust static optimum identified in the pre-disruption scenario, which represents the best historical choice subject to the objective disruption.

Even though the $C_B^{t\text{-}set}$ with respect to objective B after disruption is an optimization criterion, it is necessary to use a threshold criterion in this study to answer the question of preferability between static or adaptive strategies. In pre-disruption scenario, threshold criterion is not used for objective B, because it lacks a reference level and the threshold can be uncertain, subjective and out of context. In contrast, if disruption is supposed and adaptation is allowed, the

robust static optimum identified in the pre-disruption context, implies a deterministic level used for comparison. In this case, the performance of the robust static optimum, equal to $TRU_{tot}(t = 2090) = 849$ tons, can serve as a threshold for adaptive robustness assessment, denoted as $TRU_{th,ad}$. If an adaptive strategy has a better performance, i.e. leads to a lower TRU_{tot} in 2090 than $TRU_{th,ad}$ from the robust static optimum, then this adaptive strategy, based on a selected prior trajectory, is called robust. Both the robust adaptive strategies and the adaptive optimum, the adaptive strategy that achieved the lowest TRU_{tot} among all valid ones, are investigated for given uncertain adaptation times.

It is important to clarify the notation of robustness in adaptation scenarios. An adaptively robust strategy is defined as the combination of two parts: one comes from the prior strategy under the context before disruption, and the other is the post-disruption adaptation that leads to lower TRU_{tot} than $TRU_{th,ad}$ by 2090. Here the so-called prior trajectory denotes the trajectory meant to be adapted after disruption, supposing the implementation of a given strategy in the pre-disruption strategy. In the concept, the prior strategy is adaptively robust **if** such an adaptive strategy follows the just-in-case disruption. From a given prior trajectory, those adaptive strategies leading to lower TRU_{tot} than $TRU_{th,ad}$ by 2090 are also called robust adaptive strategies or robust adaptations for the sake of simplification.

3.3.1 Prior trajectory to be adapted and description of adaptation scenario

First of all, the prior trajectory to be adapted should be determined. It sets directly the starting point of adaptation scenario and thus influences the robustness assessment. Here, as the first step, the adaptation from the trajectory of reference strategy which was supposed to maximize R_{Subs} by 2090 before disruption is considered. As the optimal strategy for objective A, it is highly possible to implement this strategy when the disruption of objective is not well anticipated. Moreover, it is one of the extreme cases in the Pareto front, and the comparison between the adaptation on the corresponding trajectory and the robust static optimum can give as much information as possible.

To adapt to the new objective after disruption, a new transition fleet is supposed, as presented in Figure 3.11. For the development of robustness assessment method, no new technology is deployed, and parameters in existing facilities are considered for adaptation, in order to simplify the analysis of physics and system behaviors. Given the same parameters to be readjusted, the final values of adaptive strategy parameters are different from that in the prior strategy which determines the prior trajectory before disruption. This should be notably emphasized for $P_{tot,f}$ and $FrMOX_f$: in the ancient values of the prior reference strategy, they were determined respectively as 94.6 GWd/t and 1.94%; whereas in this scenario, they are "updated" for the adaptation.

Since the disruption time is uncertain, four adaptation times are considered: year 2040, 2050, 2060 and 2070, denoted as t_{ad}. Adaptation time t_{ad} stands for the starting time of readjustment, which should be distinguished from disruption time. Conceptually, adaptations must be after the disruption time. As the time horizon is set to year 2090 in this study, the adaptation scenario starts from t_{ad} to year 2090. Same parameters as in the pre-disruption scenario are considered, but the phase space is adapted to match the constraints relative to objective B. After t_{ad}, a new transition of readjustment of fuel cycle shown in Figure 3.11 is calculated for a period D that finishes before 2090. Notably, the $P_{tot,f}$ and the

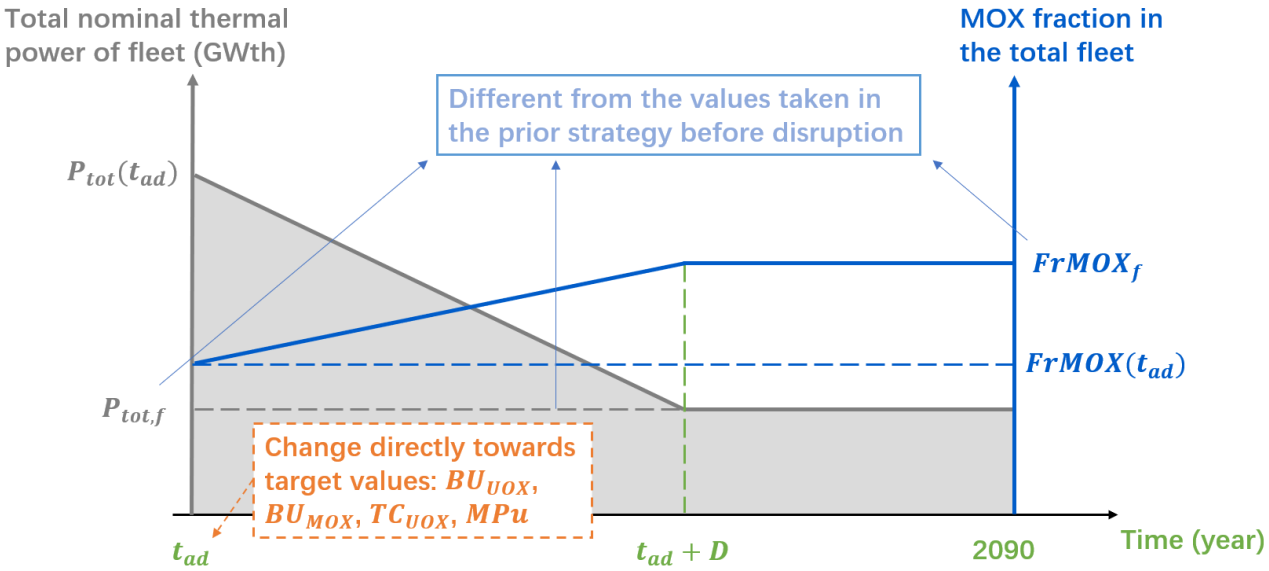

Figure 3.11: Graphical representation of the evolution of fleet in adaptation scenario. $P_{tot,f}$ and $FrMOX_f$ (and other re-sampled parameters) take different values from that in the pre-disruption scenario

$FrMOX_f$ in this DoE are different from the pre-adapted strategy. At the beginning of transition at t_{ad}, the burn-ups of two fuels BU_{UOX} and BU_{MOX}, cooling time of spent UOX fuels TC_{UOX} and the management of reprocessing order of spent UOX fuels MPu change immediately. During the transition, total power level and MOX fraction change linearly and keep constant after the transition, denoted as the final level $P_{tot,f}$ and $FrMOX_f$. The major difference from pre-disruption scenario is the variation ranges of D, $P_{tot,f}$ and $FrMOX_f$. After disruption, SFR deployment is no longer in priority. In this case, phase-out strategy is conceivable, while the power level will not increase. To minimize the TRU inventories, full core loaded with MOX in PWR s is considered feasible. To maximize the variability of these effects, an extreme short transition as one year is acceptable. In summary, seven input parameters are taken into account as shown in Table 3.10, over four options of adaptation time t_{ad}. The value of power level and MOX fraction in t_{ad}, denoted as $P_{tot}(t = t_{ad})$ and $FrMOX(t = t_{ad})$, are shown in Table 3.11. One may note that the values of $P_{tot}(t = t_{ad})$ and $FrMOX(t = t_{ad})$ do not match exactly the value of linear change, as implied by its values of inputs shown in Table 3.9. Actually, as mentioned, the simulation of macro reactors synchronizes the behaviors of same-type reactors, and the relevant changes respect the irradiation cycles. The case where t_{ad} matches exactly the reloading time is extremely rare.

Input var.	Init. Val. ($t = t_{ad}$)	Min.	Max.	Unit	Explanation
D	-	1	2090-t_{ad}	year	Duration of transition
$P_{tot,f}$	$P_{tot}(t = t_{ad})$	0.	$P_{tot}(t = t_{ad})$	GWth	Total thermal power of the fleet after transition
$FrMOX_f$	$FrMOX(t = t_{ad})$	0	100	%	MOX fraction after transition
BU_{UOX}	32.4	30	60	GWd/t	Modified burnup of UOX fuels
BU_{MOX}	41.9	30	60	GWd/t	Modified burnup of MOX fuels
TC_{UOX}	3.6	3	10	year	Modified cooling time of spent UOX fuels
MPu	1/LiFo	1/LiFo	2/FiFo	-	Modified management of spent UOX fuels

Table 3.10: Strategy space of adaptation scenario: starting from t_{ad} of the trajectory of reference strategy

For each t_{ad}, 2000 strategies are sampled by LHS [96, 97, 98] from the prior

t_{ad}	2040	2050	2060	2070	(Unit)
$P_{tot}(t = t_{ad})$	176.2	158.9	144.4	127.1	GWth
$FrMOX(t = t_{ad})$	9.5	7.7	6.6	4.6	%

Table 3.11: Starting point of level power $P_{tot,f}(t = t_{ad})$ and MOX fraction $FrMOX(t = t_{ad})$ in each adaptation scenario over t_{ad}

reference trajectory. Corresponding new trajectories are simulated by CLASS. Actually, same samples are employed for each t_{ad} except that the transition time D is normalized by the time length of scenario over t_{ad}. This choice allows to facilitate the comparison of results with respect to different t_{ad}.

One should also note that t_{ad} is not an input parameter in the adaptive strategy. Even though numerically it plays to some extent a similar role as t_{start} of pre-disruption scenario, it is important to distinguish and dissociate these two variables. On one hand, t_{ad} concerns the disruption and thus it is intrinsically uncertain, whereas t_{start} in the pre-disruption scenario is a controllable parameter as one component of pre-disruption strategy. On the other hand, the time t_{ad} determines directly the starting point of fleet in adaptation scenario. As shown in the subsequent analysis, the starting point of adaptation has significant influence on the results of adaptation, which implies the temporality of adaptive robustness.

3.3.2 Missload and validity linked to the uncertain adaptation time

In total, 8000 new trajectories are simulated by CLASS. Number of missload for each trajectory is calculated.

The first impact of uncertain t_{ad} in this time-set scenario is on the validity of explored strategies. As indicated, same samples are employed for scenarios with respect to the four considered t_{ad}. However, the percentage of valid strategies are quite different, as presented in Table 3.12.

t_{ad}	2040	2050	2060	2070
% of valid strategies	28.9%	39.7%	54.9%	80.3%
Highest N_{ML}	16	12	9	4

Table 3.12: Percentage of valid strategies in the exploratory phase space over adaptation time t_{ad} in adaptation scenario

The percentage of valid strategies in the same exploratory phase space increases over t_{ad}, while the highest number of missloads N_{ML} decreases. It is linked to the choice of prior trajectory and can be explained by two factors concerning different t_{ad}. First, in the prior reference trajectory, plutonium inventory is accumulated in interim stocks of spent UOX fuels over time, as shown in Figure 3.9. The later is t_{ad}, the more plutonium is available for MOX fabrication at the beginning of adaptation, and thus the lower is the probability to meet the plutonium shortage for MOX fabrication. The other factor concerns the time horizon hypothesis: the results of adaptation are all evaluated in year 2090, regardless t_{ad}. Actually, 10% of MOX, corresponding approximately to the current France fuel cycle, indicates the limit that will not empty the spent UOX fuels. The variability of MOX fraction in adaptation scenario is far from this value, and therefore the risk of missload for adaptive strategies with higher $FrMOX_f$ increase over time. A later t_{ad} implies a shorter simulation time period. Since the results are assessed

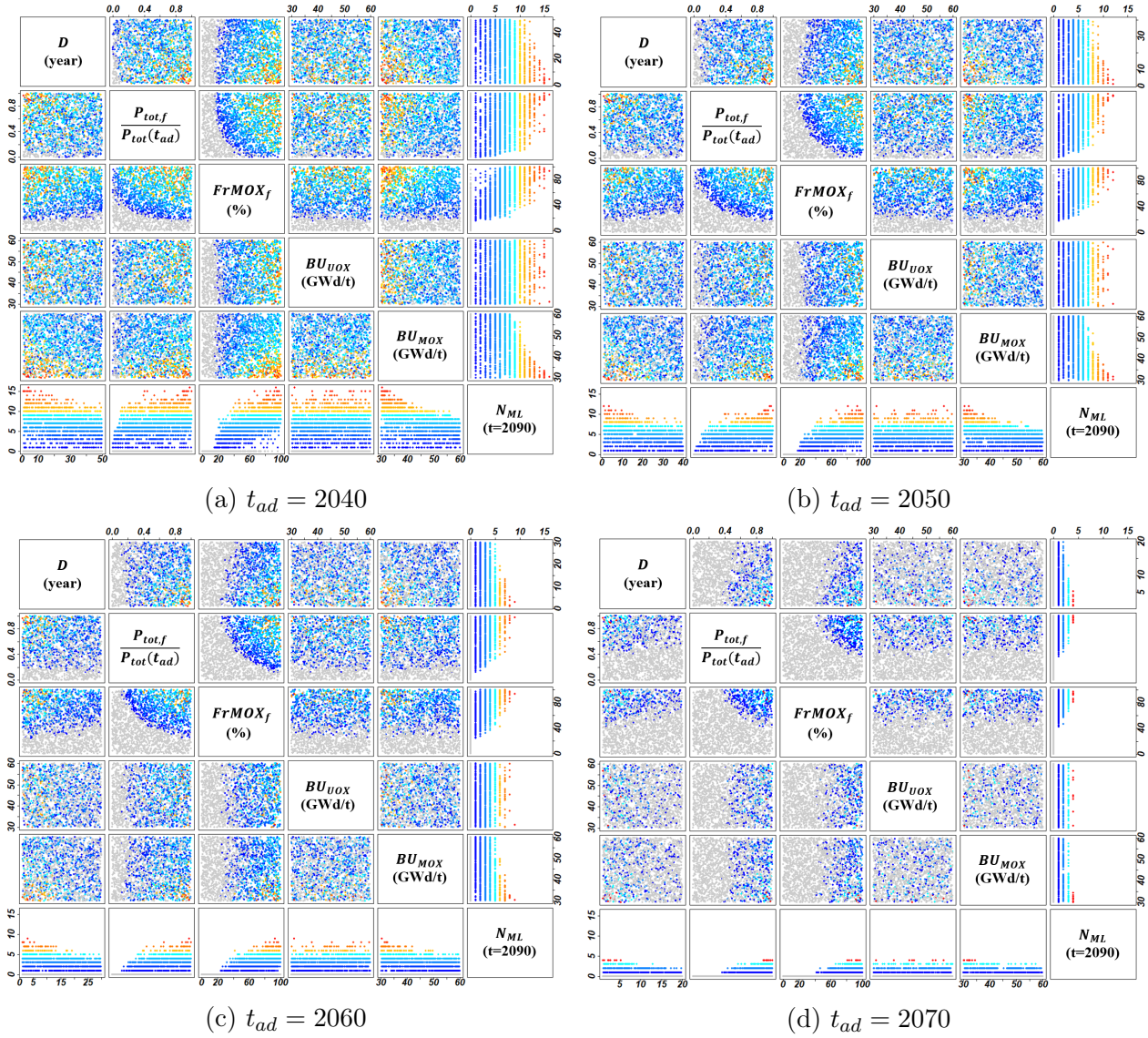

(a) $t_{ad} = 2040$ (b) $t_{ad} = 2050$

(c) $t_{ad} = 2060$ (d) $t_{ad} = 2070$

Figure 3.12: Pairs plots of important adaptive strategy inputs and output $N_{ML} > 0$, in the color of blue-to-red represented by N_{ML} with respect to different adaptation times t_{ad}

in year 2090 and the evolution afterwards is not considered, the probability of missload for a given adaptive strategy is also lower. Under these two factors, the fraction of valid adaptive strategies increases over t_{ad}.

In the analysis of pre-disruption scenario, the impacts of $FrMOX_f$ and its interaction with other parameters on the validity of strategy is presented in Section 3.2. In the adaptation scenario, the variability of inputs of interest are larger compared with the ones in pre-disruption scenario. We may expect that their effects on missloads are stronger, especially for the inputs D, $P_{tot,f}$ and $FrMOX_f$. It is therefore useful to investigate the phase space of valid strategy over t_{ad}. The values of important input variables on the number of missload N_{ML} are plotted by pairs in Figure 3.12, in the blue-to-red color represented by the number of missload $N_{ML} > 0$, while the valid strategies without missload are in grey. To compare the results of different t_{ad}, the values of $P_{tot,f}$ is normalized by $P_{tot}(t = t_{ad})$, and the axes of N_{ML} are also the same in four cases. In brief, near-blue points represent low number of N_{ML} and near-red points represent the high number, in each case. The value represented by the color can be viewed in rows or columns concerning N_{ML}. As shown in Table 3.12, highest numbers of N_{ML} are different with different t_{ad}, the same color of points in different figures of t_{ad} do not stand for the same N_{ML}.

The most directly visualized result is the impact of t_{ad} on phase space of validity. The valid zone is larger when t_{ad} becomes later, and the maximal N_{ML} of valid strategies is smaller. In all cases, red points, representing a relatively high N_{ML}, are agglomerated simultaneously in the zone of short D, high $P_{tot,f}$, high $FrMOX_f$ and low BU_{MOX}. The explanation is evident: these strategies suggest nearly full MOX for all PWRs and short irradiation cycles after a very short transition, keeping a similar power level as $P_{tot}(t = t_{ad})$, which implies an extremely high consumption rate of plutonium from spent UOX fuels without supplying it. The correlation between these inputs are also well shown in the figures.

3.3.3 Assessment over adaptation time: temporality of adaptive robustness and phase space of robust adaptations

3.3.3.1 Impact of adaptation time

In terms of TRU_{tot} analysis, only valid strategies are taken into account from now. The histogram of TRU_{tot} by 2090 resulted from valid adaptive strategies over t_{ad} are shown in Figure 3.13. The extremely late adaptation corresponds to $t_{ad} = 2090$, whose $TRU_{tot} = 1120$ tons as the prior reference trajectory represented by red dash lines. Earlier is t_{ad}, more extended is the distribution of TRU_{tot}. It is also due to the fact that all outputs are evaluated in the same given observation time, year 2090. Early t_{ad} allows longer transitions and thus the variability of outcomes is more significant; otherwise, the outcomes of adaptation converge progressively to the state of prior trajectory when t_{ad} increases.

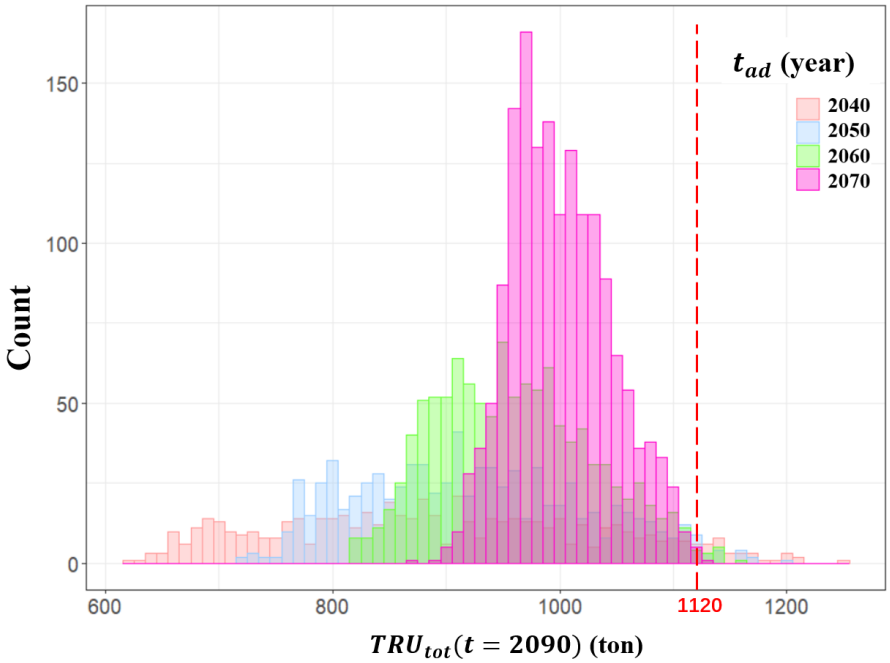

Figure 3.13: Histogram of TRU_{tot} by 2090 resulted from valid adaptive strategies over t_{ad}

For the adaptive robustness assessment, the result of robust static optimum identified in pre-disruption scenario, 849 tons of TRU_{tot}, is chosen to indicate the threshold for comparison and assessment, denoted as $TRU_{th,ad}$. As a reminder, the strategies considered adaptively robust consist of the prior strategy determining the prior trajectory before disruption, and the corresponding adaptations that lead to lower TRU_{tot} by 2090 than $TRU_{th,ad}$; and to simplify, we call those adaptations the robust adaptive strategies. Even though the early t_{ad} implies

a relatively narrow phase space of valid strategy (see in Figure 3.12), a larger fraction of them are robust as shown in Figure 3.13.

Quantitatively, the number of robust strategy and its percentage in the phase space of valid strategy over t_{ad} are presented in Table 3.13. The earlier is t_{ad}, the high is the number of robust strategies. Since the number of valid strategy increases over t_{ad}, the percentage of robust strategy in the space of valid strategy decreases dramatically. It can be explained by several factors. First, the evolution of TRU_{tot} of prior reference trajectory increases monotonously. The earlier is t_{ad}, the larger is the margin relative to $TRU_{th,ad}$, imposed by the robust static optimum. Hence, the liberty of robust adaptive strategies is higher. Meanwhile, within a given time, the TRU incineration of the nuclear system of PWR UOX and PWR MOX is extremely limited. Plutonium produced from PWR UOX cannot be totally incinerated by PWR MOX, and thus most of adaptive strategies in this adaptation scenario still tend to increase TRU_{tot} over time regarding the risk of plutonium shortages. As a result, to avoid going beyond $TRU_{th,ad}$, it is important to keep as large as possible the margin relative to $TRU_{th,ad}$ and t_{ad}. If the readjustment is performed too late, no adaptive strategy can be robust. This result can be clearly viewed in Figure 3.14, which shows the trajectories of valid adaptive strategies based on the prior reference trajectory. In this figure, the trajectories of two important static strategies identified in pre-disruption scenario, the reference strategy and the robust static optimum, are also presented. With respect to given t_{ad}, the adaptive strategy leading to the lowest TRU_{tot} by 2090 among all valid ones is called the adaptive optimum. The trajectories of the two pre-disruption strategies and the adaptive optima of different t_{ad} are emphasized in thick lines. In this study, if $t_{ad} \leq 2060$, there are always some appropriate adaptations that lead to $TRU_{tot}(t = 2090) < TRU_{th,ad}$. The increasing TRU_{tot} over time in prior reference trajectory explains the decreasing number of robust adaptive strategies over t_{ad}. When $t_{ad} = 2070$, the lowest achieved TRU_{tot} of valid adaptive strategies by 2090 is 873 tons, slightly higher than the threshold. In other words, based on the adaptation of prior reference trajectory, the time limit when there is no robust adaptive strategy is between year 2060 and 2070.

t_{ad}	2040	2050	2060	2070
Num. of rob.	231	215	35	0
(Num. of valid adapt.)	577	793	1098	1065
% in valid space	40%	27%	3%	0%

Table 3.13: Number of robust adaptive strategy and the relevant percentage in the phase space of valid strategy over t_{ad}

3.3.3.2 Phase space of robust or high-performance adaptive strategies

In the analysis of pre-disrutpion scenario, the dominance of $P_{tot,f}$ and the measurable effects of $FrMOX_f$ on the output TRU_{tot} are presented. In adaptation scenario, we may expect a more considerable gain on TRU_{tot} than in pre-disruption scenario due to larger variability of important parameters.

According to the results of TRU_{tot}, valid adaptive strategies are classified in several groups. For each adaptation scenario of given t_{ad}, robust adaptive strategies may define one group, denoted as G_{rob}; since no adaptation of $t_{ad} = 2070$ is robust, this group is empty. For the other valid strategies that are not robust (i.e. $TRU_{tot} > TRU_{th,ad}$ without missload), they are grouped according to the quartiles on TRU_{tot} excluding the robust adaptive strategies. With respect to given t_{ad},

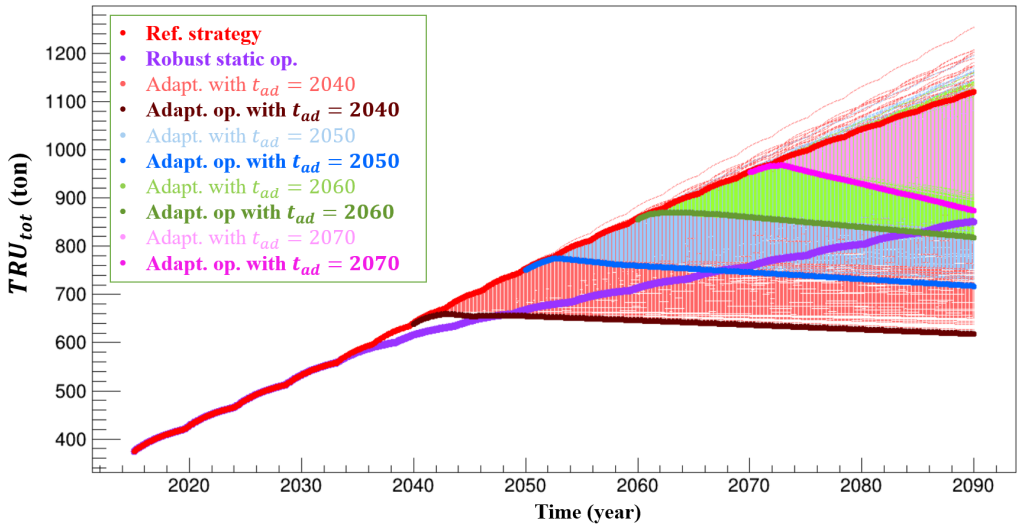

Figure 3.14: Evolutions of TRU inventories in total cycle from valid strategies over t_{ad} as well as two particular pre-disruption strategies: the reference strategy and the robust static optimum

the first quartile Q_1, the second Q_2 and the third Q_3 of TRU_{tot} are shown in Table 3.14, dividing the non-robust strategies into four groups, denoted respectively as G_1, G_2, G_3 and G_4. Each trajectory in each group satisfies the following relation $Q_{i-1} < TRU_{tot} < Q_i$. Within each clustering group, mean values of inputs are calculated, presented in Figure 3.15 for each t_{ad}. The mean values of D, $P_{tot,f}$, $FrMOX_f$ and BU_{UOX} are specifically shown in Table 3.15. In the figure and the table, the means of inputs of G_{rob} are in purple, G_1 in blue, G_2 in sky blue, G_3 in orange and G_4 in red. In the parallel plots in Figure 3.15, the connected lines indicate the values of a given group, and axes are set to the limits of variation ranges. Given the states of prior trajectory in t_{ad}, maximal values of D and $P_{tot,f}$ are different for four t_{ad}. This clustering calculation shows the average behavior of strategies of the group according to their output ranking.

Quartiles of TRU_{tot}	Q_1	Q_2	Q_3
$t_{ad} = 2040$	905	960	1040
$t_{ad} = 2050$	905	955	1020
$t_{ad} = 2060$	910	960	1010
$t_{ad} = 2070$	968	995	1030

Table 3.14: Values of TRU_{tot} (ton) corresponding to the quartiles of non-robust valid adaptive strategies with respect to given t_{ad}, where Q_i represents the i-th quartile

Cluster means of t_{ad}	D	$P_{tot,f}$	$FrMOX_f$	BU_{UOX}
$t_{ad} = 2040$	19/30/31/29/28	22.1/46.9/69.6/105.4/144.9	30.5/13.9/12.0/9.9/7.5	44.6/45.2/44.2/44.6/42.1
$t_{ad} = 2050$	13/22/25/26/23	16.2/33.8/53.3/82.1/125.5	46.3/28.2/18.0/13.8/8.6	45.1/45.2/45.6/44.3/1076
$t_{ad} = 2060$	7/12/17/19/18	21.9/21.3/39.6/63.5/101.1	83.2/54.6/35.0/21.3/11.3	47.1/45.3/45.0/45.3/43.1
$t_{ad} = 2070$	-/8/11/12/13	-/40.1/42.5/55.8/80.7	-/71.5/50.5/33.1/15.2	-/45.6/44.7/45.3/43.9
(Unit)	year	GWth	%	GWd/t

Table 3.15: Mean values of important inputs on TRU_{tot} in each clustering group with respect to t_{ad}, where colors represent the values in $G_{rob}/G_1/G_2/G_3/G_4$

In Figure 3.15, the mean values of D, $P_{tot,f}$ and $FrMOX_f$ are distinctive for different clusters, while others do not vary from a group to another and the values approximately are around the average of their sampling ranges. It implies

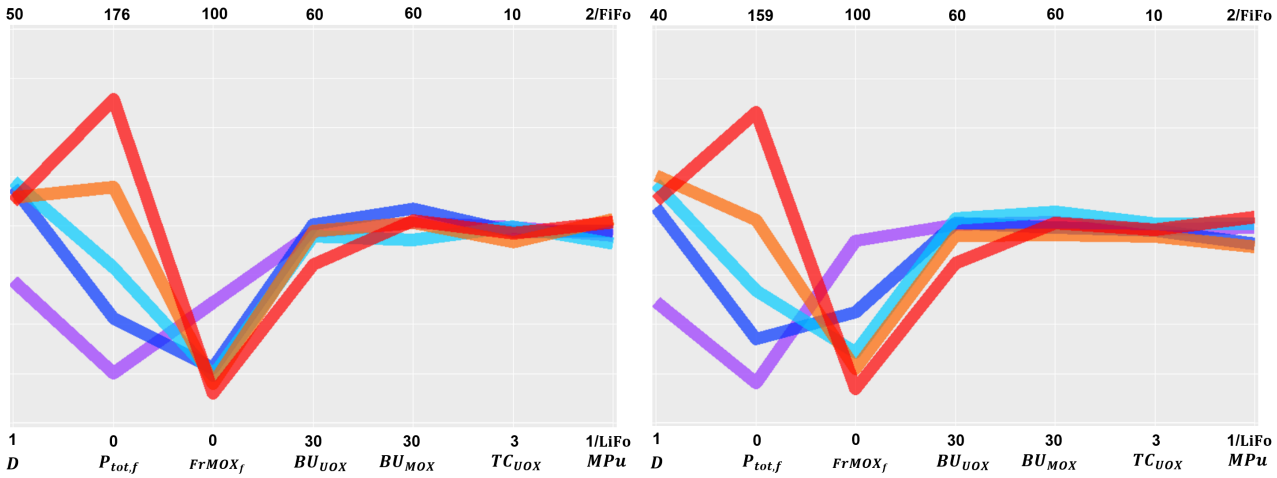

(a) $t_{ad} = 2040$ (b) $t_{ad} = 2050$

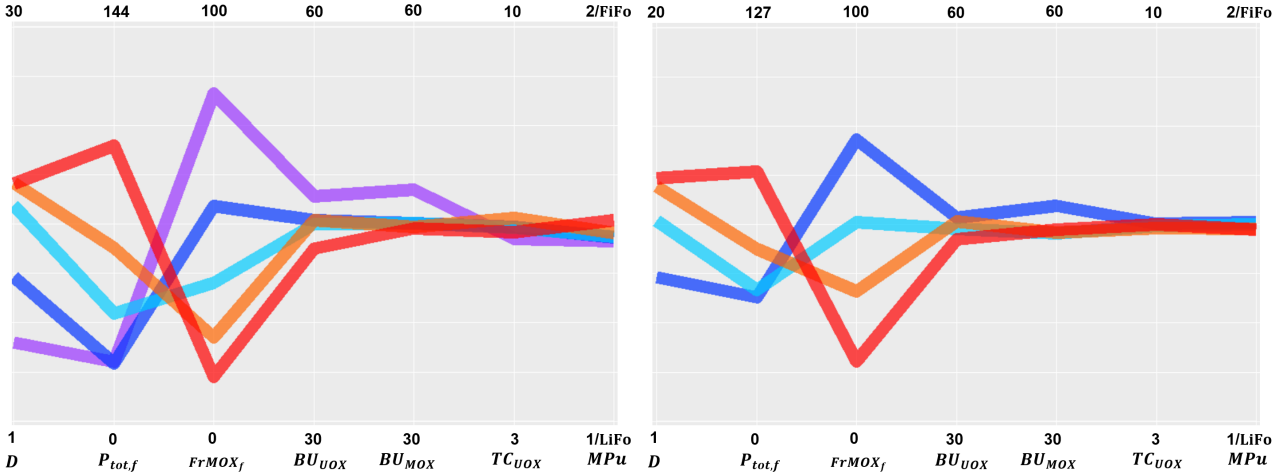

(c) $t_{ad} = 2060$ (d) $t_{ad} = 2070$

Figure 3.15: Parallel plots of the mean values of inputs and output TRU_{tot} in each clustering group with respect to given t_{ad}, where colors represent the groups $G_{rob}/G_1/G_2/G_3/G_4$

that different cluster groups have distinguishing behaviors on inputs D, $P_{tot,f}$ and $FrMOX_f$ regardless t_{ad}, while other variables are not important for the clustering. It is particularly noticeable for BU_{UOX} that had measurable effect on TRU_{tot} in the pre-disruption scenario.

The interaction between the deeply uncertain t_{ad} and these three important inputs on the clustering average behaviors can be viewed in Table 3.15. Within the same clustering group, the increasing t_{ad} results from decreasing D and $FrMOX_f$, but the interaction between $P_{tot,f}$ and t_{ad} seems not clear and depends on the groups. Nevertheless, the clustering performed here only indicates the average behaviors within a large statistical sampling, and the results of clustering should not be over-interpreted. TRU_{tot} is not a linear function of these considered inputs. The inter-dependency of inputs or the high non-linearity between output and inputs can be hidden in clustering [95].

The results can be further visualized by pairs plots of important inputs with output TRU_{tot} in Figure 3.16, which help understand the interactions between inputs and output TRU_{tot}. The importance of D, $P_{tot,f}$ and $FrMOX_f$ on TRU_{tot} are verified. Particularly, the linear dependency of TRU_{tot} on $P_{tot,f}$ and $FrMOX_f$ can be viewed. In brief, low TRU_{tot} is globally a result of short D, low $P_{tot,f}$ and high $FrMOX_f$. Intuitively, TRU_{tot} can be minimized if the fleet is fully loaded by MOX as fast as possible, while the power level is sufficiently low so that missload can be avoided before 2090. When t_{ad} increases, high $FrMOX_f$ values get more and

more available, while the $P_{tot,f}$ of low TRU_{tot} tends to shift towards a relatively high level. It can be explained by the plutonium accumulation in spent UOX and shorter simulation time period under a later t_{ad}. The effect of BU_{UOX} is much less evident than that in pre-disruption scenario. On one hand, the variability of other three important inputs are higher in adaptation scenario. In comparison, the effect of BU_{UOX} is relatively smaller. On the other hand, the UOX fraction is statistically not high, and thus the effects relevant to UOX are much less evident.

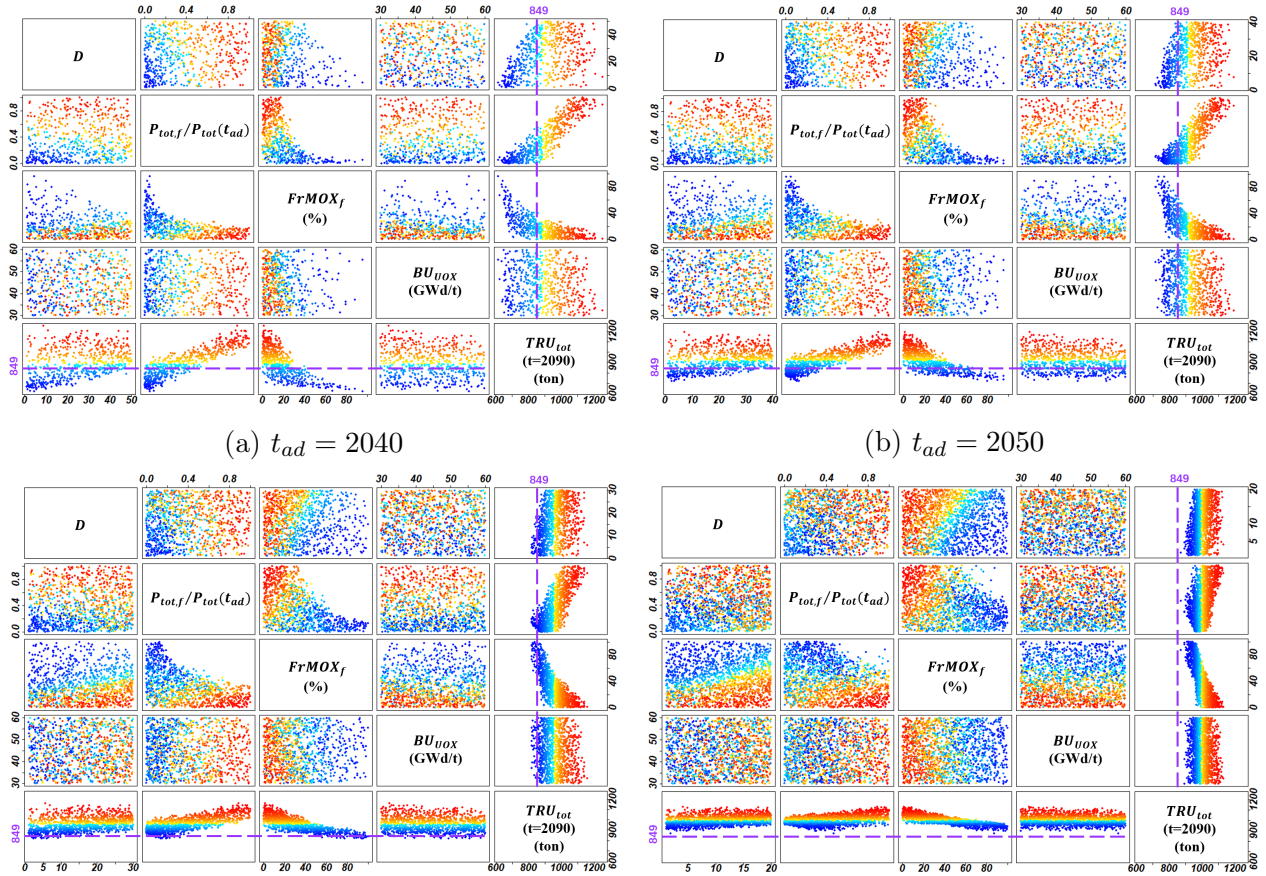

(a) $t_{ad} = 2040$ (b) $t_{ad} = 2050$

(c) $t_{ad} = 2060$ (d) $t_{ad} = 2070$

Figure 3.16: Pairs plots of important inputs D, $P_{tot,f}$, $FrMOX_f$ and possibly BU_{UOX}, and output TRU_{tot} with respect to given t_{ad}; $TRU_{th,ad} = 849$ tons is represented by purple dash lines

In terms of robust strategies leading to $TRU_{tot} < TRU_{th,ad}$, threshold effects can be observed on inputs. To limit the production of TRU in which plutonium accounts for the major part, a quite low $P_{tot,f}$ and a relatively high $FrMOX_f$ are required. When t_{ad} is early, there is still a large margin relative to the threshold $TRU_{th,ad}$, and long transitions D is allowed; however, $FrMOX_f$ cannot be too high in order to avoid missload before the end of scenario. On the contrary, if t_{ad} is relatively late, very short D of transition towards low $P_{tot,f}$ and high $FrMOX_f$ is necessary, so that the plutonium can be incinerated efficiently and rapidly.

3.3.3.3 Focus on adaptive optima

In each adaptation scenario of given t_{ad}, the adaptive strategy leading to lowest TRU_{tot} by 2090 among valid strategies is called the adaptive optimum. As analyzed, there is a time limit for the existence of robust adaptations between 2060 and 2070. At this stage, we define the temporality of adaptive robustness as the difference between the observation time and this time limit. Hence, this temporality is approximately between 20 and 30 years.

It is still useful to focus on these four adaptive optima, whose values of inputs and output TRU_{tot} are shown in Table 3.16. As analyzed, all of them present a short D, relatively low level of $P_{tot,f}$ and quite high level of $FrMOX_f$. LiFo as the reprocessing order of spent UOX fuels help use more efficiently the fissle isotopes of plutonium, and thus fortifies the incineration of plutonium and reduces the risk of missload. Another remark can be the tendency that $P_{tot,f}$ is higher when t_{ad} is later. It is coherent with the forgoing analysis that late t_{ad} implies at the same time a higher plutonium inventory in spent UOX fuels at the beginning of adaptive transition and a shorter time period of simulation, and thus leads to a lower risk of missload.

Strategy	D	$P_{tot,f}$	$FrMOX_f$	BU_{UOX}	BU_{MOX}	TC_{UOX}	MPu	TRU_{tot}
Op. of $t_{ad} = 2040$	4.5	8.9	95.7	55.4	48.0	5.9	LiFo	617
Op. of $t_{ad} = 2050$	3.5	17.5	80.1	54.4	56.2	5.5	LiFo	717
Op. of $t_{ad} = 2060$	6.0	19.6	95.4	47.2	56.8	4.1	LiFo	818
Op. of $t_{ad} = 2070$	1.8	59.5	87.2	57.9	59.7	5.9	LiFo	874
(Unit)	year	GWth	%	GWd/t	GWd/t	year	-	ton

Table 3.16: Values of inputs and output TRU_{tot} of adaptive optima with respect to t_{ad}

The evolution of TRU_{tot} of these four adaptive optima are emphasized by thick lines in Figure 3.14. There seems to be a tendency that the incineration rate of TRU_{tot} is higher when t_{ad} is later. The explanation is again the same. One may note that the evolution of adaptive optima are to some extent separated with other trajectories of adaptation with respect to given t_{ad}; in other words, the "density of lines" are optically smallerThat is because these optima aim to minimize TRU by consuming all available plutonium in spent UOX fuels and thus have a high risk of missload. The evolutions also show that the capacity of TRU/plutonium incineration of a PWR UOX and MOX system is really limited.

3.3.4 Discussion about some key hypotheses of scenario: possible impacts on the assessment

In this adaptation scenario, based on the definition of robustness and a set of hypotheses of scenario in this study, we determined the latest time for which a robust adaptation is possible, defining also the temporality of adaptive robustness. Several hypotheses, including the definitions and the method of assessment are discussed along the analysis. In this part, the validity of several hypotheses is re-investigated based on the results obtained.

First important hypothesis concerns the prior trajectory to be adapted after disruption. In this study, only the adaptation from the reference trajectory is analyzed, on which the robustness assessment depends. More precisely, the pair of the reference strategy identified in pre-disruption scenario and the related time-dependent adaptation plan before 2070 is adaptively robust. Nonetheless, as justified for the selection of robust static strategies, the determination of "reference strategy" satisfying all extra criteria of actors may depend on other various factors that are out of the scope of work. The prior reference trajectory to be adapted are only selected as an example to illustrate the method of robustness assessment. When other criteria are more relevant regarding a decision making process, the same method can be applied. Meanwhile, it is possible that the same adaptive strategy on the prior robust static optimum trajectory can lead to lower TRU_{tot} than previously. However, this last hypothesis should be verified by

a complete new set of calculations as the risks of missloads seem to be very high. We shall remind that this study does not aim to search for the lowest achievable TRU_{tot} by an exhaustive investigation of adapting all possible prior trajectories. In contrast, the purpose is to compare the consequence of adaptation on a reasonable choice before disruption with another precautionary strategy, in order to highlight the difference between the a-posteriori adaptation planning and the a-priori conservative strategy.

Second, the variability of input parameters in adaptation scenario can also impact the result of the assessment. It is constrained by the DoE which is defined in accordance to the interests of stakeholders. The achievement of adaptive robustness as well as the temporality is mainly based on the different variability of D, $P_{tot,f}$ and $FrMOX_f$ from those in pre-disruption scenario, which are important variables on the output TRU_{tot}. Therefore, the assessment and temporality of adaptive robustness can be impacted with different variability of input variables. Indeed, the high-performance adaptations suggest a quick approximate phase-out strategy with high MOX fraction; whereas stakeholders may prefer a less ambitious readjustment with a smaller gain on output TRU_{tot}.

Based on various considerations, one may impose other constraints on variation ranges, noted as Ct, than the ones in this study. For instance:

- $\boldsymbol{Ct(P)}$: the phase-out strategy after disruption, indicated by $P_{tot,f} \simeq 0$, is not acceptable according to stakeholders of nuclear industry. The lowest acceptable level is 50% of the level in t_{ad}, which means that $P_{tot,f} \geq 0.5 \times P_{tot}(t = t_{ad})$
- $\boldsymbol{Ct(D)}$: In consideration of the stabilization of electricity supply and the pace of readjustment, the new transition should always longer than 10 years, and thus $D \geq 10$.
- $\boldsymbol{Ct(P_{MOX})}$: the reprocessing capacities of spent UOX fuels and the fabrication of fresh MOX fuels cannot be too high. Since the capacity depends on the power level contributed by MOX denoted as P_{MOX}, one may give a relevant constraint that P_{MOX} after transition should be smaller than the double of current level, and thus $P_{tot,f} \times FrMOX_f \leq 188.1 \times 10\% \times 2 = 37.6$ GWth.
- $\boldsymbol{Ct(TC_{UOX})}$: in consideration of nuclear safety, cooling time of spent UOX fuels should be longer than five years, and thus $TC_{UOX} > 5$ years.

Depending on cases, these new constraints may be added to the DoE individually or cumulatively. To give a rough estimation, the results of adaptation of $t_{ad} = 2070$ are used since the number of valid strategy is relatively high; these constraints are used cumulatively in the foregoing order. The lowest achieved TRU_{tot} by accumulating the constraints in this order are shown in Table 3.17. Except the very weak effect of TC_{UOX} on TRU_{tot}, these new constraints, which imply a smaller variability of inputs, affect significantly the performance of the constraint-dependent adaptive optimum. Meanwhile, one may open other possibilities of adaptation than sticking to the previous systems by adding new input parameters, such as the use of technologies concerning the multi-recycling of plutonium in PWRs. These new variables will probably change the results of assessment, and requires further analyses.

Besides, by definition, the results of strategy assessments also depend strongly on the link between output evaluations and the observation time (here the time horizon). The dependency of objective on a given time is intuitively a natural and common choice in practise. In this study, there is no robust adaptive strategy because the trajectory of adaptive optimum leads to $TRU_{tot}(t = 2090)$ higher than

Constraints accumulated	-	$Ct(P)$	$Ct(D)$	$Ct(P_{MOX})$	$Ct(TC_{UOX})$
Lowest achieved TRU_{tot}	873	903	929	971	971

Table 3.17: Lowest achieved TRU_{tot} (in ton) accumulating new constraints on the variability of input variables

$TRU_{th,ad}$, which is determined by the robust static optimum in 2090. However, as shown in Figure 3.14, a longer simulation would lead to a lower TRU_{tot} for this optimum and thus the probable existence of robust adaptive strategies. In other words, if the time horizon of scenario is later than 2090, the adaptation of year 2070 may be robust. It requires certainly further analysis because the validity of robust static optimum and the adaptive optimum of $t_{ad} = 2070$ after year 2090 are not justified; nevertheless, it indicates the possibility of inter-temporal inconsistency in this way to assess adaptive robustness.

If the evaluation of outputs is always connected with a given observation time, the investigation based on the system of PWR UOX and MOX can be infinitely iterative. In fact, the management of MOX employed in current French fleet stabilizes the available plutonium inventory in the stock of spent UOX fuels [13]. If the stabilization is broken, leading to the reduction and not rebuilt after transition, there is always a risk of missload and requires further simulation to verify the validity.

In all, the connection of evaluation with set observation time is rather an option of objective reformulation than a problem of numeric analysis. The objective will be rephrased in another manner in next chapter, which aims to disconnect the dependency.

3.3.5 Conclusion of adaptive robustness assessment

In this section, adaptation scenarios with respect to four adaptation times t_{ad} are analyzed, based on the prior reference trajectory. The adaptive robustness assessment is performed by comparing the performance of adaptive strategies with the robust static optimum identified in pre-disruption scenario. The comparison aims to highlight the difference between post-disruption adaptation and best historical and precautionary choice regarding the disruption. It is shown that the latest adaptation time for which adaptive robustness can be achieved based on the prior reference trajectory is before year 2070, defining the temporality of adaptive robustness based on the prior reference trajectory is between 20 and 30 years. This show a limit of the adaptation process which cannot compensate the difference with the robust static optimum when only 20 years remains between the adaptation and the evaluation.

Several hypotheses of scenario are also discussed, which may impact the assessment of robustness. Therefore, the results of assessment cannot be separated with relevant hypotheses, and they are not generalizable out of the scope of study. When the aforementioned results are interpreted, the hypotheses of scenario should be also highlighted.

3.4 Complement of set time problem: another option of objective translation

As highlighted in Section 3.1, the objectives considered in this work are formulated with ambiguities (as any objective formulation for scenario studies), and numeric criteria are used to translate objectives into numerically applicable propo-

sitions by adding hypotheses. These hypotheses depend on the aim of analysts to match the interests of stakeholders. To highlight the effect of other choices of hypotheses, another reformulation of objective should be studied. In this section, the objective B is rephrased into another criterion, and the same methodology of assessment is employed.

It is worth noting that the criterion for objective B presented in Section 3.1 is quite different from the one for objective A regarding a specific parameter of primary importance : the installed capacity of the fleet. Indeed, R_{Subs} was designed to quantify the feasibility of a SFR transition regardless of the fleet power, whereas TRU_{tot} is strongly dependent on it as revealed in the previous sections. Some may argue that the power should not have the same status as other operational parameters such as reactor burn-ups or cooling time, as it represents the evolution of nuclear capacity and is then directly relative to the interest of stakeholders.The power is then subject, as objectives, to deep uncertainty. Its impact is particularly studied in the Ph.D work in [49] with firmly built paradigm of analysis. To handle it in this study, it may be more relevant to define a criterion for objective B independent from the future fleet power. Outcomes of this section will then allow us to conclude, on one hand, on the importance to translation of objectives into criteria, and on the other hand, on the power status as a specific parameter subject to deep uncertainty.

3.4.1 Another choice of criterion for objective B

Objective B considered in this work aims to minimize potential wastes in the cycle. In previous sections, TRU_{tot} is used as the output of interest. Given the high variability of energy supply, one may argue that the waste should be refered to as the quantity relative to a given energy production, for example, the TRU inventories normalized by the total energy supply, denoted as TRU_{tot}^{norm}:

$$TRU_{tot}^{norm}(t) = \frac{TRU_{tot}(t)}{E(t)} = \frac{TRU_{tot}(t)}{\int_{t_0}^{t} P_{elec}(\tau)d\tau} \tag{3.7}$$

where t_0 denotes the grid-connection time of first commercial nuclear reactor in France, and P_{elec} denotes the electric power. For all PWR simulated in this chapter, a yield of 33% is supposed. The large production of energy leads to a considerable benefit that allows wide flexibility and economic margin of waste management. Moreover, the organization of waste management can be more efficient in a large scale. These positive effects may offset somehow the negativity of proportional TRU_{tot} to the large scale of fleet. Hence, it is also of interest to investigate the wastes per unit of energy produced.

With respect to the output of interest TRU_{tot}^{norm} and the hypothesis of set time horizon, the new criterion for objective B and the new conditional criterion, denoted respectively as $C_{Bnorm}^{t\text{-}set}$ and $C_{Bnorm|A}^{t\text{-}set}$, are recast as:

- $C_{Bnorm}^{t\text{-}set}$: Minimization of the normalized TRU inventories in total cycle by 2090 $TRU_{tot}^{norm}(t = 2090)$.
- $C_{Bnorm|A}^{t\text{-}set}$: Minimization of $TRU_{tot}^{norm}(t = 2090)$ among all valid strategies which achieve $R_{Subs}(2090) > 1$.

The method of scenario analysis and robustness assessment are illustrated in previous sections. The same methods are used for the investigation with respect to the new criterion defined for objective B. Same scenario and trajectories simulated in previous analyses are used to calculate new outputs and to evaluate the strategies.

3.4.2 Assessment of static robustness in pre-disruption scenario

The cumulative energy supply of nuclear fleet in France till 2015 is calculated to give the starting point. According to the simulation of French fleet shown in Section 2.2.1, the total electricity production from 1977 to 2015 is around 1.15×10^4 TWe.h, or 1313 GWe.y, while around 372 tons of TRU inventories are accumulated. To facilitate the representation of results, TRU_{tot}^{norm} is expressed in t/(MWe.y). By 2015, $TRU_{tot}^{norm} = 283$ t/(MWe.y).

Pre-disruption scenario is described in Section 3.2. For each simulated trajectory, $TRU_{tot}^{norm}(t = 2090)$ is calculated. Similarly, under the hypothesis of evaluation in year 2090, the term "t=2090" is omitted in this study. PCA is employed to investigate the importance of the eight input parameters on TRU_{tot}^{norm}. To help complete the correlation matrix of original variable vector $\boldsymbol{X}$ where $X_{out} = TRU_{tot}^{norm}$, the correlation coefficients between inputs and TRU_{tot}^{norm} are presented in Table 3.18; note that only the correlations higher than 0.1 are presented.

Input	$\boldsymbol{t_{start}}$	$\boldsymbol{D}$	$\boldsymbol{P_{tot,f}}$	$\boldsymbol{FrMOX_f}$	$\boldsymbol{BU_{UOX}}$	$\boldsymbol{BU_{MOX}}$	$\boldsymbol{TC_{UOX}}$	$\boldsymbol{MPu}$
Cor. coef.			0.10	-0.64	-0.58	-0.12		

Table 3.18: Correlation coefficients between inputs and output TRU_{tot}^{norm} in pre-disruption scenario

Only valid strategies are taken into account for PCA . For these valid observations, the correlation matrix of $\boldsymbol{X}$ where $X_{out} = TRU_{tot}^{norm}$ is calculated, and then the principal components (PCs) are identified by calculating the pairs of eigenvalue-eigenvector. Fraction of total variance of $\boldsymbol{X}$ explained by given PC as well as the squares of correlation coefficients between $X_{out} = TRU_{tot}^{norm}$ and inputs are presented in Table 3.19. The PC_1 can explain nearly the whole variance of TRU_{tot}^{norm}, while PC_9 is approximately a constant compare to other PCs .

PC	$\boldsymbol{Y_1}$	$\boldsymbol{Y_2}$	$\boldsymbol{Y_3}$	$\boldsymbol{Y_4}$	$\boldsymbol{Y_5}$	$\boldsymbol{Y_6}$	$\boldsymbol{Y_7}$	$\boldsymbol{Y_8}$	$\boldsymbol{Y_9}$
$\boldsymbol{\lambda_j / V_{tot}}$	0.21	0.15	0.13	0.11	0.11	0.11	0.09	0.08	0.00
$\boldsymbol{\sum_k^j \lambda_k / V_{tot}}$	0.21	0.36	0.49	0.60	0.71	0.82	0.92	1.00	1.00
$\boldsymbol{\rho^2(N_{ML}, Y_j)}$	**0.92**	0.03	0.01	0.	0.	0.	0.02	0.01	0.01

Table 3.19: Statistical information of principal components in the PCA where $TRU_{tot}^{norm}(t = 2090)$ is one component of original variable vector

According to the method illustrated in Section 3.2, the composition of PC Y_1 indicates the importance of variables on PC Y_1 and thus TRU_{tot}^{norm}, while the coefficients in Y_9 imply a possible linear relation among these variables. The coefficients of inputs and output TRU_{tot}^{norm} in Y_1 and Y_9 are presented in Table 3.20. Coefficients of variables in PC Y_1 indicates the measurable importance of $FrMOX_f$ and BU_{UOX} on TRU_{tot}^{norm}, while t_{start}, D, $P_{tot,f}$ and BU_{MOX} may have some effects. The composition of Y_9 emphasizes the linear relation between $FrMOX_f$, BU_{UOX} and output TRU_{tot}^{norm}, while the effects of other variables are negligible. Hence, the composition of these two PCs confirms the high importance of $FrMOX_f$ and BU_{UOX} on TRU_{tot}^{norm}, while other inputs such as t_{start}, D, $P_{tot,f}$ and BU_{MOX} may possibly affect TRU_{tot}^{norm}.

As expected, a large difference of importance of $P_{tot,f}$ on output TRU_{tot} and on the normalized quantity TRU_{tot}^{norm} is observed. Actually, after the normalization of energy production, TRU_{tot}^{norm} is not an extensive quantity driven by scaling parameter such as $P_{tot,f}$. Instead, it measures the depth of energy released regarding

Coef. in Y_j	t_{start}	D	$P_{tot,f}$	$FrMOX_f$	BU_{UOX}	BU_{MOX}	TC_{UOX}	MPu	TRU_{tot}^{norm}
Y_1	**-0.14**	**-0.11**	**0.29**	**-0.50**	**-0.34**	**-0.15**	0.08	0.05	**0.69**
Y_9	0.07	0.05	0.	**0.52**	**0.52**	0.05	0.	0.	**0.67**

Table 3.20: Coefficients of original variables in the linear transformations of PCs Y_1 and Y_9, where $X_{out} = TRU_{tot}^{norm}$

the production of TRU, particularly the plutonium. For other input parameters, $FrMOX_f$ and BU_{UOX} have strong impacts on TRU_{tot}^{norm}, because they characterize the valorization of plutonium. The effects of t_{start}, D and BU_{MOX} are possibly measurable but cannot definitely determined.

The impacts of input parameters can be verified by the scatter plots of TRU_{tot}^{norm} by 2090 versus inputs and R_{Subs} in Figure 3.17, where blue points represent the strategies of LiFo and the red points are FiFo. The correlations between output TRU_{tot}^{norm} and important inputs $FrMOX_f$ and BU_{UOX} are clearly shown, whereas the effect of $P_{tot,f}$ is much smaller. Given the uniform distribution of two colors of points, the effect of MPu on TRU_{tot}^{norm} can be considered negligible. In terms of t_{start} and D, there seems to be a slight tendency of convergence of TRU_{tot}^{norm}, which can be the same explanation of transition time effects. While for BU_{MOX}, it seems to be slightly correlated with TRU_{tot}^{norm}, as indicated by their correlation coefficient shown in Table 3.18, but globally its effect is much smaller than other important input parameters.

To sum up, these results demonstrate a-posteriori the independence of the new-built criterion from any nuclear power transition as our willing. The uncertainty of the power evolution should then not impact our conclusions on robust strategy assessments with this new translation of objective B.

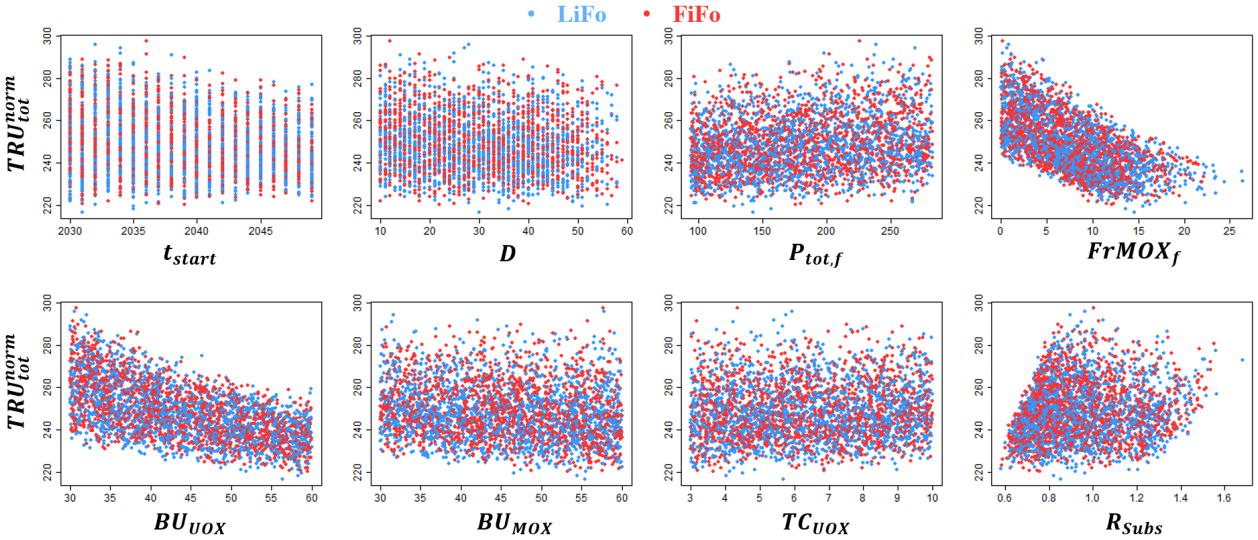

Figure 3.17: TRU_{tot}^{norm} by 2090 versus inputs and R_{Subs}, where blue points are LiFo and red points are FiFo

The impacts of possible important interactions of input parameters are verified in Figure 3.18. The strong symbiotic effect of $FrMOX_f$ and BU_{UOX} is obvious; whereas the interaction between $P_{tot,f}$ and $FrMOX_f$ accounts rather for the plutonium availability than for TRU_{tot}^{norm}. Again, due to the normalization, wide range of TRU_{tot}^{norm} is presented in all range of $P_{tot,f}$, and their dependency is not as high as in the previous study with respect to output TRU_{tot}.

The scatter plots of two outputs of interest, TRU_{tot}^{norm} versus R_{Subs}, are shown in Figure 3.19, colored respectively by $FrMOX_f$ and by BU_{UOX}. Two figures present

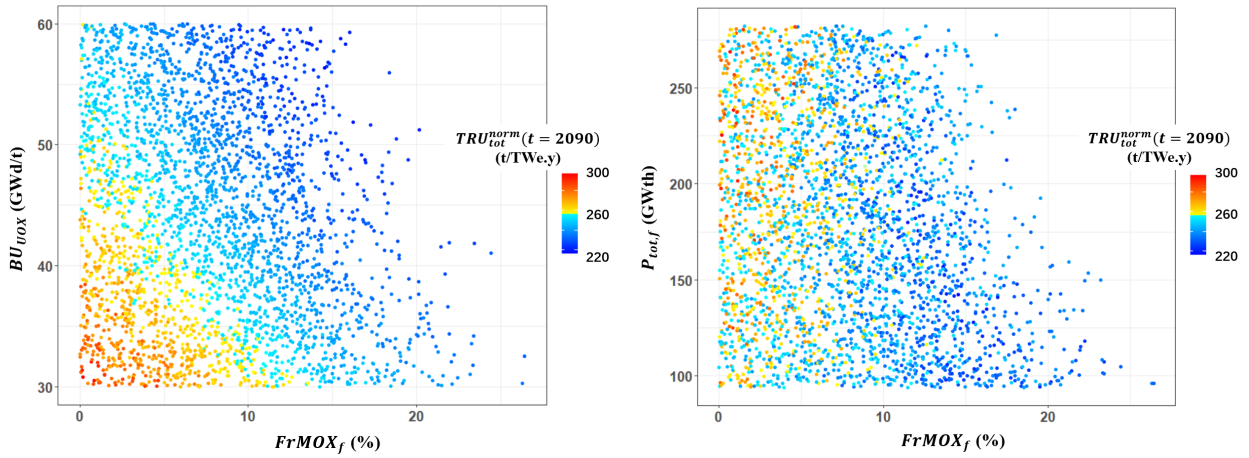

(a) (b)

Figure 3.18: Scatter plot of inputs $FrMOX_f$ versus R_{Subs} respectively BU_{UOX} and $P_{tot,f}$ colored by TRU_{tot}^{norm} by 2090

a slight difference on the color pattern, which means that the responses of the two outputs to $FrMOX_f$ and to BU_{UOX} still have some nuances. Figure 3.18a shows that when R_{Subs} is relatively low corresponding to very high level of $P_{tot,f}$ and BU_{UOX}, low-level TRU_{tot}^{norm} can still be achieved with a $FrMOX_f$ around 15%, which is much lower than the case of high R_{Subs} corresponding to low power level. Actually the high level of $P_{tot,f}$ is not compatible with high $FrMOX_f$ due to the plutonium availability.

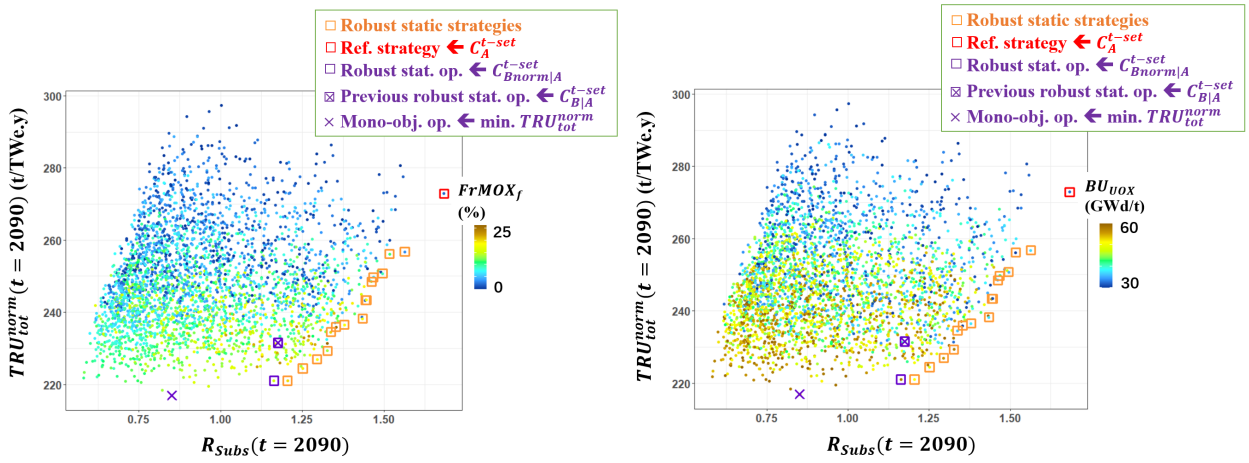

(a) (b)

Figure 3.19: Scatter plot of outputs TRU_{tot}^{norm} versus R_{Subs} by 2090, colored respectively by $FrMOX_f$ and BU_{UOX}

The strategies of Pareto front, represented as points surrounded by squares in Figure 3.19, presents a wide range of tradeoffs between the maximization of R_{Subs} and the minimization of TRU_{tot}^{norm}. They can be considered as robust static strategies depending on the requirement and interest on these two outputs. The R_{Subs} of this zone ranges in [1.16, 1.68], while TRU_{tot}^{norm} ranges in [221, 273] t/TWe.y. The front can be first achieved by low level of $P_{tot,f}$, mainly constrained by the optimization on R_{Subs}. The tradeoffs are then controlled by the choices of $FrMOX_f$ and BU_{UOX}. Note that under the priority of objective A, R_{Subs} of strategies of interest should be larger than 1; thus, the strategy achieving the lowest $TRU_{tot}^{norm} = 217$ t/TWe.y is not of interest even though it is on the Pareto

front, because its $R_{Subs} < 1$. It is represented by a cross in Figure 3.19. Because it is the global minimum, it is called mono-objective optimum satisfying $C^{t\text{-}set}_{Bnorm}$.

Two extreme cases can be investigated. The first one is the reference strategy that maximizes R_{Subs}. The other one minimizes TRU^{norm}_{tot} among valid strategies achieving $R_{Subs} > 1$; according to the new criterion $C^{t\text{-}set}_{Bnorm|A}$, this one is defined here as the robust static optimum. Those two strategies are represented respectively by red square and purple square in Figure 3.19. The reference strategy leads to 273 t/TWe.y by 2090, while the robust static strategy in this study results in 221 t/TWe.y, which is quite close to the mono-objective optimum satisfying $C^{t\text{-}set}_{Bnorm}$. The values of inputs and outputs of robust static optimum in this study are shown in Table 3.21. The previous robust static optimum that minimizes TRU_{tot} satisfying $C^{t\text{-}set}_{B}$, leads to $TRU^{norm}_{tot} = 232$ t/TWe.y and is not in the Pareto front.

Var.	t_{start}	D	$P_{tot,f}$	$FrMOX_f$	BU_{UOX}	BU_{MOX}	TC_{UOX}	MPu	R_{Subs}	TRU_{tot}	TRU^{norm}_{tot}
Valus	2036	34	98.2	15.8	58.3	47.4	9.0	LiFo	1.16	885	221
(Unit)	year	year	GWth	%	GWd/t	GWd/t	year	-	-	ton	t/TWe.y

Table 3.21: Values of inputs and outputs of the robust static optimum satisfying $C^{t\text{-}set}_{Bnorm}$

One may note that a large part of explored valid strategies lead to lower TRU^{norm}_{tot} than the initial state in 2015. Actually, the reduction of TRU^{norm}_{tot} can date back to the beginning of fleet. The evolution of TRU^{norm}_{tot} of French nuclear fleet is shown in Figure 3.20a. During the first irradiation, TRU nuclides are created; the net production rate of TRU decreases due to the nuclear reactions of TRU, specially during the plutonium mono-recycling. Since TRU_{tot} and energy production are both cumulative quantities, the influence of large deployment of new reactors on TRU^{norm}_{tot} is relatively limited. The increase of BU_{UOX} and the use of MOX fortifies the reduction TRU^{norm}_{tot} over time.

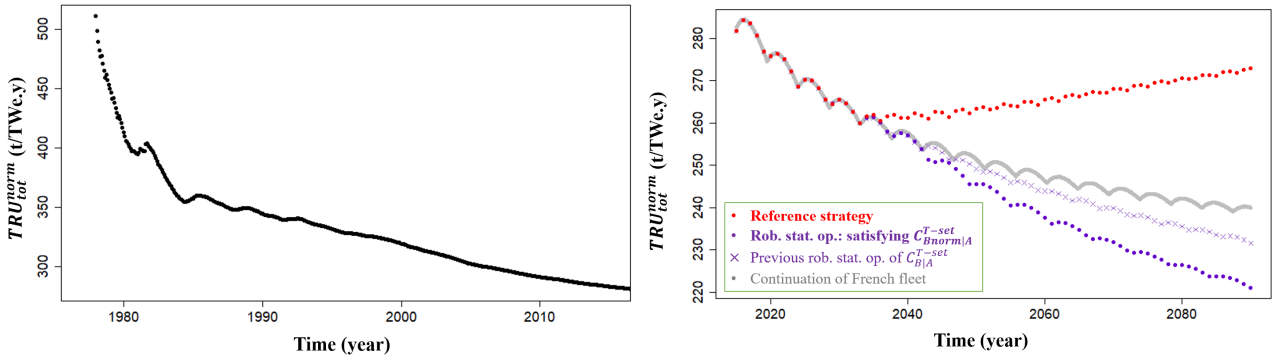

(a) Evolution of TRU^{norm}_{tot} of historical French fleet till year 2015

(b) Evolution of TRU^{norm}_{tot} of particular cases till year 2090

Figure 3.20: Evolution of TRU^{norm}_{tot} of particular trajectories

A simple dual-state system can help understand more in detail the evolution of TRU^{norm}_{tot}. Suppose that TRU^{norm}_{early} denotes the production of TRU normalized by the energy production in early irradiation cycles, characterized by low BU_{UOX} without MOX, simply called the early system; TRU^{norm}_{rec} denotes the production of TRU normalized by the energy production in recent irradiation cycles, characterized by median BU_{UOX} and a given fraction of MOX, simply called the recent system. According to the simple individual reactor simulations in Section 2.2.1.1, the use of MOX tends to reduce TRU during the electricity production. Accordingly, we may have $TRU^{norm}_{early} > TRU^{norm}_{rec}$. The French fleet starts from TRU^{norm}_{early}; following

the modification of BU_{UOX} and the use of MOX, the high value of TRU_{tot}^{norm} approximates to TRU_{early}^{norm} is little by little "diluted" by the increasing weight of TRU_{rec}^{norm}:

$$TRU_{tot}^{norm}(t) = \frac{E_{early}}{E_{early} + E_{rec}(t)} TRU_{early}^{norm} + \frac{E_{rec}(t)}{E_{early} + E_{rec}(t)} TRU_{rec}^{norm} \tag{3.8}$$

where E_{early} and E_{rec} denote the energy produced by the early system and by the recent system. Following the application of recent system and the increase of E_{rec}, the time-dependent TRU_{tot}^{norm} decreases and converges to TRU_{rec}^{unit}. It also explains why TRU_{tot}^{norm} converges to a constant value over time. This explanation is only an extremely simplified model of two system states; but also help understand how TRU_{tot}^{norm} evolves over time.

Meanwhile, this simplified explanation also helps understand why high level of $P_{tot,f}$ corresponding to very low R_{Subs}, can still achieve low TRU_{tot}^{norm} with high level of BU_{UOX} and a $FrMOX_f$ around 15%, a fraction much lower than the case of high R_{Subs}, as shown in Figure 3.19. When $P_{tot,f}$ is high, the weight of TRU_{rec}^{norm} represented by relatively high level of $FrMOX_f$ and BU_{UOX} is also high, and thus TRU_{tot}^{norm} decreases efficiently over time. While $P_{tot,f}$ is low, the relevant weight is consequently small. To achieve the similar low level of TRU_{tot}^{norm} within the same time horizon, $FrMOX_f$ should be much higher to strengthen the reduction of TRU_{tot}^{norm}.

Figure 3.20b shows the evolution of TRU_{tot}^{norm} of four particular strategies: reference strategy, the robust static optimum of this study and the one defined in Section 3.2 satisfying $C_{Bnorm}^{t\text{-}set}$, and also the prolongation of current French fleet. The two strategies concerning immediate precautionary action lead to the continuous decrease of TRU_{tot}^{norm}, since the $FrMOX_f$ and BU_{UOX} are higher than the initial levels. The continuation of French fleet, also keeps decreasing TRU_{tot}^{norm} but seems to converge without any modification of fleet. On the contrary, the TRU_{tot}^{norm} of reference strategy re-increases due to the reduction of $FrMOX_f$ and BU_{UOX}.

3.4.3 Adaptive robustness assessment with respect to TRU inventories normalized by cumulative energy production

The same adaptation scenario and samples in previous study are used, based on the prior trajectory of the reference strategy. The threshold for adaptive robustness assessment, denoted as $TRU_{th,ad}^{norm} = 221$ t/TWe.y, is deduced from the robust static optimum defined in this section. The aim is to explore adaptive strategies to minimize TRU_{tot}^{norm} by 2090.

At a first step, Figure 3.21 indicates the histogram and distribution of TRU_{tot}^{norm} of adaptive strategies by 2090 over t_{ad}. Compared to the prior reference trajectory by 2090, 273 t/TWe.y represented by red dash line in the figure, most of adaptive strategies can reduce TRU_{tot}^{norm}. According to the previous analysis, it can be explained by the fact that the major part of valid $FrMOX_f$ sampled are higher than the state in t_{ad}, which is summarized in Table 3.11. Therefore, the TRU_{tot}^{norm} can be improved by adaptive strategies compared with the prior trajectory without any readjustment. Coherent with the time effect of transition, late t_{ad} limits the effects of adaptation, and thus the results are more close to the prior reference trajectory. However, the width of distribution is similar over t_{ad}.

Similar to the study of adaptation with respect to the TRU_{tot} minimization, pairs plots of inputs and the output TRU_{tot}^{norm} of adaptive strategies allow to give an insight on the responses of fuel cycle to the variation of input parameters. The pairs plots are shown in Figure 3.22 over t_{ad}, where the points are colored by the val-

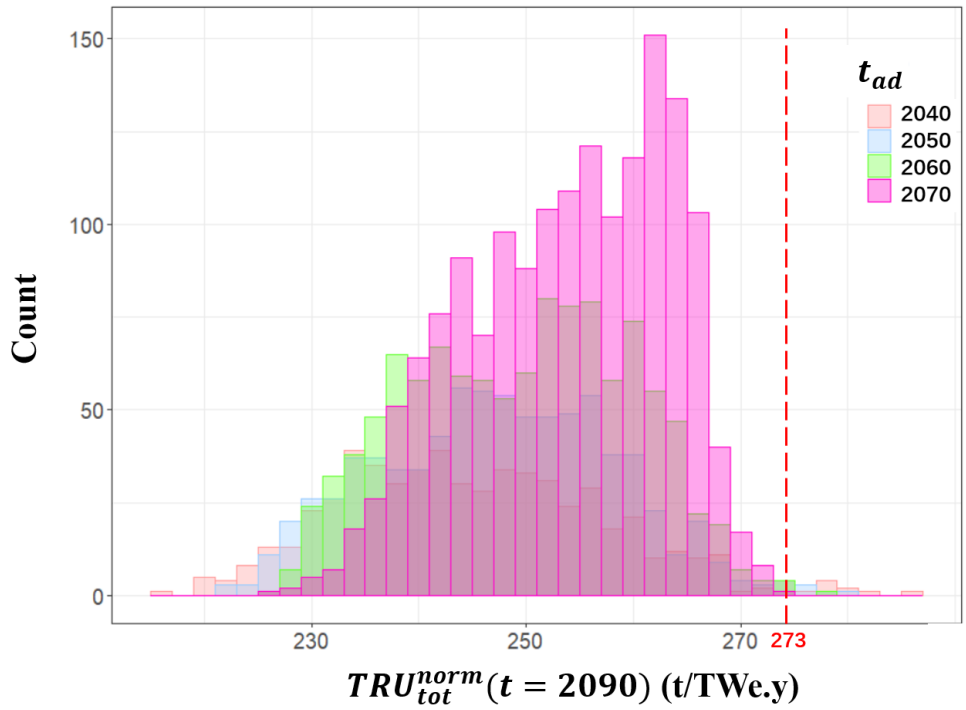

Figure 3.21: Histogram of TRU_{tot}^{norm} of adaptive strategies by 2090 over t_{ad}

ues of TRU_{tot}^{norm}; near-blue points stands for the low level of TRU_{tot}^{norm} and near-red points represent the high level. The importance of $FrMOX_f$ is verified. However, input BU_{UOX}, an important parameter in pre-disruption scenario, seems to have much smaller effects on output TRU_{tot}^{norm}. Actually, as highlighted in previous analyses in section 3.3, the global statistical effects is strongly linked to the variability of variable. In adaptation scenario, the variability of $FrMOX_f$ is much higher than in pre-disruption scenario, and the relative importance of other parameters, such as BU_{UOX}, can a-priori be reduced. In addition, when MOX fraction is high, the effects from UOX fuels and relevant parameters become restricted because of the limited share of UOX fuels. An extreme case is that if the MOX fraction is close to 100%, outputs can be insensitive to the parameters of UOX fuels.

In terms of other input parameters, the importance of $P_{tot,f}$ is still measurable. BU_{MOX} also seems to have some effects on TRU_{tot}^{norm}, especially the strategies leading to low TRU_{tot}^{norm} prefer high BU_{MOX}. It may be explained by a better use of plutonium: if BU_{MOX} is high, fresh MOX fuels demands high content and thus high inventory of plutonium, which implies that the inventory of idle plutonium in spent UOX is kept at low level. Since $^{241}\mathrm{Pu}$ is short-lived, low inventory of idle plutonium in spent UOX can improve the use of high-quality plutonium. Actually, a LiFo strategy for spent UOX management has a similar effect as well, which is verified by the adaptive optimum in the following analyses. Last but not least, the parameter D is statistically not important on TRU_{tot}^{norm}, which is totally different from its role on TRU_{tot}. Actually, its contribution is principally presented by the correlation with $FrMOX_f$. According to the analysis above, the most efficient way to minimize TRU_{tot} is to incinerate the plutonium in spent UOX fuels, so that TRU_{tot} can be reduced while increasing the energy production. Within this large range of $FrMOX_f$, even long transition of large D can empty the interim stock of spent UOX with appropriate choice of $FrMOX_f$.

To assess the adaptive robustness, trajectories of adaptive strategies, as well as the two important prior trajectories of reference strategy and robust static optimum, are shown in Figure 3.23. In the pairs plots of Figure 3.23, the threshold $TRU_{th,ad}^{norm} = 221$ t/TWe.y is also presented by purple dash lines.

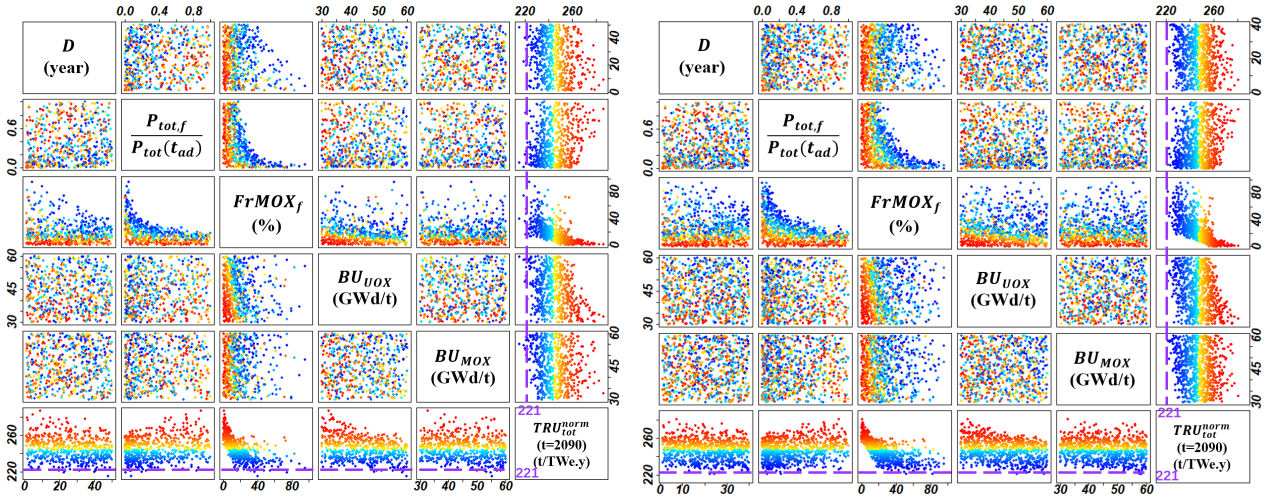

(a) $t_{ad} = 2040$ (b) $t_{ad} = 2050$

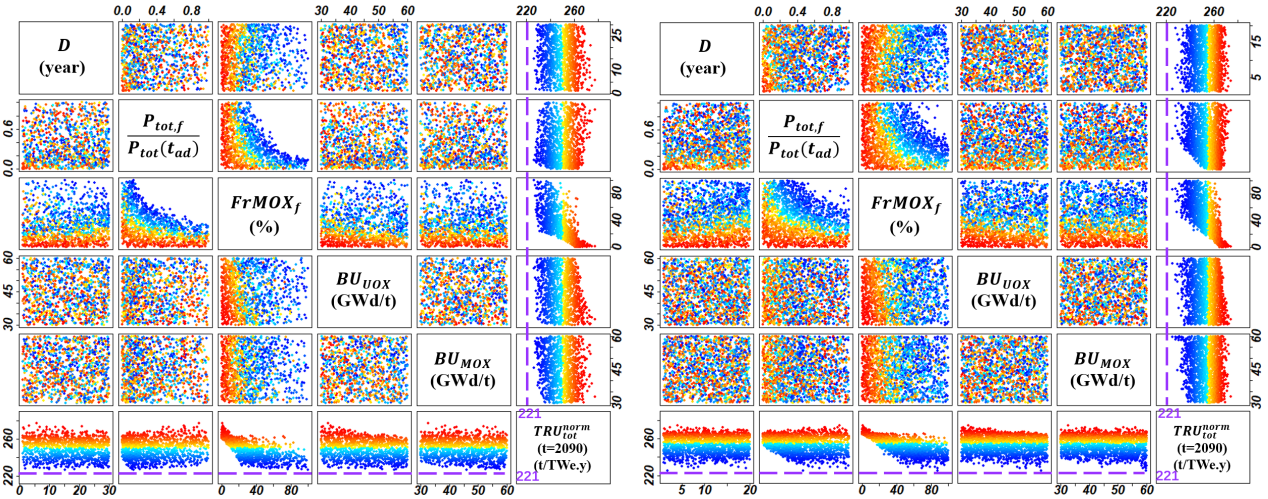

(c) $t_{ad} = 2060$ (d) $t_{ad} = 2070$

Figure 3.22: Pairs plots of output TRU_{tot}^{norm} and important inputs D, $P_{tot,f}$, $FrMOX_f$, BU_{UOX} and BU_{MOX} over t_{ad}, colored by the values of TRU_{tot}^{norm}

Compared with the robust static optimum, there exists adaptive strategies that lead to lower TRU_{tot}^{norm} by 2090 than $TRU_{th,ad}^{norm}$ if $t_{ad} = 2040$; otherwise, the TRU_{tot}^{norm} of possible adaptations are always higher than the robust static optimum. With respect to the criterion $C_{Bnorm}^{t\text{-}set}$ and the adaptation from reference trajectory, the time limit to have robust adaptations is around year 2050. In regard to the year 2090 as the time horizon, the temporality of adaptive robustness, as defined in section 3.3 is longer than 40 years.

Adaptive optimum of each case of t_{ad} indicates if the adaptation can be robust. The evolution of TRU_{tot}^{norm} of these optima are represented by thick lines in Figure 3.23, and the values of inputs and output TRU_{tot}^{norm} of adaptive optima are presented in Table 3.22. Adaptive optima after disruption lead to the values of TRU_{tot}^{norm} by 2090 quite close to the result of robust static optimum. Note that the relative discrepancy of TRU_{tot}^{norm} of adaptive optima to $TRU_{th,ad}^{norm}$ is around 3%, while the uncertainty of accumulated TRU_{tot} is also in this magnitude. Results are totally different from the previous adaptation study with respect to TRU_{tot}, where a measurable fraction of valid strategies can be considered to be robust within acceptable ambiguity. In this adaptation study, the robustness assessment depending on a delicate nuance of numeric results may be not sufficiently credible.

Instead of exhausting the exploration of robust strategies possibly without sufficient credibility, one useful information can be deduced with respect to the

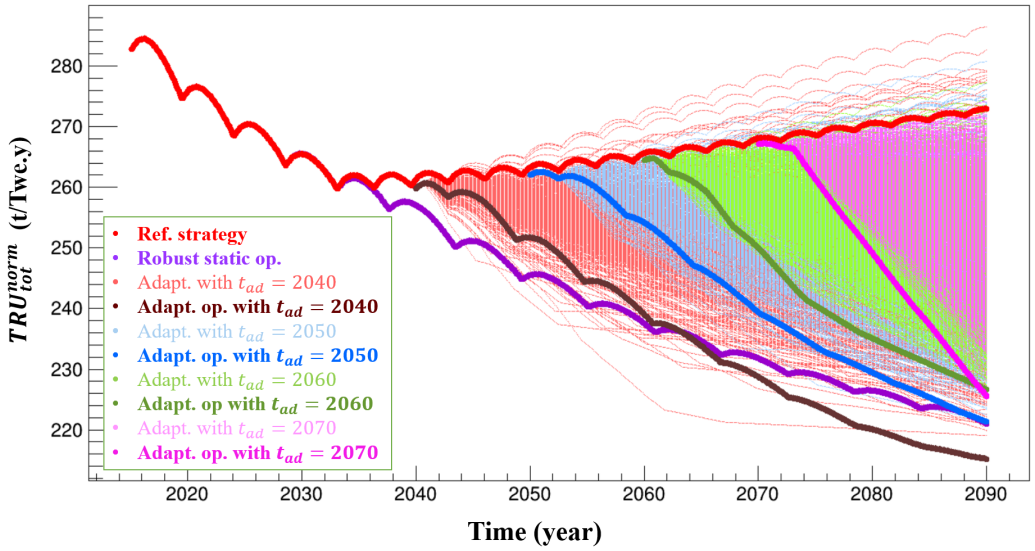

Figure 3.23: Evolution of TRU_{tot}^{norm} of adaptive strategies, and the prior trajectories of reference strategy and robust static optimum

t_{ad} of op.	D	$P_{tot,f}$	$FrMOX_f$	BU_{UOX}	BU_{MOX}	TC_{UOX}	MPu	TRU_{tot}^{norm}
$t_{ad} = 2040$	47.7	13.5	40.1	59.8	55.1	3.1	LiFo	215
$t_{ad} = 2050$	22	34.7	51.6	58.8	58.1	4.1	LiFo	221
$t_{ad} = 2060$	15	18.8	100.	55.4	45.9	8.8	LiFo	226
$t_{ad} = 2070$	2	59.5	87.2	57.9	59.7	5.9	LiFo	226
(Unit)	year	GWth	%	GWd/t	GWd/t	year	-	t/TWe.y

Table 3.22: Inputs and output TRU_{tot}^{norm} of adaptive optima over t_{ad}

minimization of TRU_{tot}^{norm}. Even though the variability of important parameter $FrMOX_f$ is much larger than the one before disruption, adaptive readjustments cannot achieve a far better performance than the immediate precautionary action suggested by the strategy of robust static optimum. Meanwhile, this optimal performance can still be approximated by adaptation even in a large range of t_{ad}, while necessarily high MOX fraction can be traded for the temporality of adaptation.

3.4.4 Conclusion of the complement analysis and the comparison with previous study without normalization on the waste

In this section, another translation of objective B is used, which aims to minimize the normalized TRU inventories in the total cycle TRU_{tot}^{norm}. The same methods of scenario analysis and robustness assessment as presented in Section 3.2 and 3.3 are employed. This study reveals that with a different translation of the same objective to numeric criterion, the mechanism of fuel cycle responses to the variation of inputs in the two cases can be completely different, and so is the robustness assessment. Analysts should then take extra care to the stakeholders interests they can not even define. Indeed, our two formulations for criterion B were built to answer the same objective which is the minimisation of potential waste.

For $C_B^{t\text{-}set}$, the relevant output of interest TRU_{tot} is an extensive quantity and depends strongly on the scale effect of $P_{tot,f}$. For most of strategies without measurable risk of missload, TRU_{tot} increases significantly over time. Since the varia-

tion scales of total power of fleet in the situation before disruption and the one for adaptation are completely different, the threshold of adaptive robustness $TRU_{th,ad}$ deduced from pre-disruption scenario is a projection far in the future much higher than the levels estimated at some given points of time, such as year 2040, 2050 and 2060; and the margin between $TRU_{th,ad}$ and $TRU_{tot}(t = t_{ad})$ is therefore relatively large to be adaptively robust with respect to the hypotheses of parameter variation. The time limit to achieve robust adaptations is then in the 2060s.

When wastes are normalized, the output TRU_{tot}^{norm} of $C_{Bnorm}^{t\text{-}set}$ is much less sensitive to $P_{tot,f}$ by construction, but much more sensitive to the use of plutonium, such as $FrMOX_f$ and BU_{UOX}. Due to the normalization, TRU_{tot}^{norm} is similar to an intensive quantity that can be "diluted" or "concentrated", but bounded by extreme states. In this case, even though the variability of the important factor $FrMOX_f$ of adaptation is far higher than pre-disruption strategy, it does not help improve the minimization of TRU_{tot}^{norm} compared to the robust static optimum before disruption. Under these implications, the adaptive robustness is far less evident. Numerically, the time limit to achieve robust adaptations is the 2040s. However, the discrepancies between the TRU_{tot}^{norm} of adaptive optima regardless t_{ad} and the threshold $TRU_{th,ad}^{norm}$ are in the similar magnitudes of uncertainties of TRU_{tot}^{norm} estimations. In comparison, both the physics explanation of fuel cycle behavior and the assessment of adaptive robustness with respect to $C_{Bnorm}^{t\text{-}set}$ is globally different from the analysis of $C_{B}^{t\text{-}set}$.

The cumulative production of energy builds the connection between these two outputs, the absolute level of TRU TRU_{tot} and the normalized one TRU_{tot}^{norm}. Because the energy produced from TRU is limited under the mono-recycling, TRU_{tot} is highly correlated with the cumulative production of energy, as shown in Figure 3.24. Figure 3.24a presents the TRU_{tot} and the cumulative production of energy by 2090 of all valid pre-disruption strategies, colored by the input $P_{tot,f}$ in pre-disruption scenario. The domination of $P_{tot,f}$ on these two outputs is evident. The dispersion of points leads to different slopes which stands for the normalized waste TRU_{tot}^{norm}, principally due to the choices of $FrMOX_f$ and BU_{UOX} as explained. Equivalently, this corresponds to different allocation options of plutonium in facilities, either stored in spent UOX fuels, or partially burned and stored in spent MOX fuels. With dynamic readjustments, the available plutonium/TRU can be used for energy production. In this case, a lowest achievable TRU_{tot}^{norm} seems highly possible to be reversible regardless the adaptation time (if neglecting the reduction of plutonium quality during storage). It is however too hard to become measurably lower than the robust static optimum in regard to criterion $C_{Bnorm|A}^{t\text{-}set}$.

In comparison, it is harder to reduce TRU_{tot} by mono-recycling once it goes beyond a given level, here determined by the corresponding robust static optimum (which fulfills $C_{B|A}^{t\text{-}set}$). As shown in Figure 3.9, this robust static optimum maximizes the use of available plutonium in the stock of spent UOX fuels. Corresponding to this high use of plutonium of mono-recycling, each increment on the cumulative energy production brings a net production of TRU_{tot}. Thus, a lower cumulative production of energy is much more effective to achieve a lower level of TRU_{tot}, and it is confirmed in Figure 3.24b. This figure shows the evolution of TRU_{tot} and the cumulative production of energy resulting from all valid pre-disruption strategies as well as the robust adaptive strategies over t_{ad}, regarding the minimization of TRU_{tot}. Most of the robust adaptations lead to a lower cumulative energy production than the robust static optimum (which minimizes TRU_{tot}). Cases that allow higher energy production by 2090 are extremely rare. As an interpretation, the cost to adapt to lower level of TRU_{tot} may be a lower eventual energy production. At the same time, readjustments should be taken sufficiently

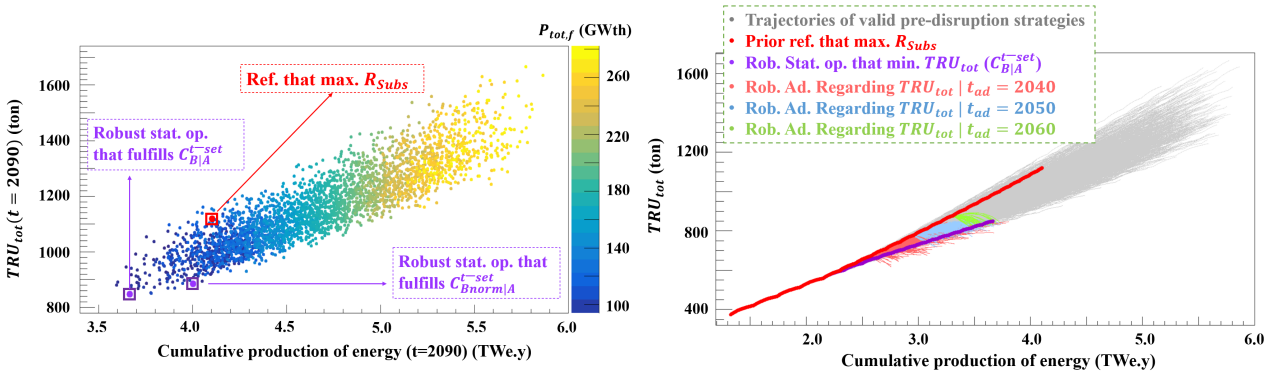

(a) (b)

Figure 3.24: TRU_{tot} versus cumulative production of energy of trajectories simulated: (a) results by 2090 of valid pre-disruption strategies; (b) evolution of two outputs, for both valid pre-disruption strategies and robust adaptive strategies regarding the minimization of TRU_{tot}

in advance to achieve a lower cumulative energy production. This explains the different approachability of TRU_{tot} from that of TRU_{tot}^{norm} if the corresponding time limit is over.

In spite of suggesting different strategies, both choices of outputs and criteria for objective B make sense, and none of them is comprehensively superior. All depends on the interest of stakeholders and the choice of analysts. It implies that the translation of objective into numeric criterion should be clarified with caution, because even a slight ambiguity of hypothesis can result in the obscurity of assessment. Furthermore, the purpose of this Ph.D is to tackle deep uncertainties in scenario studies by disruptions simulations. It seems reasonable to say that objective A and objective B are related directly to the future evolution of nuclear energy. The deep uncertainty of objectives (meaning the deep uncertainty of stakeholders interest) may involve then a deep uncertainty on the power evolution of the global fleet. The construction of criterion independent from this installed capacity may be a way to handle the uncertainty and draw conclusions of robustness assessments without any disruption simulation concerning power-related objectives.

3.5 Conclusion of this chapter

In this chapter, robustness of strategies have been assessed in a pre-determined observation time. Under this assumption, the static robustness of strategies in pre-disruption scenario and the adaptive robustness of strategies based on the prior reference trajectory have been assessed.

The maximization of R_{Subs} by year 2090 for SFR deployment is pre-selected as objective. Under uncertain disruption, it could be changed to minimizing TRU_{tot} by 2090 without any SFR deployment. Coherent with the preliminary scenario study in Chapter 2, $P_{tot,f}$, $FrMOX_f$ and BU_{UOX} are shown to be important parameters for both outputs R_{Subs} and TRU_{tot} in the pre-disruption scenario. The Pareto front of these two contradictory objectives is achieved by the minimization of $P_{tot,f}$, while the trade-offs of these robust static strategies are presented on the different choices of $FrMOX_f$ and BU_{UOX}. The reference strategy for the pre-selected objective of SFR deployment leads to $R_{Subs}(2090) = 1.68$ implying 68% of the margin of plutonium availability in 2090. 1120 tons of TRU in total cycle is accumulated. In contrast, the robust static optimum accumulates only 849 tons, but keeping only 18% of margin for plutonium availability.

The adaptation scenario starts from the prior trajectory of the reference strategy. Four adaptation times t_{ad} are considered: year 2040, 2050, 2060 and 2070. In the adaptation scenario, variables D, $P_{tot,f}$ and $FrMOX_f$ have direct impacts on the output $TRU_{tot}(2090)$. Furthermore, valid ranges of $P_{tot,f}$ and $FrMOX_f$ change over t_{ad} subject to the plutonium availability for MOX fuels. To perform the robustness assessment, the performance of adaptive strategies represented by $TRU_{tot}(2090)$ is compared with the robust static optimum one. Strategies achieving lower $TRU_{tot}(2090)$ are considered robust. Robust adaptive strategies are identified when $t_{ad} \leq 2060$, but none has been found when the adaptation occurs after 2070.

The criterion with respect to the objective linked to disruption is then formulated in another definition, considering the minimization of TRU normalized by cumulative energy production, denoted as TRU_{tot}^{norm}. This study shows the influence of uncertain formulation of objective on the strategy assessment. It has also been verified that this formulation freed the analyses from the dependency on the deep uncertainty of future fleet power. With respect to output TRU_{tot}^{norm}, the analysis verifies that $FrMOX_f$ and BU_{UOX} are the dominant factors, and the effect of $P_{tot,f}$ is much weaker than its impact on TRU_{tot}. It is explained by the fact that TRU_{tot} is an extensive quantity controlled by scale-related factor like $P_{tot,f}$, while the normalized quantity TRU_{tot}^{norm} is rather sensitive to the valorization of TRU (principally the plutonium), which is characterized by $FrMOX_f$ and BU_{UOX}. Therefore, compared with the robust static optimum standing for the historically best choice before disruption, most of adaptive strategies lead to higher TRU_{tot}^{norm}, and robust adaptive strategies are extremely rare even if t_{ad} is early. However, it also means that this best level can be approached increasing the MOX share, in spite of irreversible loss due to insufficient time and possibly the decrease of plutonium quality.

Chapter 4

Strategy evaluation and Robustness assessment disconnected from pre-determined time

A given time horizon for scenario evaluation is classically considered in lots of projects for formulation of perspectives in different studies. However, as pointed out in the discussion in Section 3.3, the analysis of adaptive robustness under a set time horizon, especially connected with a pre-determined time, may lead to inter-temporal inconsistency in practical assessments.

An option to address this issue is to disconnect the evaluation of strategy from any pre-determined time. In this case, the time horizon of scenario can be more flexible than the previous case. In this chapter, time characteristics of previous outputs evolution (R_{Subs} and TRU_{tot}) are considered, with no consideration of any pre-determined time. This implies new reformulations of objectives and their relevant numeric criteria. Using these new objectives and criteria, the physics analysis of fuel cycle as well as the robustness assessment can be quite different from the ones connected to a set time horizon in Chapter 3.

Moreover, the new analysis in this chapter can highlight and address several shortcomings of the previous adaptive robustness assessment discussed in Section 3.3. Specifically, the assumptions that only one reference trajectory is adapted, and the fact that no new technology is taken into account are discussed. Some evaluations about how these aspects impact the conclusion are also carried out.

In this study, the same two example objectives concerning the future of the future plutonium status as in the previous chapter are considered: the pre-selected objective A considers the substitution of PWR-fleet with future SFR deployment; the objective B linked to the uncertain disruption is to minimize the TRU inventories in total cycle without SFR deployment. To allow an independent evaluation from a pre-determined time of observation, the problem is reformulated with new criteria in Section 4.1, introducing new scenario assumptions. The thresholds R_{th} and TRU_{th} are defined and justified for the acceptable levels of R_{Subs} and TRU_{tot} respectively. These two thresholds are the central assumptions for the evaluation of strategy performances. Based on new assumptions, the static robustness assessment is performed in a pre-disruption scenario in Section 4.2.

The new assumption regarding the time horizon implies also a more complicated definition of validity and robustness assessment in adaptation scenarios. To give a fundamental understanding, the adaptations from the prior reference trajectory identified in pre-disruption scenario are studied for the adaptation from year 2040 in Section 4.3. Learning from the studies in Chapter 3, two aspects are complemented. The first one considers the adaptation from a set of prior trajec-

tories. This introduces the notion of adaptability of prior trajectories in Section 4.4, which help complement the robustness assessment. Under the estimation of adaptability, a set of prior trajectories are adapted from 2070, and the new adaptive robustness assessment is carried out.

The second aspect in Section 4.5 considers the use of MOX on Enriched Uranium Support (MOXEUS) in PWRs, a new option that is supposed to be unavailable before disruption for adaptation. This analysis uses the model of MOXEUS developed in [50] in which both the $^{235}\mathrm{U}$ enrichment and the plutonium content are variables for the Fuel Loading Model. The MIX fuel will be used in Chapter 5 where more realistic issues of the future French fleet are addressed. New properties of strategies concerning adaptive robustness can be expected.

4.1 Problem formulation: objectives disconnected from pre-determined point of time

As indicated in the introduction of this chapter, the same two objectives are considered to compare the assessment disconnected from a pre-determined time with the assessments in Chapter 3. Objective A aiming to the substitution of PWR-fleet with future SFR deployment is pre-selected, while the disruption of this objective is deeply uncertain. If objective A is disrupted, TRU inventories in total cycle should be minimized in the PWR-fleet system.

Corresponding to these two objectives, two outputs, the substitution ratio (R_{Subs}) and TRU inventories in total cycle (TRU_{tot}) are considered. To evaluate if the strategies of interest have acceptable performances, thresholds in terms of R_{Subs} and TRU_{tot}, written respectively as R_{th} and TRU_{th}, need to be set to represents an estimation of an acceptable level. To disconnect the evaluation of the strategy from the time horizon of the scenario, the general idea is to estimate the time when the physics quantities check the inequalities defined by the thresholds ($R_{Subs} > R_{th}$ and $TRU_{tot} > TRU_{th}$).

As discussed in Section 3.1, the choice of a relevant threshold is a difficult issue. $R_{th} = 1$ may make sense but does not take any plutonium margin into account for SFR fuel fabrication. In this study, the assumption of $R_{th} = 1$ is used, considering that the margin asked by the uncertainties on the R_{Subs} evaluation can be replaced by a margin taken for the time when $R_{Subs} > R_{th}$.

TRU_{th} involves the bibliographical research on waste disposal. Several thresholds may be considered in pre-disruption scenario; meanwhile, the threshold used in adaptation scenario can be also different from the previous ones, due to the different situations before and after disruption. To disconnect the evaluation of strategies from a pre-determined time and a preset time horizon, new notions with respect to thresholds different from the study in Chapter 3 should be defined.

4.1.1 Role of time horizon in this study

In Chapter 3, the assumption of evaluating a strategy at a given time constrains the time horizon of scenario. Although in this chapter we are aiming to free ourselves of such dependency on a pre-determined time, the time horizon of simulations and scenario cannot be indefinite. A fleet transition and outputs of interest evaluated after several centuries are not of interest. Furthermore, the simulation should stop on a reasonable time to keep the calculation time and the size of the outputs reasonable. Therefore, a time horizon needs to be determined

for both studies of pre-disruption scenario and adaptation scenario.

As presented in Section 4.2, some results of strategies may be quantifiable and others may be not, depending on the behavior of the fuel cycle and the choice of time horizon. The fact that some results are non-quantifiable can also help construct meaningful strategies. The functionality of time horizon should reflect more on the interest of studies than its impacts on the conclusion of scenario studies. With the new notions introduced in the subsequent formulations, the assessment of strategies can remain relatively consistent regarding different assumption of time horizon.

The time horizon of pre-disruption scenario can remain the same as the one in Chapter 3, from year 2015 to 2090. In short, the current fleet will be replaced successively by the new generation of reactors, such as EPR, and this new fleet may be replaced at the end of century. This time horizon covers then the fleet transition in this century and the end corresponds well the timing of the substitution with SFR.

The horizon of adaptation scenario can be freed from the one of pre-disruption scenario. To minimize TRU, a time period similar to the life of reactor can be used to investigate the behavior of fuel cycle, like 50 years from the beginning of adaptation. Such length of period is long enough to observe the dynamics of the fuel cycle, and it is not so long that too many uncertainties of long-term future involve in the study.

4.1.2 Validity and performances in pre-disruption scenario and static robustness assessment

In Chapter 3, the pre-disruption scenario is studied considering R_{Subs} and TRU_{tot} by 2090 for evaluation criteria. Here the pre-disruption assessment differs due to the different criteria defined for the disconnection between the assessment and the evaluation time, as presented in the following.

The priority is still given to objective A, while the minimization of TRU is secondary. Subject to the priority of objective A on the future deployment of SFR, missloads within the time horizon of scenario is considered unacceptable. Hence, the pre-disruption strategies leading to missloads are considered invalid and are discarded from any further analysis.

The assessment of pre-disruption strategy in this study is related to the threshold levels for the outputs of interest, R_{th} and TRU_{th}. Suppose first these two thresholds are known, and the two corresponding objectives can be recast into the criteria as:

- $C_A^{t\text{-}dcn}$: The time when R_{Subs} of each strategy becomes higher than the threshold R_{th} is studied, denoted as t_R. It should be within the time horizon of interest given the priority of objective A; minimize t_R if optimization is required.
- $C_B^{t\text{-}dcn}$: The time when TRU_{tot} of strategy becomes higher than the threshold TRU_{th} is studied, denoted as t_{TRU}. Maximize t_{TRU} according to objective B.

Mathematically, the two mentioned times of interest, t_R and t_{TRU} of a given strategy, are defined as:

$$t_R = \min\{t_r | \forall t \geq t_r, R_{Subs}(t) \geq R_{th}\} \tag{4.1}$$

$$t_{TRU} = \min\{t_{tru} | \exists t \leq t_{tru}, TRU_{tot}(t) \geq TRU_{th}\} \tag{4.2}$$

By definition, $C_A^{t\text{-}dcn}$ searches for the strategy that achieves objective A characterized by threshold R_{th} as quickly as possible. The time needed, represented by t_R, evaluates the performance in regard to objective A. Given the priority of

objective A, the valid strategies leading to quantifiable t_R which should be earlier than the time horizon, are of interest. With the same notation as used in Chapter 3, the reference strategy that is optimal for the pre-selected objective A, should minimize t_R among all valid strategies in this chapter. Concerning $C_B^{t\text{-}dcn}$, the strategies should be able to postpone the time when the TRU_{tot} exceeds the threshold TRU_{th} as late as possible. The time needed, represented by t_{TRU}, evaluates then the performance of strategy regarding a given acceptable level of TRU disposal. t_{TRU} later than the horizon (and thus not defined in our simulations) means that the TRU inventories do not go beyond the given level within the time horizon of interest. Therefore, these strategies are well performing regarding the minimization of waste.

Figure 4.1 presents graphically how to calculate the t_R and t_{TRU} of a trajectory from a given strategy, according to different choices of thresholds R_{th} and TRU_{th}. To summarize, objective A requires a sustainable material availability before the substitution of fleet, while it can be problematic when the threshold of capacity of waste deposit is exceeded for the first time. But due to the consideration of objective priority, strategies leading to quantifiable t_R within the time horizon are conceptually more of interest than those leading to non-quantifiable t_{TRU} before any disruption.

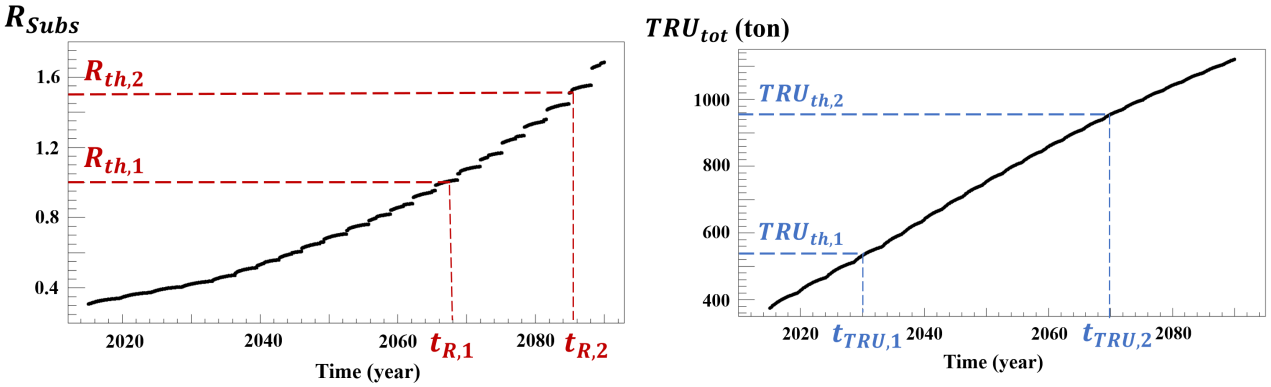

Figure 4.1: Determination of t_R and t_{TRU} of a trajectory from a given strategy, according to the choices of thresholds R_{th} and TRU_{th}

Robust static strategies should then maximize t_{TRU}, under the condition that t_R is earlier than the time horizon of interest, or even is minimized if possible. Given the contradiction between these two objectives, some trade-offs may exist on the performance of t_R and t_{TRU}. Similar to the study in Chapter 3, static strategies in Pareto front of the output space t_{TRU}-t_R can be considered robust: if t_{TRU} of all strategies can be determined within the time horizon, a single optimum can be identified by applying the conditional criterion $C_{B|A}^{t\text{-}dcn}$:

- $C_{B|A}^{t\text{-}dcn}$: Maximization of t_{TRU} under the condition that t_R is realized within the time horizon of interest.

The strategy that satisfies $C_{B|A}^{t\text{-}dcn}$ is then called the robust static optimum in the following of this chapter. It is worth noting that this robust static optimum may differ from the one identified in Chapter 3, because the criteria have different definitions.

But because t_{TRU} can be out of horizon (which also means that the TRU inventories in total cycle are always under the threshold level), it is possible that the Pareto front of this part is not well-defined. Actually, these foregoing cases depend strongly on the choices of thresholds TRU_{th}, which also influence the results of fuel cycle analysis as well as the robustness assessment. As will be presented

in Section 4.2, different TRU_{th} are used, and the impacts of their definitions on the fuel cycle analysis and robustness assessment are investigated.

4.1.3 Validity and performances in adaptation scenario and adaptive robustness assessment

For adaptation scenario, the time horizon of interest should be also determined, which is not necessarily the same as the one in pre-disruption scenario. After the disruption, the goal becomes the minimization of TRU inventories in total cycle in the PWR-fleet. Because the evaluation of strategy is separated from any pre-determined time, the validity of an adaptive strategy can be different from previous cases where we consider only the trajectories without any missload until the end of the scenario (year 2090). Similar to the assumptions made in Chapter 3, the adaptations consist in the change of parameters in a large range, including fast phase-out strategies starting from the adaptation time.

For each trajectory, the first time of missload, denoted as t_{ML}, may define its time horizon as long as it is later than the end of the new transition defined by adaptation. The first missload may happen hundreds of years after disruption (even never). Consequently, we have to define a maximal time horizon, depending on our studies. This way to proceed leads to different time horizon for a set of trajectories with adaptations.

The post-disruption planning can be characterized by the new transition of adaptation. In brief, a valid adaptive strategy should finish this transition before meeting missloads, which can be summarized as the criterion of validity, denoted as :

- $C_{V,ad}^{t\text{-}dcn}$: An adaptive strategy is valid in this adaptation scenario study if $t_{ML} > t_{ad}+D$; the well-defined duration of the corresponding trajectory is $\{t|t < t_{ML}\}$.

where D is the duration of fleet transition defined by the corresponding adaptive strategy. According to $C_{V,ad}^{t\text{-}dcn}$, the evolution of the fleet is well defined before the first missload; once the first missload is met, the level of TRU_{tot} is implicitly maintained by phase-out after the first time of plutonium shortage. This assumption ensures then the results validity of a valid adaptation within different time horizons.

In terms of the assessment of adaptive robustness, one may choose the same threshold TRU_{th} as the one in pre-disruption scenario, which relies on the estimation of waste disposals availability in the future. However, this choice is not coherent with our approach that disconnects assessment to time horizon. Indeed, this value only makes its own sense within the time horizon of pre-disruption scenario, whereas the adaptation scenario may have a different horizon. Another choice is to investigate the lowest level of $TRU_{tot}(t = t_{ad})$ among valid strategies leading to t_R within the horizon of pre-disruption scenario. Figure 4.2 presents graphically how this threshold level can be determined from prior trajectories. This value, denoted as $TRU_{th,ad}$, has to be distinguished from the threshold taken in pre-disruption scenario. It indicates the best historical choice regarding the level at adaptation time among all pre-disruption strategies pursuing objective A. Thus, the aim of adaptation is to adapt the prior trajectory to reduce TRU inventories and to go beneath $TRU_{th,ad}$, absorbing the excess of TRU relative to this best historical level by t_{ad}. In this case, a new criterion of adaptation can be used, respecting $C_{V,ad}^{t\text{-}dcn}$, in order to be distinct from the one $C_B^{t\text{-}dcn}$ in pre-disruption scenario:

- $C_{B,ad}^{t\text{-}dcn}$: Respecting $C_{V,ad}^{t\text{-}dcn}$, the time that TRU inventories in total cycle go beneath $TRU_{th,ad}$, denoted as t'_{TRU}, should be within the time horizon of adaptation scenario, and before the first missload ($t'_{TRU} < t_{ML}$). The optimum should minimize t'_{TRU}.

where t'_{TRU} of a strategy is mathematically defined as:

$$t'_{TRU} = \min\{t' | \exists t \geq t', TRU_{tot}(t) \leq TRU_{th,ad}\} \tag{4.3}$$

Thus, t'_{TRU} denotes the first time when TRU_{tot} goes beneath $TRU_{th,ad}$. Actually, when the regret of TRU_{tot} relative to $TRU_{th,ad}$ is absorbed by adaptive strategies, there exist at least a phase-out option to keep this low-level TRU_{tot}. For a given t_{ad}, t'_{TRU} also indicates the time needed to remove the excess of TRU inventories in total cycle relative to $TRU_{th,ad}$.

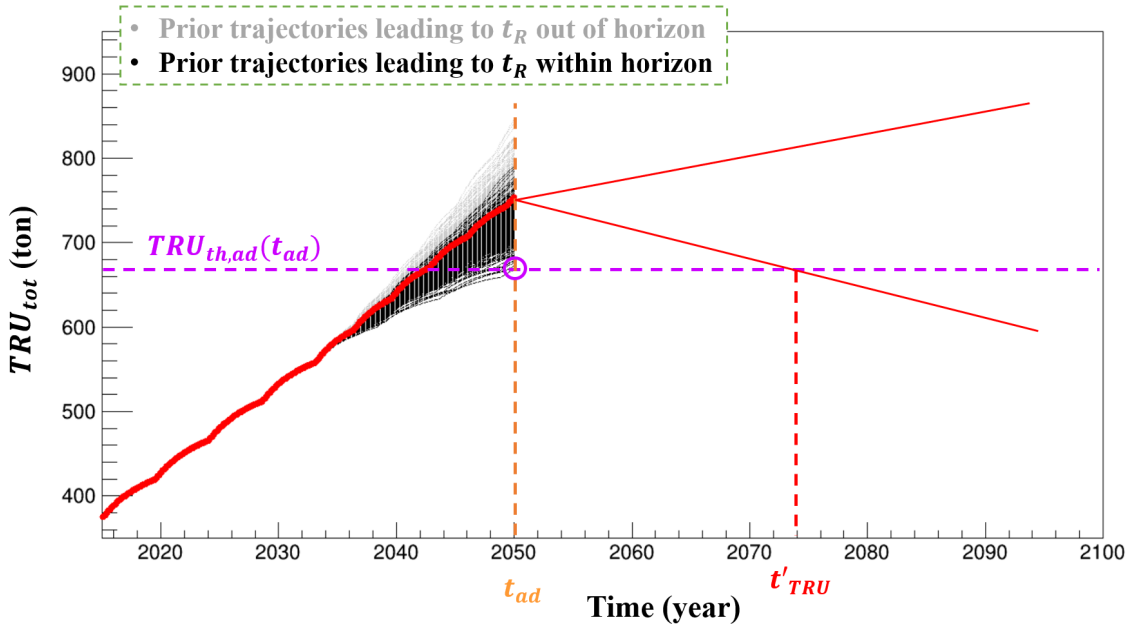

Figure 4.2: Determination of threshold level $TRU_{th,ad}$ and the time t'_{TRU} in adaptation scenario study

To summarize, the robustness assessment is carried out only for valid strategies that satisfy $C_{V,ad}^{t\text{-}dcn}$. An adaptive strategy is considered robust if it satisfies $C_{B,ad}^{t\text{-}dcn}$. Moreover, the performance of adaptive robustness can be estimated by the output t'_{TRU}. The earlier is t'_{TRU}, the less time is needed to go beneath $TRU_{th,ad}$, and so the better is the robust adaptive strategy.

4.2 Pre-disruption scenario and static robustness analysis

The methodology concerning the static robustness assessment is well developed and presented in Chapter 3, in which the results are connected with predetermined evaluation time. The method is not directly suitable for the analysis in this study: due to the disconnection from any predetermined time, t_R or t_{TRU} of an explored strategy can be out of time horizon of simulation and thus non-quantifiable, while it is valid without missload. This issue depends directly on the thresholds used to define these two outputs of interest.

To establish the framework for this new pre-disruption scenario study with sufficient clarity, the analysis of fuel cycle and strategy assessment are performed in various assumptions, and the results under these assumptions are compared.

Three assumptions are addressed: the thresholds used to calculate the outputs, the subset of samples used to perform the fuel cycle analysis, and the assessment of static robustness depending on the two previous conditions.

4.2.1 Possible problems in the application of new concepts in pre-disruption scenario study

4.2.1.1 Pre-disruption scenario and possible phase space of outputs of interest

As justified in Chapter 3, a time horizon from year 2015 to year 2090 is of interest. Accordingly, the simulation of fuel cycle stops by 2090. Since the context of this study is not modified, the global idea of this scenario study is similar to the analysis in Section 3.2.1, summarized in Figure 3.1 and in Table 3.1. The same exploration space of pre-disruption scenario is considered. The particularity of the pre-disruption scenario study in this chapter is to evaluate the time needed to go beyond a given threshold with respect to two objectives within the time horizon of interest, represented by t_R and t_{TRU} respectively. Those times are the outputs of interest in this study and the assessment method of robustness are defined in Section 4.1. The goal is to minimize t_R, which brings forward the capacity to replace the fleet as fast as possible, while maximizing t_{TRU} at the same time, which postpone the accumulation of TRU inventories as late as possible. Within the same strategy space, there is no need to launch new simulation, and only the computation of outputs t_R and t_{TRU} is required for each simulated trajectories.

Given the priority of the planning of future SFR deployment, a strategy in this pre-disruption scenario is considered valid if it does not have any missload before 2090. The analysis of validity is performed in Section 3.2. Since the time horizon of interest is set to year 2090, simulations stop by year 2090, and the t_R of a strategy that does not exist within the horizon is considered too far. Equivalently, a strategy leading to $t_R \leq 2090$ means that the substitution of fleet can be fulfilled from the angle of plutonium availability within the time horizon, and thus this strategy can achieve objective A. Meanwhile, a strategy leading to $t_{TRU} \geq 2090$ means that within the time horizon, TRU inventories in total cycle will not reach the threshold, and thus it is a well-performing strategy for objective B. In general, the output space t_{TRU}-t_R of valid static strategies can be divided into four subsets according to the given horizon of interest, as shown in Figure 4.3:

- $S_{A\wedge B^+}$: the strategy leads to $t_R \leq 2090$, achieving objective A; it also leads to $t_{TRU} \geq 2090$, relatively well-performing regarding the uncertain disruption.
- $S_{A\wedge B^-}$: the strategy leads to $t_R \leq 2090$, achieving objective A; but it leads to $t_{TRU} < 2090$, which means that a larger TRU inventories than TRU_{th} should be anticipated within the time horizon of interest.
- $S_{\neg A\wedge B^+}$: the strategy leads to $t_R < 2090$, and thus it cannot achieve objective A; while it leads to $t_{TRU} \geq 2090$, relatively well-performing regarding the uncertain disruption.
- $S_{\neg A\wedge B^-}$: the strategy leads to $t_R < 2090$ and $t_{TRU} > 2090$, and thus it cannot achieve objective A, while a larger TRU inventories than TRU_{th} should be anticipated within the time horizon of interest.

In practice, the t_R and t_{TRU} out of horizon are deduced respectively by a linear fit of R_{Subs} and TRU_{tot}, over their evolution during the last ten years. The fitted values may complete the information on the times of interest, but they are hypothetical with some bias not well quantified. For instance, those fitted values do not make any sense if the first missload happens before.

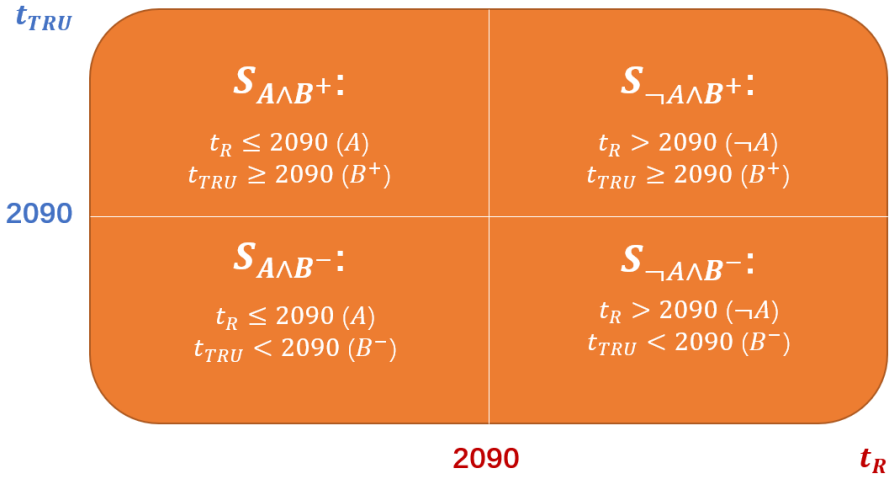

Figure 4.3: Division of the output space t_{TRU}-t_R

4.2.1.2 Possible choice of thresholds to determine the outputs of interest

Before all, one should define the thresholds used for the calculation of t_R and t_{TRU}. The position of R_{th} and TRU_{th} is important for the numeric results of these two outputs. Given the results of trajectories simulated, Figure 4.4a provides a qualitative representation of the time-dependent TRU_{tot} versus R_{Subs} from the valid strategies in pre-disruption scenario, colored as a function of time. The gradual change of color shows the dynamic approach of R_{Subs} relative to R_{th} and TRU_{tot} relative to TRU_{th} over time. The figure also illustrates how the positions of thresholds affect these two times of interest. $R_{th} = 1$ is a reasonable choice

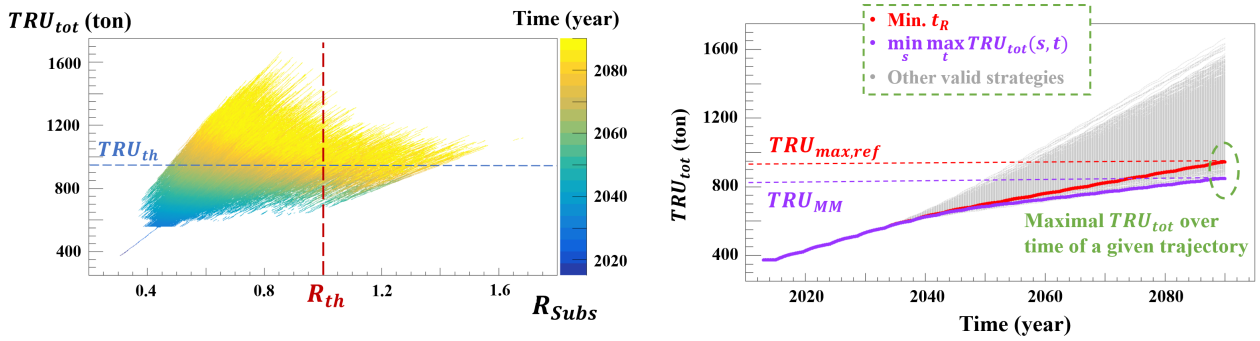

Figure 4.4: Graphical explanation about the effects of choice of thresholds: (a) TRU_{tot} vs R_{Subs} over time of the trajectories of valid strategies in the pre-disruption scenario, colored by the time; (b) How TRU_{MM} and $TRU_{max,ref}$ are determined as threshold TRU_{th}.

regarding objective A. It implies that the in-cycle plutonium inventories allows theoretically the substitution of PWR-fleet with SFR. However, the options for TRU_{th} are diverse and relatively problematic. Instead of searching for a threshold responding to the uncertain interest of stakeholders without clear concession, TRU_{th} here is chosen by the result of a "particular" strategy, which may present a special status in this pre-disruption scenario study. In this framework, two values are available:

- $TRU_{max,ref}$: the maximal TRU inventories over time in the trajectory of the reference strategy (which minimizes t_R) is used.
- TRU_{MM}: For each valid strategy strategy, the maximal TRU_{tot} over time is calculated; the minimum of those maxima among all valid strategies is used

as threshold. This is a minimax determination.

Mathematically, they are defined as:

$$TRU_{max,ref} = \max_{t} TRU_{tot}(s_{ref}, t) \tag{4.4}$$

$$TRU_{MM} = \min_{s|t_R \leq 2090} (\max_{t} TRU_{tot}(s, t)) \tag{4.5}$$

where s_{ref} in Equation 4.4 is the reference strategy that minimizes t_R, and $s|t_R \leq 2090$ in Equation 4.5 implies the condition that the considered valid static strategy achieves the objective A within the time horizon. Actually, given the monotone increase of TRU_{tot} over time of all valid static strategies in this pre-disruption scenario, these two thresholds can be equivalently simplified as $TRU_{max,ref} = TRU_{tot}(s_{ref}, t = 2090)$ and $TRU_{MM} = \min_{s|t_R \leq 2090} TRU_{tot}(s, t = 2090)$. Figure 4.4b presents the determination of the values of TRU_{MM} and $TRU_{max,ref}$. The most important issue of the assessment is then the interpretation of these two thresholds.

$TRU_{max,ref}$ means that the highest accepted TRU_{tot} is given by the reference strategy optimized for objective A. By definition, we have $t_{TRU}(s_{ref}) = 2090$. If the reference strategy is implemented for objective A, a corresponding capacity of disposal of $TRU_{max,ref}$ may be envisaged subject to the uncertain disruption. If another strategy leading to a later t_R accumulates larger inventories of TRU than the reference strategy, it is comprehensively a worse strategy regarding these two possible objectives. On the contrary, if a strategy s allows $t_{TRU}(s) > 2090 = t_{TRU}(s_{ref})$, tradeoffs with a later t_R is also of interest, and this strategy can then be considered robust. In this case, the robust static strategies (s_{rob}) lead to $t_R(s_{ref}) < t_R(s_{rob}) \leq 2090$ and $t_{TRU}(s_{rob}) \geq 2090$. Equivalently, the strategies in the subset $S_{A \wedge B^+}$ are considered robust.

TRU_{MM} implies a strict condition on TRU_{tot} within the time horizon of interest under the condition of achieving objective A. If TRU_{MM} is used as the threshold, the t_{TRU} of strategies achieving objective A ($t_R \leq 2090$) can be all quantified. Actually, given the relation $TRU_{MM} = \min_{s} TRU_{tot}(s, t = 2090)$, TRU_{MM} is given by the previous robust static optimum identified in the study of Section 3.2. This value is actually the global minimum of the highest achieved TRU_{tot} of all valid strategies. Therefore, t_{TRU} of all valid strategies (including those leading to $t_R > 2090$) can be quantified. $S_{A \wedge B^+}$ only contains one strategy and $S_{\neg A \wedge B^+}$ is empty if TRU_{MM} is employed. In this case, a single optimum that satisfies $C^{t\text{-}dcn}_{B|A}$ can be identified; a Pareto front concerning the tradeoffs between the minimization of t_R and the maximization of t_{TRU} exists as well, in which the strategies can be considered robust.

It seems difficult to settle as none of these two choices is completely better than the other one. It is therefore important to take the assumption of the choice of thresholds into account when the results of static robustness are interpreted.

4.2.1.3 Sample space employed for the analysis of fuel cycle by PCA

PCA can be employed to investigate the relation between t_R and t_{TRU} and the input parameters of the fuel cycle. However, as shown in Figure 4.3, the determination of the subsets taken for PCA can be problematic due to the t_R or t_{TRU} out of horizon of interest. For example, to study t_R over static strategy characterized by eight input parameters, three sets are possible and they correspond to different interest and interpretation: $S_A = S_{A \wedge B^+} \cup S_{A \wedge B^-}$, $S_{A \wedge B^-}$, and the set of all valid strategies S_V^{pre} in the pre-disruption scenario.

Strategies of other subsets than S_A are not necessarily of interest as they lead to non-quantifiable t_R. Hence, a PCA with respect to this output is a first possible choice.

The use of S_A for the analysis of t_R implies by the same logic the use of the set $S_{B^-} = S_{A \wedge B^-} \cup S_{\neg A \wedge B^-}$ for the analysis of t_{TRU}. In this case, one may doubt the coherence of two PCAs because the samples used in two analyses are not the same. As an alternative, using $S_{A \wedge B^-}$ can ensure the coherence using the same set of samples. But in this case, the samples are implicitly cut, even though their results also make sense in the respective analysis. The cut creates potentially some more correlations which are not well anticipated nor relevant in S_A or in S_{B^-}.

The main concern of the use of S_A or only the part $S_{A \wedge B^-}$ for the analysis of t_R is the extrapolation of the results on the whole valid space. Similarly, the use of these two subsets for the analysis of t_R implies a cut-off on the valid strategies taken into the analysis, imposing additional correlations on input variables in the phase space of valid strategies. Whether the results of this analysis can be applied to the cases with non-quantifiable t_R (which are beforehand unknown), should be investigated. Meanwhile, if the valid strategies leading to $t_R > 2090$ are used in the PCA concerning t_R, some bias is directly introduced. It is worth noting that this issue of subset definition for PCA would appear whatever the definition of time horizon.

Each of these three choices for the PCA with respect to t_R has shortcomings and advantages. These same remarks can be made for the PCA with respect to t_{TRU}. The interpretation of results should correspond to the set of samples used for the analysis of fuel cycle. The choice of sample set can be also coupled with the choice of threshold TRU_{th}, which can be viewed as an extension of the discussion on the advantages and the drawbacks of the Morris method and PCA.

In comparison, the choice of samples for PCA in the pre-disruption scenario study in Chapter 3 is much less problematic than the one in this study. In that previous study where the strategy evaluation is connected with a given time, the outputs of interest R_{Subs} and TRU_{tot} at year 2090 can be well quantified by deterministic runs for all valid strategies (the ones without missload). But in this study, the strategy validity of scenario does not implies that the results of simulation are quantifiable for PCA.

4.2.1.4 Summary of the problems and the outline of pre-disruption scenario study

Even though the methodology of static robustness assessment is well developed and presented in the study of set time horizon in Chapter 3, it cannot be directly transposed in this study where the evaluation are separated from a predetermined time. In summary, three principal issues need dedicated analysis:

- Which thresholds are used to calculate the outputs of interest, t_R and t_{TRU}? A specific focus is put on the threshold of TRU_{tot} in this study.
- Based on the results of t_R and t_{TRU}, which part of samples are taken for PCA?
- Which part of strategies are regarded as robust static strategies?

These three questions are dependent. In both PCAs concerning t_R and t_{TRU} and different choices of sample subset, two thresholds $TRU_{th} = TRU_{max,ref}$ and TRU_{MM} are used and the results are then compared. In that way, the consistency of using different hypotheses can be studied.

4.2.2 PCA using various subsets of samples with respect to two outputs of interest

4.2.2.1 Basic information about the valid strategies

In total, 3124 strategies from our sampling are valid. For each of them, t_R is calculated under the assumption of $R_{th} = 1$. To determine t_{TRU}, $TRU_{th} = TRU_{max,ref}$ defined in Equation 4.4 and $TRU_{th} = TRU_{MM}$ defined in Equation 4.5 are used. Given the monotone increase of TRU_{tot} over time, $TRU_{max,ref} = TRU_{tot}(s_{ref}, t = 2090) = 946$ tons, where s_{ref} denotes the reference strategy in this pre-disruption scenario which minimizes t_R; $TRU_{MM} = TRU_{tot}(s_{op}, t = 2090) = 849$ tons, where s_{op} denotes the robust static optimum identified in the previous pre-disruption scenario study in Chapter 3. According to the thresholds used, the results of t_R and t_{TRU} of a strategy may vary, and so is its position in the phase space. The histograms of t_R and t_{TRU} over the choice of threshold TRU_{th} are presented in Figure 4.5. Note that the total count of t_R in Figure 4.5a and in Figure 4.5b are identical, because the choice of threshold TRU_{th} does not change t_R of any strategy. In all four figures, the t_R or t_{TRU} later than 2090 are values deduced from an extrapolation of a linear fit of each relevant outputs. Year 2200 of t_R means that under the implementation of corresponding strategy, R_{Subs} by 2200 is still smaller than R_{th} according to the fitting. Hence, the count in year 2200 represents all trajectories of $t_R > 2200$. Compared to t_R, the distribution of t_{TRU} is more concentrated. Actually the two thresholds considered for TRU_{th} are close to the minimum value of the output space, and the TRU_{tot} of most of explored strategies reach the threshold within the horizon of scenario.

The size of samples in the four subsets shown in Figure 4.3 are presented in Table 4.1, corresponding to the two choices of TRU_{th}. The values highlight that when $TRU_{th} = TRU_{MM}$, the subset S_A contains only one more strategy than $S_{A \wedge B^-}$. The statistical information of these two sets are therefore extremely similar.

Conditions of subset	$\boldsymbol{A}$: $\boldsymbol{t_R \leq 2090}$	$\boldsymbol{\neg A}$: $\boldsymbol{t_R > 2090}$
$\boldsymbol{B^+}$: $\boldsymbol{t_{TRU} \geq 2090}$	1/87	0/4
$\boldsymbol{B^-}$: $\boldsymbol{t_{TRU} < 2090}$	1083/997	2040/2036

Table 4.1: Size of valid strategies in the subset $S_{A \wedge B^+}$, $S_{A \wedge B^-}$, $S_{\neg A \wedge B^+}$ and $S_{\neg A \wedge B^-}$ related to two choices of TRU_{th}; values correspond to the choice of $TRU_{MM} = 849/TRU_{max,ref} = 946$ tons

4.2.2.2 PCA with respect to t_R

To study the effects of input parameters on t_R, three subsets of valid strategies are possible: $S_{A \wedge B^-}$, $S_A = S_{A \wedge B^+} \cup S_{A \wedge B^-}$, and the total set of valid strategies S_V^{pre}. The original variable vector becomes $\boldsymbol{X} = (t_{start}, ..., t_R)$. When $TRU_{th} = TRU_{MM}$, the results using S_A and the ones of $S_{A \wedge B^-}$ are identical; the subset S_A as well as S_V^{pre} keeps the same regardless of the choice of TRU_{th}, since it does not change the result of t_R.

To carry out the PCA, the correlation matrix of vector $\boldsymbol{X}$ in the subset S_A is presented in Table 4.2. Correlations are independent from the definition of TRU_{th}, because it does not affect t_R of strategies. The correlation matrix in Table 4.3 corresponds to the correlations considering the smaller subspace $S_{A \wedge B^-}$, where the upper triangle presents the results under the assumption of $TRU_{th} = TRU_{MM}$, and the lower one under $TRU_{th} = TRU_{max,ref}$. Only the coefficients larger than 0.1 are presented; the results in gray in Table 4.3 underlines the impacts of TRU_{th}: when

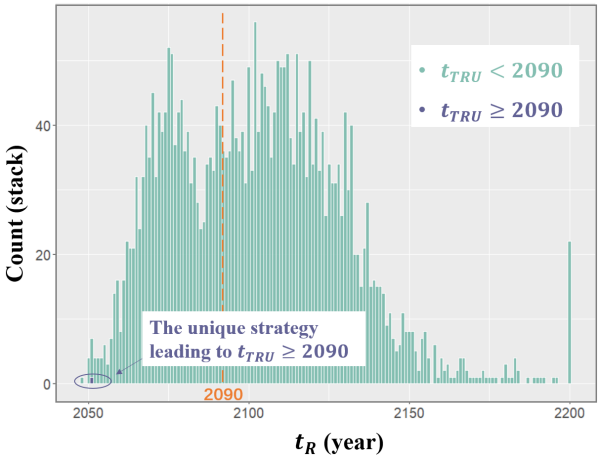

(a) Histogram of t_R when $TRU_{th} = TRU_{MM}$

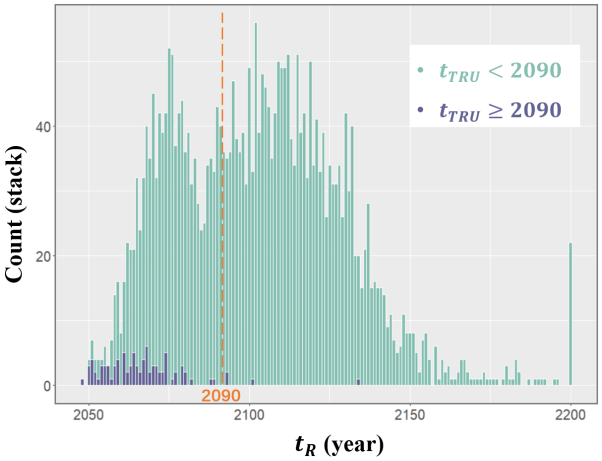

(b) Histogram of t_R when $TRU_{th} = TRU_{max,ref}$

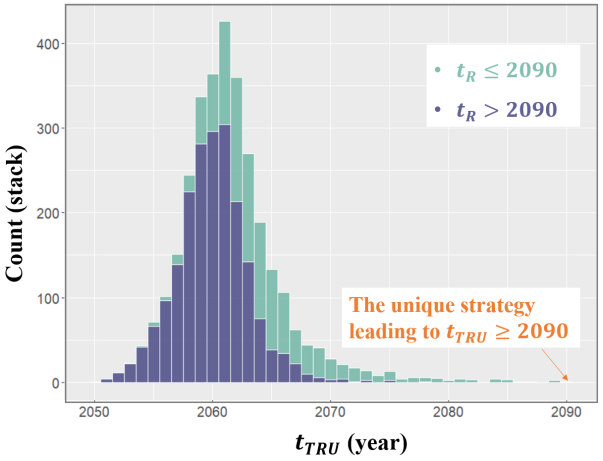

(c) Histogram of t_{TRU} when $TRU_{th} = TRU_{MM}$

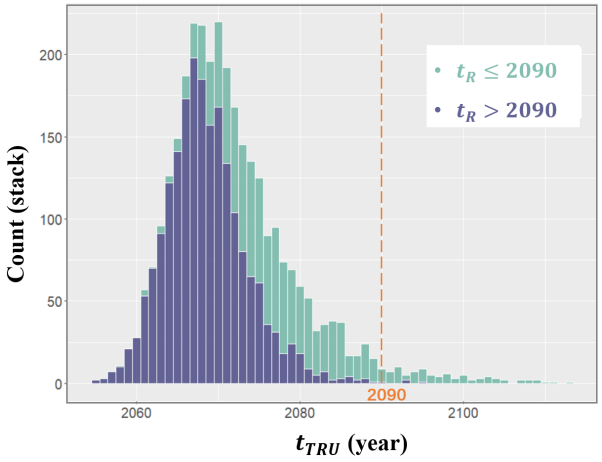

(d) Histogram of t_{TRU} when $TRU_{th} = TRU_{max,ref}$

Figure 4.5: Histogram of t_R (stack of $t_{TRU} < 2090$ and $t_{TRU} \geq 2090$) and t_{TRU} (stack of $t_R \leq 2090$ and $t_R > 2090$) over the choice of TRU_{th}; bin width = 1 year

TRU_{MM} is considered, these correlations are smaller than 0.1; and if $TRU_{max,ref}$ is used they are larger than 0.1. Note that when $TRU_{th} = TRU_{MM}$, S_A contains one more strategy than $S_{A \wedge B^-}$, and thus the upper triangles of Table 4.2 and 4.3 are identical. If S_V^{pre} is considered, the correlations between input variables have been presented in Table 3.2; the analysis of t_R requires additionally the correlations between t_R and inputs, which are presented in Table 4.4.

The comparison between Table 3.2 (input correlation matrix in the pre-disruption scenario study in Section 3.2) and Table 4.2 underlines the effects of the strategy space considered for PCA. Compared with Table 3.2 in the study of Chapter 3, Table 4.2 discards the valid strategies leading to $t_R > 2090$ (from S_V^{pre} to S_A). As shown in Table 4.1, this reduction of subset excludes a large part of valid strategies. A slight dependency between the time variables (t_{start} and D) and $FrMOX_f$, and between $P_{tot,f}$ and BU_{UOX} are created.

The comparison between Table 4.2 and 4.3 reveals the impact of the definition of TRU_{th} and the constraint $t_{TRU} < 2090$ (from S_A to $S_{A \wedge B^-}$). These two effects are evidently dependent.

The principle of PCA is well illustrated in Section 3.2. In brief, PCA is used to deduce the PCs according to the correlation matrix of original variable vector $\boldsymbol{X}$. The output of interest, t_R in this study, is a component of the original variable vector, besides the other eight input variables. Two metrics are considered to reveal the relation between the inputs and the ouput t_R: the fraction of total variance explained by a PC Y_j, denoted as λ_j / V_{tot}, and the square of correlation

Cor. Coef.	t_{start}	D	$P_{tot,f}$	$FrMOX_f$	BU_{UOX}	BU_{MOX}	TC_{UOX}	MPu	t_R
t_{start}	1.	-0.21		0.11					
D		1.		0.12					0.32
$P_{tot,f}$			1.	-0.36	-0.23				0.73
$FrMOX_f$				1.	-0.18				
BU_{UOX}					1.				
BU_{MOX}						1.			
TC_{UOX}				(symmetrical)			1.		
MPu								1.	
t_R									1.

Table 4.2: Correlation matrix of original variable vector $\boldsymbol{X} = (t_{start}, ..., t_R)$, taking the subset S_A; the results of t_R is not sensitive to the choice of TRU_{th}

Cor. Coef.	t_{start}	D	$P_{tot,f}$	$FrMOX_f$	BU_{UOX}	BU_{MOX}	TC_{UOX}	MPu	t_R
t_{start}	1.	-0.21	-0.09	0.11	0.05				
D	-0.26	1.	-0.05	0.12					0.32
$P_{tot,f}$	-0.16	-0.12	1.	-0.36	-0.23				0.73
$FrMOX_f$	0.16	0.17	-0.32	1.	-0.18				
BU_{UOX}	0.10		-0.19	-0.23	1.				0.05
BU_{MOX}						1.			
TC_{UOX}							1.		
MPu								1.	
t_R		0.27	0.72		0.11				1.

Table 4.3: Correlation matrix of original variable vector $\boldsymbol{X} = (t_{start}, ..., t_R)$, taking the subset $S_{A\wedge B^-}$; upper triangle presents the values using the threshold $TRU_{th} = TRU_{MM}$ to calculate t_R, and lower triangle presents the values using the threshold $TRU_{th} = TRU_{max,ref}$ to calculate t_R

between t_R and a PC Y_j, denoted as $\rho^2(t_R, Y_j)$. The PCs that have measurable correlations with the t_R imply their interpretability on the variation of t_R; and the PCs that are nearly constants imply a linear dependency between original variables. Therefore, the composition of these PCs indicate the importance of original variables, principally those eight input variables, on the output t_R.

The results of the two metrics aforementioned are shown in Table 4.5. In all cases of subset and threshold TRU_{th}, the last PC (Y_9) only explains 1% of total variance of the original variable vector, and thus the composition of such PC in respective case can give the information on the linear dependency between t_R and the input variables. Meanwhile, when all valid strategies in the set S_V^{pre} are used for PCA, the first PC (Y_1) can explains 87% of the variance of t_R. If additional cut is imposed on this set (in the case of S_A or $S_{A\wedge B^-}$), the variance of t_R is mainly

Input	t_{start}	D	$P_{tot,f}$	$FrMOX_f$	BU_{UOX}	BU_{MOX}	TC_{UOX}	MPu
Cor. Coef.		0.12	0.83		0.21			

Table 4.4: Correlation coefficients between t_R and input variables using the whole set of valid strategies S_V^{pre}, regardless of the choice of TRU_{th}

Set of samples	TRU_{th}	Metrics	Y_1	Y_2	Y_3	Y_4	Y_5	Y_6	Y_7	Y_8	Y_9
$S_{A\wedge B^-}$	TRU_{MM}	λ_j/V_{tot}	0.21	0.14	0.13	0.12	0.12	0.11	0.11	0.06	0.01
		$\rho^2(t_R, Y_j)$	**0.75**	0.05	0.01	**0.12**	0.	0.01	0.01	0.02	0.03
	$TRU_{max,ref}$	λ_j/V_{tot}	0.20	0.15	0.13	0.12	0.11	0.11	0.10	0.06	0.01
		$\rho^2(t_R, Y_j)$	**0.73**	0.04	0.02	**0.15**	0.	0.	0.02	0.01	0.03
S_A	Both	Same results as in the case when $S_{A\wedge B^-}$ is taken and $TRU_{th} = TRU_{MM}$									
S_V^{pre}	Both	λ_j/V_{tot}	0.21	0.14	0.13	0.11	0.11	0.11	0.10	0.08	0.01
		$\rho^2(t_R, Y_j)$	**0.87**	0.03	0.04	0.	0.	0.	0.03	0.01	0.03

Table 4.5: Fraction of variance of original variable vector $\boldsymbol{X}$ explained by j-th PC Y_j, λ_j/V_{tot}, and correlation squares between t_R and PC Y_j, $\rho^2(t_R, Y_j)$, under the choices of subsets and TRU_{th} in the PCA with respect to t_R

shared by two PC, Y_1 and Y_4. Therefore, the composition of Y_1, Y_4 and Y_9 when $S_{A\wedge B^-}$ or S_A defines the subset for analysis, and the composition of Y_1 and Y_9 when S_V^{pre} is considered, are investigated.

The coefficients of original variables in these PCs in the respective cases are shown in Table 4.6. Note that the PCs are calculated in each PCA given the choice of sample set and the TRU_{th}. For any i, the Y_i in one given configuration for PCA is conceptually unrelated to the Y_i in the other one.

Set of samples	TRU_{th}	Y_j	t_{start}	D	$P_{tot,f}$	$FrMOX_f$	BU_{UOX}	BU_{MOX}	TC_{UOX}	MPu	t_R
$S_{A\wedge B^-}$	TRU_{MM}	Y_1	**-0.13**	**0.17**	**0.68**	**-0.29**	-0.09	-0.05	-0.02	0.02	**0.63**
		Y_4	**0.62**	0.10	-0.07	0.13	**0.61**	0.24	-0.20	-0.06	**0.34**
		Y_9	-0.10	**-0.24**	**-0.67**	**-0.24**	**-0.22**	-0.03	-0.02	-0.05	**0.62**
	$TRU_{max,ref}$	Y_1	**-0.24**	**0.14**	**0.68**	**-0.25**	-0.03	0.	-0.01	0.02	**0.63**
		Y_4	**0.58**	0.12	-0.07	0.17	**0.63**	0.24	-0.08	-0.12	**0.37**
		Y_9	-0.09	**-0.22**	**-0.66**	**-0.26**	**-0.24**	-0.03	-0.03	-0.05	**0.62**
S_A	Both	Same results as in the case when $S_{A\wedge B^-}$ is taken and $TRU_{th} = TRU_{MM}$									
S_V^{pre}	Both	Y_1	-0.01	0.04	**0.68**	**-0.19**	**0.20**	0.05	0.02	0.	**0.68**
		Y_9	-0.06	-0.10	**-0.66**	**-0.23**	**-0.21**	-0.02	0.	-0.03	**0.67**

Table 4.6: Coefficients of original variables in the PCs of interest in the respective PCA under the choices of subset and TRU_{th} in the study of t_R

As shown by the results in Table 4.5 and 4.6, all cases share a common feature: Y_1 explains most of the variance of output variable t_R, and Y_9 implies linear dependency between original variables; both of them are mainly composed of the input variable $P_{tot,f}$ and the output t_R itself. In other words, for all possible assumptions on the choice of subset and threshold TRU_{th} in this study, $P_{tot,f}$ is always the most important input parameter for t_R. Their signs in Y_9 indicate that they have a strong positive correlation, verifying the results in the correlation matrix. It is also coherent with the study presented in Chapter 3 where $P_{tot,f}$ is the most impacting factor on R_{Subs}. The reduction of total installed capacity of fleet is the most efficient manner to increase R_{Subs} during short term, helping get close to or go beyond the threshold R_{th}, and thus brings forward t_R.

Meanwhile, the coefficient of $FrMOX_f$ in Y_1 and Y_9 in all cases is not negligible. The influence of $FrMOX_f$ on t_R cannot be deduced from their correlation from a mono-variate point of view, as their correlation is always smaller than 0.1. Actually, the impact of $FrMOX_f$ on t_R is a symbiotic effect with $P_{tot,f}$. As the sign of the $FrMOX_f$ coefficients in Y_9 suggests, the increase of $FrMOX_f$ under a given power level of fleet leads to the reduction of plutonium inventories in the cycle, and thus delays t_R. Further graphical representations may help visualize this ef-

fect as shown in the next subsection. BU_{UOX} also seems to play a consistent role on t_R in all cases, even though it does not account for Y_1 when S_A or $S_{A\wedge B^-}$ is considered for analysis.

Some effects of the choice of subset on the statistical analysis can be observed. In consideration of the set S_A or $S_{A\wedge B^-}$, Y_4 accounts for more than 10% of the variance of the output t_R, whereas it is not of interest in the analysis considering S_V^{pre}. Actually, this PC Y_4, regardless of the use of S_A or $S_{A\wedge B^-}$, is mainly weighed by the variable t_{start} and BU_{UOX}, while the coefficient of t_R itself is also measurable. Nevertheless, Y_4 does not imply that t_{start} or BU_{UOX} is important for t_R. If we suppose that these nine variables are independent (even though it is not the case), the term $\alpha_{49}t_R$ in Y_4 can explain approximately the fraction of variance of t_R indicated by the value of $\rho^2(t_R, Y_4)$, where α_{49} denotes the $(4, 9)$-th element of the transformation matrix $\boldsymbol{A}$ (or equivalently, the coefficient of t_R in Y_4). In other words, the non-negligible interpretability of Y_4 on the variance of t_R may be contributed by the part t_R itself, but not by other variables.

Secondly, taking S_A or $S_{A\wedge B^-}$ seems to indicate the non-negligible effect of time variables, t_{start} and D, on t_R, whereas this transition timing effect vanishes when all valid strategies are considered. It can be explained by a simplified relation between time variables and the outputs. In general, the responses of most of outputs to these two variables can be represented in Figure 4.6: given the variation range of other parameters, the timing of transition control the variability of outputs. Early t_{start} and short D amplify the effect of the modification of fuel cycle, while late t_{start} and long D mitigate it. The all-range t_{start} or D has a global tendency of converging to the values of initial state in the output space. As shown by the mono-variate correlation coefficients, t_R is slightly correlated with D but statistically uncorrelated with t_{start} when S_V^{pre} is taken. If the constraint of $t_R < 2090$ is imposed, the correlation between t_R and two time variables is strengthened, as schematically explained in Figure 4.6 after the cut. The strengthened correlation can be verified by the corresponding correlation coefficients of t_R and D with respect to different subsets; but the correlation of t_R and t_{start} is still globally weak. On the contrary, the PCs of analysis reveals the stronger effects of the dynamics of transition on t_R, characterized by t_{start} and D, in consideration of the variation of other parameters. Similar to the effect of $FrMOX_f$, the complement of graphical techniques can help visualize these symbiotic effects of input parameters.

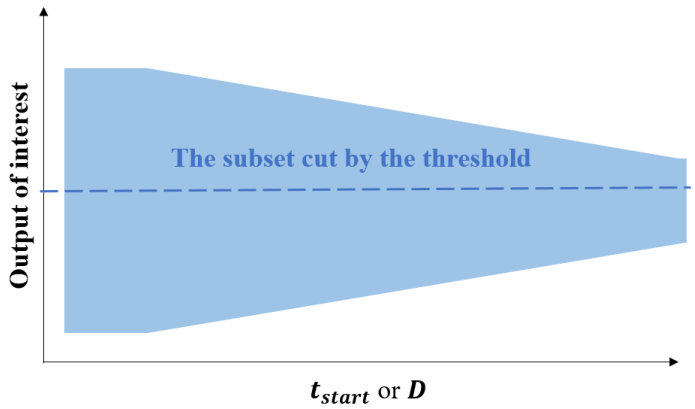

Figure 4.6: Simplified graphical representation of responses of possible outputs to transition timing variables t_{start} and D

Last but not least, taking the subset $S_{A\wedge B^-}$ into the analysis allows to show the influence of the choice of TRU_{th}, as presented in Table 4.5 and 4.6.

Although the results are numerically different, they share lots of similarities

concerning the importance of input parameters on t_R. In summary, it is a common result that the input $P_{tot,f}$ is the most impacting factor on the output t_R, regardless the choice of subsets or threshold TRU_{th} in this study. The symbiotic effects concerning $FrMOX_f$ and possibly BU_{UOX} are also revealed by PCA. The effects of transition timing (from t_{start} and D) appear when the strategies leading to $t_R > 2090$ are cut. The visibility of the effects of $FrMOX_f$ in this analysis emphasizes again the advantage of using PCA instead of simple correlation coefficients.

4.2.2.3 PCA with respect to t_{TRU}

To perform PCA with respect to t_{TRU}, three subsets may be considered: $S_{A\wedge B^-}$, $S_{B^-} = S_{A\wedge B^-} \cup S_{\neg A\wedge B^-}$, and S_V^{pre}. The original variable vector becomes $\boldsymbol{X} = (t_{start}, ..., t_{TRU})$. The correlation matrix of $\boldsymbol{X}$ concerning the subset S_{B^-} is shown in Table 4.7, where upper triangle presents the results of $TRU_{th} = TRU_{MM}$, and the lower triangle corresponds to $TRU_{th} = TRU_{max,ref}$. Only the values strictly larger than 0.1 are presented. The values in gray means that the value of this correlation is strictly smaller than 0.1, whereas it is strictly larger in the counterpart triangle. Since only one valid strategy leads to $t_{TRU} > 2090$ when $TRU_{th} = TRU_{MM}$, the correlation between input variables (results in the upper triangle except the column of t_{TRU}) are identical to the ones of all valid strategies presented in Table 3.2. The small differences between Table 3.2 (input correlation matrix in the pre-disruption scenario study in Section 3.2) and 4.7 indicates the negligible effects of the cut of valid strategies leading to $t_{TRU} \geq 2090$ (from S_V^{pre} to S_{B^-}) on the correlations between input variables. Meanwhile, the comparison between Table 4.7 and 4.3 underlines the additional correlations between input variables due to the constraint of $t_R \leq 2090$. In terms of $S_{A\wedge B^-}$ and S_V^{pre}, the correlations between input variables (components in $\boldsymbol{X}$ except t_{TRU}) have been presented in Table 4.3 and 3.2 respectively.

Cor. Coef.	t_{start}	D	$P_{tot,f}$	$FrMOX_f$	BU_{UOX}	BU_{MOX}	TC_{UOX}	MPu	t_{TRU}
t_{start}	1.	-0.23							0.01
D	-0.25	1.		0.10					
$P_{tot,f}$			1.	-0.24					-0.68
$FrMOX_f$		0.11	-0.20	1.	-0.21				0.32
BU_{UOX}				-0.23	1.				0.38
BU_{MOX}						1.			0.10
TC_{UOX}							1.		
MPu								1.	
t_{TRU}	0.10		-0.79	0.38	0.31	0.06			1.

Table 4.7: Correlation matrix of original variable vector $\boldsymbol{X} = (t_{start}, ..., t_{TRU})$, taking the subset S_{B^-}; upper triangle presents the values using $TRU_{th} = TRU_{MM}$ to calculate t_{TRU}, while lower triangle presents the values using $TRU_{th} = TRU_{max,ref}$ to calculate t_{TRU}

The complement of correlations between t_{TRU} and input variables concerning these two subsets are presented in Table 4.8. When TRU_{MM} is used as threshold, the correlations between t_{TRU} and input variables are approximately identical in two subsets S_{B^-} and S_V^{pre}, because only one strategy makes the difference between the two sets. But even if $TRU_{max,ref}$ is used, these correlations do not differ much in the two sets of strategies. For all possible subsets considered, the correlations between t_{TRU} and input variables seem to change over the choice of TRU_{th}.

Set of samples	TRU_{th}	t_{start}	D	$P_{tot,f}$	$FrMOX_f$	BU_{UOX}	BU_{MOX}	TC_{UOX}	MPu
$S_{A\wedge B^-}$	TRU_{MM}	-0.25	-0.24	-0.55	0.32	0.47	0.17		
	$TRU_{max,ref}$		-0.13	-0.67	0.46	0.46	0.10		
S_V^{pre}	TRU_{MM}			-0.68	0.32	0.37	0.10		
	$TRU_{max,ref}$			-0.76	0.41	0.31	0.09		

Table 4.8: Correlation coefficients between t_{TRU} and input variables, taking the subset $S_{A\wedge B^-}$ and the subset of all valid strategies S_V^{pre}, with respect to two choices of TRU_{th}

Given the correlation matrices under the choices of subsets and threshold TRU_{th}, the PCA is carried out for each subset. Once the PCs are identified, the fraction of the total variance of $\boldsymbol{X}$ explained by the j-th PC Y_j, denoted as λ_j/V_{tot}, as well as the square of correlation coefficient between t_{TRU} and Y_j, denoted as $\rho^2(t_{TRU}, Y_j)$, is calculated for each PCA. These two output metrics regarding a given PC are presented in Table 4.9.

Set of samples	TRU_{th}	Metrics	Y_1	Y_2	Y_3	Y_4	Y_5	Y_6	Y_7	Y_8	Y_9
$S_{A\wedge B^-}$	TRU_{MM}	λ_j/V_{tot}	0.22	0.14	0.14	0.12	0.11	0.11	0.10	0.05	0.01
		$\rho^2(t_R, Y_j)$	**0.81**	0.05	0.	0.	0.02	0.	0.05	0.01	0.05
	$TRU_{max,ref}$	λ_j/V_{tot}	0.24	0.14	0.14	0.11	0.11	0.11	0.09	0.06	0.01
		$\rho^2(t_R, Y_j)$	**0.85**	0.01	0.01	0.	0.	0.	0.09	0.02	0.02
S_{B^-}	TRU_{MM}	λ_j/V_{tot}	0.21	0.14	0.13	0.11	0.11	0.11	0.09	0.07	0.02
		$\rho^2(t_R, Y_j)$	**0.86**	0.02	0.02	0.	0.	0.	0.	0.	0.09
	$TRU_{max,ref}$	λ_j/V_{tot}	0.22	0.14	0.13	0.11	0.11	0.11	0.09	0.07	0.01
		$\rho^2(t_R, Y_j)$	**0.91**	0.02	0.02	0.	0.	0.	0.	0.	0.04
S_v^{pre}	TRU_{MM}	λ_j/V_{tot}	Same results as in the case when S_{B^-} is taken and TRU_{th}= TRU_{MM}								
		$\rho^2(t_R, Y_j)$									
	$TRU_{max,ref}$	λ_j/V_{tot}	0.22	0.14	0.13	0.11	0.11	0.11	0.09	0.07	0.01
		$\rho^2(t_R, Y_j)$	**0.90**	0.02	0.02	0.	0.	0.	0.	0.	0.06

Table 4.9: Fraction of variance of original variable vector $\boldsymbol{X}$ explained by j-th PC Y_j, λ_j/V_{tot}, and correlation squares between t_{TRU} and PC Y_j, $\rho^2(t_{TRU}, Y_j)$, under the choices of subsets and TRU_{th} in the PCA with respect to t_{TRU}

In all cases, Y_1 can explain most of the variance of t_{TRU}, while the last PC Y_9 accounts for negligible variation of $\boldsymbol{X}$, and thus implies linear dependency between the components of $\boldsymbol{X}$. Therefore, the composition of Y_1 and Y_9 in respective PCA under different choices of subset and TRU_{th} are investigated, presented in Table 4.10.

Y_1 and Y_9 in all combinations of assumptions (choice of subset and threshold) justify the measurable impacts of $P_{tot,f}$, $FrMOX_f$ and BU_{UOX} on t_{TRU}. The signs of corresponding coefficients in Y_9 indicate that t_{TRU} increases if $P_{tot,f}$ decreases, and if $FrMOX_f$ or BU_{UOX} increases. It is consistent with the correlation coefficients between t_{TRU} and these three variables, and also coherent with the analysis of TRU_{tot} in Chapter 3. Low $P_{tot,f}$, high $FrMOX_f$ and high BU_{UOX} mitigate the accumulation of TRU_{tot} over time, and thus delay the time to surpass the threshold.

The nuances of the importance of input variables can be observed on t_{start}, D and $P_{tot,f}$ within different combinations of assumptions, as shown in Table 4.10. When $S_{A\wedge B^-}$ is taken, the coefficients of t_{start} and D in Y_9 are on the same magnitude of other important factors, and $P_{tot,f}$ is not strongly dominant. When S_{B^-} or S_V^{pre} is considered, the time variables seem to have a negligible impact and $P_{tot,f}$ is more important for t_{TRU}. In other words, the cut of strategies of $t_R > 2090$, creates the dependency of t_{TRU} on the transition timing (characterized by t_{start} and D), while the importance of $P_{tot,f}$ is reduced. The reduction on the importance of $P_{tot,f}$

Set of samples	TRU_{th}	Y_j	t_{start}	D	$P_{tot,f}$	$FrMOX_f$	BU_{UOX}	BU_{MOX}	TC_{UOX}	MPu	t_{TRU}
$S_{A\wedge B^-}$	TRU_{MM}	Y_1	-0.04	-0.06	**-0.56**	**0.34**	**0.36**	**0.16**	0.02	0.01	**0.64**
		Y_9	**0.36**	**0.34**	**0.25**	**-0.30**	**-0.38**	-0.06	0.	0.01	**0.67**
	$TRU_{max,ref}$	Y_1	**0.17**	0.02	**-0.57**	**0.39**	**0.29**	0.07	0.02	0.	**0.63**
		Y_9	**0.24**	**0.28**	**0.34**	**-0.39**	**-0.39**	-0.05	0.	0.01	**0.66**
S_{B^-}	TRU_{MM}	Y_1	0.05	0.01	**-0.60**	**0.36**	**0.20**	0.10	-0.05	-0.01	**0.67**
		Y_9	0.07	0.10	**0.53**	**-0.23**	**-0.38**	-0.06	-0.01	0.	**0.71**
	$TRU_{max,ref}$	Y_1	**0.12**	0.07	**-0.61**	**0.37**	**0.12**	0.04	-0.05	0.	**0.67**
		Y_9	0.	0.03	**0.57**	**-0.25**	**-0.32**	-0.04	0.	-0.01	**0.71**
S_V^{pre}	TRU_{MM}	Y_1	Same results as in the case when S_{B^-} is taken and $TRU_{th}=TRU_{MM}$								
		Y_9									
	$TRU_{max,ref}$	Y_1	0.05	0.03	**-0.60**	**0.40**	**0.12**	0.08	-0.05	-0.01	**0.67**
		Y_9	0.05	0.07	**0.55**	**-0.27**	**-0.31**	-0.05	-0.01	0.	**0.72**

Table 4.10: Coefficients of original variables in the PCs of interest in the respective PCA under the choices of subset and TRU_{th} in the study of t_{TRU}

can be explained by the strong dependency of R_{Subs} or t_R on $P_{tot,f}$, as shown by the study of R_{Subs} in Chapter 3 and of t_R aforementioned. Actually, the constraint of $t_R \leq 2090$ demands implicitly a relatively low level of $P_{tot,f}$; hence, with the cut of those of $t_R > 2090$, the $P_{tot,f}$ of strategies in $S_{A\wedge B^-}$ are relatively low. As analyzed, the reduction of the variability of $P_{tot,f}$ may highlight the effects of other important variables, such as $FrMOX_f$ and BU_{UOX}. Meanwhile, those cut strategies with $t_R > 2090$ lead to averagely earlier t_{TRU} than those retained in $S_{A\wedge B^-}$, according to the histograms of t_{TRU} shown in Figure 4.5c and 4.5d. By the similar explanation of Figure 4.6, the cut of these strategies with relatively early t_{TRU} creates a negative correlations between t_{TRU} and two time variables, t_{start} and D. Besides this statistical explanation, for the strategies leading to $t_R \leq 2090$ in $S_{A\wedge B^-}$, late t_{start} and long D implies a heavy inertia of initial system state which accumulates faster the TRU inventories than the low-power-level fleet after transition, and thus the TRU_{tot} of the corresponding strategy surpasses earlier the threshold TRU_{th}.

Comparing the case using $TRU_{max,ref}$ with the one using TRU_{MM} as threshold, we can find that the coefficient of t_{start} in Y_1 is larger, whereas in Y_9 it is smaller. Globally, the discrepancies of results between the use of these two thresholds are relatively limited, and thus the results are considered consistent with respect to these two choices of threshold.

In summary, the PCAs in this section, based on different assumptions on the definition of thresholds and subsets considered, share the common point that three input parameters, $P_{tot,f}$, $FrMOX_f$ and BU_{UOX} have measurable impacts on the output t_{TRU}. The constraint of $t_R \leq 2090$ tends to accentuate the influence of transition timing, characterized by t_{start} and D. Furthermore, the importance of inputs on t_{TRU} seems insensitive to the choice of threshold TRU_{th}.

4.2.2.4 Summary of PCA

This sub-section presents the PCAs that look into the input-output relation in the pre-disruption scenario, with different choices of sample subsets and thresholds to calculate the outputs considered.

For both outputs, the global consistency of the importance of input parameters is verified. $P_{tot,f}$ is the dominant factor in most of cases, and both $FrMOX_f$ and BU_{UOX} have measurable effects on these two outputs. The status of input parameters relevant to t_{TRU} seems insensitive to the TRU_{th} definition. But the cut of strategies of $t_R > 2090$ may highlight the importance of the transition timing on

these two outputs, characterized by t_{start} and D.

Given the consistency of results, the subset $S_{A\wedge B^-}$ and S_V^{pre} are considered and $TRU_{max,ref}$ is used to deduce t_{TRU} for the complementary graphical analysis presented in the next section.

4.2.3 Complement by graphical techniques for the analysis

Since the effects of inputs BU_{MOX}, TC_{UOX} and MPu on the two times of interest in this study are not measurable, they are not presented in the following graphical representations.

Under the assumption $TRU_{th} = TRU_{max,ref}$, the pairs plot of t_{start}, D, $P_{tot,f}$, $FrMOX_f$, BU_{UOX} and the output t_R are shown in Figure 4.7, colored by the value of t_R. Figure 4.7a considers all valid strategies, including those fitted values for $t_R > 2090$. Figure 4.7b considers only the subset $S_{A\wedge B^-}$. Note that the values of $t_R > 2090$ are deduced from the fitting process instead of simulation except that $t_R = 2200$ represents all cases of $t_R > 2200$ according to the fit. The axes of variables, especially the $P_{tot,f}$ and t_R, are not the same in two figures.

The dominance of $P_{tot,f}$ on t_R among input parameters is clearly proved. $FrMOX_f$ or BU_{UOX} cannot modify t_R in a large degree, but their synergy with $P_{tot,f}$ changes more efficiently t_R, as shown by the distribution of colors in the sub-figure of $P_{tot,f}$ versus $FrMOX_f$ and the subfigure of $P_{tot,f}$ versus BU_{UOX}.

Two variables concerning the transition timing characterized, t_{start} and D, have limited effect on t_R when all valid strategies are considered in Figure 4.7a, while their positive correlations with t_R are more accentuated in $S_{A\wedge B^-}$ in Figure 4.7b. One may argue that Figure 4.7a shows indeed a slight positive correlation between t_R and D, which can be verified by the correlation value in Table 4.4. This may be somehow contradictory to the foregoing analysis explained in Figure 4.6 which suppose that their correlation should be near zero. This can be explained by the discarding of short-D strategies that lead to late t_R by the validity. In fact, if a short transition will lead to late t_R, it means that the final state of fleet after transition is characterized by high $P_{tot,f}$ but also relatively high $FrMOX_f$. This configuration of fleet may lack plutonium for MOX fabrication and thus is highly possible to be invalid.

Similarly, the pairs plot of t_{start}, D, $P_{tot,f}$, $FrMOX_f$, BU_{UOX} and the output t_{TRU} is shown in Figure 4.8, colored by the value of t_{TRU}. Figure 4.8a considers all valid strategies including those fitted values of $t_{TRU} > 2090$. Figure 4.8b zooms into $S_{A\wedge B^-}$. The axes of variables, especially the ones of $P_{tot,f}$ and t_{TRU}, are not the same in two figures. In both figures, the importance of $P_{tot,f}$, $FrMOX_f$ and BU_{UOX}, and their synergy on t_{TRU} are verified. While in terms of the transition timing, the symbiotic effects of t_{start}, D and $P_{tot,f}$ is highlighted after the cut, as shown by the distribution of colors in the sub-figures of $P_{tot,f}$ versus t_{start} and $P_{tot,f}$ versus D.

In brief, the results deduced from the pairs plot are consistent with the ones in PCA. $P_{tot,f}$, $FrMOX_f$ and BU_{UOX} and their interactions have measurable effects on both times of interest, t_R and t_{TRU} in this pre-disruption scenario. The influence of transition timing, in particular the symbiotic effects of t_{start}, D and other important input parameters, are highlighted if the subset $S_{A\wedge B^-}$ is taken for the analysis.

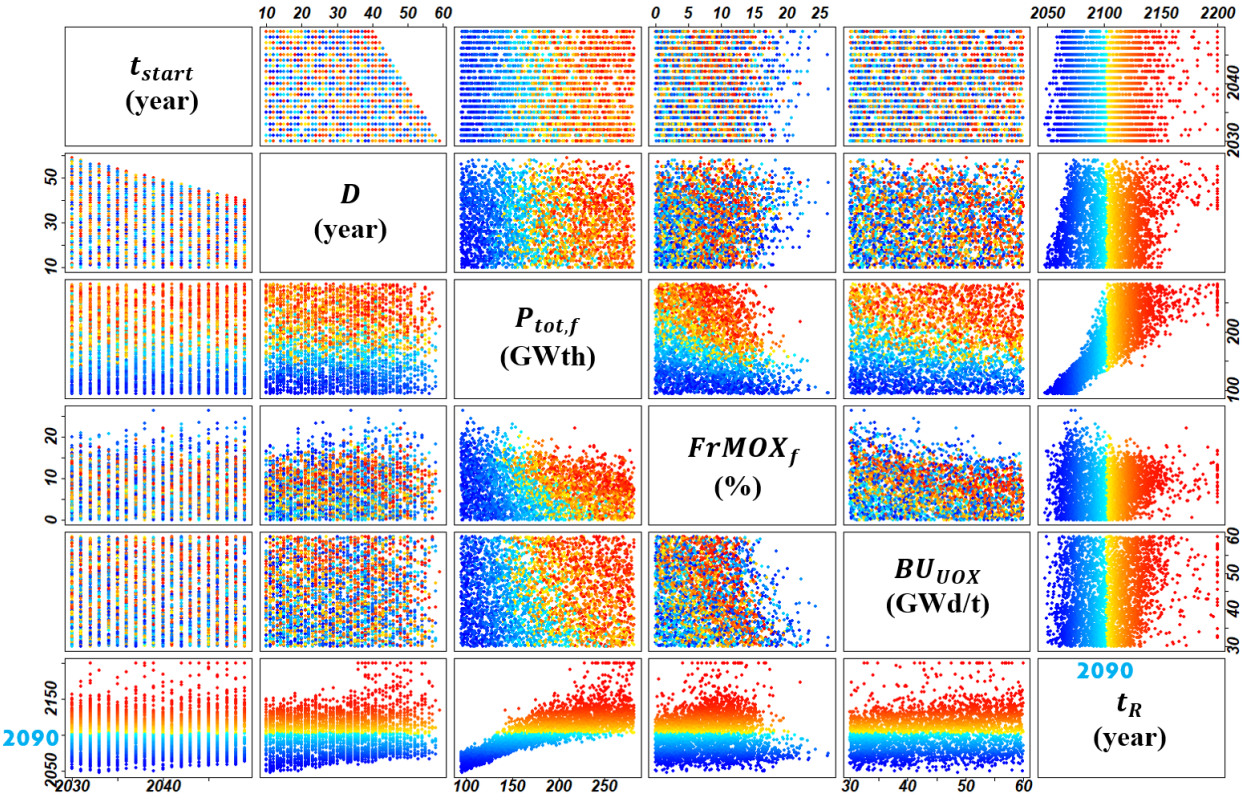

(a) Pairs plot of t_{start}, D, $P_{tot,f}$, $FrMOX_f$, BU_{UOX} and output t_R, colored by the value of t_R. Strategies in S_V^{pre} are considered.

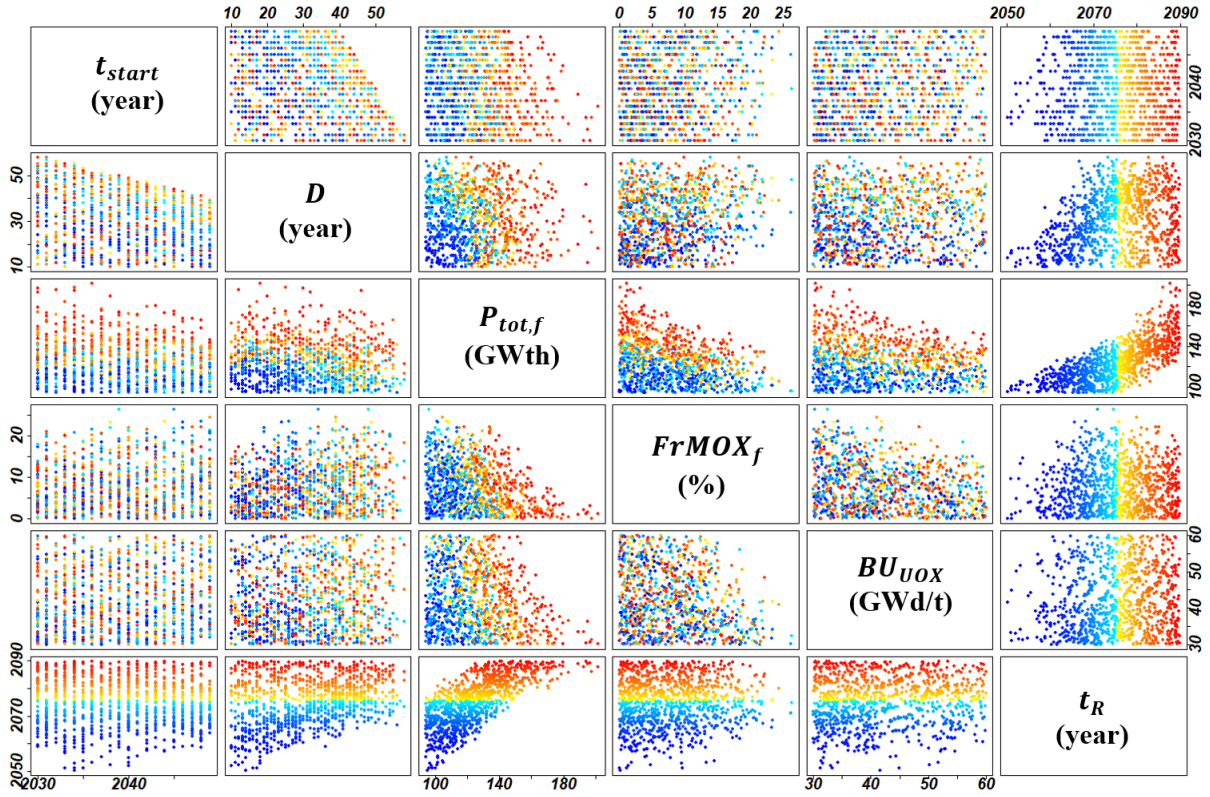

(b) Pairs plot of t_{start}, D, $P_{tot,f}$, $FrMOX_f$, BU_{UOX} and output t_R, colored by the value of t_R. Strategies in $S_{A\wedge B^-}$ are zoomed.

Figure 4.7: Pairs plots of t_{start}, D, $P_{tot,f}$, $FrMOX_f$, BU_{UOX} and output t_R, colored by the value of t_R, considering $TRU_{max,ref}$ as threshold TRU_{th}, taking strategies in S_V^{pre} and a zoom in $S_{A\wedge B^-}$

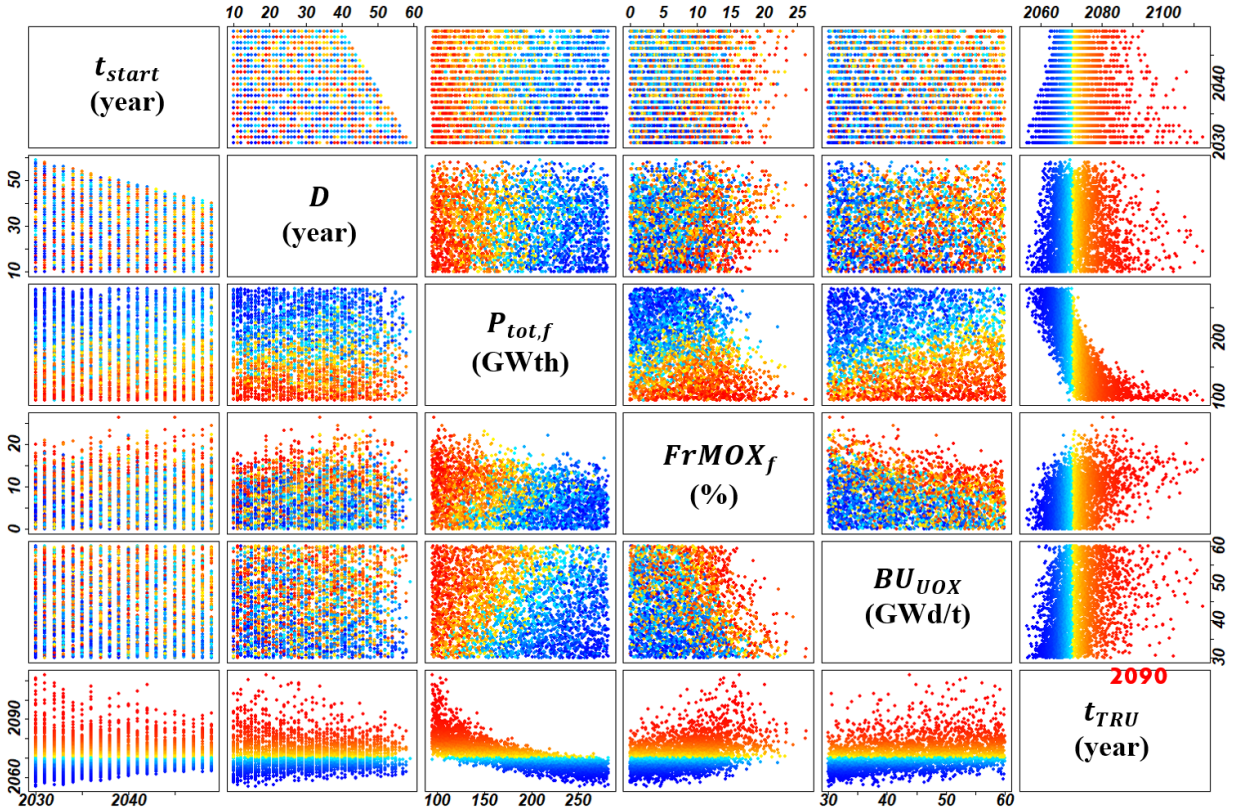

(a) Pairs plot of t_{start}, D, $P_{tot,f}$, $FrMOX_f$, BU_{UOX} and output t_{TRU}, colored by the value of t_{TRU}. Strategies in S_V^{pre} are considered.

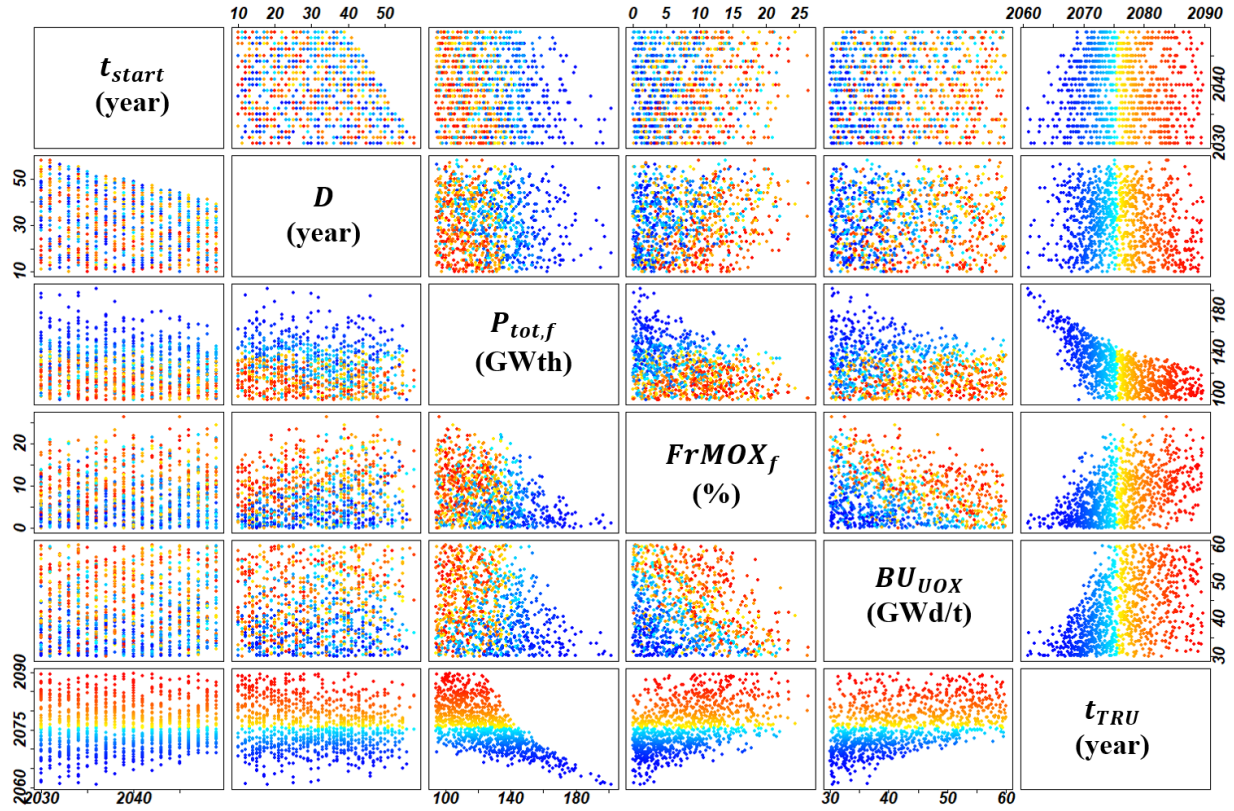

(b) Pairs plot of t_{start}, D, $P_{tot,f}$, $FrMOX_f$, BU_{UOX} and output t_{TRU}, colored by the value of t_{TRU}. Strategies in $S_{A\wedge B^-}$ are zoomed.

Figure 4.8: Pairs plots of t_{start}, D, $P_{tot,f}$, $FrMOX_f$, BU_{UOX} and output t_{TRU}, colored by the value of t_{TRU}, considering $TRU_{max,ref}$ as threshold TRU_{th}, taking strategies in S_V^{pre} and a zoom in $S_{A\wedge B^-}$

4.2.4 Static robustness assessment

As the times of interest depend on the choice of thresholds, the determination of robust strategy does as well.

Under the assumption of $TRU_{th} = TRU_{MM}$, t_{TRU} of all valid strategies can be quantified. Accordingly, the trade-offs between the minimization of t_R and the maximization of t_{TRU} present among the strategies in the Pareto front. The trade-offs can be visualized in the scatter plot of t_{TRU} versus t_R, shown in Figure 4.9. Figure 4.9a considers all valid strategies and the color depends on the input $P_{tot,f}$. The importance of $P_{tot,f}$, especially on the output t_R, is clearly presented. The strategies in the Pareto front, represented as the points surrounded by squares, share relatively low $P_{tot,f}$. Figure 4.9b zooms into strategies in S_A whose $t_R \leq 2090$, and they are colored by input $FrMOX_f$. Under a low $P_{tot,f}$ condition, the trade-offs on the Pareto front depend on the choice of $FrMOX_f$ as seen for the four strategies of interest. The trade-offs imply that within a small increase of $FrMOX_f$, the gain on t_{TRU} is much larger than the delay on t_R.

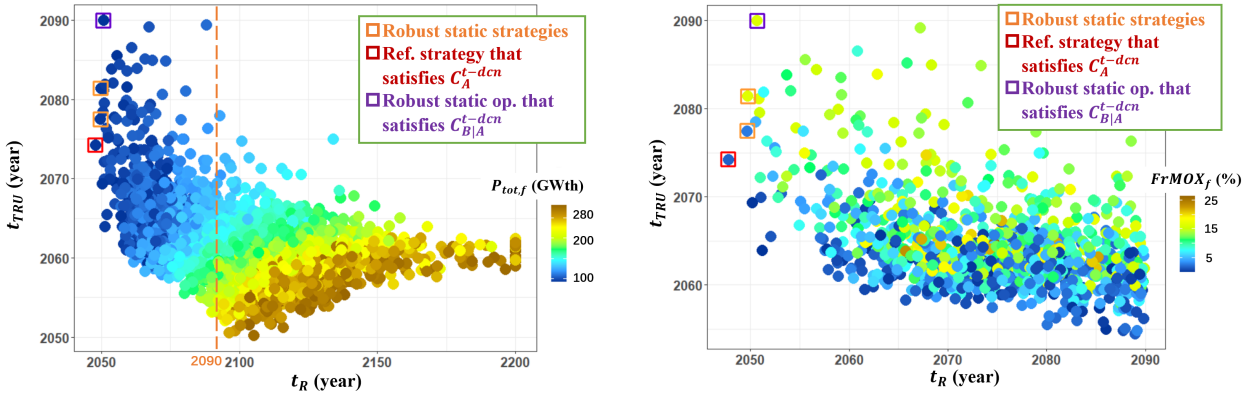

(a) (b)

Figure 4.9: Scatter plots of t_{TRU} versus t_R, under the assumption $TRU_{th} = TRU_{MM}$: (a) colored by input $P_{tot,f}$ taking S_V^{pre}; (b) colored by input $FrMOX_f$ zooming in S_A

On the Pareto front, two extreme cases are of interest. The first one is the unique strategy that leads to $t_R \leq 2090$ and $t_{TRU} \geq 2090$ simultaneously, represented as the point surrounded by purple square in Figure 4.9. Retaining the plutonium availability to satisfy objective A within the time horizon, this strategy takes the most precaution relative to the accumulation of TRU inventories. Note that the margin of t_{TRU} not only represents the discrepancy between the TRU_{tot} of trajectory and the threshold, but also considers the dynamic change of TRU_{tot} owing to the inertia of fuel cycle. Hence, it can be regarded somehow as an optimum, or called robust static optimum.

The other case of particular interest minimizes t_R, represented as the point surrounded by red square. Under the context of mono-objective where objective A is pre-selected, this strategy represents the optimum respecting the criterion $C_A^{t\text{-}dcn}$, and thus it is called the reference strategy in this pre-disruption scenario study. The earliest achieved t_R is year 2048, while the time when the accumulated TRU inventories surpass threshold $TRU_{th} = TRU_{MM}$ in year 2074. If this threshold is regarded as an alarming level, hedging actions should be prepared before year 2074 concerning the TRU inventories in total cycle.

The parameters and outputs of interest of these two strategies are presented in Table 4.11. The robust static optimum is the same as the one in Chapter 3. To complement, the values of inputs and outputs of two other strategies in the Pareto front, denoted as $s_{PF,1}$ and $s_{PF,2}$ respectively, are added in Table 4.11. The

values of inputs verify that the Pareto front can be achieved by a relatively early and short transition towards quite low level of $P_{tot,f}$, while the tradeoffs depend on the choice of $FrMOX_f$ and BU_{UOX}.

Strategy	t_{start}	D	$P_{tot,f}$	$FrMOX_f$	BU_{UOX}	BU_{MOX}	TC_{UOX}	MPu	t_R	t_{TRU}
Rob. stat. op.	2031	19	94.3	16.3	43.9	39.0	9.5	LiFo	2051	2090
$s_{PF,1}$	2039	10	95.3	16.6	37.7	43.0	7.7	FiFo	2050	2081
$s_{PF,2}$	2034	11	95.1	2.7	59.9	43.8	4.5	FiFo	2050	2078
Ref.	2033	11	95.2	1.8	48.6	46.6	3.3	FiFo	2048	2074
(Unit)	year	year	GWth	%	GWd/t	GWd/t	year	-	year	year

Table 4.11: The values of inputs and outputs of robust static optimum and reference strategy; to complement, the information of two other strategies in the Pareto front, denoted as $s_{PF,1}$ and $s_{PF,2}$, are added

The pattern of scatter points distribution in the output space of t_{TRU}-t_R is globally insensitive to the choice of threshold TRU_{th}. The similar pattern of distribution under the assumption $TRU_{th} = TRU_{max,ref}$ is shown in Figure 4.10. In fact, t_R does not depend on TRU_{th}, while TRU_{th} shifts the t_{TRU} of strategies in the same direction. Similarly, the values of $t_R > 2090$ and $t_{TRU} > 2090$ are fitted from the last ten years of scenario.

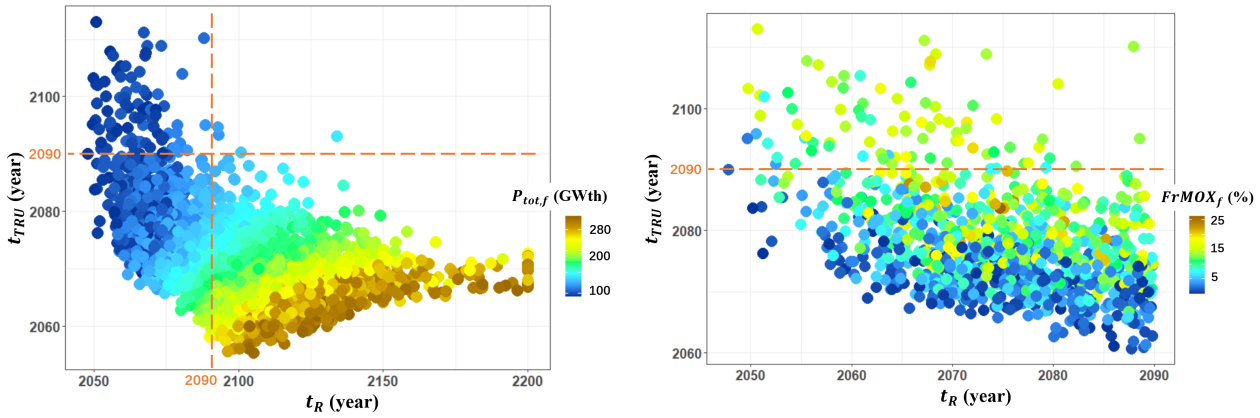

(a) (b)

Figure 4.10: Scatter plots of t_{TRU} versus t_R, under the assumption $TRU_{th} = TRU_{max,ref}$: (a) colored by input $P_{tot,f}$ taking S_V^{pre}; (b) colored by input $FrMOX_f$ zooming in S_A

It is worth noting that the choice of TRU_{th} makes conceptually a difference on the robustness assessment. In the case of $TRU_{th} = TRU_{max,ref}$, t_{TRU} that are strictly later than 2090 are not precisely quantified. Most importantly, the validity of corresponding strategy until the fitted time is not justified. Thus, the fitted t_{TRU} only indicates the margin left concerning the TRU inventories. The determination of Pareto front lacks then sufficient precision. Instead, the strategies resulting in $t_R \leq 2090$ and $t_{TRU} \geq 2090$, indicate that the material availability to replace 100% of fleet with SFRs can be achieved within the time horizon of interest, while the TRU inventories in total cycle are always under the threshold considered. It is therefore reasonable to define these strategies as robust static strategies. In this case, a single optimum cannot be identified.

As shown in Figure 4.10b, the trade-offs of robust static strategies between the minimization of t_R and the maximization of t_{TRU} seem not obvious. The pairs plots of important input parameters of robust static strategies are preformed, colored by t_R in Figure 4.11 and the fitted t_{TRU} in Figure 4.12 respectively, under the

assumption of $TRU_{th} = TRU_{max,ref}$. Note that the range of $P_{tot,f}$ of these strategies is different from the original sampling range, since the constraint of $t_R \leq 2090$ requires relatively low level of $P_{tot,f}$. For these robust static strategies, early t_R requires short D and low $P_{tot,f}$. The symbiotic effects between short D and low $P_{tot,f}$, and between high $FrMOX_f$ and high BU_{UOX} are also obvious. As for t_{TRU}, late fitted t_{TRU} prefers relatively high $FrMOX_f$. The synergy of early t_{start}, short D, low $P_{tot,f}$ and high $FrMOX_f$ help postpone t_{TRU}. Therefore, the trade-offs between the t_R achieved and the margin deduced from t_{TRU} may still depend on the choice of $FrMOX_f$ and its synergy with other input parameters.

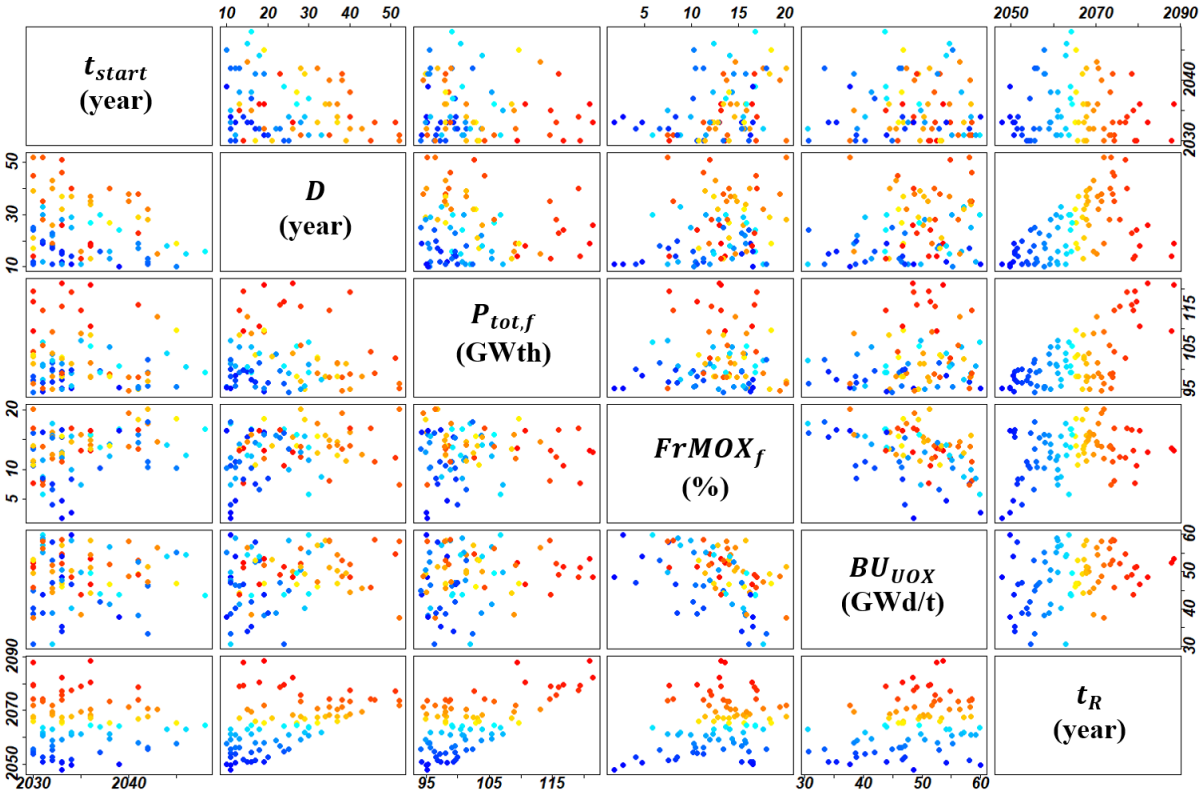

Figure 4.11: Pairs plots of output $t_R \leq 2090$ and inputs t_{start}, D, $P_{tot,f}$, $FrMOX_f$, BU_{UOX} of robust static strategies (thus simultaneously $t_{TRU} \geq 2090$) under the assumption of $TRU_{th} = TRU_{max,ref}$, colored by t_R

4.2.5 Summary of the pre-disruption scenario study and comparison with the study depending on the evaluation at given time

In this section, a pre-disruption scenario subject to the deep uncertainty of disruption of objective is studied, in which the evaluation of strategy is separated from a given time. Two outputs of interest, t_R and t_{TRU}, are used to quantify the performance of strategies regarding two uncertain objectives. On one hand, t_R characterizes the time needed to allow the substitution ratio R_{Subs} to go beyond the threshold R_{th}. Objective A demands the minimization of t_R, implying that the in-cycle inventory of plutonium is accumulated as quickly as possible in order to replace the fleet with SFRs. On the other hand, t_{TRU} points out the time when TRU_{tot} surpasses the threshold TRU_{th}. Regarding the objective B linked to the disruption, one may aim to postpone t_{TRU} as late as possible.

Those two outputs are strongly related to the choice of relevant thresholds. There is no standard choice for threshold TRU_{th} concerning the TRU inventory in total cycle, which is an issue. Two choices of TRU_{th} are then considered, denoted

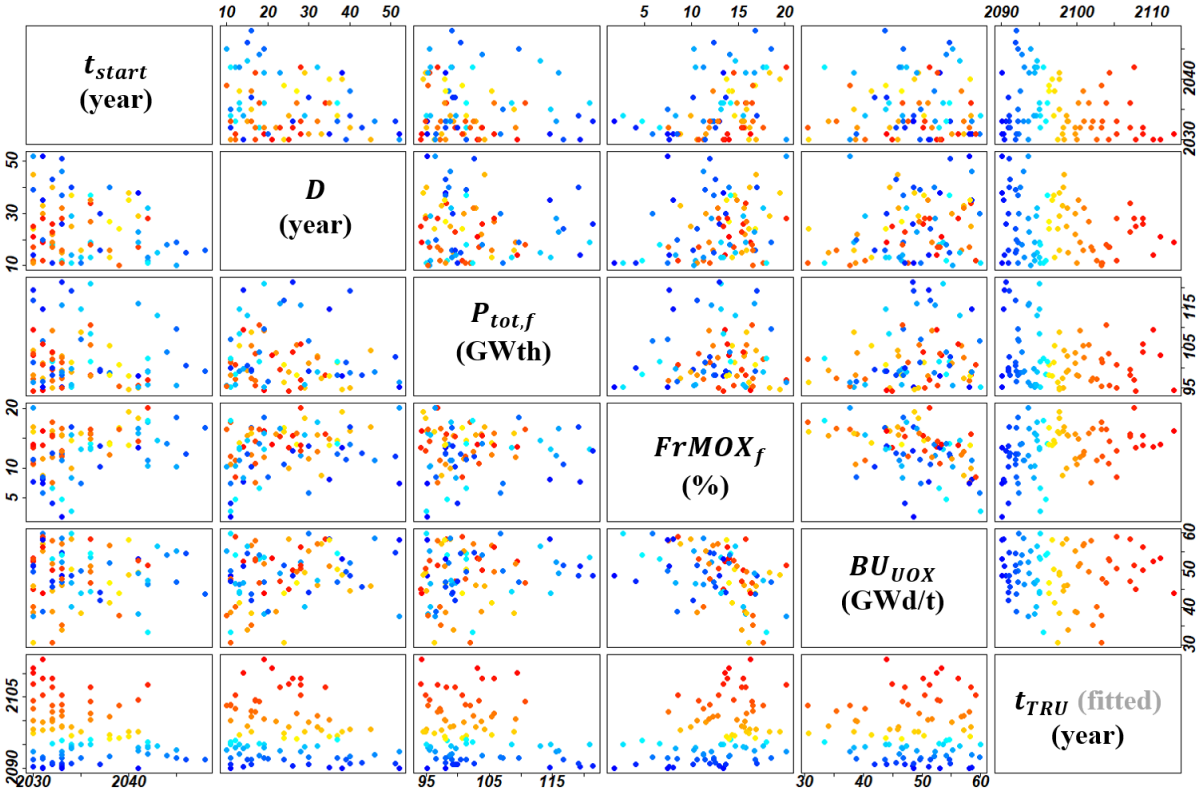

Figure 4.12: Pairs plots of fitted output $t_{TRU} \geq 2090$ and inputs t_{start}, D, $P_{tot,f}$, $FrMOX_f$, BU_{UOX} of robust static strategies (thus simultaneously $t_R \leq 2090$) under the assumption of $TRU_{th} = TRU_{max,ref}$, colored by t_{TRU}

as TRU_{MM} and $TRU_{max,ref}$, determined respectively from the most conservative strategy and the reference strategy minimizing t_R.

Several subsets have been considered for the PCA because the t_R or t_{TRU} of some strategies is not quantifiable. In practise, these values of corresponding strategies are deduced from a linear fit of last ten-year evolution of R_{Subs} and TRU_{tot} respectively. To verify the consistency of analysis, principally on the choice of the subset in the statistical analysis and on the choice of TRU_{th} on both the statistical and robustness evaluation of strategy, a systematic comparison using different combinations of assumptions is performed.

PCA is used to investigate the response of fuel cycle concerning the output t_R or t_{TRU} to the strategies characterized by eight input parameters. Combinations of the choice of TRU_{th} and subsets considered for PCA are enumerated and investigated. The comparison of these combinations shows that the results are qualitatively insensitive to the choice of TRU_{th}. It is evident that t_R is unrelated to TRU_{th}. The TRU_{th} does not change substantially the relative results of t_{TRU} either, given the monotone increase of TRU_{tot} of all valid strategies. The importance of $P_{tot,f}$, $FrMOX_f$ and BU_{UOX} on two times of interest are also consistent in all choices of sample subsets, while the effects of time variables t_{start} and D are statistically highlighted without taking the valid strategies leading to $t_R > 2090$.

The scatter plots of t_{TRU}-t_R are used to visualize the distribution of performance of valid strategies, helping assess the static robustness. Although the choice of TRU_{th} does not change the relative distribution, it may affect the robustness assessment. In the case of $TRU_{th} = TRU_{MM}$, one unique strategy leads simultaneously to $t_R \leq 2090$ and $t_{TRU} \geq 2090$. Regarding the priority of objective A and the precaution on the uncertain disruption, this strategy is defined now as the robust static optimum. Related to reference strategy that minimizes t_R, a Pareto front can be identified. The front can be achieved by early and short tran-

sition towards relatively low level of installed capacity. The tradeoffs between the minimization of t_R and maximization of t_{TRU} depend then on $FrMOX_f$ and BU_{UOX}. While in the case of $TRU_{th} = TRU_{max,ref}$, a non-negligible size of set of valid strategies lead simultaneously to $t_R \leq 2090$ and $t_{TRU} \geq 2090$, and they can also be defined as a set of robust static strategies. The set shares relatively low $P_{tot,f}$ but no trends for other parameters can be pointed out. In general, those achieving early t_R requires low $FrMOX_f$ and BU_{UOX}, and the ones maximizing the gain on the delay of t_{TRU} demands high $FrMOX_f$. The transition timing characterized by t_{start} and D limits the bounds of these effects.

In all, the results are consistent regarding the definition of subsets and thresholds TRU_{th} for the PCA, whereas the choice of TRU_{th} may change the determination of robust static strategies.

This study of pre-disruption scenario and static robustness assessment is worth a comparison with the one in Chapter 3 where TRU_{tot} is used as output of interest and evaluated at the end of scenario. The time horizon in this chapter is regarded as the horizon of interest, while in Chapter 3 it plays an important role on the results. Even though the problem and the outputs of interest are formulated differently, the analyses of fuel cycle are similar and coherent. The similarity is actually expected, because the t_R is strongly correlated with $R_{Subs}(t = 2090)$ and t_{TRU} is strongly correlated with $TRU_{tot}(t = 2090)$ for the valid strategies, as shown in Table 4.12. A drop of correlation $\rho(t_R, R_{Subs}(t = 2090))$ can be observed when the subset considered passes from S_V^{pre} to $S_{A\wedge B^-}$. It can be explained by the fact that more than a half of valid strategies lead to $t_R > 2090$, and the fitted values from the evolution of R_{Subs} strengthen the correlation; but for strategies in S_A, the discontinuities of R_{Subs} evolution soften the correlation between R_{Subs} and t_R. Nevertheless, these correlations are high regardless of the assumptions. t_R and $R_{Subs}(t = 2090)$ are therefore good indicators for each other, and so are t_{TRU} and $TRU_{tot}(t = 2090)$.

$\boldsymbol{TRU_{th}}$	Set of samples	$\boldsymbol{\rho(t_R, R_{Subs}(t = 2090))}$	$\boldsymbol{\rho(t_{TRU}, TRU_{tot}(t = 2090))}$
$\boldsymbol{TRU_{MM}}$	$\boldsymbol{S_V^{pre}}$	-0.91	-0.86
	$\boldsymbol{S_{A\wedge B^-}}$	-0.72	-0.83
$\boldsymbol{TRU_{max,ref}}$	$\boldsymbol{S_V^{pre}}$	-0.91	-0.90
	$\boldsymbol{S_{A\wedge B^-}}$	-0.77	-0.93

Table 4.12: Correlations (denoted as ρ) between t_R and $R_{Subs}(t = 2090)$ and between t_{TRU} and $TRU_{tot}(t = 2090)$ of strategies under the choice of TRU_{th} and the subset

Despite the coherence of numeric results, these two studies are built on entirely different purposes and angles of vision. In the study in Chapter 3, in accordance with the same point of comparison, both the analyses of static strategy and the adaptations should be stuck to a given time. The vulnerability of this assumption is the potential inter-temporal inconsistency of adaptive robustness assessment. This study liberates the evaluation from this constraint; as presented in the following Section 4.3 and 4.4, it is not necessary for the analysis of adaptation scenario to consider the same time horizon. In that case, the adaptive robustness assessment is consistent over the extension of the time horizon of scenario.

4.3 Adaptive robustness assessment: adaptation by year 2040 as an example

By definition, the adaptation scenario supposes that readjustments are taken in order to respond to the disruption of objective. In general, a robust adaptive strategy may be looked for, which can recover the impacts of disruption through some appropriate adjustments.

As indicated in Section 4.1, the choice of time horizon of scenario matches the horizon of interest of analysts or stakeholders. In this study of adaptation scenario, 50 years after the adaptation time t_{ad} is defined as a primary time horizon for the simulation, and thus the adaptation scenario starts from t_{ad} and ends by $t_{ad} + 50$. This definition covers the remaining life time of reactors operation. An adaptive strategy, based on a given prior trajectory, is considered valid if it satisfies $C_{V,ad}^{t\text{-}dcn}$, meaning that the first missload takes place after the planned transition. The time of first missload is denoted as t_{ML} and $C_{V,ad}^{t\text{-}dcn}$ demands $t_{ML} > t_{ad} + D$. The adaptation is considered robust if it satisfies $C_{B,ad}^{t\text{-}dcn}$, meaning that the TRU inventory in the total cycle should be reduced beneath a given threshold $TRU_{th,ad}$. The corresponding output of interest, t'_{TRU}, indicates the time when TRU inventory in total cycle decreases beneath $TRU_{th,ad}$.

Intuitively the choice of $TRU_{th,ad}$ can affect to a large degree the result of the robustness assessment. One may use the same threshold as in the pre-disruption scenario; but the choices in pre-disruption scenario are determined within its own time horizon of interest. To address this issue of dependency, one can also use a threshold value from bibliographical review and industrial feed-backs that represents real interest and estimation. But given the complexity and uncertainty of accessing such value, a "historically lowest TRU_{tot} by t_{ad}" is used as $TRU_{th,ad}$, denoted as $TRU_{min}^{A}(t_{ad})$. Mathematically, it is determined by

$$TRU_{min}^{A}(t) = \min_{s \in S_A} TRU_{tot}(s,t) \tag{4.6}$$

where S_A denotes the set of strategies in the pre-disruption scenario that achieve $t_R \leq 2090$. In other words, $TRU_{min}^{A}(t)$ indicates the lowest achieved TRU_{tot} at a given time t, among the valid strategies prioritizing objective A. In the following illustrations, both notations TRU_{min}^{A} and $TRU_{th,ad}$ are used, depending on the context: TRU_{min}^{A} makes sense when the pre-disruption strategies are analyzed, while $TRU_{th,ad}$ is more informative when the adaptations after disruption are considered.

Based on the new definitions of validity and adaptive robustness introduced, an adaptation scenario is studied for year 2040 as the adaptation time in this section. It starts from the prior trajectory of the reference strategy, which was supposed to minimize t_R before disruption.

4.3.1 Adaptation scenario with flexible time horizon

To liberate the evaluation of strategy from given time, new concepts and definitions are introduced, complicating the problems related to the uncertain t_{ad}. For the first step, only $t_{ad} = 2040$ is studied in this section. Correspondingly, the time horizon of scenario lasts from year 2040 to 2090, and we have $TRU_{min}^{A}(t = 2040) = 616$ tons as the threshold.

In a mono-objective context where the deployment of SFR is pre-selected, it is reasonable to implement the reference strategy that minimizes t_R. The assessment of adaptive robustness that adapts the prior reference trajectory can

give primary information on the impacts of disruption. Besides the parameters of prior reference trajectory shown in Table 4.11, $P_{tot}(t = 2040) = 151.0$ GWth and $FrMOX(t = 2040) = 7.6\%$ should be also noted. Compared to the threshold $TRU_{th,ad} = 616$ tons, the evolution of TRU starts from $TRU_{tot}(t = 2040) = 628$ tons. In spite of the different starting point, the adaptation scenario is very similar to the one suggested in Section 3.3, summarized in Table 3.10. In brief, starting from the state of prior trajectory by t_{ad}, an adaptive transition of fleet is considered to minimize t'_{TRU}. The nuclear system of interest is still PWR UOX and PWR MOX in this section. Since SFR deployment is no longer in priority after the disruption, the final total power of fleet $P_{tot,f}$ ranges in [0%, 100%] of the level by t_{ad}, while the MOX fraction $FrMOX_f$ can reach 100%. To maximize the effects of the modification of fuel cycle parameters, a transition as short as one year is considered acceptable. The only change of sampling space concerns the lower bound of $FrMOX_f$, which is 10% instead of 0%. 10%, corresponding to the current global fraction of MOX in the whole fleet, results in a stable increase of TRU inventories in total cycle. But with respect to the threshold $TRU_{th,ad}$ determined in this adaptation scenario, robust adaptive strategies should lead to net incineration of TRU. Hence, a higher fraction of MOX than 10% is expected for robust adaptations.

The interest of introducing this exploration space into this adaptation scenario reinforces the necessity of the new definition of strategy validity. The current management strategy concerning MOX in France is able to stabilize the flow of plutonium between the reprocessing rate of spent fuels and the fabrication of fresh MOX fuels [13]. It is highly possible that a TRU-burning strategy breaks the stabilization and leads to plutonium shortage, while the time of this shortage is a-priori unknown. Under the demand of inter-temporal consistency, a valid strategy should preserve its validity subject to the change of time horizon of scenario.

4.3.2 Results of adaptation on prior reference trajectory from year 2040

4.3.2.1 Analysis of validity

The definition of strategy validity is now different from the one in pre-disruption scenario. Hence, it is useful to perform a dedicated analysis on the responses of t_{ML} (defined as the first missload time) to input parameters.

Similar to the analyses concerning t_R and t_{TRU} in Section 4.2, the statistical analysis concerning t_{ML} may raise some issues on the selection of samples. This is mainly due to the fact that a large part of explored strategies lead to $t_{ML} > 2090$ which are not quantifiable. A solution like a linear fit as done previously in 4.2 is even not a suitable solution, because the available plutonium inventories in spent UOX fuels can be gradually accumulated for a non-negligible part of trajectories. In these cases, t_{ML} tends to infinity. To simplify, only the strategies with plutonium shortages within the time horizon are taken for the PCA, and this subset of strategies is denoted as S_{ML}. Its subset of valid strategies denoted as $S_{ML,v}$, and that of invalid strategies $S_{ML,nv}$, are also considered. To facilitate the representations of subsequent analyses, the set without missload is denoted as S_{noML}, which must be a subset of valid strategies. Obviously the set of valid adaptive strategies is the sum of S_{noML} and $S_{ML,v}$, denoted as S_V^{ad}. A simple graphical representation of these subsets depending on the value of t_{ML} is shown in Figure 4.13.

To evaluate the effects of inputs on the quantifiable t_{ML}, three subsets of total sampling can be of interest for the study of validity characterized by t_{ML}: S_{ML} and its subsets, $S_{ML,v}$ and $S_{ML,nv}$. The analysis on $S_{ML,v}$ provides the information about

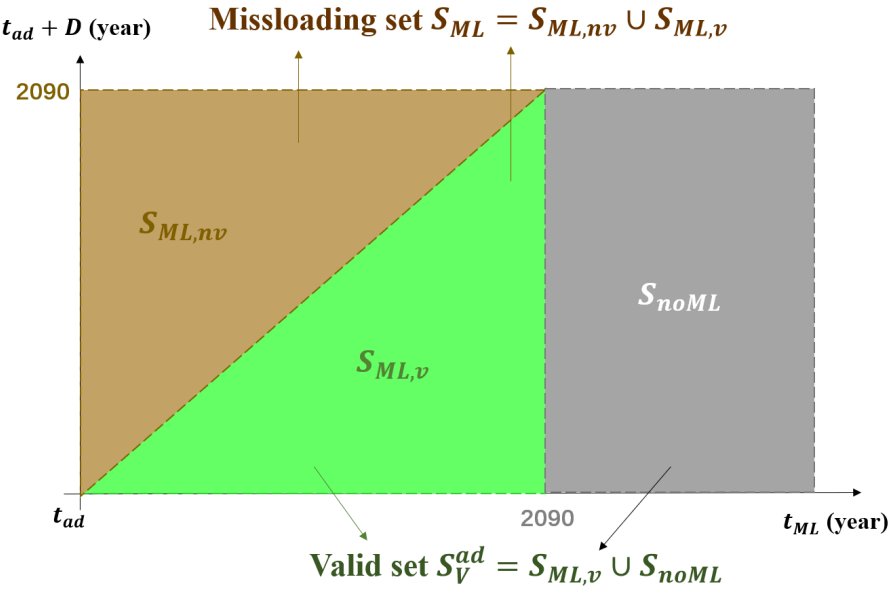

Figure 4.13: Graphical representations of subsets of adaptive strategy according to their values of t_{ML}: S_{ML} (strategies with the first missload before $t_{ad} + 50$), $S_{ML,nv}$ (non-valid strategies with the first missload before $t_{ad} + 50$), $S_{ML,v}$ (valid strategies with the first missload before $t_{ad} + 50$), S_{noML} (strategies with no missload) and S_V^{ad} (valid adaptation strategies)

t_{ML} from valid strategies. One may also focus on the space of invalid strategy and to deduce backward the properties of validity, considering $S_{ML,nv}$ into analysis. The consideration of the sum of these two subsets complements then the analysis with each other.

2000 adaptive strategies by LHS in the total adaptation space are simulated based on the prior reference trajectory (which was supposed to minimize t_R before disruption). The size and the approximate percentage of these subsets of interest in the total space presented in Table 4.13 give a basic grasp on the feature of the exploration space concerning the validity. Accordingly, the part of missloading set S_{ML} accounts for 78% of the total sampling, while the valid set S_V^{ad} takes 47%.

Set of sample	$\boldsymbol{S_{ML,nv}}$	$\boldsymbol{S_{ML,v}}$	$\boldsymbol{S_{noML}}$
Size	1060	506	434
% of total space	53.0%	25.3%	21.7%

Table 4.13: Size of subsets $\boldsymbol{S_{ML,nv}}$, $\boldsymbol{S_{ML,v}}$ and $\boldsymbol{S_{noML}}$, and their percentage in the whole space of adaptive strategy

The correlation matrix with respect to different choice of subsets (S_{ML} and its subsets $S_{ML,v}$ and $S_{ML,nv}$) are shown in Table 4.14. Those lower than 0.1 are omitted in the matrix. In all cases, the importance of D, $P_{tot,f}$ and $FrMOX_f$ on the study of t_{ML} is highlighted. The upper triangle indicates the correlations in the subset S_{ML}, corresponding to the constraint of $t_{ML} < 2090$ in S_{ML}. This constraint creates the correlations between $P_{tot,f}$ and $FrMOX_f$, which is coherent with the analysis on the missloads N_{ML}. The lower triangle presents the correlations in the two subsets, in the order of $S_{ML,v}$/$S_{ML,nv}$, corresponding respectively to the additional constraint of validity and invalidity. The validity constraint with respect to $S_{ML,v}$ highlights the correlations of $FrMOX_f$ with timing effect D and with $P_{tot,f}$, whereas the constraint of invalidity in $S_{ML,nv}$ creates lower correlations concerning $FrMOX_f$, but enhances the correlation between D and $P_{tot,f}$. One may also note that the correlation between t_{ML} and D is measurably lower in the set S_{ML}

than that in both its two subsets. The division between valid and invalid subset emphasizes the correlation between D and t_{ML}.

Cor. coef.	D	$P_{tot,f}$	$FrMOX_f$	t_{ML}
D	1.	-0.07	0.02	0.33
$P_{tot,f}$	-0.05/-0.18	1.	-0.16	-0.26
$FrMOX_f$	-0.45/-0.25	-0.38/-0.13	1.	-0.67
t_{ML}	0.68/0.68	-0.28/-0.25	-0.60/-0.71	1.

Table 4.14: Correlation matrix of original variable vector $\boldsymbol{X} = (D, .., t_{ML})$: upper triangle indicates the correlations under the set S_{ML}; lower triangle indicates the values in the order of $S_{ML,v}/S_{ML,nv}$. Correlations lower than 0.1 are not indicated.

With respect to three possible choices of sets, the PCAs are separately performed. The fraction of total variance of $\boldsymbol{X}$ explained by the j-th PC Y_j, denoted as λ_j/V_{tot}, as well as the correlation square between t_{ML} and Y_j, denoted as $\rho^2(t_{ML}, Y_j)$, is shown in Table 4.15. The results of λ_8/V_{tot} indicate that Y_8 of respective analysis may indicate a linear dependency among the original variables, and according to the values of all ρ^2, Y_1 for all subsets considered account for more than 80% of variance of t_{ML}. The coefficients of original variables in the composition of Y_1 and Y_8 in the respective PCA are then of interest and presented in Table 4.16.

Set of samples	Metrics	Y_1	Y_2	Y_3	Y_4	Y_5	Y_6	Y_7	Y_8
$S_{ML,v}$	λ_j/V_{tot}	0.27	0.16	0.13	0.13	0.12	0.11	0.05	0.01
	$\rho^2(t_{ML}, Y_j)$	**0.82**	0.08	0.	0.	0.	0.	0.04	0.06
$S_{ML,nv}$	λ_j/V_{tot}	0.27	0.14	0.13	0.13	0.12	0.12	0.08	0.01
	$\rho^2(t_{ML}, Y_j)$	**0.94**	0.	0.	0.	0.	0.	0.01	0.05
S_{ML}	λ_j/V_{tot}	0.22	0.15	0.13	0.13	0.12	0.12	0.11	0.02
	$\rho^2(t_{ML}, Y_j)$	**0.91**	0.	0.01	0.	0.	0.	0.01	0.07

Table 4.15: Fraction of variance of original variable vector $\boldsymbol{X}$ explained by j-th PC Y_j, λ_j/V_{tot}, and correlation squares between t_{ML} and PC Y_j, $\rho^2(t_{ML}, Y_j)$, under the choices of subsets in the PCA with respect to t_{ML}

Set of samples	Y_j	D	$P_{tot,f}$	$FrMOX_f$	BU_{UOX}	BU_{MOX}	TC_{UOX}	MPu	t_{ML}
$S_{ML,v}$	Y_1	**0.57**	0.	**-0.53**	-0.05	-0.01	-0.03	0.06	**0.61**
	Y_8	**-0.22**	**0.44**	**0.54**	0.01	0.	0.04	0.	**0.68**
$S_{ML,nv}$	Y_1	**0.52**	**-0.17**	**-0.50**	-0.05	-0.06	0.06	**-0.11**	**0.66**
	Y_8	**-0.37**	**0.20**	**0.51**	0.05	-0.04	0.07	0.02	**0.74**
S_{ML}	Y_1	**0.31**	**-0.15**	**-0.59**	-0.06	-0.04	-0.08	-0.06	**0.72**
	Y_8	**-0.26**	**0.30**	**0.61**	0.02	-0.03	0.07	0.	**0.68**

Table 4.16: Coefficients of original variables in the PCs of interest in the respective PCA with respect to t_{ML}

In all sets of sample, $FrMOX_f$ is the most important factor on the quantifiable result of t_{ML}. It is also coherent with the missloading study concerning the output N_{ML} in Chapter 3. The coefficient sign of $FrMOX_f$ in Y_8 indicates that t_{ML} is

brought forward over the increase of $FrMOX_f$, explained by the higher consumption rate of plutonium from spent UOX fuels. $P_{tot,f}$ also plays a similar role but brings smaller effect, which requires a sufficient high level of $FrMOX_f$.

The coefficient of D in Y_1 is higher in the analysis taking the subsets $S_{ML,v}$ or $S_{ML,nv}$ than in the case of S_{ML}. As explained for the correlation matrix, it is mainly due to the correlation between t_{ML} and D reinforced by the constraint of validity/invalidity. On the contrary, the part of D in Y_8 is similar in three cases, which reveal the consistence of contribution of D to t_{ML}, regardless of the validity.

Despite this result consistency over the subsets $S_{ML,v}$ and $S_{ML,nv}$ considered for PCA, one should note the importance of differentiating these two subsets. Pairs plot of D, $P_{tot,f}$, $FrMOX_f$ and t_{ML} help visualize the distribution of these strategies, shown in Figure 4.14. The scatter plots are colored by the value of t_{ML}, where near-blue points indicate early t_{ML} and near-red points correspond to late t_{ML}. Gray points are those without missloads in the set S_{noML}, and the t_{ML} are set to 2100 in the figure in order to represent the corresponding strategies in the plots. To distinguish, the invalid strategies in $S_{ML,nv}$ are represented by crosses. The scatter plot of t_{ML} versus D verifies their enhanced correlation in the subset $S_{ML,v}$ and $S_{ML,nv}$, while it is reduced in the sum of two. Coherent with the missloading study in Chapter 3, the boundary between S_{noML} and S_{ML} is relatively clear, mainly characterized in the plot of $P_{tot,f}$ versus $FrMOX_f$. In case of inevitable missloads within the horizon, valid and invalid strategies are not well distinguished in the set S_{ML} as visualized.

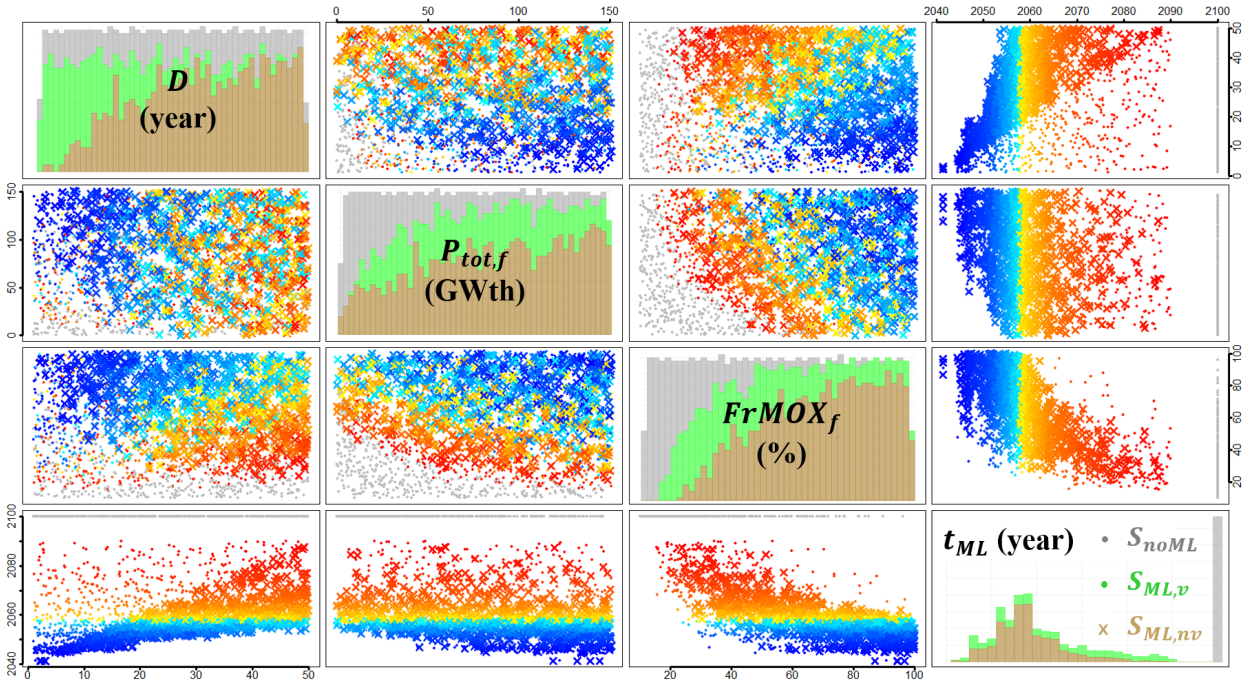

Figure 4.14: Pairs plot between D, $P_{tot,f}$, $FrMOX_f$ and t_{ML}, scatter points colored by the value of t_{ML}. Strategies in $S_{ML,nv}$ are represented by crosses. Strategies in S_{noML} are in gray, and their t_{ML} are set in 2100 to be fit in the figures. Diagonal figures give the stack histograms of corresponding variable, with S_{noML} in gray, $S_{ML,v}$ in green and $S_{ML,nv}$ in brown

Diagonal sub-figures give the stack histograms of corresponding variables, distinct in three subsets: strategies of S_{noML} in gray, $S_{ML,v}$ in green and $S_{ML,nv}$ in brown. While the missloading is well distinguished by the choice of $P_{tot,f}$ and $FrMOX_f$ (in gray), the validity with missloads (in green) is mainly characterized by short D. Short transition requires simply a stable plutonium supply during short term and thus has a higher probability to meet the plutonium shortage

after transition. If we look for valid strategies in S_{noML} and/or $S_{ML,v}$, short D and low $FrMOX_f$ are evidently preferred.

Even though other input parameters have little effect on t_{ML}, it is worth noticing that a "structural" pattern can be observed on the plot of t_{ML} versus BU_{MOX}, as shown in Figure 4.15. Radial-shape lines seem to indicate linear relation between these two quantities. Because the missload only happens on the loading of MOX fuel, t_{ML} is correlated to the length of irradiation cycle of MOX, and so to BU_{MOX}. Each radial-shape line indicates the missload with respect to the same irradiation cycle of MOX given different values of BU_{MOX}. As the number of cycle increases, the discrepancy on the starting time of cycle is accumulated. Hence, the slope of radial-shape lines increases if the first missload happens on a later irradiation cycle of MOX. Anyway, BU_{MOX} is not impactful regarding t_{ML} from a statistical point of view, but they are linear dependent under the condition where the plutonium shortage is met on the same irradiation cycle of MOX.

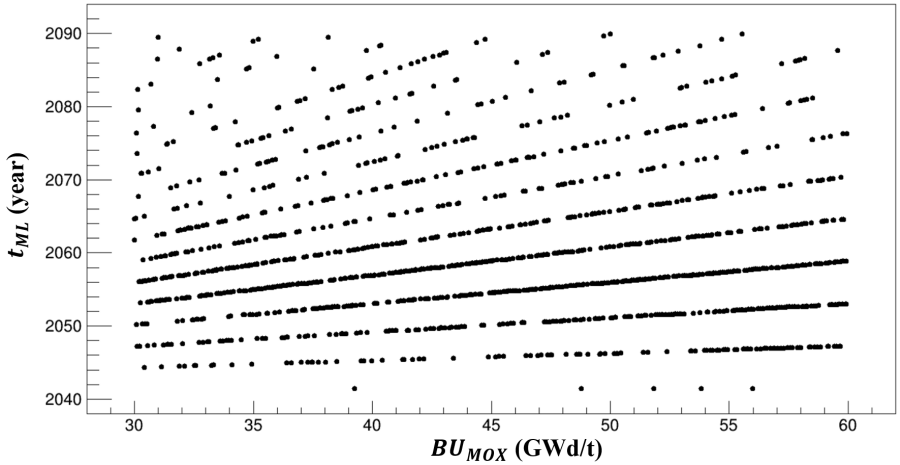

Figure 4.15: Scatter plot of t_{ML} versus BU_{MOX} for the trajectories with t_{ML} realized before the end of scenario

4.3.2.2 Analysis of outputs: performance of strategy

In the study of adaptive strategy performances, we only focus on the valid strategies in S_V^{ad}. However, t'_{TRU} is actually not an appropriate output to explain the behavior of fuel cycle. Indeed, most of the adaptive strategies cannot result in a meaningful t'_{TRU} due to the increasing TRU_{tot} over time. Here, other more general outputs are considered: the minimal achieved TRU_{tot} within the well-defined part of trajectory, denoted as TRU_{min}, and the corresponding time t_{min}. Mathematically, for a valid adaptive strategy $s \in S_V^{ad}$, these two quantities are defined as

$$TRU_{min}(s) = \min_{t<t_{ML}} TRU_{tot}(s,t) \tag{4.7}$$

$$t_{min} = min\{t | t < t_{ML}, TRU_{tot}(s,t) = TRU_{min}(s)\} \tag{4.8}$$

where the time t is implicitly in the range of $[t_{ad}, t_{ad}+50]$. The strategies leading to net increase of TRU_{tot} over time after adaptation account for a measurable part of S_V^{ad}. They result commonly in $TRU_{min} = TRU_{tot}(t = t_{ad})$ and $t_{min} = t_{ad}$. Therefore, they are not of interest in this adaptation scenario. Those leading to net incineration of TRU implying $TRU_{min} < TRU_{tot}(t = t_{ad})$ are potentially of interest, denoted as S_{burn}. According to the definition, an adaptive strategy is robust with meaningful t'_{TRU} if $TRU_{min} < TRU_{th,ad}$.

Before the analysis in detail, one should first note the inertia of the reactor fleet after t_{ad}. The adaptation respects the irradiation cycle, implying that the

macro PWR UOX and MOX continue their planned services determined before adaptation till their first EOC after t_{ad}. The trajectories of all valid adaptive strategies follow then similar evolution at the beginning of adaptation. Based on the prior reference trajectory, the evolution of TRU_{tot} begins with an inevitable increment during the first years. The TRU-incineration strategies in S_{burn} should be capable to offset this part of TRU. To give an order of magnitude of this excess quantity, the effective TRU inventories in total cycle denoted as TRU_{eff} can be defined:

$$TRU_{eff} = TRU_{tot}(t_{ad}) + \sum_{r}(TRU_r(EOC_r) - TRU_r(t_{ad})) \tag{4.9}$$

where index r denotes PWR UOX or MOX. Both TRU_r and EOC_r, the quantity of TRU in reactor r depend also on the strategy s, and it is omitted in the equation. In regards to t_{ad}, TRU_{eff} considers the inventories that is going to be discharged at the EOC of each reactor. If an adaptive strategy is not able to incinerate the quantity of discrepancy $TRU_{eff} - TRU_{tot}$ (if it is positive), we will have $TRU_{min} > TRU_{tot}(t_{ad})$, and thus this adaptation is not of interest. For the prior reference trajectory, $TRU_{eff}(t = 2040) = 647$ tons, and the difference relative to $TRU_{tot}(t = 2040)$ is 19 tons, consistent with the range estimated in Section 3.1.

The calculation of TRU_{min} of valid strategies in S_V^{ad} shows that only 72 adaptive strategies are in S_{burn}, representing approximately 7.7% of the valid set S_V^{ad} and 3.6% of the overall sampling space. Such number is too small to carry out a credible statistical analysis. Pairs plots of D, $P_{tot,f}$ and $FrMOX_f$ with output TRU_{min} and t_{min} may still give some indications on the response of these two outputs over the strategy of S_{burn}, shown in Figure 4.16. Two sub-figures are respectively colored by TRU_{min} and t_{min}, where the upper triangles show the correlations of investigated variable pairs.

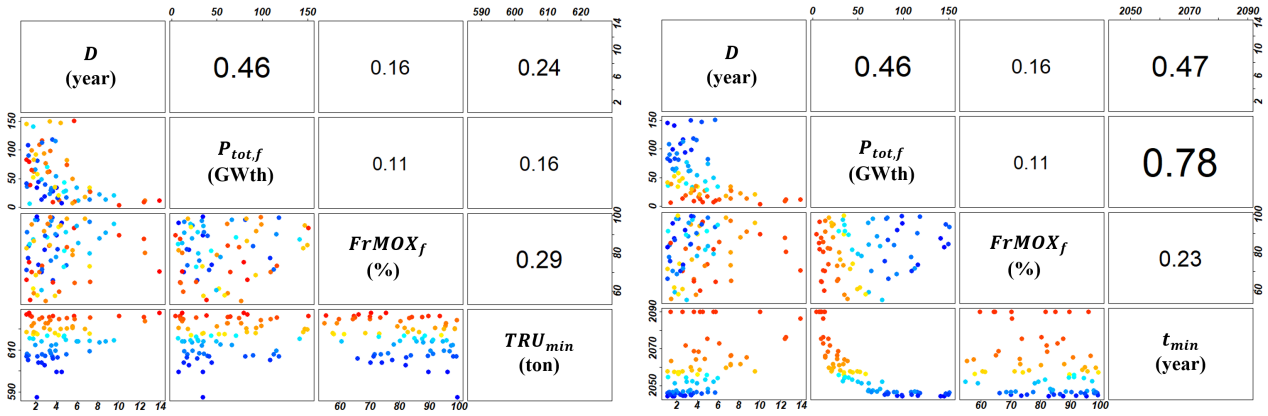

(a) Colored by the output TRU_{min} (b) Colored by the output t_{min}

Figure 4.16: Pairs plots of D, $P_{tot,f}$ and $FrMOX_f$ with: (a) TRU_{min}, (b) t_{min}. Only TRU-incineration strategies in S_{burn} are considered. Upper triangle shows the correlation matrix.

The first remark that should be noted is the ranges of these three important inputs: threshold effect can be observed for D and $FrMOX_f$, while $P_{tot,f}$ is available in a relatively large range. The net incineration of TRU in the total cycle by this nuclear system demands a rapid loading of MOX, within a transition shorter than 14 years, towards a global fraction higher than 50%. Such short transition is approximately equivalent to two or three irradiation cycles. The all initial range of $P_{tot,f}$ can satisfy the criterion of validity and the constraint of TRU incineration which is correlated measurably with the choice of D. In other words, the plutonium in spent UOX fuels should be rapidly recovered and incinerated by the use of MOX.

Under the significant cut of strategy space, these adaptations lead to a relatively narrow range of TRU_{min}. One singular case can be observed, which suggests a transition as short as two years, loading MOX into nearly 100% core of all PWRs, remaining 35 GWth after the transition. $TRU_{min} = 587$ tons is achieved by $t_{min} = 2057$ followed by the first missload. Except for this singular strategy, a simultaneous synergy between three inputs on TRU_{min} is slightly visible but globally not measurable. On the contrary, t_{min} is strongly correlated with $P_{tot,f}$, especially impacted by the synergy between $P_{tot,f}$ and $FrMOX_f$.

This result can be simply explained by the limited capacity of TRU incineration by the fleet of PWR UOX and MOX. In a fleet of PWR UOX and MOX, each inventory of plutonium produced in UOX after t_{ad} lifts up the lowest achieved TRU_{min}, because it cannot be thoroughly burned by the use of MOX. As a result, the lower bound of TRU_{min} is controlled by the available inventory of plutonium in spent UOX fuels at t_{ad}. A TRU-incineration strategy in S_{burn} in this scenario suggests then loading as much as possible MOX, so that the production during the depletion of the UOX fuels can be minimized, and the incineration by the irradiation of MOX fuels can be maximized. Given this limited capacity of incineration by mono-recycling (approximately between 10% and 30% of plutonium in the fresh MOX can be incinerated), the maximal quantity that can be incinerated is close to the discrepancy between TRU_{eff} and TRU_{tot} at t_{ad}. In consideration of these factors, the constraint $TRU_{min} < TRU_{tot}(t = 2040)$ in S_{burn} imposes a strong cut in the strategy space, presenting a uniform pattern over the the output-input space. Given similar TRU_{min} achieved, the pace of consumption of plutonium in spent UOX fuels is controlled by the choice of adaptive strategy, mainly subject to the combination of $P_{tot,f}$ and $FrMOX_f$ of the short-transition.

4.3.2.3 Robustness assessment of adaptive strategies

According to the criterion $C^{t\text{-}dcn}_{B,ad}$, the robust adaptive strategies must be in a subset of S_{burn}. The evolution of TRU_{tot} for the corresponding strategies is shown in Figure 4.17. Curves are colored by the final power level contributed by MOX given by $P_{tot,f} \times FrMOX_f$. In S_{burn}, TRU_{min} is achieved either in $t_{min} = t_{ML}$ for the strategies that meet plutonium shortages, or at the end of scenario for other strategies, given the monotonic decrease of TRU_{tot} after the transition.

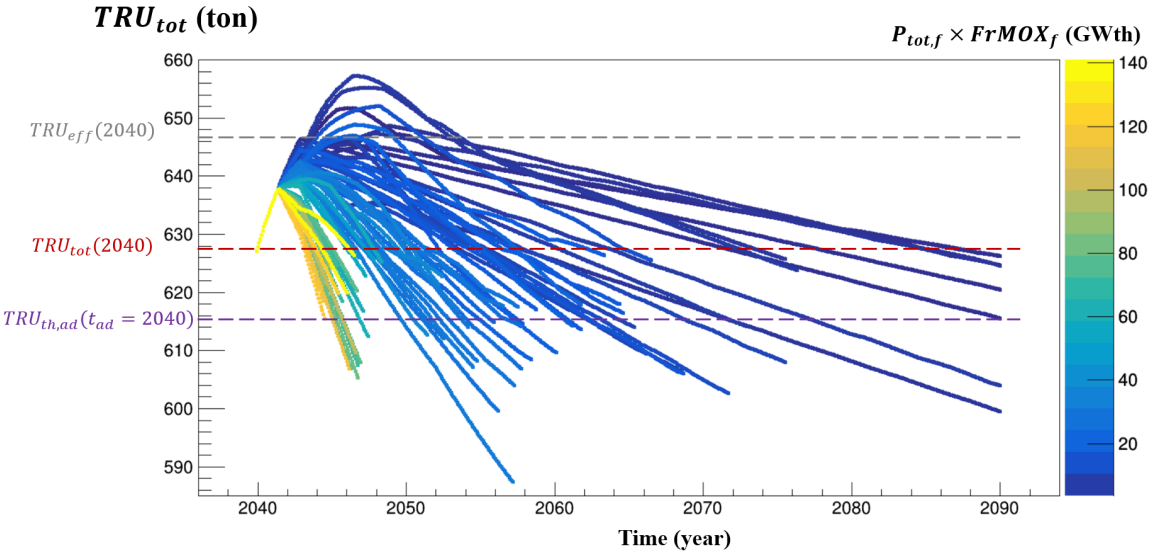

Figure 4.17: Evolution of TRU_{tot} of S_{burn} strategies, colored by final MOX power level $P_{tot,f} \times FrMOX_f$

The possible robust adaptations share actually the similar characteristics of

strategies in S_{burn}, with stricter requirements on the adapted parameters. In general, the plutonium in spent UOX fuels are recovered as fast as possible within a sufficient short transition, and loaded in MOX fuels. The time t'_{TRU} is then a function of the TRU_{tot} incineration rate, well characterized by $P_{tot,f} \times FrMOX_f$. In total, 34 adaptive strategies are defined here as robust. The t_{ML} versus t'_{TRU} of these robust strategies is shown in Figure 4.18, colored by the final power level ofMOX $P_{tot,f} \times FrMOX_f$.

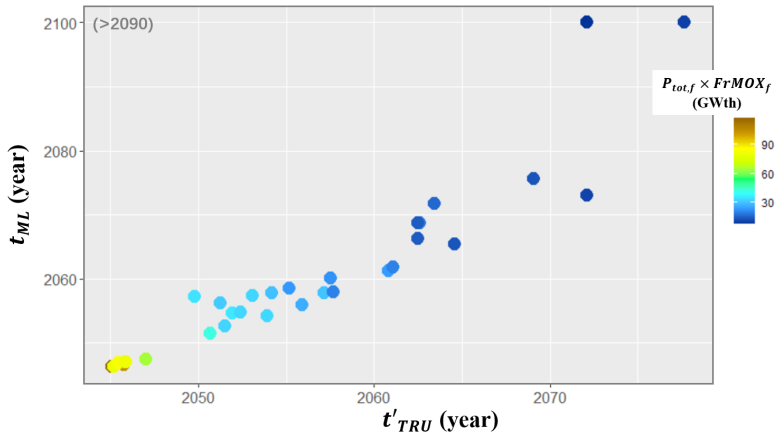

Figure 4.18: t_{ML} versus t'_{TRU} of robust adaptive strategies, colored by the final power level of MOX $P_{tot,f} \times FrMOX_f$

For most of these robust strategies, the first missload follows rapidly t'_{TRU}. As analyzed previously, MOX fuels are loaded rapidly in a very high fraction of PWRs, and the decrease rate of TRU_{tot} is controlled by the power level. Even though the difference between $TRU_{tot}(t = t_{ad})$ based on the prior trajectory and the threshold $TRU_{th,ad}$ is not significant in the whole evolution within the horizon, it is extremely difficult to remove this part of TRU. Even a slight increment requires a radical and brutal change of fuel cycle to offset it.

The difference of TRU to be burnt, $(TRU_{tot} - TRU_{th,ad})(2040)$ in this study, is close to the capacity of TRU incineration by PWR MOX. As we can see in Figure 4.17, most of robust adaptations TRU_{min} are close to the threshold $TRU_{th,ad}$. Subject to this condition, the assessment of adaptive robustness can be easily influenced by some outer factors, such as modelling errors and subtle uncertainties of scenario assumptions. The resistance and the credibility of assessment results are then reduced.

In terms of the uncertainty of t_{ad}, the difference between the TRU_{tot} of prior reference trajectory and TRU^A_{min} increases over time. Intuitively, later t_{ad} leads to a smaller phase space for robust adaptations with t_{ad} increase. The space becomes more and more strict on the demand of MOX loading and the pace of transition. In consideration of the increasing cost of search and the fragility of the assessment result aforementioned, the systematic comparison of adaptation on this prior reference trajectory over different t_{ad} is not performed in this section.

4.3.3 Comparison of strategy assessments connected with/disconnected from a pre-determined time

This section presents a study of adaptive robustness assessment which separates the evaluation of strategies from a pre-determined time. With these new introduced definitions, the assessment of an adaptive strategy can be generalized within extended time horizon, enhancing the inter-temporal consistency of

analysis, which is an issue in the study connecting the evaluation to a given time in Chapter 3.

The disconnection is done by the change on the definition of threshold levels. In the adaptation study in Chapter 3, the threshold levels are still attached with a projection in the future, being variable over the assumption on the time horizon. In this adaptation scenario study, a "historical level" relative to the adaptation time is taken as threshold, which is invariant for the future afterwards. But this threshold varies over the adaptation time. Correspondingly, one other major change is the validity of strategies. Due to the independence of assessment from a given time, the validity of strategies is generalized such that it only focuses on the duration of each adaptation transition. If the transition can be carried out without plutonium shortage, this adaptive strategy is considered valid.

Under these changes of definitions, the adaptive robustness assessment is performed for an early adaptation $t_{ad} = 2040$, based on the prior reference trajectory that minimized t_R in pre-disruption scenario. Even though the adaptation is early, the fraction of robust adaptive strategy in the exploration space is small. Actually, net incineration of TRU inventories is a necessary condition of being robust, whereas the fleet of plutonium mono-recycling has a weak capability of TRU incineration. Even a tiny increase of TRU in total cycle requires a huge modification of the fuel cycle to burn it out.

4.4 Adaptability in case of disruption

Section 4.3 shows that a slight increment of TRU inventories requires a huge change on the fuel cycle to be offset completely. The difficulty of healing such vulnerability requires us to be more precautionary in the pre-disruption context, minimizing the regrets on TRU accumulation relative to the so-called lowest achieved level. In this section, adaptations from a set of prior trajectories are investigated, aiming to give more comprehensive assessments on both pre-disruption and adaptive strategies.

To do this, we define the adaptability of a given pre-disruption strategy as the fraction of robust adaptive strategies over the total sampling of adaptation. For the reference strategy that minimizes t_R in the pre-disruption scenario, it is 1.6% (32/2000) as shown in Section 4.3 for the case $t_{ad} = 2040$. From this prior reference trajectory, the quantity of the TRU that should be incinerated (in order to be adaptively robust), which can be represented by $TRU_{eff} - TRU^{A}_{min}$, is actually close to the maximal burnt TRU achieved by PWR MOX. If this small difference is a common outcome for all possible prior trajectories, it may reduce dramatically the credibility of the numeric values of adaptability for a set of pre-disruption strategies investigated.

Otherwise, if the difference of adaptability between two pre-disruption strategies is sufficiently large, 10% versus 1% for instance, a qualitative conclusion can still be drawn. The phase space of robust adaptation is a-priori less restrained for the high-adaptability pre-disruption strategies than for the low-adaptability ones. Accordingly, not only the adaptive planning characterized by the phase space of robust adaptations is an important criterion for the robustness assessment, but the adaptability is also informative for the choice before disruption.

However, it is not realistic to apply a large size of LHS to all prior trajectories of interest to deduce their adaptability. Associated with the identical DoE of adaptation space, the adaptability of prior trajectories depends on themselves that is completely controlled by eight input variables of pre-disruption strategy. In this section, some intermediate outputs of prior trajectories are analyzed to help un-

derstand how our notion of adaptability builds the link between pre-disruption strategies and robust adaptations. With the help of these outputs, a test is performed for the adaptation from year 2070, as a complement about the uncertainty of the disruption time.

4.4.1 Indicator of adaptability

The adaptation scenario in this study looks back to the outcomes before or at t_{ad}, neglecting the performance and evolution of trajectories afterwards in case of disruption. The trajectory state at t_{ad} is informative to deduce the adaptability of the corresponding pre-disruption strategy. Given the limited capacity of incineration of TRU by PWR MOX, two intermediate outputs of prior trajectory at t_{ad} can describe the potential of adaptability.

The first one is the TRU inventory at t_{ad}, or more precisely TRU_{eff}, the effective TRU inventory in consideration of the complete irradiation cycles of reactors, as defined in Equation 4.9. To be robust, the adaptive strategy should be able to incinerate enough TRU to bridge the gap between TRU_{eff} and the threshold considered: $TRU_{th,ad} = TRU^{A}_{min}(2040) = 616$ tons. As the incineration capability of considered technologies is very limited, it is highly possible that the adaptability drops sharply even with a small increase on TRU_{eff} over different pre-disruption strategies.

We shall remind that only plutonium from UOX spent fuel can be recycled. Consequently, the available plutonium inventories for MOX fabrication, denoted as Pu_{toMOX}, should also be looked at in detail. Pu_{toMOX} considers the plutonium inventories available for the MOX fabrication after t_{ad}, including those in the cooling pool and the interim stock of spent UOX, the inventory staying in the fabrication plant of MOX, as well as the ones that will be discharged from PWR UOX just after t_{ad}. A larger Pu_{toMOX} indicates directly a larger burnable mass of plutonium, which accounts for the major TRU incineration. The isotopic vector may modify the fraction to be incinerated, but it is only a second order effect, relatively minor compared with Pu_{toMOX}.

Figure 4.19 presents the evolution of these two intermediate outputs, TRU_{eff} and Pu_{toMOX}, in the prior trajectories of pre-disruption scenario. Figure 4.19a shows the evolution of TRU_{eff}, and the minimal achieved TRU TRU^{A}_{min} considered for the threshold level in adaptation scenario, colored by Pu_{eff} for given time. Figure 4.19b, as a complement, presents the evolution of Pu_{toMOX}, colored by the difference between TRU_{eff} and the threshold level TRU^{A}_{min} in case of disruption. These two figures provide complementary indications on the possible adaptability of prior trajectory. Under the uncertain t_{ad}, the difference between TRU_{eff} and TRU^{A}_{min} is a better metric to characterize the adaptability than the simple consideration of TRU_{eff} or TRU_{tot}.

Figure 4.20 explains why TRU_{eff} and Pu_{toMOX} are important indicators of adaptability for a given t_{ad}. From a global point of view, the final trajectory is a result on a prior pre-disruption strategy (s^{pre}) concatenated with a post-disruption adaptive strategy (s^{ad}). Starting from a given state of prior trajectory, the TRU_{tot} evolution is generally monotone under the TRU-incineration strategies. In these TRU-incineration trajectories, the TRU_{tot} variation rate after t_{ad} is directly determined by the adaptive strategy, principally through $P_{tot,f}$ and $FrMOX_f$ of s^{ad}. This TRU_{tot} variation rate is then specifically linked to t'_{TRU}, which characterizes the performance of adaptive robustness. Regardless, the variation of TRU_{eff} and Pu_{toMOX} may shift the TRU_{tot} evolution and impact the TRU_{min} achieved by a given adaptive strategy. As a result, both the adaptability of pre-disruption strategies and the t'_{TRU} after adaptations, are impacted by these two indicators regardless of t_{ad}.

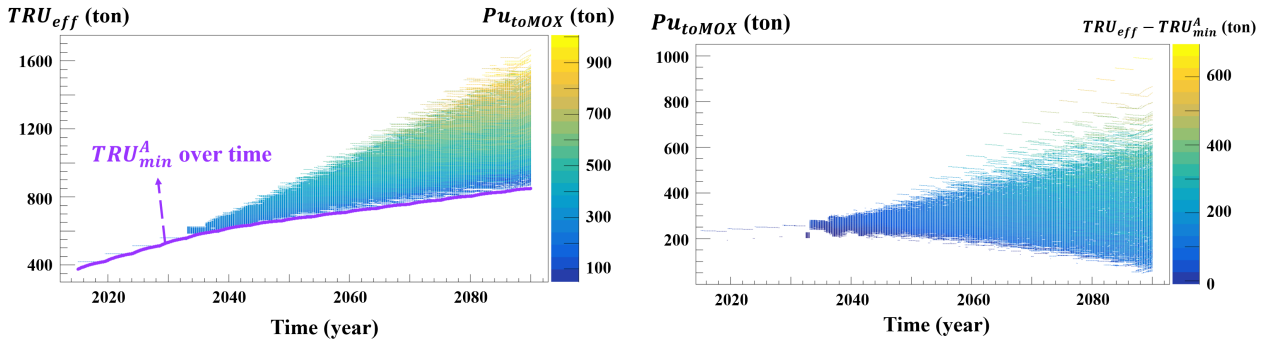

Figure 4.19: Evolution of TRU_{eff} colored by Pu_{toMOX}, and Pu_{toMOX} colored by the difference $TRU_{eff} - TRU^{A}_{min}$

Nevertheless, one should note the approximation of these two quantities on the adaptability. As it can be anticipated (and presented previously in section 4.3), all robust adaptive strategies suggest a relatively high power level of MOX. Under the assumption of macro-reactor, the first missload can happen even if a considerable inventory of Pu is still available in spent UOX fuels. Meanwhile, because the robust adaptive strategies need to be valid strategies, the vague boundary between valid and invalid adaptive strategies may complicate and affect the estimation of the adaptability of pre-disruption strategies. As a result, both the value of adaptability and its dependency on both TRU_{eff} and Pu_{toMOX} are approximate, and the nuances of adaptability between different pre-disruption trajectories should not be over-interpreted.

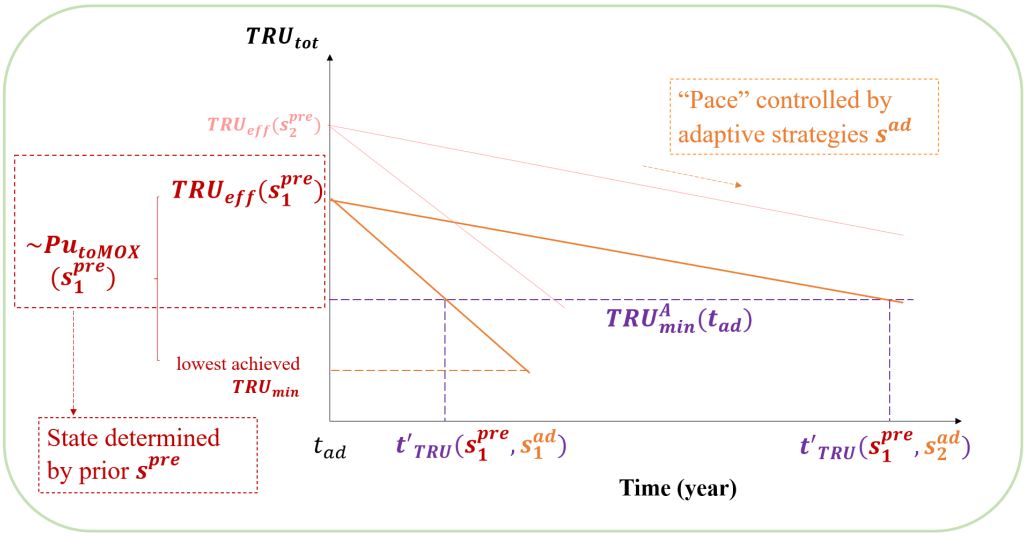

Figure 4.20: Graphical representation of the influence of prior pre-disruption strategy and adaptive strategy on TRU_{tot} evolution, in the fleet of PWR UOX and MOX

4.4.2 Analysis of two indicators of adaptability by 2040

To verify the importance of indicators TRU_{eff} and Pu_{toMOX} and to carry out the study on adaptability, 18 prior trajectories, characterized by the corresponding pre-disruption strategy, are chosen for adaptation. $t_{ad} = 2040$ is taken as an example. Note that an adaptation scenario is always based on the disruption of objective under the pre-disruption context; thus, the prior trajectories chosen should lead to $t_R < 2090$. Among these chosen strategies, only one allows $t_{start} > 2040$,

since all prior trajectories with $t_{start} > 2040$ are identical at $t_{ad} = 2040$. TRU_{eff} and Pu_{toMOX} of chosen prior trajectories should vary in a large range for the chosen strategies, as shown in Figure 4.21.

In Figure 4.21a, these two intermediate outputs, TRU_{eff} and Pu_{toMOX} in 2040, are actually highly correlated. In fact, just after several years of transition in the pre-disruption scenario, the variation of TRU_{eff} of trajectories is mainly reflected by the incineration during MOX depletion for one or two irradiation cycles. A lower Pu_{toMOX} results from a larger consumption of plutonium in spent UOX fuels, and implies then a lower TRU_{eff}. But because the high values of these two quantities have potentially opposite effects on the adaptability, their positive correlation may enhance their competition of their effects on the adaptability. To complement, the chosen strategies are also widely distributed in the output space of t_{TRU}-t_R, as shown in Figure 4.21b (only those of $t_R \leq 2090$ are presented). It emphasizes again that t_R and t_{TRU} are not appropriate indicators of adaptability, because the strategies of $t_{start} > 2040$ lead to considerable variability of these two outputs, while their adaptability with respect to t_{ad} are identical.

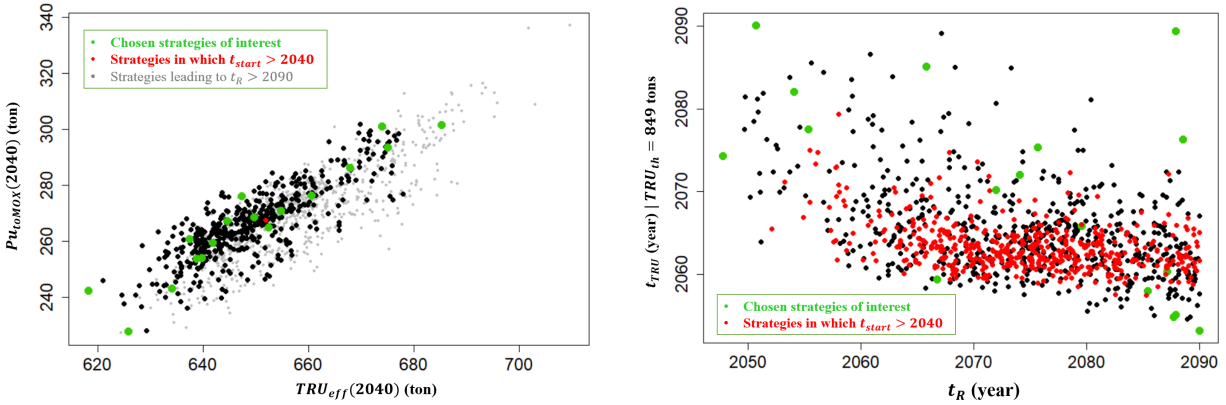

(a) $Pu_{toMOX}(2040)$ versus $TRU_{eff}(2040)$ (b) t_{TRU} versus t_R

Figure 4.21: Chosen strategies among the valid ones achieving $t_R \leq 2090$ for the study of indicators of adaptability: (a) the output space of $Pu_{toMOX}(2040)$ versus $TRU_{eff}(2040)$; (b) the output space of t_{TRU} versus t_R ($TRU_{th} = TRU_{MM} = 849$ tons)

The same DoE of adaptation is applied to these 18 prior trajectories. Robust adaptive strategies are counted for each prior trajectory so that the adaptability is approximately deduced, shown in Figure 4.22a. Two over these 18 pre-disruption strategies cannot be adapted robustly. The adaptability shows a global decreasing tendency over the difference $TRU_{eff} - TRU^A_{min}$. Some fluctuation of adaptability occurs over the increase of this difference: certain cases with higher difference $TRU_{eff} - TRU^A_{min}$ seems to achieve higher adaptability than several other cases with smaller difference. This fluctuation may be accounted by the larger Pu_{toMOX}, as presented in Figure 4.22b. A much larger Pu_{toMOX} indicates to the first degree of approximation a larger burnable inventory of plutonium, and may induce a gain on the adaptability due to the dominance of plutonium in TRU in this fuel cycle. But this effect is still secondary compared to the domination of TRU_{eff}.

A particular adaptive strategy s^{ad}_{40}, i.e. a set of parameters for the adaptation, is taken to show the effect of TRU_{eff} of different prior trajectories on the performance of adaptation. It is chosen because it can adapt robustly 14 prior trajectories of the 18 sampled, much more than all other adaptive strategies. The input parameters of s^{ad}_{40} is presented in Table 4.17. Instead of absolute power level $P_{tot,f}$, the ratio relative to $P_{tot}(t = t_{ad})$ is presented, because the starting point of all prior

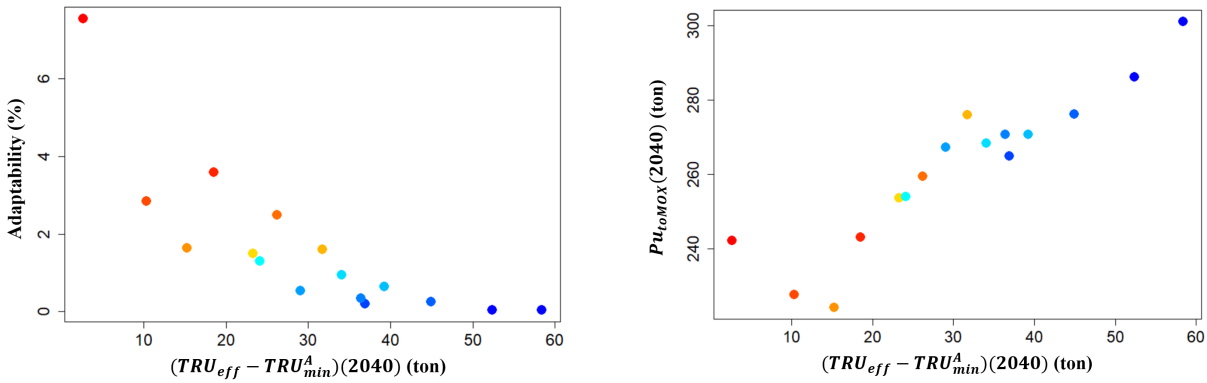

(a) (b)

Figure 4.22: Scatter plots of adaptability, the difference $TRU_{eff} - TRU^{A}_{min}$ and Pu_{toMOX}, with respect to $t_{ad} = 2040$; both figures are colored by the level of adaptability, where TRU^{A}_{min} stands for the threshold level of adaptation by 2040

trajectories are different. As shown in Figure 4.23, the difference between TRU_{eff} and the threshold TRU^{A}_{min} shifts proportionally the TRU_{min} after adaptation, based on the same readjustment plan. Given the same adaptive space for possible prior trajectories, the higher TRU_{eff} is, the lower the adaptability is.

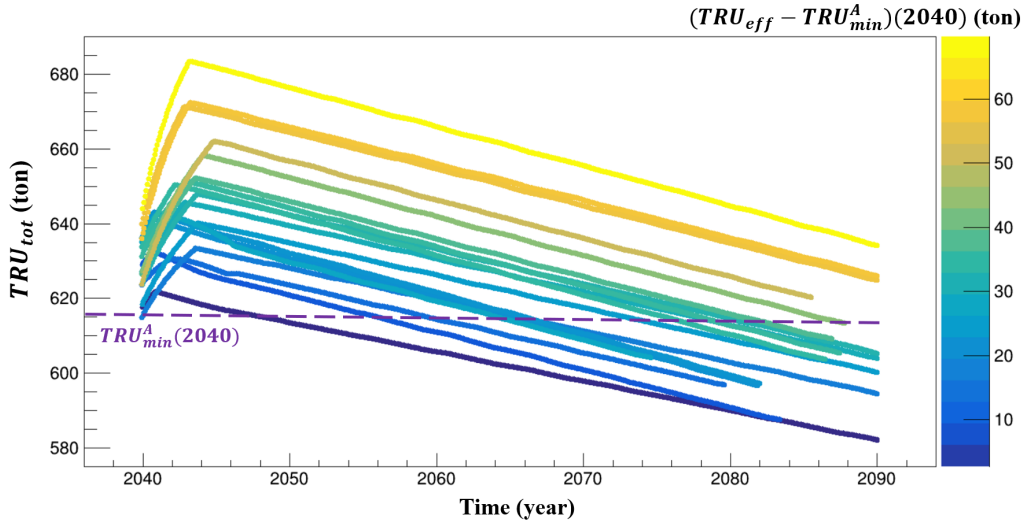

Figure 4.23: Evolution of TRU_{tot} under the adaptation of s^{ad}_{40}, based on 18 sampled prior trajectories

Once the importance of TRU_{eff} and Pu_{toMOX} on the adaptability is verified, we can investigate the relationship between them and the input parameters of pre-disruption strategies characterizing each prior trajectory. This may give us an insight even before simulating trajectories of adaptation from those potentially adaptable ones. The scatter plots of TRU_{eff} versus input parameters of pre-disruption strategy over t_{ad} are shown in Figure 4.24. In the case of $t_{ad} = 2040$, only strategies of $t_{start} < 2040$ are shown. The inputs TC_{UOX} and MPu are omitted due to their non-measurable effects on TRU_{eff}. Gray points stand for the strategies leading to $t_R > 2090$, which verifies that the black points of interest are distributed by the value of TRU_{eff} instead of the constraint $t_R \leq 2090$.

Even though those of $t_{start} > 2040$ are cut, some strategies that starts the transition after 2040 are still left, because the irradiation cycles are not yet finished by 2040. A line of constant $TRU_{eff}(2040)$ can be first remarked in the case of $t_{ad} = 2040$ and is created by these trajectories.

Strategy	D	$P_{tot,f}/P_{tot}(t=t_{ad})$	$FrMOX_f$	BU_{UOX}	BU_{MOX}	TC_{UOX}	MPu
s_{40}^{ad}	3	17.1	70.2	46.5	58.3	3.7	LiFo
s_{70}^{ad}	2	28.0	85.3	55.9	59.2	7.5	FiFo
(Unit)	year	%	%	GWd/t	GWd/t	year	-

Table 4.17: Input parameters of particular adaptive strategies s_{40}^{ad} and s_{70}^{ad}

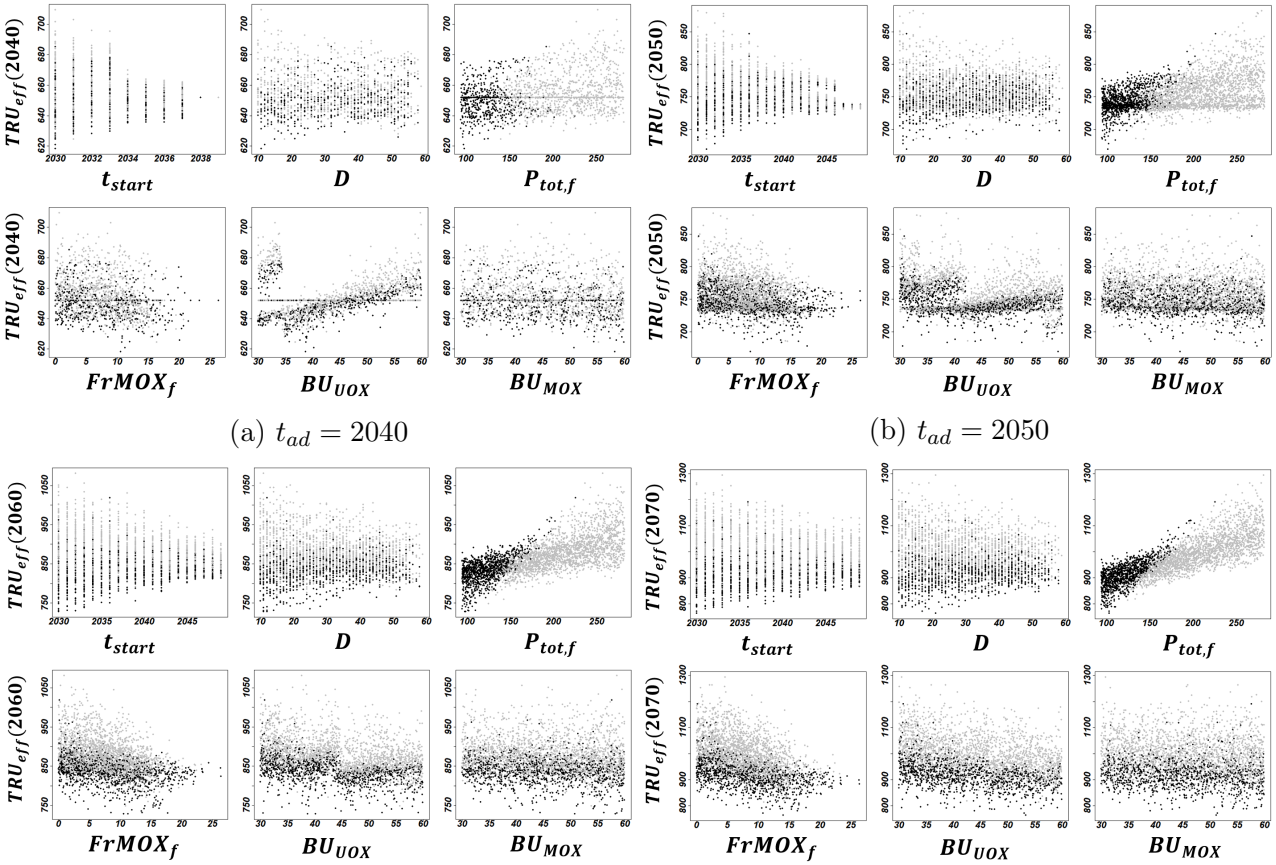

(a) $t_{ad} = 2040$ (b) $t_{ad} = 2050$

(c) $t_{ad} = 2060$ (d) $t_{ad} = 2070$

Figure 4.24: Scatter plots of TRU_{eff} and input parameters of pre-disruption strategies over t_{ad}. Gray points stand for the strategies leading to $t_R > 2090$.

For $t_{ad} = 2040$, a singular agglomeration of points appears in the region of high TRU_{eff} and low BU_{UOX}. This set of trajectories passes one more irradiation cycle when they finish the cycle of 2040 than others, due to the short cycle of low BU_{UOX} and a matching t_{start}. Apart from this cluster, TRU_{eff} increases with BU_{UOX}, which seems contradictory to the previous studies. Actually, within a very short term after the divergence of strategies, most of trajectories go through the same number of irradiation cycles except the ones in that singular cluster aforementioned. The advantage of high BU_{UOX} on the reduction of plutonium/TRU is not yet effective; on the contrary, a longer cycle of UOX depletion leads to a measurably higher production of plutonium at EOC. Similarly, the effects of other parameters are not evident due to the limited time of divergence.

As time goes by, TRU_{eff} of trajectories diverge. The effect on the lower production of TRU by high BU_{UOX} gets stronger, and $P_{tot,f}$ becomes gradually dominant. After decades of divergence of strategies, the importance of inputs on TRU_{eff} is extremely similar to the importance on TRU_{tot}. The difference between them becomes minor in the long term.

The relation between input parameters of pre-disruption strategies and the

output Pu_{toMOX} shares lots of similarities with the relation concerning the output TRU_{eff}. A slight tendency of inflection of Pu_{toMOX} on the medium-level BU_{MOX} can be observed when $t_{ad} = 2040$. When BU_{MOX} is high (>50 GWd/t), the Pu_{toMOX} seems statistically lower than that of the medium BU_{MOX} (between 40 and 50 GWd/t). In fact, within the identical number of irradiation cycles, high BU_{MOX} consume larger inventory of plutonium. While BU_{MOX} is sufficiently low, one more irradiation cycle is taken which consumes also one more part of plutonium. This effect of synchronization vanishes over the time. The increasing impact of $FrMOX_f$ on Pu_{toMOX} much more measurable than on TRU_{eff} should be highlighted as well.

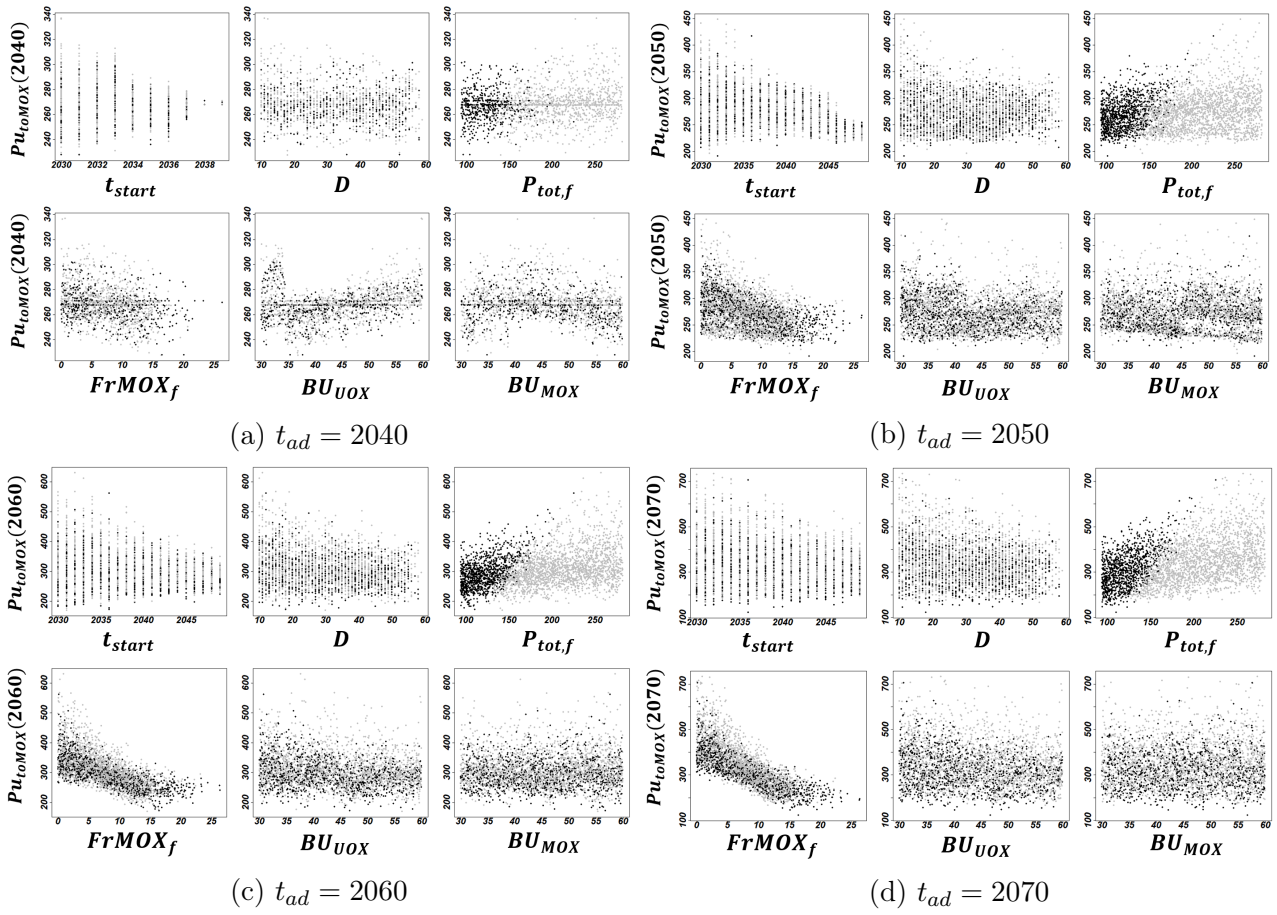

(a) $t_{ad} = 2040$ (b) $t_{ad} = 2050$

(c) $t_{ad} = 2060$ (d) $t_{ad} = 2070$

Figure 4.25: Scatter plots of Pu_{toMOX} and input parameters of pre-disruption strategies over t_{ad}. Gray points stand for the strategies leading to $t_R > 2090$.

4.4.3 Complement of adaptation by 2070: applying the indicators of adaptability

To complement the adaptation scenario study with respect to $t_{ad} = 2070$ which stands for a late disruption, TRU_{eff} and Pu_{toMOX} are used to perform the first screening of prior trajectories. The principle is that for a given prior trajectory, the Pu_{toMOX} should, under an optimistic estimation, allows an incineration of plutonium larger than the difference between TRU_{eff} and threshold TRU^A_{min} at t_{ad}. Because of the mono-recycling, an additional production of plutonium by UOX depletion after t_{ad} is regarded as a net increment of TRU. Putting all available plutonium into MOX as adaptation minimizes intuitively the achievable TRU_{min}.

It is therefore important to investigate the Pu_{toMOX} of pre-disruption strategies over the difference $TRU_{eff} - TRU^A_{min}$ for the study of adaptability. Figure 4.26 shows the Pu_{toMOX} versus this difference of pre-disruption strategies over possible t_{ad} of year 2040, 2050, 2060 and 2070. Those leading to $t_R > 2090$ are

presented by crosses. The reference strategy that minimizes t_R is surrounded by a square. It situates on the boundary of high Pu_{toMOX} due to its low $FrMOX_f$; and it has relatively low $TRU_{eff} - TRU^A_{min}$, because the low $P_{tot,f}$ prevents it from a too large TRU accumulation. Gloabally, a linear dependency between Pu_{toMOX} and $TRU_{eff} - TRU^A_{min}$ can still be drawn for all t_{ad}. Nevertheless, the scattered points disperse when t_{ad} increases, mainly due to the divergence of the trajectories under different pre-disruption strategies. If all Pu_{toMOX} is supposed to be used for MOX and no UOX is considered, one may wonder how deep the TRU incineration could be. The simulation of PWR MOX by CLASS in the study of [69] shows that within a very large variability of plutonium isotopic composition, the maximal fraction of initial mass of plutonium in fresh MOX fuels to be incinerated is around 30%. This limit is drawn in Figure 4.26. For the case $t_{ad} = 2070$, the threshold for robust adaptation is $TRU^A_{min}(2070) = 757$ tons. This limit criterion is able to cut a large amount of pre-disruption strategies that would not have any robust adaptation.

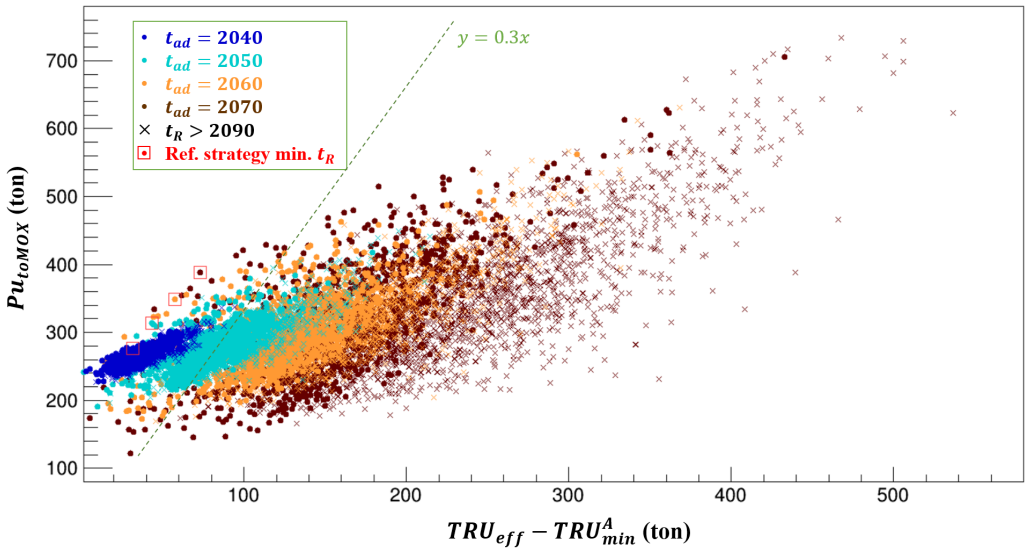

Figure 4.26: Pu_{toMOX} versus the difference $TRU_{eff} - TRU^A_{min}$ of pre-disruption strategies

For the available prior trajectories after the cut, a simplified exercise of adaptation is performed. For each of them, a quick transition converting all reactors of the fleet to full-MOX just after the adaptation time is simulated. If the level of TRU_{tot} after emptying the interim stock is still higher than the threshold TRU^A_{min}, there is evidently no robust adaptive strategy available for this prior trajectory.

After these two steps of screening, 16 prior trajectories are left for adaptation in 2070. The other ones are supposed not to be adaptable, meaning that no robust strategies can be identified. Similar to the previous exercises, 2000 adaptive strategies for each of these 16 prior trajectories are simulated and analysed for robustness assessment.

The adaptability over the difference $TRU_{eff} - TRU^A_{min}$ and Pu_{toMOX} of prior trajectories with respect to $t_{ad} = 2070$ is shown in Figure 4.27, colored by the value of adaptability. With a significant divergence of prior trajectories after decades of transition, the correlation between TRU_{eff} and Pu_{toMOX} becomes weaker than that of $t_{ad} = 2040$ presented in Section 4.3, which enhances the importance of Pu_{toMOX}. That's why the adaptability over TRU_{eff} (or the difference relative to TRU^A_{min}) gets more disperse than in the case of $t_{ad} = 2040$. Particularly, in the interval of [30, 45] tons of $TRU_{eff} - TRU^A_{min}$ at 2070, a large variability of Pu_{toMOX} can be observed, and so is the adaptability of pre-disruption strategies. For two of these 16 prior trajectories, no robust adaptation is identified, meaning that

none of 2000 adaptations can lead to $TRU_{tot} < TRU_{th,ad}(2070)$ within the time horizon.These two present respectively a difference $TRU_{eff} - TRU^{A}_{min}$ of 60 and 70 tons and Pu_{toMOX} of 350 and 300 tons by $t_{ad} = 2070$. It emphasizes again that the adaptability deduced by the sampling and these two indicators are only estimators and should not be over-interpreted. But even with this limitation, the strong dependency of adaptability on both these two indicators are verified and remains credible with a different t_{ad}.

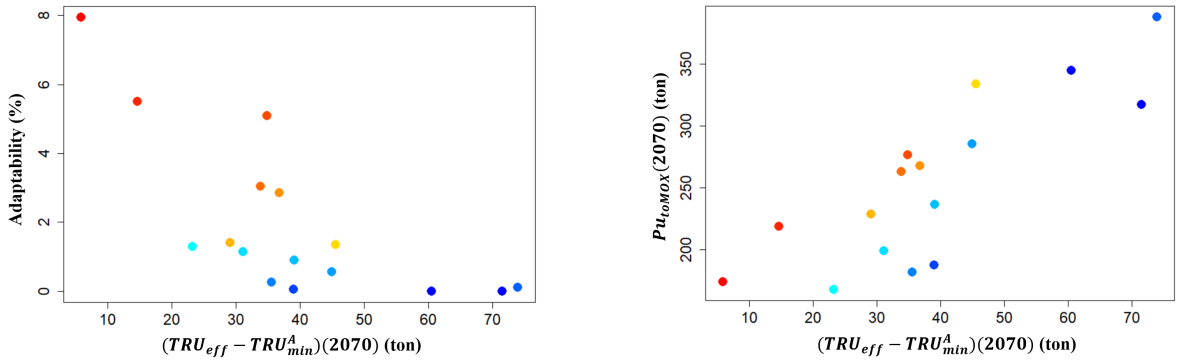

(a) (b)

Figure 4.27: Scatter plots of adaptability, the difference $TRU_{eff} - TRU^{A}_{min}$ and Pu_{toMOX}, with respect to $t_{ad} = 2070$; both figures are colored by the level of adaptability, where TRU^{A}_{min} stands for the threshold level of adaptation by 2040

The evolution of TRU_{tot} of several particular trajectories after adaptation are presented in Figure 4.28, showing the combined effects of prior pre-disruption strategies and adaptive strategies. Figure 4.28a considers the TRU-incineration adaptations based on three prior trajectories. The first one is from the prior reference strategy aiming to minimize t_R in the pre-disruption scenario, which starts from the orange square in the figure. For this prior reference trajectory, a large inventory of plutonium is stored in the spent UOX fuels. The consumption rate of plutonium characterized by the adaptive $P_{tot,f} \times FrMOX_f$ can be kept during relatively long time, and the quantity of TRU burned is also significant. But due to a large difference from the threshold level $TRU_{th} = TRU^{A}_{min}(2070)$, only several adaptive strategies can lead to adaptive robustness. In contrast, the prior trajectory of robust static optimum which maximizes t_{TRU} in the pre-disruption scenario, leads to a relatively small difference to TRU^{A}_{min} by 2070; but it has a relatively limited inventory of plutonium available for the mono-recycling. The most adaptable prior trajectory by 2070 is also considered, represented by gray curves. As verified in Figure 4.27a, the difference of $TRU_{eff} - TRU^{A}_{min}$ of this trajectory is only several tons while more than 170 tons of plutonium is available for MOX fabrication. These two considerations allow a relatively large choice for robust adaptive strategies. In general, the performance of robust adaptation, characterized by the time t'_{TRU}, still depends strongly on the power level contributed by MOX fuels, which is coherent with the previous analysis.

Figure 4.28b focuses on two adaptive strategies applied to all investigated prior trajectories. One is the s^{ad}_{40} presented in the analysis of adaptation by 2040, presented by gray curves, and the other is denoted as s^{ad}_{70} which adapts robustly 14 prior trajectories over 16 for this study of $t_{ad} = 2070$. The input parameters of s^{ad}_{70} are presented in Table 4.17. The colored curve and the gray curve which start from the same point stand for the evolution of these two adaptations from the same prior trajectory. Even though s^{ad}_{40} seems universal to be robust subject to the unknown prior trajectory in the case of $t_{ad} = 2040$ (but only 18 prior trajectories are considered in this case), it is not the same when the adaptation is

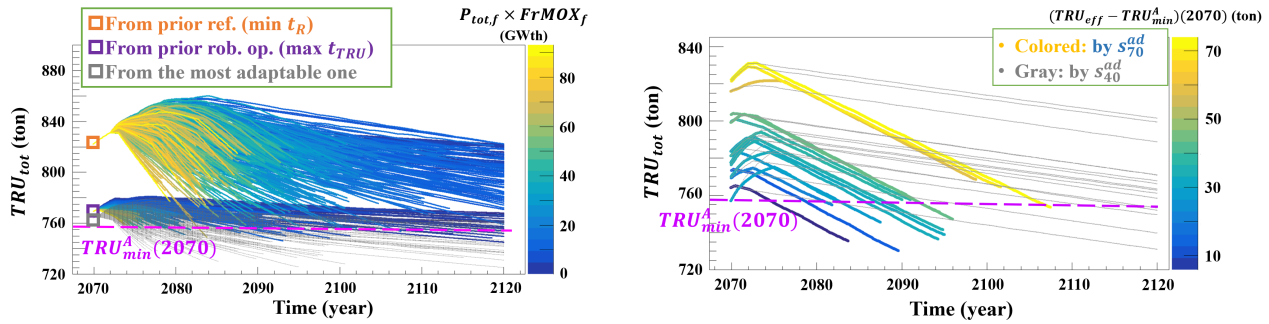

Figure 4.28: Evolution of TRU_{tot} of particular trajectories: (a) trajectories with adaptation on three prior trajectories; (b) two particular adaptive strategies on all investigated prior trajectories

taken in 2070. It can be explained by the different power level contributed by MOX between these two strategies, which is also a numeric difference from the scenario assumptions. Actually, if $t_{ad} = 2040$, this level should be sufficiently low to be valid, because the available plutonium inventory for MOX fabrication is low. The ratio $P_{tot,f}/P_{tot}(t = t_{ad})$ stays the same regardless of t_{ad}. The final level $P_{tot,f}$ is therefore relatively high, because $P_{tot}(t = 2040)$ of prior trajectories are still high. For $t_{ad} = 2070$, the plutonium consumption rate of MOX suggested by s^{ad}_{40} becomes much smaller, leaving a large part of it in the spent UOX fuels. Then the incineration is not maximized. s^{ad}_{70} suggests, on the contrary, a higher power of MOX as well as high BU_{UOX}. Such changes highlight, at the same time, the interactions between pre-disruption strategies, adaptive strategies and the uncertainty of t_{ad} on the results.

4.4.4 Beyond the times of interest: feed-back of adaptability on available choices under uncertain disruption

In the pre-disruption scenario study, the importance of two times of interest, t_R and t_{TRU}, are analyzed. The precaution for the uncertain disruption of objective is pronounced on the value of t_{TRU}, depending on corresponding threshold definition. In case of disruption, the adaptability, defined in this work as the proportion of robust adaptations over all exploratory space, is also a helpful criterion on the choice of pre-disruption strategy.As verified in two studies of adaptation in 2040 and in 2070, the robust static strategies are not necessarily the most adaptable ones in case of disruption. In other words, even if a good tradeoff is achieved between t_R and t_{TRU}, the corresponding trajectory can be hard to readjust back to the lowest achievable TRU among historical choices.

One should note that irradiation cycle is supposed to be respected for any adaptation. Given the limited TRU incineration capability of PWR MOX, the inertia of the fleet can impact strongly the adaptability of pre-disruption strategies. If, approximated at the first order, the burnable plutonium inventory is of the same magnitude as the plutonium produced by one irradiation cycle of the macro PWR, then the adaptability of the same pre-disruption strategy can differ measurably around one or two years of t_{ad}. The assumption of macro reactor can also have some influences. In this case, the adaptability may not be a very meaning full quantity.

Regardless, $TRU_{eff} - TRU^A_{min}$ and Pu_{toMOX} can be used as indicators to rank the available strategies. The evolution of these two intermediate outputs, as shown in Figure 4.19, gives an insight on the dynamic change of adaptability.

One may also calculate the time-average values of these two indicators, in order to perform a time-independent ranking. The use of these two quantities are dependent on this study context, such as the assumption of PWR UOX and MOX for the fleet adaptation. If other assumptions are considered, the use of them should be checked, or other new indicators can be defined.

4.5 Adaptation with advanced technology: multi-recycling of plutonium in PWR

The previous studies show how hard is to incinerate the excess of TRU relative to another by PWR MOX, and how limited is the robust adaptation space. It implies extremely precautionary choices before disruption to guarantee the possible adaptability.

Instead of sticking to existing technologies, it is possible to apply advanced design for adaptation, in order to free the fleet from narrow space of well-performing adaptations. For example, the technology of multi-recycling plutonium in PWR can be applied, in case SFR deployments are not considered any more [18]. To investigate the impact of using different advanced technology from the fleet before disruption, the MOXEUS fuel is considered for adaptation in this section. It is worth noting that MOXEUS is different from MIX fuel which is considered in Chapter 5 of this manuscript.

4.5.1 Introduction of MOXEUS

The plutonium quality of MOX decreases during depletion in the reactors. Therefore the recycling of plutonium from spent MOX fuels for current MOX assemblies is not possible. To circumvent this problem, one option is to mix homogeneously in the same fuel pellets the ^{235}U-enriched UOX and plutonium oxides allowing the use of multi-recycled plutonium. This allows to compensate the decrease of plutonium quality and respect the limit of plutonium content regarding nuclear safety. The MOXEUS fuel design applies this principle.

The modelling of MOXEUS in CLASS is well illustrated in [74, 50], in which the physic properties of MOXEUS fuels and plutonium-/TRU-stabilization scenarios are studied in detail. In practise, this fuel design varies first the plutonium content to achieve the target burn-up. If the plutonium quality cannot guarantee the target burn-up with a plutonium content below a given limit, ^{235}U needs to be enriched. If all plutonium is used but cannot reach lower limit of plutonium content, MOXEUS fuel cannot be loaded in the reactor. Technically this low plutonium content may result from either the severe plutonium shortages, or a very high-quality plutonium. If the quality of plutonium is too low and the addition of enriched ^{235}U is not able to guarantee the required burn-up, the missload will be triggered as well.

With the application of multi-recycling of plutonium and the enrichment of ^{235}U, fewer cases with missloads and a wider space of robust adaptive strategies can be expected.

In this new adaptation scenario, the prior reference trajectory that minimizes t_R before disruption is adapted, in 2040 and in 2070. The input variables of interest and their ranges are summarized in Table 4.18. The MOXEUS fuel replaces the mono-MOX fuel of the previous adaptation scenario, and the final MOXEUS fraction, denoted as $FrMXE_f$ in this section, ranges in [20%, 100%], while other hypotheses concerning the input parameters remain unchanged. The smaller

range of MOXEUS final fraction than the one of MOX in the previous scenario studies aims to generate more useful observations for TRU-incineration or robust adaptations. In short, a new transition is supposed after the adaptation time t_{ad}. The burn-up of fuels, the cooling time of spent UOX, and the reprocessing strategy (LiFo/FiFo) change at t_{ad}. During the transition, the total power level of fleet and MOXEUS fraction change linearly; they are kept constant after the transition. The cooling times are set to five years, remaining the same as in the scenario using MOX. On the other hand, the reprocessing strategy of spent MOXEUS fuels is an additional variable. In this study, it follows the same law as spent UOX reprocessing: either both types of spent fuels take LiFo, or both of them are FiFo. The input variable of MOXEUS fraction is denoted as $FrMXE_f$, and the MOXEUS burn-up is denoted as BU_{MXE}. The transition phase between the use of MOX in prior trajectory and the use of MOXEUS for adaptation is neglected. The use of MOXEUS is considered mature enough when adaptive strategy is implemented. Thus, the evolution of MOXEUS fraction starts from the MOX fraction by t_{ad} of prior trajectory, as indicated in Table 4.18. Other operational and fuel cycle parameters concerning MOXEUS fuel should be specified as well. The plutonium content of fresh MOXEUS fuel is variable and determined by the FLM of MOXEUS. The maximal plutonium content is still set to 12%, as used for MOX fuel, even though other values are also possible. Its minimal content is set to 4.5%. The highest enrichment of ^{235}U is set to 5%.

Input var.	Init. Val. ($t = t_{ad}$)	Min.	Max.	Unit	Explanation
D	-	1	50	year	Duration of transition
$P_{tot,f}$	$P_{tot}(t = t_{ad})$	0.	$P_{tot}(t = t_{ad})$	GWth	Total thermal power of the fleet after transition
$FrMXE_f$	$FrMOX(t = t_{ad})$	20	100	%	MOXEUS fraction after transition
BU_{UOX}	32.4	30	60	GWd/t	Modified burnup of UOX fuels
BU_{MXE}	41.9	30	60	GWd/t	Modified burnup of MOXEUS fuels
TC_{UOX}	3.6	3	10	year	Modified cooling time of spent UOX fuels
MPu	1/LiFo	1/LiFo	2/FiFo	-	Modified management of spent fuels

Table 4.18: Strategy space of adaptation scenario allowing the use of MOXEUS: starting from t_{ad} of the trajectory of reference strategy that minimizes t_R

The same DoE of 2000 samples from LHS is performed for this adaptation scenario with respect to $t_{ad} = 2040$ and $t_{ad} = 2070$. The starting value of power level and MOXEUS fraction are described in Table 4.19. The use of the same DoE allows a direct comparison with the adaptations using MOX.

t_{ad}	2040	2070	(Unit)
$P_{tot}(t = t_{ad})$	151.0	95.2	GWth
$FrMOX(t = t_{ad})$	7.6	1.8	%

Table 4.19: Starting point of level power $P_{tot,f}(t = t_{ad})$ and MOX fraction $FrMOX(t = t_{ad})$ in each adaptation scenario over t_{ad}

4.5.2 Analysis of valid strategies

Same notions as in Section 4.3 are used to group the strategies regarding the validity and missloads. S_{noML} means strategies without plutonium shortage within the time horizon. $S_{ML,v}$ stands for the strategies leading to missloads within

the horizon but satisfying the validity criterion $C_{V,ad}^{t\text{-}dcn}$. Finally $S_{ML,nv}$ stands for the invalid strategies that do not satisfy $C_{V,ad}^{t\text{-}dcn}$. $S_{ML} = S_{ML,v} \cup S_{ML,nv}$ is the then the group of all missloading strategies, including the valid and invalid ones. $S_V^{ad} = S_{noML} \cup S_{ML,v}$ contains all valid strategies. Using MOXEUS for adaptation, the space structure of validity is completely different from the previous one of using MOX, as shown in Table 4.20.

t_{ad}	2040			2070		
Set of sample	$S_{ML,nv}$	$S_{ML,v}$	S_{noML}	$S_{ML,nv}$	$S_{ML,v}$	S_{noML}
Size using MOXEUS	90	284	1626	1	49	1950
% of total space using MOXEUS	4.5%	14.2%	81.3%	0.0%	2.5%	97.5%
Size using MOX	1060	506	434	1011	630	359
% of total space using MOX	53.0%	25.3%	21.7%	50.5%	31.5%	18.0%

Table 4.20: Under the use of MOXEUS fuels for adaptations from the prior reference trajectory, size of subsets $\boldsymbol{S_{ML,nv}}$, $\boldsymbol{S_{ML,v}}$ and $\boldsymbol{S_{noML}}$, and their percentage in the whole space of adaptive strategy. Comparison with the use of MOX for adaptations.

With MOXEUS, a major part of the adaptations are valid, even without missload. The validity of adaptive strategies using MOXEUS differs a lot from that using MOX, especially from the angle of plutonium availability within the whole horizon. The large part of adaptive strategies without missload with the use of MOXEUS highlights the high sustainability of material flow even when high MOXEUS fraction is considered. The ^{235}U enrichment is a key point to ensure this sustainability when the plutonium is not sufficient for a target burn-up.

Given the relatively small number of strategies with quantifiable t_{ML}, only graphical techniques are used to investigate the impacts of adaptive strategy input parameters on t_{ML}. The pairs plots of D, $P_{tot,f}$ and $FrMXE_f$ of adaptive strategies, with the output t_{ML}, are presented in Figure 4.29, colored by the value of t_{ML}. In these pairs plots, gray points stand for strategies without missload, and their t_{ML} are set arbitrarily to 10 years after the end of scenario in the figures. Crosses stand for the invalid strategies. Note that $P_{tot,f}$ in two cases are not in the same range, due to the different starting point of $P_{tot}(2040)$ and $P_{tot}(2070)$.

We assume that these three parameters are the most important for the determination of quantifiable t_{ML}. The missload occurs when both $P_{tot,f}$ and $FrMXE_f$ are close to the maximum. t_{ML} depends on the combined effects of 3 input variables: $P_{tot,f}$, $FrMXE_f$ and D. They characterize the dynamic evolution of the proportion of the power produced by MOXEUS. The correlation between t_{ML} and $P_{tot,f} \times FrMXE_f/D$ is around -0.73. It can be simply explained by the fact that a fast transition towards a high consumption rate of plutonium of available stocks may meet quickly the shortage of plutonium, even if a large amount of plutonium stays in the cooling pool and would be available later. If the transition gets slower, more plutonium can be accumulated by the depletion of UOX during transition, and there is a larger margin of plutonium availability for MOXEUS fabrication. Thus, slower transitions delay the missload, especially when it is an adaptation for TRU-incineration.

With later t_{ad}, more available plutonium is accumulated to sustain the multi-recycling, and the maximum achievable $P_{tot,f}$ is lower, according to the prior reference trajectory. Thus, the adaptation scenario of $t_{ad} = 2070$ has much fewer cases with missloads.

There is also a dependency between t_{ML} and BU_{MXE}, as it is observed in the case of MOX shown in Figure 4.15. Similarly, when the missload on the same

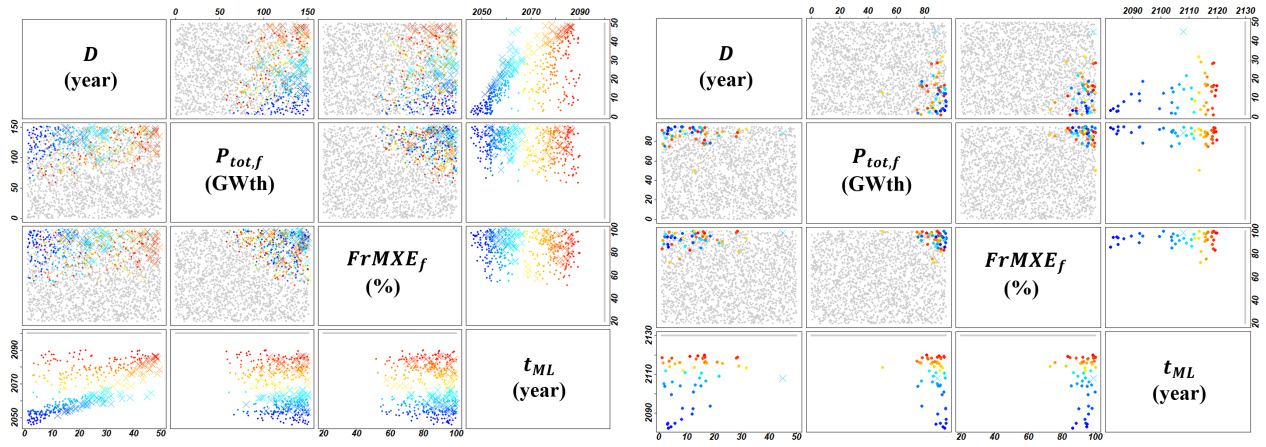

(a) $t_{ad} = 2040$ (b) $t_{ad} = 2070$

Figure 4.29: Pairs plot of D, $P_{tot,f}$ and $FrMXE_f$ of adaptive strategies, with output t_{ML}, with respect to $t_{ad} = 2040$ and $t_{ad} = 2070$, colored by the value of t_{ML}. Gray points stand for strategies without missload, and their t_{ML} are set to 10 years after the end of scenario in the figures. Invalid strategies are represented by crosses.

irradiation cycle is observed, a linear dependency between t_{ML} and BU_{MXE} is present. But statistically, these two quantities are not strongly correlated.

4.5.3 Analysis of outputs concerning the performance of adaptation

For each valid strategy, the minimal TRU_{tot} achieved in the trajectory before missload is calculated, denoted as TRU_{min}. The time when achieving TRU_{min} is also informative, denoted as t_{min}. Among all valid adaptive strategies, those allowing net incineration of TRU inventories, implying $TRU_{min} < TRU_{tot}(t_{ad})$, are of interest. The notation S_{burn} stands for this subset of valid adaptive strategy allowing the incineration of TRU inventories. TRU_{min} help understand the behavior of fuel cycle subject to the demand of incineration of TRU in a wider range than the focus on robust adaptations. Besides, the time needed to be robust, characterized by t'_{TRU}, is also studied.

4.5.3.1 Analysis of minimal achieved TRU of given adaptation

Because the use of MOXEUS help sustain the recycling and loading of plutonium, the size of subset S_{burn} is relatively large. In 2000 samples, there are 522 valid TRU-incineration strategies in the case of $t_{ad} = 2040$, and 802 in the case of $t_{ad} = 2070$. With such a size of trajectories of interest, the PCA is performed for the study of TRU_{min}.

One should note that the constraint of TRU-incineration creates an evident cut on the adaptation space, especially on D and $FrMXE_f$, and correlates the input variables. The 8-dimension original variable vector $\boldsymbol{X}$ $\boldsymbol{X} = (D, ..., TRU_{min})$ is considered to perform the PCA. The correlation matrix of $\boldsymbol{X}$ is shown in Table 4.21. Lower triangle presents the correlations of the case of $t_{ad} = 2040$, and the upper triangle presents the correlations of the case of $t_{ad} = 2070$. The correlations concerning inputs BU_{UOX}, BU_{MXE}, TC_{UOX} and MPu are smaller than 0.1 and are not presented. The correlations between D and $P_{tot,f}$ and between $P_{tot,f}$ and TRU_{min} are marked in red, which present opposite signs for two t_{ad}. They indicate that both the interaction between input parameters (especially between D and $P_{tot,f}$) and the relation between output TRU_{min} and those inputs (especially $P_{tot,f}$), subject to the constraint of TRU incineration, depends on the adaptation time.

Cor. coef.	D	$P_{tot,f}$	$FrMOX_f$	TRU_{min}
D	1.	0.17	0.37	0.40
$P_{tot,f}$	-0.29	1.		-0.37
$FrMOX_f$	0.355		1.	-0.41
TRU_{min}	0.28	0.26	-0.31	1.

Table 4.21: Correlation matrix of original variable vector $\boldsymbol{X} = (D, .., TRU_{min})$ of TRU-incineration adaptations: lower triangle indicates the correlations of $t_{ad} = 2040$; upper triangle indicates the values in the case of $t_{ad} = 2070$. Correlations lower than 0.1 are not indicated. Opposite signs in two t_{ad} are marked in red.

Based on the correlation matrix, the PCA is performed. Similarly, two important metrics are investigated. One is the fraction of total variability explained by j-th PC Y_j, represented by λ_j/V_{tot}, where λ_j is the j-th largest eigenvalue of the correlation matrix. The smallest λ_j/V_{tot} is approximately a constant, it may indicate a linear dependency between the original components of $\boldsymbol{X}$. The other one is the square of correlation between the output TRU_{min} and PC Y_j, denoted as $\rho^2(TRU_{min}, Y_j)$. The composition of Y_j achieving the highest $\rho^2(TRU_{min}, Y_j)$ indicates the importance of input variables on TRU_{min}.

The values of these two metrics in the PCA of two t_{ad} are shown in Table 4.22. In both cases of t_{ad}, the last PC, Y_8 in respective analysis, explains respectively 3% and 1% of the total variance of original variable vector $\boldsymbol{X}$, which is far smaller than the average contribution of single variable to the total variance. The composition of Y_8 indicates then a linear dependency and should be investigated. Y_2 in the case of $t_{ad} = 2040$ and Y_1 in the case of $t_{ad} = 2070$ present measurable correlations with the output TRU_{min}. Their compositions are of interest as well. Last but not least, Y_1 for $t_{ad} = 2040$ and Y_2 for $t_{ad} = 2070$ also account for non-negligible but limited variances of the respective TRU_{min}, and thus their compositions are investigated.

t_{ad}	Metrics	Y_1	Y_2	Y_3	Y_4	Y_5	Y_6	Y_7	Y_8
2040	λ_j/V_{tot}	0.20	0.16	0.13	0.13	0.12	0.12	0.11	0.03
	$\rho^2(TRU_{min}, Y_j)$	**0.19**	**0.67**	0.01	0.03	0.	0.01	0.	0.08
2070	λ_j/V_{tot}	0.19	0.17	0.13	0.13	0.12	0.12	0.11	0.01
	$\rho^2(TRU_{min}, Y_j)$	**0.81**	**0.14**	0.	0.	0.	0.	0.	0.03

Table 4.22: Fraction of variance of original variable vector $\boldsymbol{X}$ explained by j-th PC Y_j, λ_j/V_{tot}, and correlation squares between TRU_{min} and PC Y_j, $\rho^2(TRU_{min}, Y_j)$, regarding the TRU-incineration adaptation using MOXEUS

The composition of Y_1, Y_2 and Y_8 in both PCAs are presented in Table 4.23. Y_1 in the PCA of $t_{ad} = 2040$ and Y_2 in $t_{ad} = 2070$ are first checked. Y_1 in $t_{ad} = 2040$ is principally a combination of D, $P_{tot,f}$, $FrMXE_f$ and TRU_{min}. BU_{UOX} and BU_{MXE} also have some weights on Y_1. The 19% of TRU_{min} variance explained by Y_1 comes mainly from the part of TRU_{min} itself. The limited accountable fraction of TRU_{min} variance does not allow Y_1 to provide more information on the importance of input parameters on the output. Among all PCs, Y_1 accounts most of variance of all variables $\boldsymbol{X}$, because it captures the strong correlations of input parameters created by the constraint of TRU incineration. It is the similar for Y_2 in $t_{ad} = 2070$, which is principally composed of D, with some weights on $FrMXE_f$ and TRU_{min}

as well. Since these two PCs provide little information on the relation between input parameters and output TRU_{min}, other PCs of interest are needed.

t_{ad}	Y_j	D	$P_{tot,f}$	$FrMXE_f$	BU_{UOX}	BU_{MXE}	TC_{UOX}	MPu	TRU_{min}
2040	Y_1	**-0.47**	**0.51**	**-0.59**	**0.12**	**0.12**	0.02	-0.06	**0.35**
	Y_2	**0.63**	0.02	-0.03	**0.17**	-0.02	**0.19**	**0.13**	**0.72**
	Y_8	**-0.58**	**-0.37**	**0.47**	-0.02	0.03	0.	-0.01	**0.55**
2070	Y_1	0.04	**-0.46**	**-0.50**	-0.09	0.	-0.01	-0.04	**0.72**
	Y_2	**0.81**	0.06	**0.46**	0.06	0.03	**0.15**	0.08	**0.31**
	Y_8	**-0.53**	**0.35**	**0.49**	0.05	-0.02	-0.02	0.	**0.60**

Table 4.23: Coefficients of original variables in the PCs of interest in the PCA of TRU-incineration adaptations, for the output TRU_{min}

In the case of $t_{ad} = 2040$, 67% of the variance of TRU_{min} explained by Y_2 which is principally composed of D and the output TRU_{min} itself. According to their correlation and their coefficients in Y_2, this accountable fraction of TRU_{min} variance can be actually decomposed to the part of TRU_{min} in Y_2 and its correlation with D. This PC cannot therefore give new information. On the contrary, the composition of Y_8 shows a strong synergy of D, $P_{tot,f}$ and $FrMXE_f$ on TRU_{min}. For $t_{ad} = 2070$, 81% of variance of TRU_{min} can be explained by Y_1, and its composition highlights the importance of $P_{tot,f}$ and $FrMXE_f$. The composition of Y_8 also emphasizes the importance of D in addition to these two input parameters.

The importance of D, $P_{tot,f}$ and $FrMXE_f$ revealed by respective PCA seems not intuitive to be interpreted from a physics point of view. For the effect of D on TRU_{min}, a longer transition continues the prior trajectory tendency of TRU accumulation, and a lower TRU_{min} becomes harder to achieve. According to the signs of coefficients in Y_8, the effects of D and of $FrMXE_f$ on TRU_{min} are consistent over two t_{ad}, whereas the sign of $P_{tot,f}$ is different. It is also indicated by the correlations between TRU_{min} and $P_{tot,f}$ and between D and $P_{tot,f}$ presented in Table 4.21. The dependency of TRU_{min} on $P_{tot,f}$ and $FrMXE_f$ involves the interaction with the constraint of validity. Graphical representations are needed to visualize their effects.

The evolution of TRU_{tot} in the valid part of trajectory of those TRU-incineration adaptation in S_{burn} is shown in Figure 4.30, over the value of $P_{tot,f}$ and colored over $FrMXE_f$. Given the understandable behavior of TRU_{min} over D, only those with $D < 5$ years are chosen to simplify the graphical representation.

From a statistically point of view, high $FrMXE_f$ of fleet has a deeper potential of TRU incineration and may lead to lower TRU_{min}, even though some plutonium/TRU-stabilization fleets with $FrMXE_f = 100\%$ have been identified in other studies [9, 50]. As shown in Figure 4.30, a higher $FrMXE_f$ has a larger potential to achieve a lower TRU_{min}, in particular when $P_{tot,f}$ is well chosen. Other factors may interact with the choice of $FrMXE_f$ and complicate indirectly the behavior of TRU_{min} on $FrMXE_f$. For example, a fleet with high $FrMXE_f$ may need a relatively high enrichment of ^{235}U because the plutonium content is not sufficient to reach the specified BU_{MXE}. In this case, an increasing $FrMXE_f$ weakens then the capability of plutonium incineration. Still, it is secondary in comparison to the scale effect characterized by $FrMXE_f$.

For $P_{tot,f}$, the correlation with $FrMXE_f$ as mentioned can be viewed in Figure 4.30. In particular, when $t_{ad} = 2040$ the trajectories of high $P_{tot,f}$ and high $FrMXE_f$ simultaneously meet very early the first missload, and thus the level of

TRU_{min} stays at a high level. That is because the available inventory of plutonium for MOXEUS fabrication is still limited by 2040, while the power level $P_{tot}(2040)$ is high. The high level of both $P_{tot,f}$ and $FrMXE_f$ results in a significant consumption of plutonium for each irradiation cycle of MOXEUS. Since the recycling of plutonium needs a certain time (e.g. the cooling of spent fuels and the fabrication time), such high consumption rate may empty rapidly the interim storage and there is not enough available plutonium for MOXEUS fabrication (note that the lower bound of plutonium content in MOXEUS is set to 4.5%; if the content cannot reach this threshold when all available plutonium is loaded, the loading is missed). It is under this constraint of validity that the minimization of TRU_{min} needs a matching between $P_{tot,f}$ and $FrMXE_f$, in order to sustain the plutonium supply for MOXEUS fabrication and deepen the TRU incineration. When $t_{ad} = 2070$, the plutonium in the cycle is much more available and the maximum achieved power level $P_{tot}(2070)$ is lower according to the features of the prior reference trajectory. In this case, most of adaptive trajectories with high $P_{tot,f}$ and high $FrMXE_f$ meet the missload later than the case of $t_{ad} = 2040$, and the level of $P_{tot,f}$ that achieves low TRU_{min} is higher.

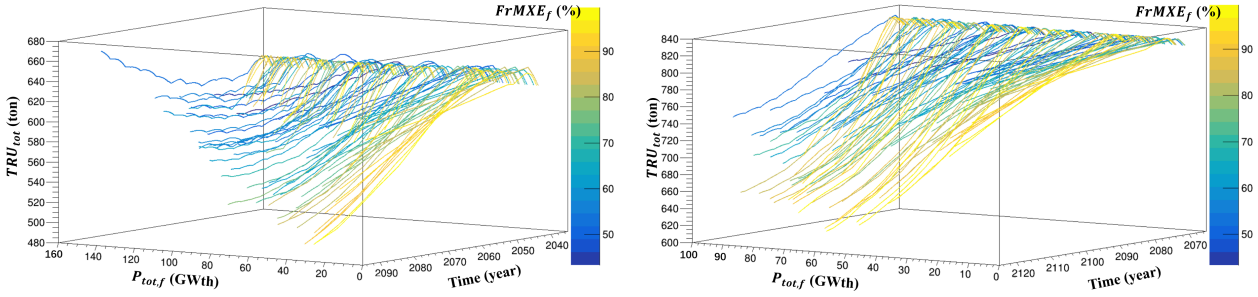

(a) $t_{ad} = 2040$ (b) $t_{ad} = 2070$

Figure 4.30: Evolution of TRU_{tot} in the valid part of trajectories over $P_{tot,f}$ and colored over $FrMXE_f$, under the constraint of $D < 5$ years of those TRU-incineration adaptations in S_{burn}

The pairs plots shown in Figure 4.31 help visualize and verifies such change over t_{ad}, where the scatter points are colored by the value of TRU_{min}. Note that the axes of variables respect the ranges of TRU-incineration adaptations in the respective cases, and it is completely reduced from the original sampling space. The strong cutting effect of the constraint of TRU-incineration $TRU_{min} < TRU_{tot}(t_{ad})$ can be observed on these three important parameters, particularly on D and $FrMXE_f$, while the value of $P_{tot,f}$ depends on the choices of other two parameters. The consistent effect of D and $FrMXE_f$ on the minimization of TRU_{min} over t_{ad} is clearly shown. Coherent with the dependency aforementioned, the value of $P_{tot,f}$ achieving minimal TRU_{min} moves over the adaptation time. There may be some optical effects that amplify this change because the axis of $P_{tot,f}$ in the two cases are different. Short D and near 100% of $FrMXE_f$ are necessary conditions for the minimization of TRU_{min}; under these conditions, the TRU_{min} can be minimized with a compromised level of $P_{tot,f}$ that allows a rapid but also continuous incineration of TRU inventories. As the plutonium is more available for MOXEUS fabrication when the prior trajectory is adapted later, this compromised $P_{tot,f}$ shifts to a higher level in the case of later adaptation. Hence, from a global viewpoint upon the respective sampling space, the correlation between TRU_{min} and $P_{tot,f}$ has different sign in the case of $t_{ad} = 2040$ and in $t_{ad} = 2070$.

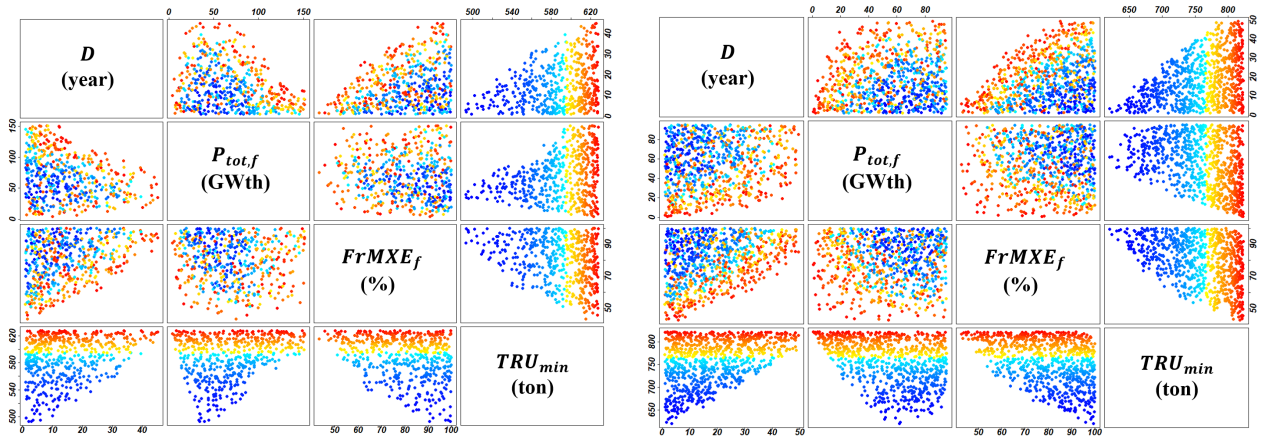

(a) $t_{ad} = 2040$ (b) $t_{ad} = 2070$

Figure 4.31: Pairs plots of D, $P_{tot,f}$ and $FrMXE_f$ with the output TRU_{min}, for the TRU-incineration adaptations, with respect to $t_{ad} = 2040$ and $t_{ad} = 2070$, colored by the value of TRU_{min}

4.5.3.2 Particularities of using MOXEUS: minimal TRU achieved in the middle of trajectory

In the previous study of MOX, we notice that the evolution of TRU_{tot} of TRU-incineration strategies is monotone, which leads to $t_{min} = t_{ML}$ or the end of scenario. If MOXEUS is used for adaptation, new behaviors can be observed, as shown by the red points in Figure 4.32. Besides the two cases mentioned, we may also observe that some strategies reach TRU_{min} in the middle of their trajectories, which means that the evolution of TRU_{tot} is not necessarily monotone. The t_{min} of these trajectories is achieved before both the first missload and the end of scenario. But compared with the total size of TRU-incineration strategies S_{burn}, the number of these strategies is relatively small (68/522 for $t_{ad} = 2040$ and 23/802 for $t_{ad} = 2070$).

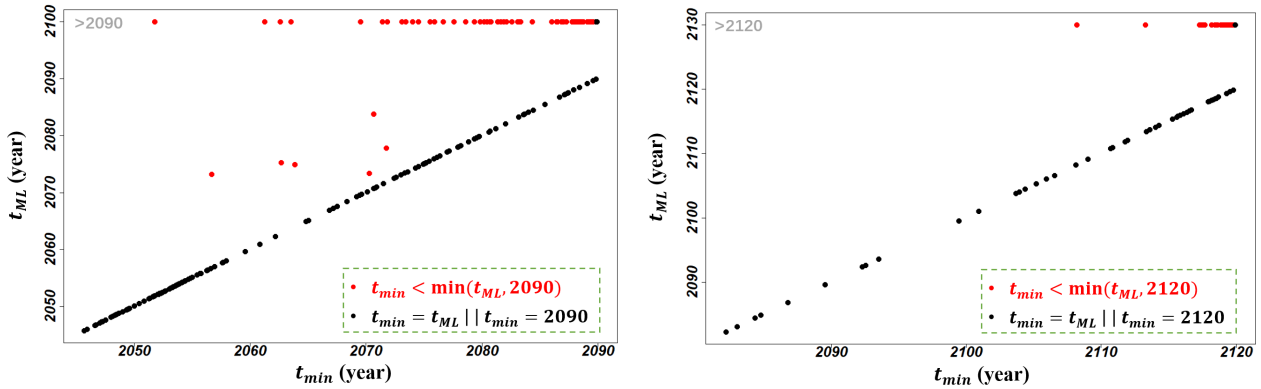

(a) $t_{ad} = 2040$ (b) $t_{ad} = 2070$

Figure 4.32: t_{ML} vs t_{min} with respect to $t_{ad} = 2040$ and $t_{ad} = 2070$, in the adaptation scenario using MOXEUS

The evolution of TRU_{tot} of these particular strategies are shown in Figure 4.33. The curves are colored by D. The gradual change of color confirms that a longer D slows down the transition. The increase of TRU_{tot} at the beginning of adaptation, owing to the inertia of prior trajectory, is highlighted by longer D.

Some trajectories without missload achieve TRU_{min} near the end of scenario (t_{min} close to the end which is $t_{ad} + 50$), within the last irradiation cycle. These

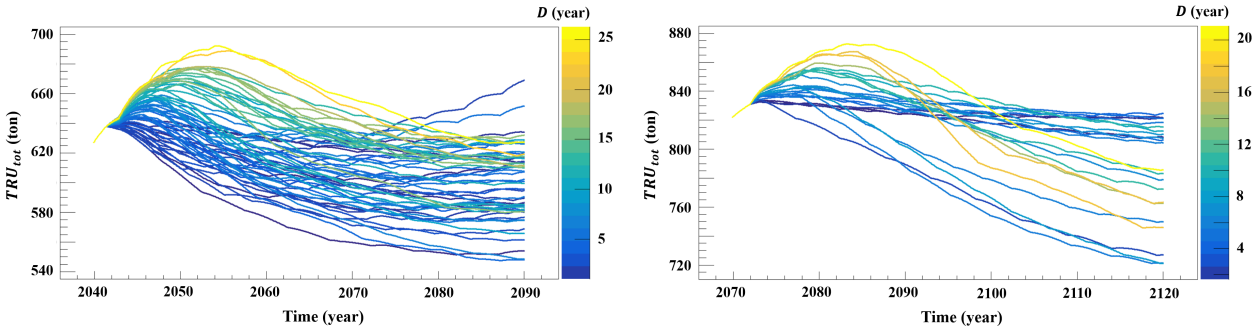

(a) $t_{ad} = 2040$ (b) $t_{ad} = 2070$

Figure 4.33: Evolution of TRU_{tot} of strategies reaching TRU_{min} at the middle of trajectory (t_{min} achieved before t_{ML} and before the end of scenario), colored by D

strategies seem therefore not yet to reach stabilization and may be not of interest. For most of others, their TRU_{tot} seem to reach or approach to stabilization. The fluctuations around their stable levels explain why t_{min} is realized in the middle of trajectory. The conditions of TRU stabilization and incineration in total cycle by using MOXEUS fuels are well studied in [50]. The goal of this study of TRU_{min} and t_{min} is to minimize TRU and not to stabilize it, and therefore the strategy space of TRU-stabilization regardless of the final level of TRU is not investigated in detail.

Two singular cases can be observed in the case of $t_{ad} = 2040$, in which TRU_{tot} achieves TRU_{min} early and re-increases measurably afterwards. These strategies change rapidly to a medium-level of $FrMXE_f$ and keeps high $P_{tot,f}$ near to the initial $P_{tot}(2040)$. This condition takes lots of plutonium for each irradiation cycle of MOXEUS, while keeps a relatively high power level of PWR UOX as well. After several cycles of MOXEUS, there is not enough plutonium inventory for MOXEUS to reach target burn-up (and thus the plutonium content in fresh fuels is low) and high enrichment of ^{235}U is needed. In this case, the plutonium incineration by MOXEUS is limited and the behavior may be less similar to MOX, and thus TRU_{tot} re-increase. Conceptually, it is not a real TRU-incineration adaptive strategy if the trajectory continues after t_{min}. One may consider an additional output $max(TRU_{min}, TRU_{tot}(t_{ad} + 50))$ to screen TRU-incineration adaptations, but this may complicate the further interpretation of results. It shows the complexity of analysis of introducing MOXEUS in this study.

4.5.3.3 Analysis of adaptive robustness

The multi-recycling of plutonium help deepen the incineration of TRU inventories in the total cycle. A larger space of robust adaptive strategies than the use of MOX for adaptation can be expected.

According to the criterion $C_{B,ad}^{t\text{-}dcn}$, the size of robust adaptive strategies is 409 for $t_{ad} = 2040$ and 362 for $t_{ad} = 2070$, accounting for respectively 20.5% and 18.1% of the total sampling space (2000 adaptive strategies). Note that $C_{B,ad}^{t\text{-}dcn}$ does not exclude the several strategies leading to the re-increase of TRU_{tot} after t_{min} as shown in Figure 4.33. As discussed in Section 4.1, this kind of strategies still have the potential to bring the situation back to a sufficiently low TRU_{tot} as the threshold level, and this level can be kept by phase-out strategy. In comparison, if only MOX is used for the incineration in adaptation, there are only 32 robust adaptive strategies for $t_{ad} = 2040$ and 5 for $t_{ad} = 2070$.

In the previous analysis of TRU_{min}, the importance of D, $P_{tot,f}$ and $FrMXE_f$ are well presented. For robustness assessment, strategies that lead to lower

TRU_{min} than the threshold level TRU^{A}_{min} are considered robust. Given this relation between TRU_{min} and adaptive robustness and given the importance of input parameters on TRU_{min}, it is reasonable to see inputs D, $P_{tot,f}$ and $FrMXE_f$ as important factors for output t'_{TRU} which indicates the performance on strategy robustness. Regardless, TRU_{min} stands for the minimal inventory achieved and t'_{TRU} indicates the time to let TRU_{tot} of a given trajectory reach the threshold level, and thus they have substantial difference. Graphical skills are used to verify this derivation, and to reveal different combination effects of inputs on t'_{TRU} from that of TRU_{min}.

For the t'_{TRU} of these robust adaptive strategies, the effects of these three inputs, D, $P_{tot,f}$ and $FrMXE_f$, can be verified in Figure 4.34, colored by the reprocessing strategy MPu. It is worth noting that the plots only take the robust adaptive strategies and are not scaled by the original sampling space. Particularly, the cut in the range of D and $FrMXE_f$ should be noted. The non-measurable effects of BU_{UOX}, BU_{MXE}, TC_{UOX} and MPu are also verified. The distributions of MPu in these scatter plots for both t_{ad} are uniform.

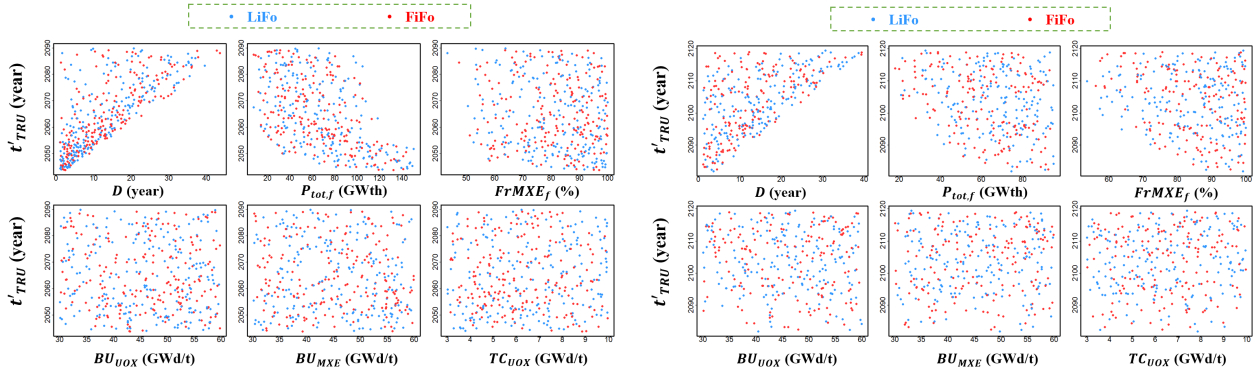

(a) $t_{ad} = 2040$ (b) $t_{ad} = 2070$

Figure 4.34: Scatter plots of t'_{TRU} over the inputs D, $P_{tot,f}$, $FrMXE_f$ of robust adaptive strategies, colored by the reprocessing strategy MPu

To understand the synergy of inputs, the pairs plots of the three important input parameters and the output t'_{TRU} of two t_{ad} are shown in Figure 4.35. The distribution patterns regarding the input pairs are very similar to the plots in the study of TRU_{min} in Figure 4.31, because robust adaptive strategies are literally a subset of TRU-incineration S_{burn}, imposing stricter constraints on those important parameters such as D, $P_{tot,f}$ and $FrMXE_f$ on the set S_{burn}. The distributions of color in the pairs of input parameters confirm their strong synergy on t'_{TRU}. Particularly, late t'_{TRU} under high $P_{tot,f}$ seems achievable for $t_{ad} = 2070$ but not for earlier $t_{ad} = 2040$. This difference comes mainly from the availability of plutonium for enormous demand of MOXEUS loading as mentioned. This high $P_{tot,f}$ matches very high $FrMXE_f$ and short D so that t'_{TRU} is achieved earlier than the missload. In brief, the t'_{TRU} can be minimized by a very short transition towards an almost full-MOXEUS fleet, keeping a similar power level as before adaptation.

One may note that the minimization of t'_{TRU} and of TRU_{min} do not lead to the same conditions of adaptation for $t_{ad} = 2040$, as shown by Figure 4.31 and 4.35. The difference presents mainly on the choice of $P_{tot,f}$. According to the definition of adaptive robustness in this study, the most robust adaptive strategy minimizing t'_{TRU} requires relatively high $P_{tot,f}$. As t_{ad} gets later like year 2070, both minimizations require high $P_{tot,f}$, and these two sets of strategies overlap. To explain this difference, Figure 4.36 compares the trajectories concerning the minimization of t'_{TRU} and the minimization of TRU_{min}. For both t_{ad}, the trajectories

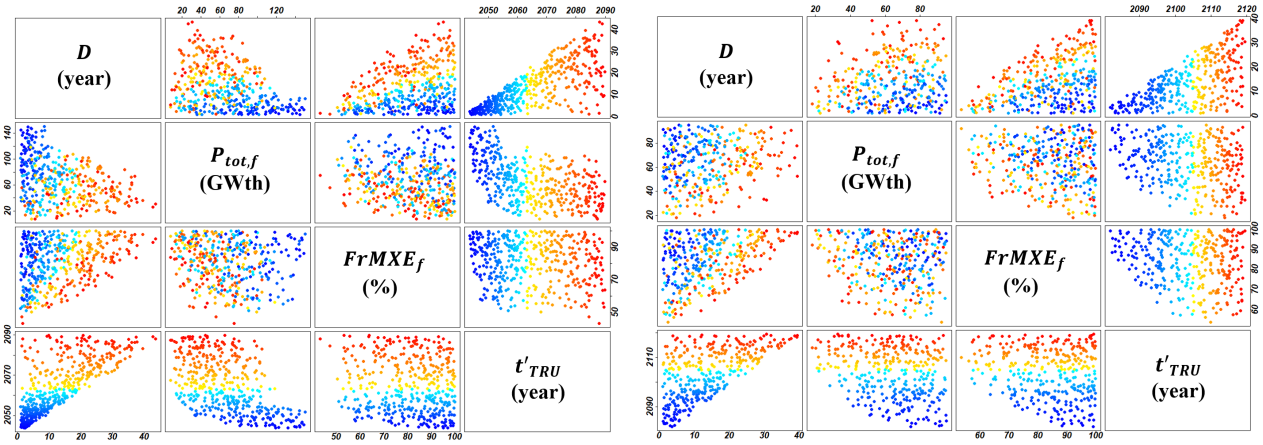

(a) $t_{ad} = 2040$ (b) $t_{ad} = 2070$

Figure 4.35: Pairs plot of D, $P_{tot,f}$, $FrMXE_f$ and t'_{TRU} of robust adaptive strategies, colored by the value of t'_{TRU}

achieving the 10% earliest t'_{TRU} of all robust adaptive strategies are presented by red curves, and the ones achieving the 10% lowest TRU_{min} of all TRU-incineration adaptations in the subset S_{burn} are presented by green curves. Note that some trajectories fulfill both criteria and they are in brown in the figure.

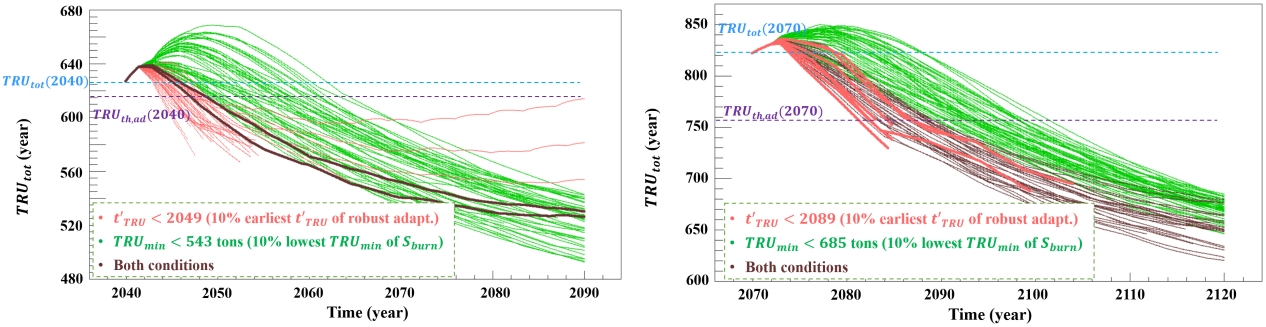

(a) $t_{ad} = 2040$ (b) $t_{ad} = 2070$

Figure 4.36: Contrast of trajectories on the minimization of t'_{TRU} and the minimization of TRU_{min}. Some strategies are overlapped in two example groups

When $t_{ad} = 2040$, most of early-t'_{TRU} trajectories meet plutonium shortage early as well, due to the low available inventory of plutonium but a high demand from MOXEUS. Because of the massive loading of MOXEUS, the plutonium is rapidly incinerated so that TRU_{tot} decreases fast beneath the threshold as well. The depth is relatively limited due to the early shortage of plutonium. On the contrary, the low-TRU_{min} trajectories trade some performance of t'_{TRU} for a stable supply of plutonium during the multi-recycling. The continuation of MOXEUS loading ensures a deeper incineration of plutonium.

When $t_{ad} = 2070$, available inventories of plutonium for MOXEUS loading become larger. Therefore, the well-performing strategies on t'_{TRU} with simultaneously high $P_{tot,f}$ and $FrMXE_f$ achieve also low TRU_{min}.

4.5.4 Conclusion on the adaptation using MOXEUS and its difference from the adaptation using MOX

The outcomes of allowing multi-recycling of plutonium is thoroughly different from the case sticking to the use of MOX. When only MOX is allowed, the only

available plutonium to be used remains in the spent UOX; and once it is emptied, no further measure can bring improvement. It is extremely hard to keep the same level of TRU inventories, and even a small increase requires a brutal change of fuel cycle to burn it out. An abrupt transition of fleet, recycling all available plutonium in spent UOX fuels for the MOX fabrication, is consequently demanded. In contrast, one direct advantage of using MOXEUS is that the use of plutonium from spent MOX as well as the ^{235}U enrichment avoids missload and sustain the operation of reactors, subject to the demand of incinerating TRU. As a result, the fraction of subsets concerning the validity in the original sampling space are much larger with the use of MOXEUS (take the early adaptation of $t_{ad} = 2040$ as example): the no-missload subset S_{noML} and the valid subset S_V^{ad} with MOXEUS accounts for more than 80% and 95% respectively of total sampling, while smaller than a quarter of them do not have missload in the case of MOX and the fraction valid subset is smaller than a half.

A longer duration of TRU incineration can be liberated from the mono-recycling constraint, and it is intuitively conducive to improve the performance of strategies. If the adaptation is as early as year 2040, the minimal TRU before a quick phase-out can be lower than 500 tons with MOXEUS (around 580 tons if only MOX is considered). Transitions as long as 40 years can still be robust, if $P_{tot,f}$ and $FrMXE_f$ are well chosen. Different from the fleet only using MOX for incineration, phase-out is not the unique strategy to maintain a given level of TRU in total cycle by MOXEUS, and $P_{tot,f}$ can be kept at a reasonable level to stabilize it. The use of MOXEUS also unlocks the option of trading performance of adaptive robustness, quantified by the time t'_{TRU}, for the availability of recycled plutonium and thus for a deeper incineration of plutonium/TRU.

4.6 Conclusion of this chapter

Compared to the scenario study in Chapter 3, this chapter shows another vision of robustness assessment of different strategies, disconnected from predetermined observation time. The method developed in this chapter pay a special attention to the inter-temporal consistency of robustness assessment. To achieve this, we focus on the time needed to reach a given threshold.

In the pre-disruption scenario, t_R and t_{TRU} are defined as the output to evaluate strategies for two possible objectives. They stand respectively for the time needed for the corresponding physical quantities R_{Subs} and TRU_{tot} to go beyond given thresholds. $t_R \leq 2090$ implies that the R_{Subs} can achieve the (desirable) level before year 2090, and $t_{TRU} \geq 2090$ means that the TRU_{tot} will not reach the (undesirable) level before 2090. Under the assumption of thresholds used, the PCA has been performed to reveal the importance of input variables. $P_{tot,f}$, $FrMOX_f$ and BU_{UOX} are shown to have large influences on t_R and t_{TRU}. This result is coherent to the physical analysis on the relevant outputs R_{Subs} and TRU_{tot} in Chapter 3. By definition, the reference strategy for objective A minimizes t_R in year 2048. While for the robust static strategies, trade-offs can be observed between the maximization of t_{TRU} and the minimization of t_R, depending on the choice of thresholds.

In adaptation scenario, the strategy validity for adaptation is different from previous studies. To be valid, it is sufficient to finish the adaptive transition before the plutonium shortage. Afterwards, phase-out strategies are considered acceptable to keep the of TRU inventory when it lacks plutonium for MOX fuels. Similar to the pre-disruption scenario, we focus on the the time when the TRU_{tot} can decrease beneath the threshold level deduced from the historical best strat-

egy before disruption, denoted as t'_{TRU}. In particular, the threshold is deduced from the history before disruption, so that it does not change over different time horizons of adaptation scenario. This evaluation method is first applied to an early adaptation from year 2040, based on the prior reference trajectory that was supposed to minimize t_R before disruption.

To complete the adaptive robustness assessment, the notion of adaptability of pre-disruption strategy is introduced. It is defined as the fraction of robust adaptations in the exploratory strategy space. Subject to the nuclear system defined by PWR UOX and MOX, two indicators deduced from the corresponding prior trajectories are analyzed: the effective TRU inventory TRU_{eff}, and the available plutonium for MOX fabrication Pu_{toMOX}. These two outputs can characterize the difficulty of a given prior trajectory to be adaptively robust. They help screen and get adaptable prior trajectories to complement the study of adaptation in 2070.

Finally, the use of MOXEUS fuels for the plutonium multi-recycling is taken as a new option for adaptation that was not available before disruption. This advanced fuel design liberates the adaptation from limited plutonium availability, and thus leads to deeper TRU incineration than MOX fuel. As a result, the adaptability of pre-disruption strategy becomes much higher.

In summary, the methodology of robustness assessment is adapted and enhances the inter-temporal consistency. In comparison to 3, a quite different phase space of robust strategies is identified, which are valid within an extended time horizon of adaptation. From the numeric point of view, the difference space is directly linked to a different threshold used for adaptation. Furthermore, sticking to one possible prior trajectories, and to the same technology of plutonium mono-recycling, are two principal limits mentioned in Section 3.3.4 of Chapter 3, while these two constraints are liberated in this chapter. All these considerations improve the methodology development from different aspects, giving a relatively comprehensive frame of work.

Chapter 5

Application: impact of disruption to the plutonium multi-recycling in PWR and in SFR

In the previous two chapters, the methodology of robustness assessment under uncertain disruption of objective is developed within different assumptions on the time horizon of the studied scenario. The physical analyses provide explanations about how a fuel cycle constituted of PWR UOX and MOX responds to the modification of parameters; more specifically, these scenario studies give an insight about how all these parameter interact with a change of objective, which is an important factor for prospective studies, deeply uncertain and out of any physical aspect. These studies are based on statistical analyses and they neglects industrial constraints in order to make analyses more comprehensible. Lots of approximations had to be introduced to simplify the simulations and to reduce computational costs.

Based on the understanding acquired from previous studies, the robustness assessment methodology is applied to a more concrete scenarios close to possible French nuclear fleet transitions without diving into large sampling or statistical analysis in this chapter. Inspired from those possible transition strategies in France, we focus on two prior trajectories concerning different options for the future of nuclear power before any disruption, and their respective post-disruption scenarios are considered:

- Prior **TRJ MIX**: plutonium is multi-recycled in PWRs using MIX fuels. This pathway corresponds to the context where SFR technology is not ecnomic competitive, and plutonium should be stabilized by PWR-related technology.
- Prior **TRJ SFR**: SFRs are deployed, substituting for the PWR-fleet. This pathway corresponds to the high risk of uranium shortages in the near-term future.
- **SCN MIX2SFR** after the disruption of the trajectory **TRJ MIX**: when plutonium is recycled in PWRs, SFR deployment is reconsidered after the new estimation of uranium resources availability. The interest is to see if the plutonium multi-recycling in PWRs would necessarily postpone the deployment of SFR.
- **SCN SFR2MOXEUS** after the disruption of the trajectory **TRJ SFR**: in the middle of the SFR deployment, no new SFR is put into service owing to economic factors, and thus the plutonium should be multi-recycled in PWRs by MOXEUS. The interest is to maximize the use of plutonium, represented by

the plutonium inventory in interim storage (called *idle plutonium*), and to compare it with the level without SFR deployment as in the trajectory **TRJ MIX**. The small distinction between the use of MIX and MOXEUS will be detailed in the subsequent description of scenarios.

MOXEUS and MIX for plutonium-recycling PWR assemblies present a slight difference on the control of the plutonium content in fresh fuels. In MOXEUS, plutonium content in fresh fuel is variable. In the simulation of MIX, the plutonium content is given whatever its isotopic quality and then the enrichment of $^{235}\mathrm{U}$ is adjusted to achieve the given burn-up. A medium level in [31], 9.54%, is used in the MIX-related scenarios in this study. MIX plays a more important role than MOXEUS in current R&D of innovative fuels for plutonium multi-recycling, as shown in [31, 32, 33, 16]. But MOXEUS is still used for the **SCN SFR2MOXEUS** scenario, in order to be more flexible regarding the plutonium quality variation from different spent fuels when several SFRs are deployed just before disruption. This will be further explained in the description of scenario in Section 5.2.

There are thus two families of adaptation scenarios: **SCN MIX2SFR** adapting the prior trajectory **TRJ MIX**, and **SCN SFR2MOXEUS** adapting the prior trajectory **TRJ SFR**. The prior trajectory of one family may set a comparison reference for the other. Regardless, two families lies on different context, assumptions and objectives with which the adaptive strategy assessment should be connected.

"Expert scenarios" from [18, 31, 21, 16] are taken as inspiration for our modeling with CLASS of previous defined strategies. These studies set the baselines of each possible future in industrial estimations, and avoid the unnecessary statistical information that complicate the following analysis. The macro reactor assumption is used in this work. Different outputs are observed to evaluate the strategies as comprehensively as possible. For the adaptation after disruption, the optimization method of Nelder-Mead [103] is used, instead of a large sampling as in the previous studies.

Scenarios are presented in detail in dedicated sections. The descriptions and analyses of prior trajectories are presented in Section 5.1, and that of post-disruption trajectories are studied in Section 5.2. As different nuclear systems are involved in the transition trajectories, one should clarify the hypotheses on the different concepts, such as electric and thermal power, and particularly the fuel type or the reactor type fraction concerning the contribution on electric or thermal power contribution. To distinguish, the notation of MOX denotes specifically the MOX fuel for PWR, while the MOX fuel for SFR is called simply the SFR fuel in this chapter.

5.1 Analysis of prior trajectories before disruption

The prior trajectories **TRJ MIX** and **TRJ SFR** are based on scenarios of plausible futures studied in the literature, principally using [31] for **TRJ MIX** and [21] for **TRJ SFR**. In this study, they are adapted with respect to the instructions of PPE [18]. To set a baseline reference for the transition until the time horizon, the continuation of the current French fleet of plutonium mono-recycling is simulated as well, and the trajectory is denoted as **TRJ FrMono**. This simulation sets especially a reference level of installed capacities which plays a dominant role in the previous scenarios (if the change of 50% of the current level is allowed). This assumption avoids then the impact of the deep uncertainty of installed capacity as discussed in [49]. After that, a set of outputs are taken to compare the consequences of these two strategies.

5.1.1 Description of pre-disruption scenarios

5.1.1.1 Simulation of TRJ FrMono

For the scenarios in this chapter, the time horizon from PPE should be extended, because the SFR deployment that substitutes EPRs by the end of century should be considered. Furthermore, the dynamics concerning disruption and adaptation should be taken into account. The horizon from year 2015 to 2160 is chosen, during which the details of SFR deployment or post-disruption adaptation will be presented in corresponding paragraphs.

The simulation of **TRJ FrMono** focuses first on the fleet transition before 2035, using report PPE [18] as reference. This report indicates that two 900-MWe PWRs in the Fessenheim site started decommissioning by 2020, and most of PWRs of current generation will start their decommissioning from year 2027 and replaced by EPRs. Following the decommissioning of old reactors and the fleet renewal, the electricity production from nuclear will decrease to a level between 250 and 325 TWh/y, corresponding to 50% of total French electricity production. This level is supposed to be maintained till 2050. The nuclear fuels and designs used in this simulation are always PWR UOX and PWR MOX, accounting for respectively 90% and 10% of the total power.

Correspondingly, the nominal installed capacity decreases linearly to 75% of its initial level during the transition between year 2027 and 2035. Then it is considered constant till the end of scenario. An ideal transition of nominal installed capacity of the fleet can be presented in Figure 5.1a. Despite a higher loading factor during recent several years, 72.8% normalized from the historical operation is used to deduce the effective level of annual electricity production, which is presented in Figure 5.1b. It shows that under these foregoing assumptions, the annual electricity production by nuclear power is about 297 TWh/y, corresponding well to the interval supposed in PPE.

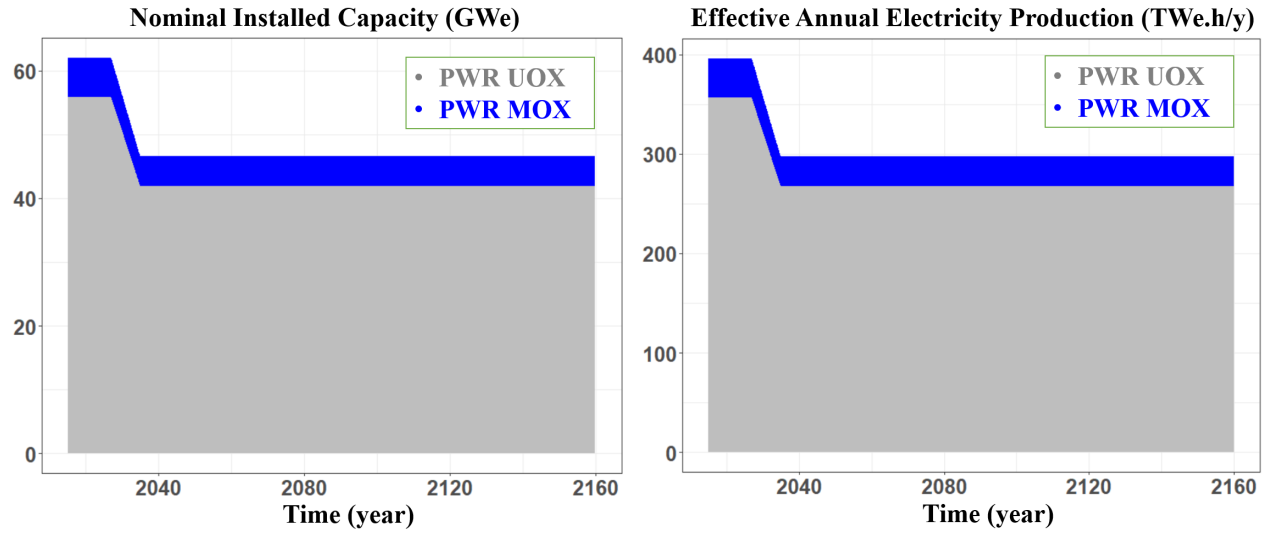

(a) (b)

Figure 5.1: Ideal transition of electricity production in **TRJ FrMono**: (a) Evolution of nominal installed capacity; (b) Evolution of effective annual electricity production by nuclear power

In practise, simplifications should be made for the simulation of this fuel cycle evolution. Notably, macro-reactor assumption is used. It is worth noting that CLASS simulates the thermal power of reactor which is directly linked to the physics analysis, whereas the electric power is more informative for relevant decision-making. To build the connection between the physics modelling and

strategy assessment, 33% and 35% are considered for the energy conversion efficiency of PWRs of current generation and that of EPRs respectively. Nevertheless, the physics model used by CLASS for these two water reactors are identical; the use of two names in this study only highlights their different energy conversion efficiencies and thus a slight difference on the thermal power level.

The timeline of transition simulation is presented in Figure 5.2. P_e and P_{th} denote respectively the electric and thermal power of fleet in the figure. Several key phases can be listed to help build conceptually the schedule:

- **Year 2015:** start from the current fleet characterized by normalized parameters of fuel cycle;
- **Year 2027-2035:** reduction of electricity production by nuclear power;
  - **Year 2027:** decrease to 95% of the initial electric power level $P_{e,0}$;
  - **Year 2030**: the first EPR in France is supposed to start (it is conceptually considered for the subsequent reactor life calculation, but not taken in simulation);
  - **Around 2031 (one irradiation cycle after):** decrease to 85% of $P_{e,0}$;
  - **Year 2035:** decrease to 75% of $P_{e,0}$;
- **Year 2035-2160:** constant electric power at the level of 75% of $P_{e,0}$, subject to the renewal of fleet.
  - **Year 2040-2060:** replacement of PWRs with EPRs; due to different energy conversion capacity, the thermal power of fleet is assumed to change linearly
  - **Year 2060**: the burn-ups of both UOX and MOX fuels are set to 55 GWd/t;
  - **Year 2080-2120:** renewal with new EPRs (no change in the simulation)

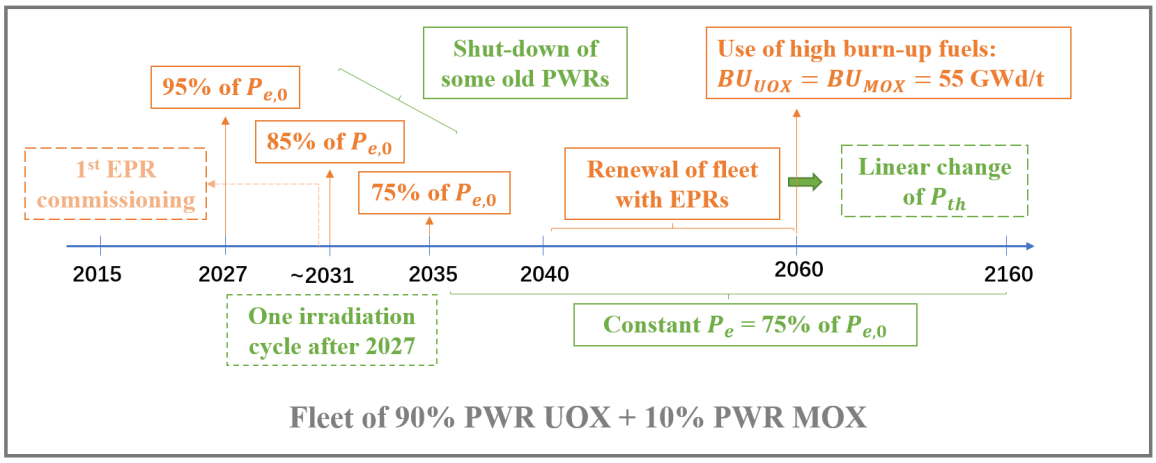

Figure 5.2: Schematic representations of timeline in the simulation of **TRJ FrMono**

This simulation sets the baseline of electric power evolution for all scenarios in this Chapter. In particular, the phase between year 2027 and 2035 sets the common starting point. Figure 5.3 shows the thermal power evolution of simulation. The staircase curve during the transition is a direct result of the macro-reactor assumption. To approach realistic assessments, the power evolution shown in Figure 5.3a is smoothed by 6-year average, as presented in Figure 5.3b which considers also a loading factor of 72.8%. Between year 2040 and 2060, a slight

reduction of thermal power can be observed, due to a higher energy conversion capacity of EPR than the one of PWR of current generation.

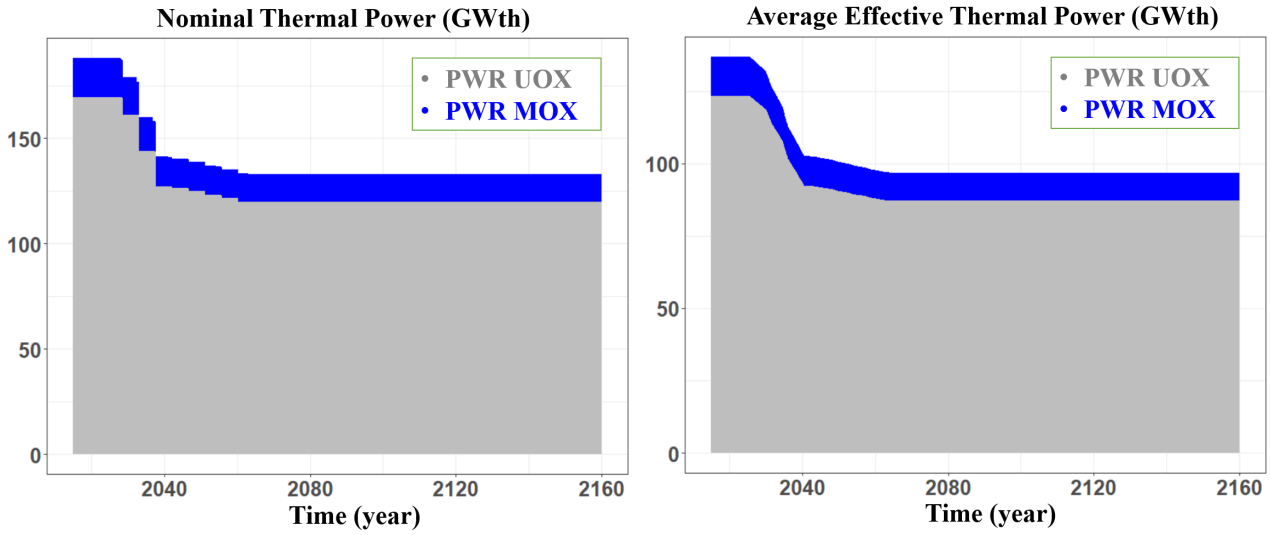

(a) (b)

Figure 5.3: Thermal power evolution in the simulation of **TRJ FrMono**: (a) nominal level; (b) 6-year-average effective level

In the following analysis concerning plutonium multi-recycling, year 2040 is the hinge time that considers the use of advanced designs. They share the same evolution before 2040 as indicated above, and differs afterwards, subject to the constant installed capacity.

5.1.1.2 Simulation of TRJ MIX

[31, 16] is used as a reference to simulate fuel cycle of plutonium multi-recycling in PWRs, subject to the assumption of installed capacity transition indicated in Figure 5.1. The aim of multi-recycling in PWRs is to stabilize the in-cycle plutonium inventory and lighten the burden on the spent fuel storage. Among all possible designs of multi-recycling in PWRs, the preset plutonium content of 9.54% for the fresh fuel is taken in this study. In the relevant perspective, MIX fuel accounts for around 34% in the energy production of fleet.

In this scenario, the simulation of **TRJ MIX** follows the timeline schematized in Figure 5.4a. Before year 2040, the same fleet transition in **TRJ FrMono** is considered. After 2040, key steps of fleet transition can be listed:

- **Year 2040-2060:** transition with modified fuel fractions within the PWR-fleet;
  - **Total thermal power:** change linearly due to the replacement of PWRs of current generation with EPRs;
  - **Fuel type fraction:** MIX fraction in the energy production change linearly, replacing first the MOX, then part of UOX;
- **Year 2060:** burn-up of UOX becomes 55 GWd/t, and the fraction of MIX reaches 34%, which is kept constant till the end.

The renewal of fleet with new EPRs from 2080 to 2120 is conceptually considered, but it does not make any change in our simulation due to our simulation hypotheses. The burn-up of MIX fuel is set to 55 GWd/t.

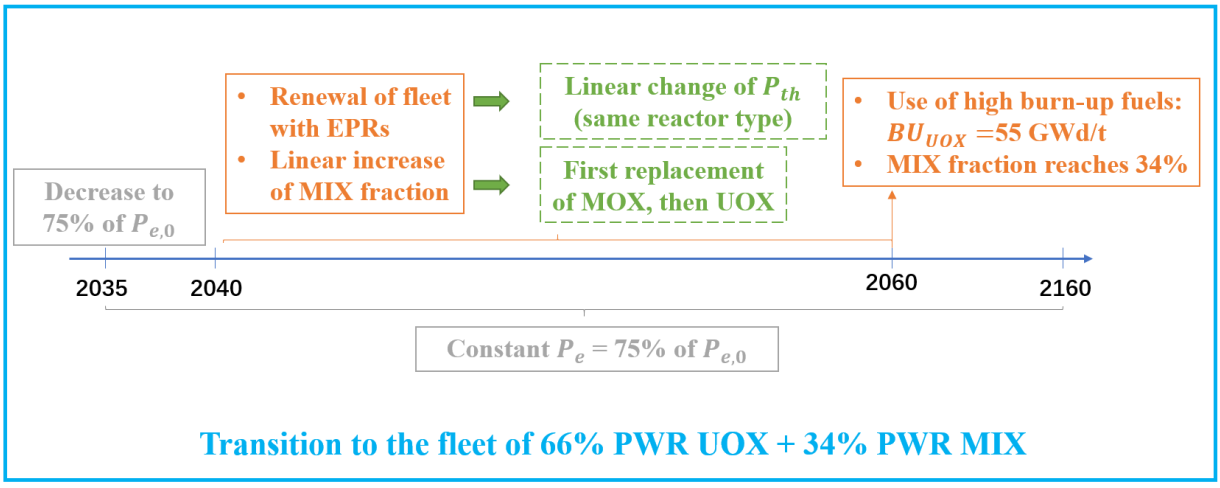

(a) Schematic representations of timeline in the simulation of **TRJ MIX**

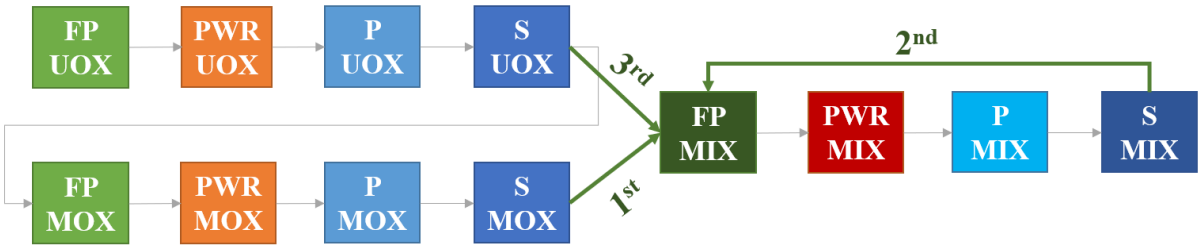

(b) Schematic representations of the fuel cycle in the simulation of **TRJ MIX**

Figure 5.4: Simulation scheme of **TRJ MIX**

Regarding the mass flow management concerning the fabrication of fresh MIX fuels, the plutonium recycling follows the path shown in Figure 5.4b: the fabrication plant of MIX looks first for the plutonium in the interim stock of spent MOX fuels; if there is not sufficient plutonium, the stock of spent MIX fuels is checked; finally it may turn to the stock of spent UOX fuels. Currently CLASS is not able to mix the material with given fractions of flows from different stocks and thus a preset order is essential; otherwise, it may also respect the global arrival time order of spent fuels in stocks. It is also important to note that because the plutonium content is set to 9.54% for fresh MIX, missload may happen if the plutonium quality is too good. In that case, a lower content may be needed. To avoid this absurdity breaking the validity of simulation, spent MIX fuels is ranked prior to spent UOX for the multi-recycling path.

Under this schedule, the power evolution of each fuel type is shown in Figure 5.5. Figure 5.5a presents the ideal evolution of fuel type fraction in the electricity production, while Figure 5.5b averages the effective thermal power level within six years. Both figures considers the loading factor.

5.1.1.3 Simulation of TRJ SFR

An accelerated planning of SFR deployment is considered in this study in order to be comparable with **TRJ MIX** under the similar time horizon. A similar schedule is studied in [21]. In practise, such accelerated transition towards a 100% fleet of SFR may face a number of engineering problems and other practical issues. Nevertheless it is still considered for this study to emphasize the difference between choices for the plutonium multi-recycling and the possible outcomes of uncertain disruption.

Using [21] as reference, the timeline of **TRJ SFR** is summarized in Figure 5.6a. Key steps are detailed as following:

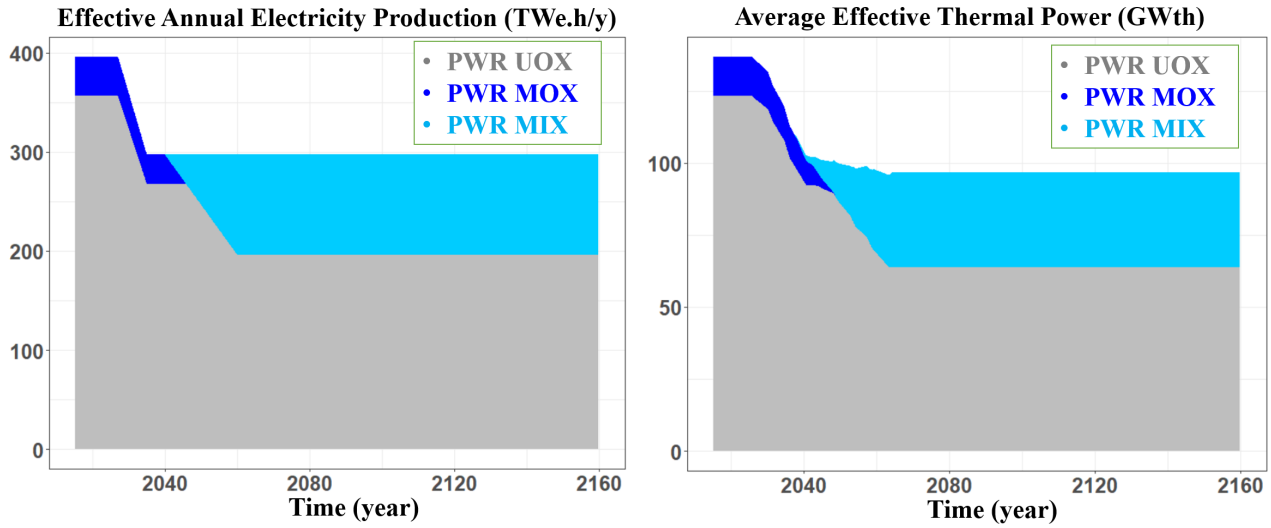

(a) (b)

Figure 5.5: Evolution of fuel contribution on the nuclear power for **TRJ MIX**: (a) ideal effective annual electricity production; (b) 6-year-average effective thermal power in the simulation

- **Year 2040:** operation of an SFR demonstrator, accounting for 1.3% of electricity production;
- **Year 2040-2060:** replacement of PWRs of current generation with EPRs;
- **Year 2060:** burn-ups of UOX and MOX in EPRs are set to 55 GWd/t; new SFRs are deployed, and thus 5% of the fleet electric power is contributed by SFR;
- **Year 2080-2120:** replacement of EPRs with new-constructed SFRs
  - **SFRs:** fraction in total electric power increases linearly;
  - **EPRs:** fraction decreases progressively, while the MOX fraction in EPRs is 5% in the irradiation cycle around 2090, and no MOX is used in EPRs after 2095;
- **Year 2120:** SFRs are deployed for 100% of fleet

The reprocessing order of spent fuels for SFR fuel fabrication in **TRJ SFR** is presented in Figure 5.6b. Stock of spent MOX fuels is also the prioritized stock. In fact, one of the goal of multi-recycling is to address the issue on the volume of spent fuels, currently problematic for the storage of spent MOX fuels in France. Spent SFR fuel is the last one in the priority order, because in the reference scenarios studies [21, 16] the reprocessing of spent SFR fuels usually starts after their massive deployment.

Simulations of SFR use the flexible model from [77], which allows to modify the number of blanket layers based on depleted uranium oxides. The burn-up of the active core is set to 100 GWd/t. For the first demonstration phase from 2040 and the completion of deployment after 2120, no blanket is added. For the simulation between 2060 and 2120, two rows of blanket assemblies are added for an effecient accumulation of plutonium.

One should note that the evolution of total thermal power P_{th} in this trajectory is not regular, due to different energy conversion capacities of different reactor designs. Figure 5.7 shows how the power or the electricity production of each fuel or reactor type changes over time. Under the constraint of ideal transition indicated in Figure 5.7a, Figure 5.7b presents the fluctuations of thermal

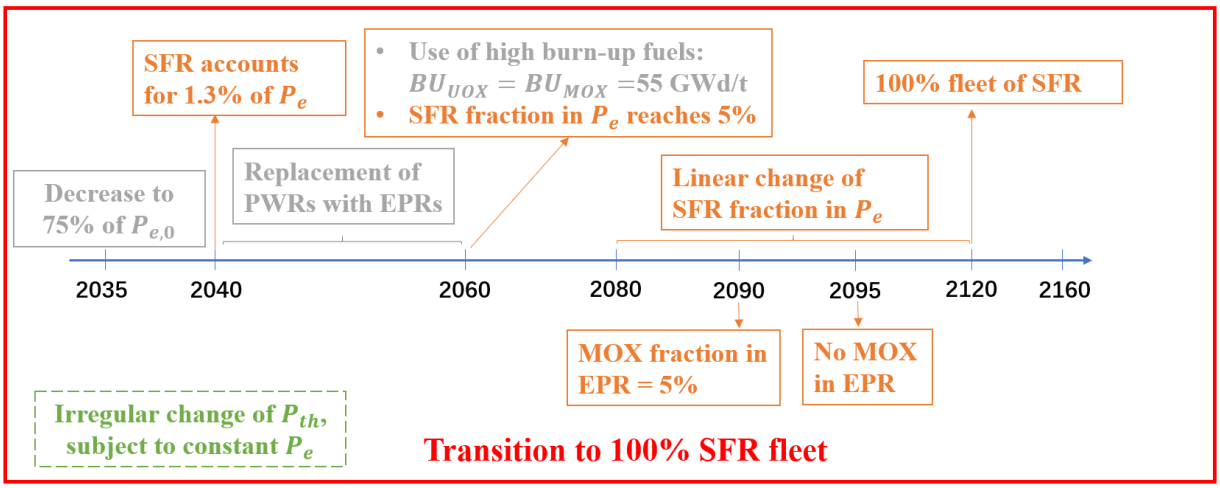

(a) Schematic representations of timeline in the simulation of **TRJ SFR**

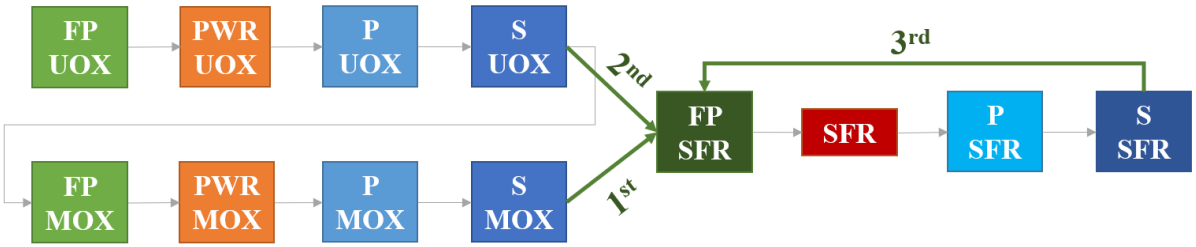

(b) Schematic representations of fuel cycle in the simulation of **TRJ SFR**

Figure 5.6: Simulation scheme of **TRJ SFR**

power, mainly due to the macro-reactor assumption, which can not completely smoothed by the average. The total thermal power of fleet decreases over time until the total substitution with SFRs, because the energy conversion capacity of SFR, 40%, is measurably higher than water reactors.

TRJ SFR shows that under this deployment schedule and management of fuel cycle parameters, the fleet can transition to 100% fleet of SFRs with sufficient plutonium inventories, verified by the simulation of SFR. Those assumptions to estimate the availability of plutonium in Chapter 3 and 4 are no longer needed.

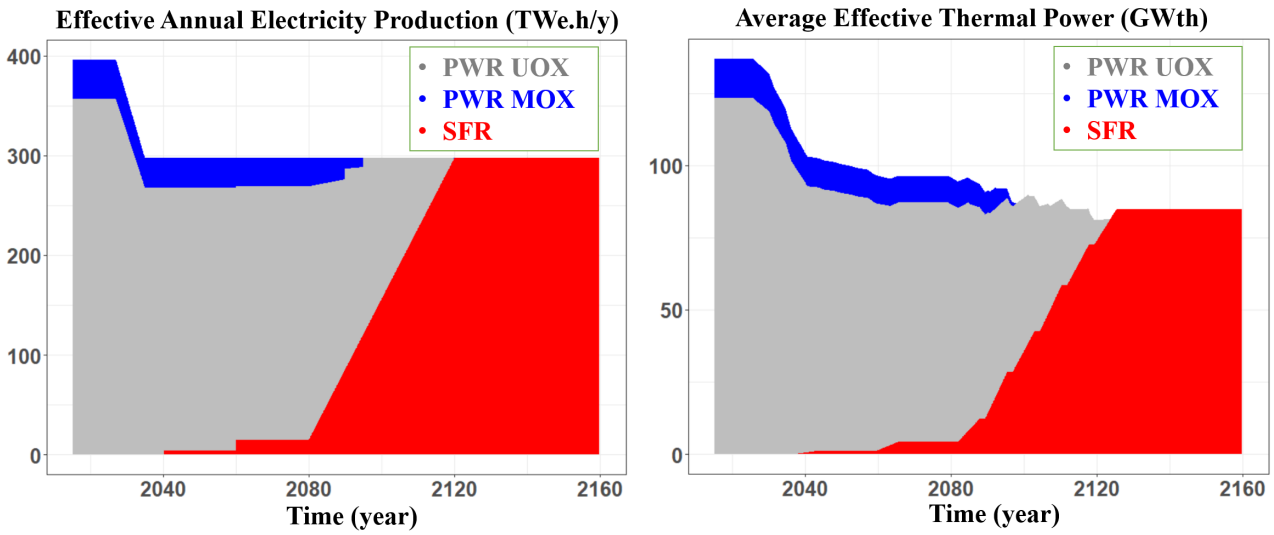

Figure 5.7: Evolution of fuel contribution on the nuclear power for **TRJ SFR**: (a) ideal effective annual electricity production; (b) 6-year-average effective thermal power in the simulation

5.1.2 Analysis of optional trajectories in pre-disruption scenario

In total three trajectories are simulated for this pre-disruption scenario. **TRJ Fr-Mono** provides the baseline of installed capacity of the fleet and reference values of some outputs of interest. **TRJ MIX** and **TRJ SFR** represents two completely different options for plutonium multi-recycling.

5.1.2.1 Estimation of reactor lifespan

Before the physical analysis, it is useful to estimate the reactor lifespan, an important industrial and economic constraint for electro-nuclear scenario studies. For **TRJ MIX**, it is not problematic because the renewal of fleet can be easily adapted to the updated planning of reactor decommissioning which makes no difference in the simulation. For **TRJ SFR**, the operation of a new SFR often follows the decommissioning of an old PWR/EPR, especially during the massive deployment of SFR. But in this simulation of macro reactors, it is not convenient to plan a-priori the operation-decommissioning of each individual reactor and to imply indirectly the transition. Instead, the evolution of power level is preset for each macro reactor. In this case, the lifespan of each shut-down PWR/EPR during the phase of power reduction should be checked.

The check of reactor lifespans during the transitions is divided into two phases. The first one tracks the replacement of current-generation PWRs reaching their lifespan limit. To keep the approximately constant electric power level, the operation of new EPRs should follow the decommissioning of old reactors. This indicates the start time of operation for the EPRs. The second phase follows the power decrease of EPRs under the preset planning, and deduce the lifespan of EPRs. The power level of macro-EPR is smoothed by six-year average, in order to provide a regular rhythm of individual reactors decommissioning.

The first phase focuses on the period from 2040 to 2060. PWRs that reach the life limit during this period start decommissioning. The constant power level should be kept by the start of new EPR operation. Several assumptions should be made for this process:

- 20 oldest among 34 900MW-class PWRs are supposed to start decommissioning before 2040, and the estimation process starts from 2040;

- Life limit of current-generation PWRs is 60 years;
- Nominal capacity of EPR is 1500 MWe;
- Decommissioning of one 1300-MWe or 1400-MWe PWR, or of two 900-MWe PWR is followed by the start of one EPR;
- Before 2040, one EPR is supposed to start operation in 2030;
- In total, 30 EPRs are supposed to be in service by 2060.

Under these assumptions, the decommissioning time of current-generation PWRs and the start time of new-built EPRs can be deduced.

The second phase tracks the EPRs decommissioning time deduced from the decreasing EPR power. Specifically, it gives particular attention on the period from 2080 to 2120 in **TRJ SFR** when the SFRs are massively deployed. When the power reduction reaches cumulatively the power of one EPR, the corresponding rounding number of the oldest EPRs are supposed to start decommissioning. Because their start time are registered in the previous phase, their lifespan can be deduced.

Different from the PWRs of current generation, life limit is not given for EPR. One may note that this decommissioning is passively constrained by the increasing deployment of SFR, which is logically opposite to the real life. As mentioned, the SFR simulation in this study of macro-reactors is not driven by the commissioning-decommissioning tracking of individual reactors. The method illustrated here is only used to help understand approximately the dynamics of individual EPRs and identify possible contradictions between the lifespan of reactor and the preset schedule of SFR deployment in the simulations.

The consistency between this start/decommissioning schemes of EPRs and the simulation can be verified by the power level in Figure 5.8a, in which the red curve denotes the simulation level and the grey curve is deduced from the start/decommissioning dynamics of PWRs/EPRs. Despite the fluctuations between year 2040 and 2050, two evolutions are globally similar.

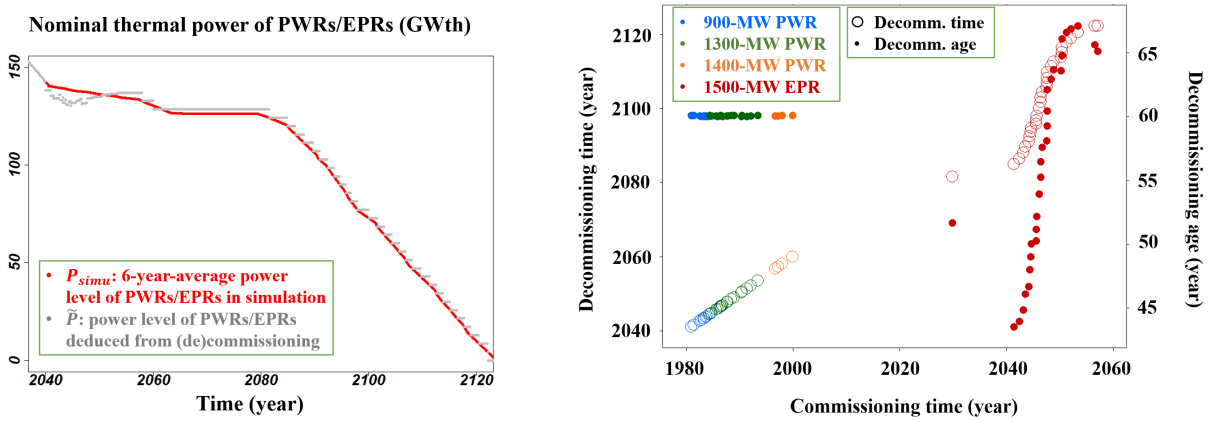

Figure 5.8: Estimation of PWRs/EPRs start/decommissioning dynamics: (a) verification of the power level; (b) (de)start time and age.

Under these assumptions, the start/decommissioning time and age of reactors are shown in Figure 5.8b. PWRs have, evidently, 60 years of age when they start decommissioning. At the beginning of the massive SFR deployment from 2080, the first EPR starting operation from 2030 should be shut down, at the age of 52 years. Following the increasing SFR deployment, EPRs deployed after 2040 starts

decommissioning, at the ages ranging from 40 to more than 60 years. This interval of reactor lifespan is coherent with the current estimation of nuclear facilities. Nevertheless, the life of reactor tends to be extended in order to maximize their economic profit, especially for EPRs. It may imply bringing forward the operation of first several EPRs and postpone the phase of massive SFR deployment relative to the assumption of this study.

5.1.2.2 Material evolution

Evolution of materials can be informative to evaluate the performances of each strategy. Material evolutions under irradiation in reactors drive the evolution of global inventories in the cycle. Figure 5.9 shows the evolution of important component contents in PWR MIX and in SFR.

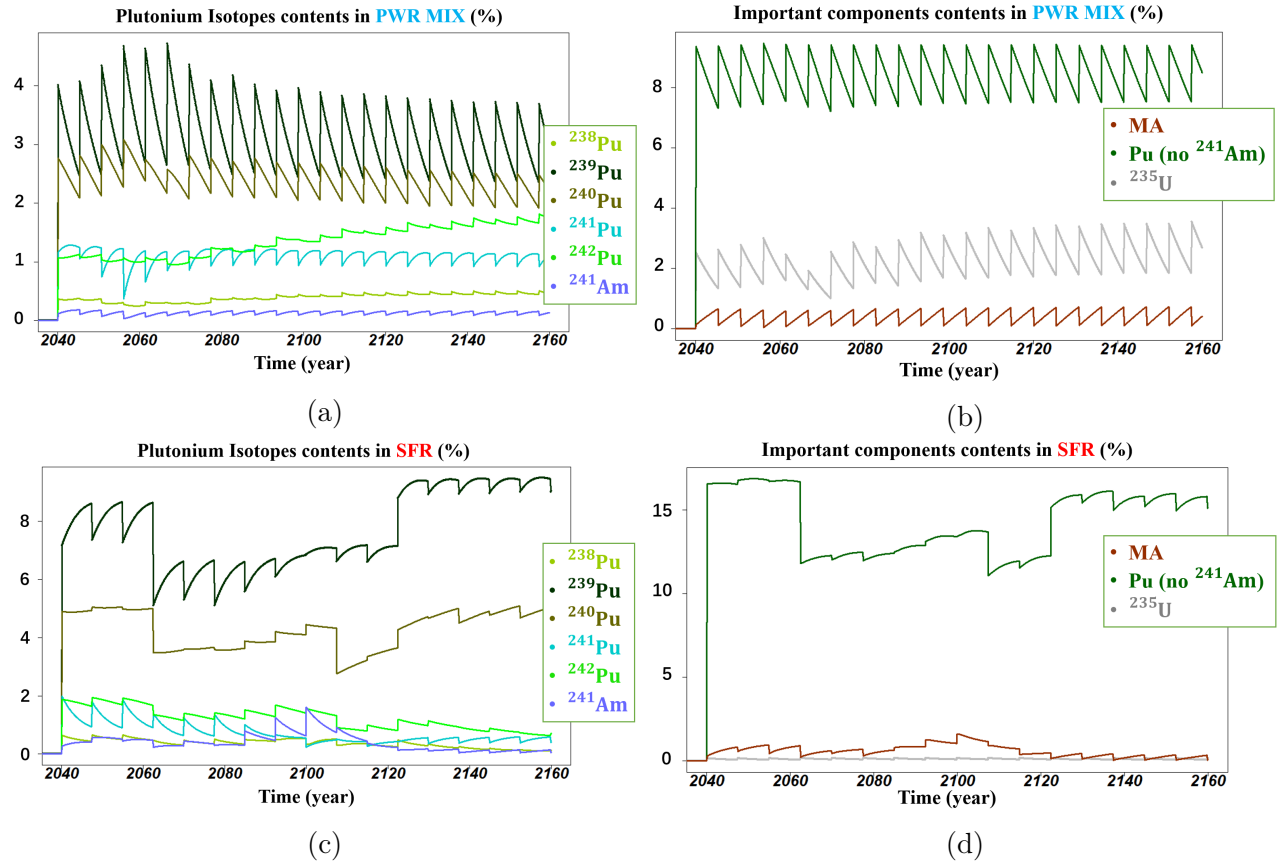

Figure 5.9: Material content evolution under irradiation in new nuclear system, concerning the ^{235}U, plutonium isotopes, and MA: (a) and (b) in PWR MIX, (c) and (d) in SFR

Figure 5.9a and 5.9b describe the contents of interest in PWR MIX. In the core with MIX fuels, a similar behavior of plutonium isotopic contents as irradiated in MOX fuels (Figure 2.6 in Section 2.2.1) can be observed in Figure 5.9a. The principal difference is the lower plutonium quality in MIX fuels than the one in MOX fuels, because the irradiation in PWR tends to burn out a large quantity of $^{239}\boldsymbol{Pu}$ without sufficient generation from the neutron capture reaction of ^{238}U. Meanwhile, some even-number isotopes like ^{238}Pu and ^{242}Pu at BOC (in the fresh fuel) increase progressively under multi-recycling. As viewed in Figure 5.9b, the evolution of plutonium content in PWR MIX is stable during more than 100 years of multi-recycling. The decreasing plutonium quality is compensated by the slowly increasing ^{235}U enrichment. This enrichment starts from about 2% at the beginning of the multi-recycling by 2040. In the 2060s, the enrichment becomes lower due to the use of higher-quality plutonium from spent UOX fuels. After one or two

cycles, it re-increases up to 4% by the end of the scenario, which is close to the enrichment for fresh UOX fuels. In contrast, the evolution of MA content is similar in different cycles of irradiation, mainly due to the similar plutonium content evolution.

Figure 5.9c and 5.9d present the contents of key components under the irradiation in SFR. A generally high plutonium contents can be observed before year 2060 and after year 2120. In fact, the contents presented here are normalized by the heavy metal in total core including the depleted-uranium blankets. Before 2060 and after 2120, no blanket are considered for SFR and thus the average plutonium contents are higher than that during the irradiation between 2060 and 2120 when two blankets are added.

As shown in Figure 5.9c, $^{239}\mathrm{Pu}$ increases in all irradiation cycles, while other isotopes have various behaviours depending on the isotopy at BOC. During the massive SFR deployment, a sharp drop of BOC content of $^{240}\mathrm{Pu}$ can be observed around year 2110. That is because after the empty of spent MOX fuels, spent UOX fuels are reprocessed for SFR fuel fabrication, containing low $^{240}\mathrm{Pu}$ content. One cycle after, spent SFR fuels are also reprocessed for SFR fuel fabrication, and thus BOC-$^{240}\mathrm{Pu}$ re-increases. One may note a relatively high BOC content of ^{241}Am during this massive SFR deployment phase as well. It can be explained by the significant production of ^{241}Am from ^{241}Pu in the wait for the reuse. Meanwhile, the SFR model in this study does not reject ^{241}Am during the SFR fuel fabrication phase [77], which is different from the FLM of other recycling-based fuel models in CLASS. The fresh fuel content of ^{241}Am reaches the peak around year 2100. For this cycle, all remaining spent MOX fuels are reprocessed for fresh SFR fuel fabrication. Because of the LiFo mode by default, the ^{241}Am content in these oldest spent MOX fuels reaches the highest level. After this irradiation cycle, the ^{241}Am BOC content decreases and keeps relatively low after year 2120, because the spent fuels are quickly reprocessed after discharge.

Figure 5.9d shows mainly plutonium and MA contents; depleted uranium is used for SFR fuel and thus $^{235}\mathrm{U}$ is always at a low level. The drop of plutonium content at the BOC in 2110 can be explained by the aforementioned drop of $^{240}\mathrm{Pu}$. In this cycle, the plutonium quality is sufficiently high to satisfy the criticality criterion. After 2120, the calculation shows that the core with no blanket is not necessarily break-even. The breeding behavior relies actually on the isotopic effects [42]. Depending on the number of blanket, plutonium content in fresh fuel ranges from 10% to 16%, far different from the simulation of ASTRID in [42] (between 22% and 28%). This highlights the importance of model and reactor design in the study. Nevertheless, the material variation between BOC and EOC is still representative for the estimation of global inventory evolution. As for MA, it is particularly driven by ^{241}Am.

This short analysis of material evolution under irradiation provides the physical explanation for the following studies, concerning the material evolution in the cycle and in the stocks. Four mass-related quantities are considered, shown in Figure 5.10: plutonium inventory in total cycle, idle plutonium in interim stocks that are available for the recycling after cooling, the cumulative consumption of natural uranium and MA inventory in total cycle that includes the ones in all facilities and in waste canisters.

Stabilization of total-cycle plutonium is one of the objective for the strategy using MIX fuels. As shown in Figure 5.10a, total-cycle plutonium is stabilized at the level around 550 tons soon after 2060 in **TRJ MIX** when the MIX fraction reaches the target value. If only mono-recycling is permitted, plutonium inventory will continue increasing over 1000 tons in the second half of next century. In contrast, the SFR deployment in **TRJ SFR** accumulates more slowly the pluto-

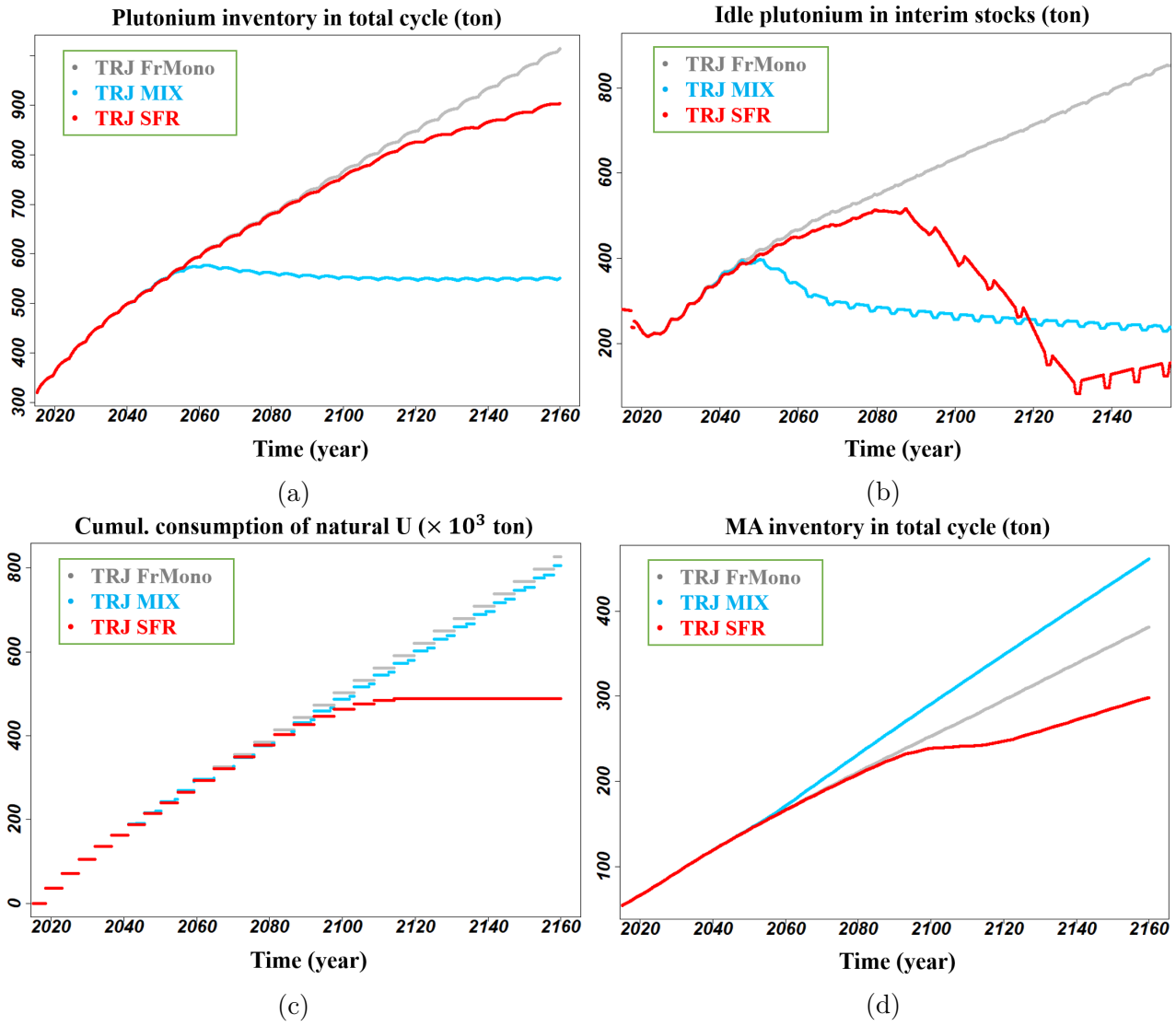

Figure 5.10: Evolution of materials in the prior trajectories: (a) plutonium inventory in total cycle; (b) idle plutonium inventory in interim stocks; (c) cumulative consumption of natural uranium; (d) MA inventory in total cycle

nium than the fleet of mono-recycling. Even if no blanket is used after 2120, the SFRs are still breeder. With other designs, SFR may be break-even and it would be possible to stabilize the total-cycle plutonium after 2120.

For the idle plutonium in interim storage, the time-dependent inventory is averaged within six years as for the power level calculation above. As shown in Figure 5.10b, the idle plutonium in **TRJ MIX** is stabilized (with a slight tendency of decrease) at the level of 250 tons, approximate to the current level. It verifies that the use of MIX fuels in 34% of EPR-fleet has the potential to stabilize spent fuel inventory in interim stocks. Without the multi-recycling, more than 800 tons of idle plutonium will be accumulated, which account for the major part of total-cycle plutonium. For **TRJ SFR**, idle plutonium is rapidly consumed during the increasing deployment of SFRs. It drops to around 83 tons when the transition of SFR deployment in 100% of fleet finishes.

The cumulative consumption of natural uranium shown in Figure 5.10c is also an important indicator. In **TRJ SFR**, extremely limited quantities of natural uranium are needed once SFRs are all deployed, because a huge stock of depleted uranium can be reused. This matches well the objective of SFR deployment. In contrast, **TRJ FrMono** and **TRJ MIX** lead to a very similar consumption of uranium. Although the plutonium is multi-recycled and contributes to the energy

production, ^{235}U enrichment of MIX fuels can still be up to several percents depending on the plutonium quality. In this case, the need of natural uranium in **TRJ MIX** is close to that in **TRJ FrMono**.

MA inventory complements the information about the management of nuclear wastes for the options of interest. As shown in Figure 5.10d, the use of MIX in **TRJ MIX** leads to a faster accumulation of MA inventory than **TRJ FrMono**. This is expected because MA isotopes are more produced during the plutonium multi-recycling [9]. It is also worth noting that in **TRJ MIX** the total-cycle MA inventory is comparable to the plutonium in the next century. In that case, it is rather MA than plutonium that becomes the major concern of nuclear wastes. For SFR deployment in **TRJ SFR**, MA seems to meet the stabilization during the transition between 2080 and 2120, due to the modelling features as explained above.

5.1.2.3 Operational capacity of facility

Operational capacity of facilities, such as the fabrication of fresh fuels and reprocessing of spent fuels, are important industrial constraints that are not taken into account in previous studies. [13] gives an order of magnitude about the operational capacity of facilities. For the fresh UOX fuel fabrication, the current need is around 1045 tHM/y and the maximal capacity of the fabrication plant of Framatome is 1400 tHM/y. For MOX fuel the current need is 120 tML/y, and the capacity of MELOX can theoretically reach 195 tHM/y. In terms of the reprocessing capacity in the plants of La Hague, the quantity of reprocessed spent UOX fuels range from 1000 to 1250 tHM/y.

The mass flows cannot be directly given by simulation, because the management by CLASS responds to the instant demand of the associated back-end facility. To get reasonable level of continuous mass flow, the instant peaks of mass transport are normalized by the "spare time" between the adjacent demands of the identical facility (each fabrication/reprocessing demand of each fuel type). With the time-average calculation, the annual fabrication of fresh fuels and the annual reprocessing of spent fuels of each fuel type are then deduced, shown in Figure 5.11.

5.11a presents the evolution of annual fabrication of heavy metal concerning different sorts of fuel in **TRJ MIX**. The starting point of fresh UOX and fresh MOX fabrication matches well the values indicated in [13]. Following the decrease of installed capacity from year 2027 to 2035 and the increase of MIX fraction from year 2040 to 2060, the annual demand of fresh UOX fuels drop rapidly and is stabilized at the level of 430 tHM/y. For the MIX fuel fabrication, a capacity higher than 220 tHM/y may be needed after the transition, which is obviously over the current nominal capacity of MELOX. It is coherent because the energy production by MIX fuels after the transition is higher than the that of current use of MOX. Nevertheless, it is only marginally higher than the maximal level of MELOX and thus reasonable. The future plant for the plutonium multi-recycling in PWRs should consider well such demand.

For the fabrication in **SCN SFR** presented in Figure 5.11b, two levels are considered for the fabrication of SFR fuels. One only accounts for the SFR MOX in the active core, and the other considers the sum with depleted-uranium blankets. Regardless, these two levels are very close. When SFRs are deployed for 100% of fleet, 312 tHM/y is needed for the fabrication of SFR fuels. This value is higher than that for **TRJ MIX**, but still conceivable. At the same time, the higher plutonium content in fresh SFR fuels than the MOX or MIX fuels, as shown in Figure 5.9d, should be taken into account. It may implies the need of innovative process for the fuel fabrication.

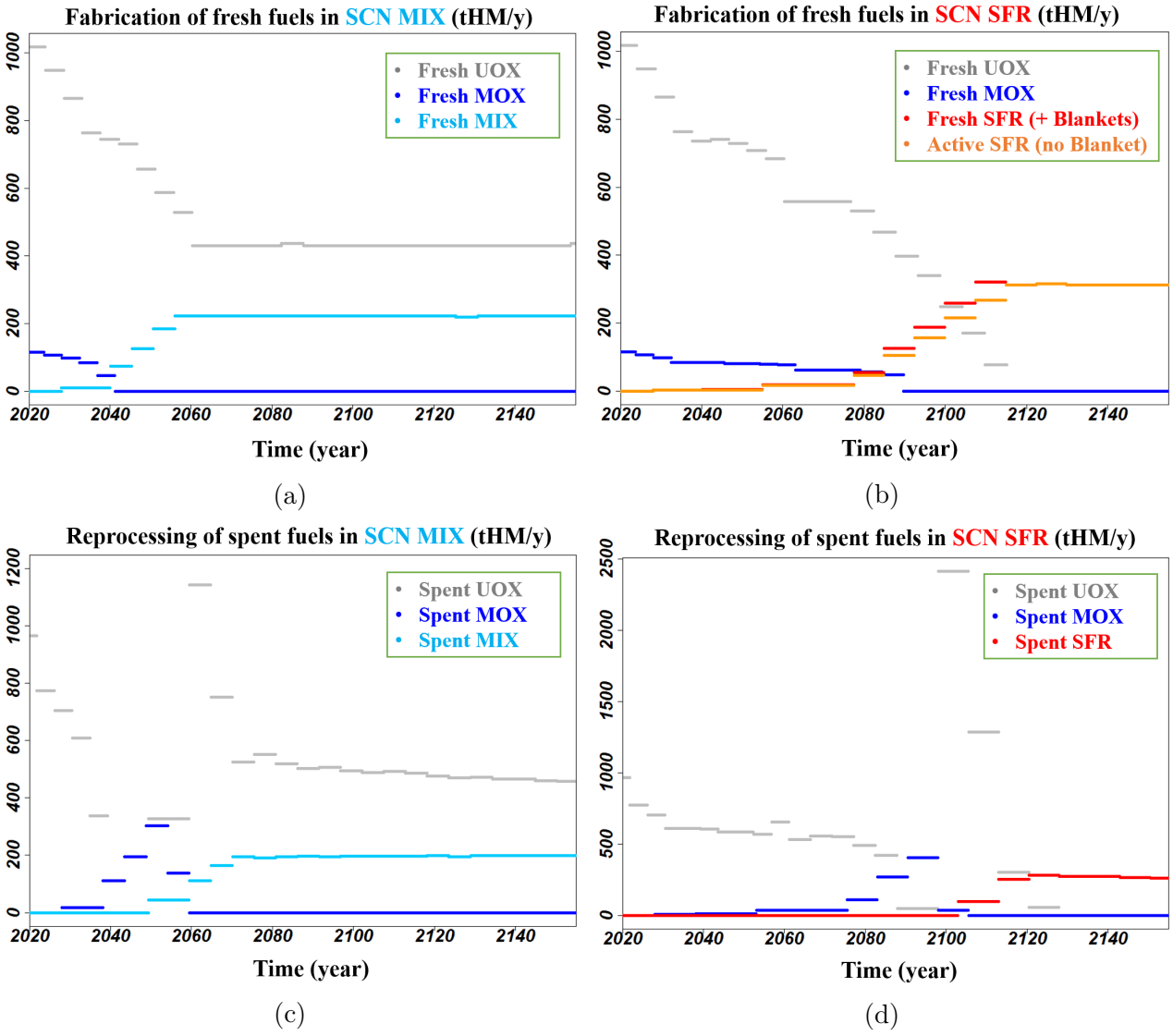

Figure 5.11: Requirement of facility capacity for the plutonium multi-recycling: (a) annual fabrication of fresh fuels in **TRJ MIX**; (b) annual fabrication of fresh fuels in **TRJ SFR**; (c) annual reprocessing of spent fuels in **TRJ MIX**; (d) annual reprocessing of spent fuels in **TRJ SFR**

Figure 5.11c and 5.11d present the requirement of reprocessing capacity of each type of spent fuels in respectively **TRJ MIX** and **TRJ SFR**. One may note the sudden peaks, at 1140 tHM/y in **TRJ MIX** and 2410 tHM/y in **TRJ SFR**. It can be explained by the fact that around the time of peaks, the stock of spent MOX fuel is nearly emptied, and it is necessary to recycle the plutonium from spent UOX fuels. However, the plutonium content in spent UOX fuels is around 1%, and to feed the demand of plutonium-based fuels at that time requires the reprocessing of a large quantity of spent UOX fuels. These peaks can be problematic for the facility operation. In practise, at least two ways can tackle the issues of these peaks. One is to anticipate this huge reprocessing requirement and to maintain a reasonably high but stable level of reprocessing in advance, in order to lighten the burden afterwards. The other may opt to mix the plutonium from different stocks, ensuring the availability of high-plutonium-content spent fuels. In the latter case, the need of spent UOX fuels reprocessing can be much lower than when these high-plutonium-content spent fuels are not available.

5.1.3 Summary of pre-disruption study

In this section, three trajectories are simulated and analyzed in detail: **TRJ Fr-Mono**, **TRJ MIX** and **TRJ SFR**. This pre-disruption scenario study aims to assess the transition strategy before any disruption under a more realistic framework and provide informative outcomes for the subsequent adaptation scenario study.

Based on the instructions of PPE [18], **TRJ FrMono** sets the baseline of installed capacity evolution for scenarios of interest in this study. Respecting this electric power evolution of fleet, two options on the plutonium multi-recycling are studied: **TRJ MIX** recycles the plutonium in PWRs/EPRs using the MIX fuels, and in **TRJ SFR** SFRs are deployed for 100% fleet.

A small algorithm is used to estimate the life of PWRs/EPRs when they start decommissioning in **TRJ SFR**. It verifies that the schedule of SFR deployment in **TRJ SFR** is coherent with the lifespan estimation of power plants. It may be useful for the lifespan estimation of decommissioning reactors in subsequent post-disruption scenarios studies.

Materials evolution such as the plutonium in interim stocks and in total cycle, the cumulative consumption of natural uranium and MA in total cycle are studied for these trajectories. **TRJ MIX** achieves the stabilization of plutonium in interim stocks and in total cycle soon after the transition by 2060, but has approximately the same consumption of natural uranium and accumulates the total-cycle MA inventory faster than the mono-recycling trajectory. **TRJ SFR** continues to accumulate plutonium in the cycle for the substitution for the EPR-fleet with SFRs. During the massive SFR deployment, idle plutonium in interim stocks are rapidly consumed. Once the substitution finishes, the fleet is almost independent from the fissile resources of natural uranium. Compared with **TRJ MIX**, **TRJ SFR** accumulates more slowly the MA in total cycle.

For future fabrication plant, **TRJ MIX** requires the capacity of about 220 tHM/y of MIX fuels, and in contrast, 310 tHM/y is necessary for the SFR fuels in **TRJ SFR**. Besides this capacity difference on the mass flow, one should also note the discrepancy of plutonium content in SFR fuel relative to MOX or MIX fuels. It may requires new design for fabrication designs and bring another practical and engineering challenges. As for future reprocessing plant, relevant anticipation or mixing plutonium from different types of spent fuel should be taken, in order to avoid an abrupt and huge demand of reprocessing of spent UOX fuels due to their relatively low plutonium content.

Besides these physical analyses, one should note the contradiction between these two trajectories depending on different context and nuclear technologies. For instance, the strategy of plutonium multi-recycling in PWRs by MIX fuels is not statically robust in case the SFR deployment is reconsidered, owing to the plutonium availability. Meanwhile, if the new SFRs cannot be put into service in the middle of **TRJ SFR** due to some economic effects, one may wonder how to maximize the use of idle plutonium. As emphasized all the time in this work, these deep uncertainties should be considered for these possible transition strategies. Given the lack of static robustness, the adaptive robustness of these two prior strategies can be investigated.

5.2 Analysis of adaptive trajectories after disruption

Following the update of information and decision-making, the prior trajectories may be disrupted. In this section, two families of post-disruption adaptive strategies are studied: one is the adaptation based on the prior trajectory **TRJ MIX**,

which reconsiders the SFR deployment, denoted as **SCN MIX2SFR**; the other is based on the prior trajectory **TRJ SFR** which stops the new SFR in operation in the middle of SFR deployment and recycles the plutonium in EPRs by MOXEUS fuels, denoted as **SCN SFR2MOXEUS**. As a reminder, the MIX fuel is not used for adaptation here, because the variable plutonium content in fresh MOXEUS fuels is more flexible regarding a large variability of plutonium quality in different types of spent fuels. To include the uncertainty of disruption time, three adaptation times t_{ad} are considered: year 2065, 2085 and 2100.

The change from **TRJ MIX** towards **SCN MIX2SFR** can be triggered by the re-adoption of massive nuclear deployment strategy in other countries, accelerating the consumption of $^{235}\mathrm{U}$ in natural uranium. Under the rising risk of resource shortage, SFR deployment may be needed after the second half of the century. The objective of adaptation is then to minimize the time needed for the 100% fleet substitution with SFRs. It can be interesting to compare with the timeline of **TRJ SFR** in which the multi-recycling of plutonium in PWRs/EPRs is not taken. One may note that the late adaptation of $t_{ad} = 2100$ is not contradictory to the indications in PPE [18], which suggests maintaining SFR-related researches for possible need by the end of century.

The change from **TRJ SFR** towards **SCN SFR2MOEUXS** may result from the new estimation of the cost of SFR in comparison with other technologies, which makes stakeholders take more conservative attitudes regarding the SFR deployment. To handle the significant quantity of in-cycle plutonium and spent fuels, the plutonium multi-recycling in EPRs is considered. Lots of spent MOX fuels containing low-quality plutonium have been reprocessed for the SFR fuels before disruption, while a large quantity of spent UOX fuels containing high-quality plutonium is accumulated. MOXEUS design instead of MIX is then used to adapt more easily to various plutonium quality in different types of spent fuels. Nevertheless, this choice is only an assumption to simplify the simulation and the analysis. Given the significant plutonium accumulation for pre-disruption SFR deployment, the post-disruption adaptation aims to maximize the use of idle plutonium. The adaptation performances are then compared with **TRJ MIX** in which SFR deployment is a-priori not considered.

The optimization based on the simplex method called Nelder-Mead optimization is introduced [103] to identify adaptive strategies of interest. This optimization method is used to deduce the earliest time when SFRs can be deployed for the whole fleet in **SCN MIX2SFR** and to minimize the idle plutonium inventory in **SCN SFR2MOXEUS**. WPS techniques is not used because of its relatively low efficiency in this study where we would identify one of those possible optimal solutions. With respect to three possible adaptation times t_{ad}, the optimal adaptive strategies are looked for, and the corresponding trajectories are analyzed in consideration of a set of outputs of interest as presented in Section 5.1.

5.2.1 Description of adaptation scenarios

5.2.1.1 Adaptation scenario of SCN MIX2SFR

As indicated, **SCN MIX2SFR** disrupts the prior trajectory **TRJ MIX** and reconsiders the SFR deployment. The objective is to substitute for the EPR-fleet with SFRs as fast as possible after the disruption.

In this adaptation study, five input variables are considered: the time $t_{e,MIX}$ to end the use of MIX fuels in EPRs, the time $t_{s,2SFR}$ for the start of the first SFR, the time $t_{e,2SFR}$ defining the ending time of the fleet replacement with SFRs, and both the burn-ups of UOX and MIX fuels, BU_{UOX} and BU_{MIX}. The adaptation scenario

SCN MIX2SFR can then be characterized by these five variables, as described in Figure 5.12. When adaptation starts in t_{ad}, the burn-ups BU_{UOX} and BU_{MIX} change immediately to the new adapted values. The MIX fraction in the macro-EPR decreases linearly to 0% from t_{ad} to $t_{e,MIX}$. The first SFR starts operation from $t_{s,2SFR}$. The fraction of SFR in the total fleet increases then linearly to 100% by $t_{e,2SFR}$.

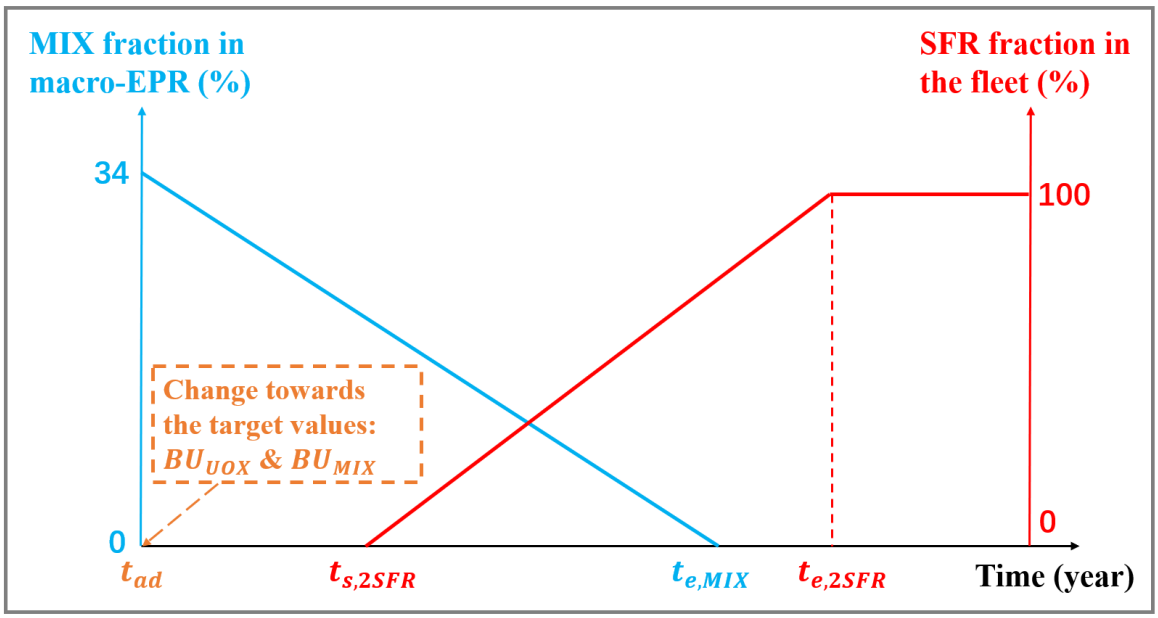

Figure 5.12: Graphical representation of the adaptation scenario **SCN MIX2SFR**

The variation ranges of these five variables are summarized in Table 5.1. First, the use of MIX fuel restrains evidently the accumulation of plutonium for the deployment of SFR. The variation of $t_{e,MIX}$ indicates the permitted dynamics for the transition of MIX fraction in EPRs, avoiding abrupt changes which are not realistic in practise. Meanwhile, the study of **TRJ SFR** in Section 5.1 shows the risk of plutonium shortage if MOX is used till year 2095. Therefore, it is not necessary to consider $t_{e,MIX} > 2095$ if $t_{ad} < 2095$; if adaptation is taken later than 2095 ($t_{ad} = 2100$ in this study), the use of MIX is assumed to be stopped in short time (1 year available).

The starting time of SFR deployment, $t_{s,2SFR}$, should be after year 2070, being coherent with the reactor lifespans and the necessary time for the development of SFR technology. The deployment should start with a demonstration-like phase, contributing to 5% of electricity production. The massive deployment will follow one irradiation cycle after. Thus, even in the case of early adaptation like $t_{ad} = 2065$, no SFR can be deployed before year 2070, and the earliest possible massive SFR deployment may begin by around 2078, consistent with the **TRJ SFR**. After 2120, the substitution for EPR-fleet with SFRs can be problematic, because EPRs may be renewed between 2080 and 2120 and most of them are not operated for a long time just after 2120. There is then no need to consider $t_{s,2SFR} > 2120$. The ending time of transition $t_{e,2SFR}$ ranges from year 2120 to year 2150. Actually, if $t_{e,2SFR} = 2120$ can be achieved, the SFR deployment can end as early as **TRJ SFR**, and the corresponding adaptation from **TRJ MIX** can be considered equally performing as **TRJ SFR**, regarding the the SFR deployment timeline. In this case, the previous multi-recycling of plutonium in PWRs/EPRs as well as the disruption has limited impacts on this timeline, mainly from the angle of plutonium availability. In terms of the burn-ups BU_{UOX} and BU_{MIX}, they are considered variable parameters to allow more efficient accumulation of plu-

tonium for the SFR deployment.

Var.	Min.	Max.	Unit	Explanation
$t_{e,MIX}$	$t_{ad}+1$	$\max(t_{ad}+1, 2095)$	year	Time to end the use of MIX fuels.
$t_{s,2SFR}$	$\max(t_{ad}, 2070)$	2120	year	Time for the first SFR starts operation.
$t_{e,2SFR}$	2120	2150	year	Time to finish the transition towards the SFR-fleet.
BU_{UOX}	30	60	GWd/t	Burn-up of UOX fuels after t_{ad}.
BU_{MIX}	30	60	GWd/t	Burn-up of MIX fuels after t_{ad}.

Table 5.1: Ranges of input variables in the adaptation scenario **SCN MIX2SFR**

In practise, the objective in this scenario is reformulated and becomes the minimization of $t_{e,2SFR}$ subject to the plutonium availability. The adaptive strategies identified by the optimization process are then compared with the deployment timeline in the prior trajectory **TRJ SFR**. The difference between the minimal achievable $t_{e,2SFR}$ and year 2120, the time when SFRs are completely deployed in the fleet in **TRJ SFR**, can be quantified as the direct influence of the previous multi-recycling of plutonium in PWRs/EPRs on the temporality of SFR deployment. To complement, the outcomes such as the material evolution and the requirement of facility capacity should be analyzed, which can be regarded also as the relevant impacts.

5.2.1.2 Adaptation scenario of SCN SFR2MOXEUS

SCN SFR2MOXEUS assumes that during the implementation of prior SFR deployment strategy, the uranium is estimated to be sufficient for the future and SFR technology becomes much less competitive economically; therefore, stakeholders stop deploying new SFRs. To respect the economic criteria, in-service SFRs continue their operation after the disruption until their life limit. The plutonium multi-recycling can be carried out by the EPR system and the existing SFRs. The plutonium in the cycle should then be valorized as much as possible.

For plutonium multi-recycling in EPRs, MOXEUS is used instead of MIX. In other words, the plutonium content in the fresh fuels for the multi-recycling in EPRs is variable. That is because the first two phases of SFR deployment before 2080 reprocess a large quantity of spent MOX fuels in which the plutonium quality is relatively low. In case of disruption, plutonium used for the multi-recycling in EPRs comes mainly from spent UOX fuels at the beginning of adaptation. This plutonium quality is higher than that from spent MOX, and a lower content than the 9.54% in **TRJ MIX** is sufficient; but the level of content is a-priori not determined. Following the multi-recycling, the plutonium quality will drop and a level like 9.54% or higher can be needed. Therefore, the more flexible model of MOXEUS is used to adapt to a large variability of plutonium quality for the whole time horizon of scenario.

In this adaptation scenario, the fuel cycle can be divided into two parts: the first one focuses on the EPR-fleet, and the other one is the SFR fuel cycle, as shown in Figure 5.13. In short, the plutonium of MOXEUS fuels comes principally from the spent UOX and spent MOX/MOXEUS fuels of EPRs, while the fabrication of fresh SFR fuels gets its plutonium from spent SFR fuels. To avoid unrealistic plutonium shortages, these two fuel cycles can still communicate for the use of plutonium but with a lower priority.

In this adaptation scenario, four variables are taken into account to minimize the idle plutonium: the fraction of MOXEUS in EPR system $FrMXE_{inEPR,f}$, the time when MOXEUS fraction reaches its target value $t_{e,2MXE}$, and the burn-ups of UOX

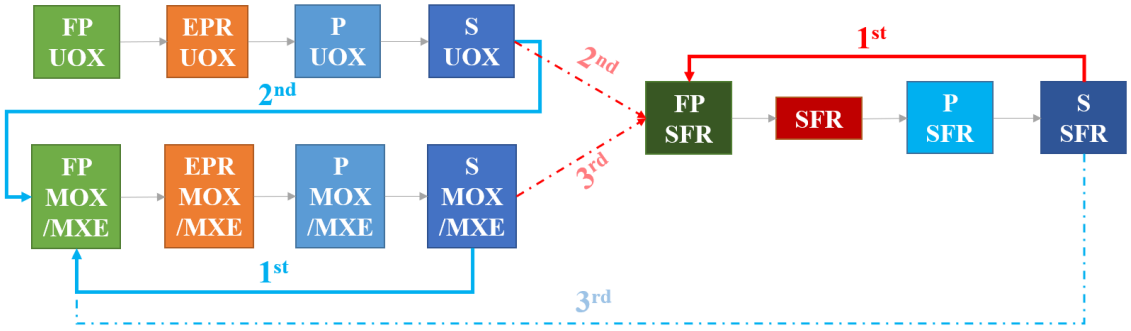

Figure 5.13: Fuel cycle in **SCN SFR2MOXEUS**

and MOXEUS (BU_{UOX} and BU_{MXE} respectively). The process of scenario is graphically presented in Figure 5.14. In t_{ad}, the new burn-ups BU_{UOX} and BU_{MXE} are determined. The macro-SFR keeps the constant power which means the continuation of in-service SFRs, and no blanket is added. Within the macro-EPR, MOXEUS fraction increases linearly and reaches $FrMXE_{inEPR,f}$ in $t_{e,2MXE}$. By 2120, the SFR share in the total electricity production in nuclear fleet decreases, because the SFRs deployed in/before 2060 which accounts for 5% of electric power of the fleet reach their life limit and should enter their decommissioning phase. If $t_{ad} < 2080$, the SFR fraction is originally 5%, and thus all SFRs are shut down by 2120. Otherwise, those SFRs deployed after year 2080 are supposed to start decommissioning in 2140. For each SFR entering decommissioning phase, the corresponding electricity production is complemented by new-built EPRs with the ongoing MOXEUS fraction in the macro-EPR, in order to keep the constant electric power. The ranges of these four variables are summarized in Table 5.2.

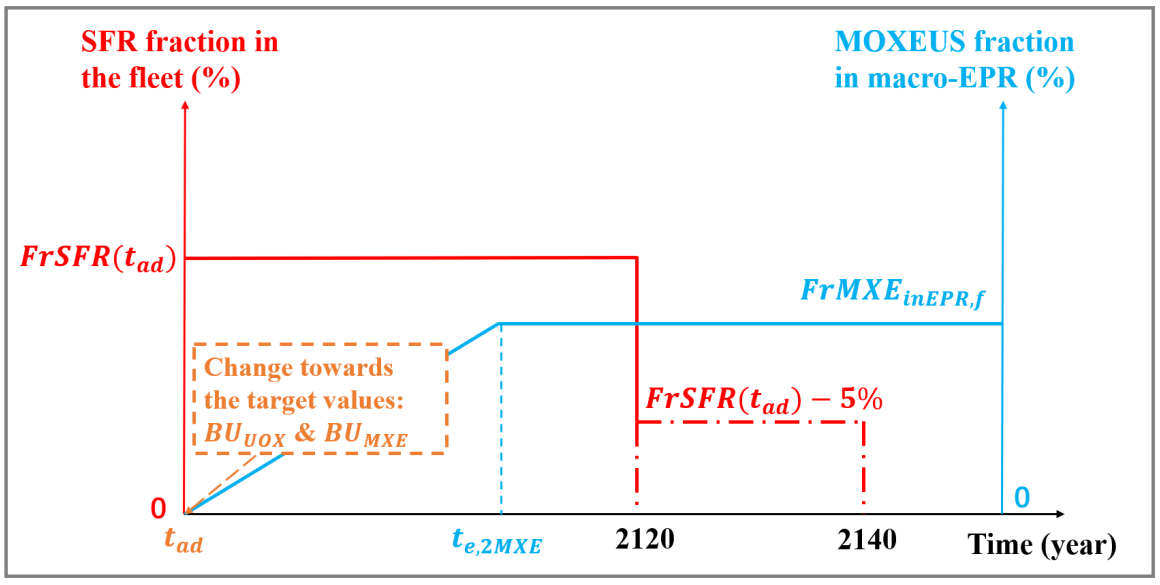

Figure 5.14: Graphical representation of the adaptation scenario **SCN SFR2MOXEUS**

Var.	Min.	Max.	Unit	Explanation
$FrMXE_{inEPR,f}$	0	100	%	Final fraction of MOXEUS in EPR system.
$t_{e,2MXE}$	$t_{ad}+1$	2120	year	Time when MOXEUS fraction in EPR system reaches $FrMXE_{inEPR,f}$
BU_{UOX}	30	60	GWd/t	Burn-up of UOX fuels after t_{ad}.
BU_{MIX}	30	60	GWd/t	Burn-up of MIX fuels after t_{ad}.

Table 5.2: Ranges of input variables in the adaptation scenario **SCN SFR2MOXEUS**

The variation of these four variables helps search for the strategy that minimizes the idle plutonium, which is a time-dependent quantity and thus not a single value. One may also note that the plutonium in spent SFR fuels after the decommissioning of all SFRs becomes definitively idle, but for each adaptation scenario of same t_{ad}, this quantity is systematically the same. To take all these factors into account, the maximum of the 6-year-average idle plutonium from 2140 to 2160 is defined as the output of interest, denoted as $Pu_{idle,max}$. With respect to the objective of adaptation, $Pu_{idle,max}$ should be minimized. The time interval between year 2140 and 2160 allows the stabilization of mass flows and ensures the arrival of spent SFR fuels in interim stocks.

5.2.2 Nelder-Mead simplex-based optimization

The Nelder-Mead optimization is a simplex-based approach to minimize the function value $y = f(x)$ without constraint. For a N-dimensional input vector $\boldsymbol{X}$, each step of iteration is based on the simplex of $N+1$ points and their function values. The steps of iteration scheme can be summarized as:

- **Step 0 - Initialization:**
  - Give $N+1$ initial points: $(\boldsymbol{X}_1, ..., \boldsymbol{X}_{N+1})$;
  - Calculate their function value $y_i = f(\boldsymbol{X}_i)$ for all i;
- **Step 1 - Update:**
  - Identify the highest output y_h, the second highest y_s and the lowest y_l, and their corresponding inputs $\boldsymbol{X}_h$, $\boldsymbol{X}_s$ and $\boldsymbol{X}_l$;
  - Identify the centroid $\boldsymbol{X}_c$ of these inputs without considering $\boldsymbol{X}_h$;
- **Step 2 - Replacement:**
  - Do ***reflection*** (Equation 5.1): reflect $\boldsymbol{X}_h$ on $\boldsymbol{X}_{rf}$, relative to $\boldsymbol{X}_c$;
  - Calculate $y_{rf} = f(\boldsymbol{X}_{rf})$;
  - If $y_{rf} < y_s$, do ***Expansion*** (Equation 5.2): expand the reflection $\boldsymbol{X}_{rf}$ to $\boldsymbol{X}_{ep}$, relative to $\boldsymbol{X}_c$;
    - If $y_{ep} \leq y_l$: replace $\boldsymbol{X}_h$ with $\boldsymbol{X}_{ep}$;
    - Else: expansion fails, and replace $\boldsymbol{X}_h$ with $\boldsymbol{X}_{rf}$;
    - Go to step 3;
  - Else ($y_{rf} \geq y_s$), do ***Contraction*** (Equation 5.3): contract the reflection $\boldsymbol{X}_{rf}$ to $\boldsymbol{X}_{ctr}$ if $y_{rf} < y_h$ (called *outside contraction*), or contract $\boldsymbol{X}_h$ if $y_{rf} \geq y_h$ (called *inside contraction*), relative to $\boldsymbol{X}_c$, and calculate $y_{ctr} = f(\boldsymbol{X}_{ctr})$;
    - If $y_{ctr} < min(y_{rf}, y_h)$: replace $\boldsymbol{X}_h$ with $\boldsymbol{X}_{ctr}$, and go to step 3;
    - Else, contraction fails, and do the ***Shrinkage*** (Equation 5.4): replace $\boldsymbol{X}_i$ by shrinking it towards $\boldsymbol{X}_l$, then back to step 1;
- **Step 3 - Exit criteria:** back to step 1 if none of criteria is fulfilled, exit otherwise.

These four key operations involve: reflection, expansion, contraction and shrinkage. In practise, these operations can be carried out under these forms:

$$\text{Reflection: } \boldsymbol{X}_{rf} = \boldsymbol{X}_c + \alpha(\boldsymbol{X}_c - \boldsymbol{X}_h) \tag{5.1}$$

$$\text{Expansion: } \boldsymbol{X}_{ep} = \boldsymbol{X}_c + \gamma(\boldsymbol{X}_{rf} - \boldsymbol{X}_c) \tag{5.2}$$

$$\text{Outside contraction: } \boldsymbol{X}_{ctr} = \boldsymbol{X}_c + \beta(\boldsymbol{X}_{rf} - \boldsymbol{X}_c) \tag{5.3a}$$
$$\text{Inside contraction: } \boldsymbol{X}_{ctr} = \boldsymbol{X}_c + \beta(\boldsymbol{X}_h - \boldsymbol{X}_c) \tag{5.3b}$$

$$\text{Shrinkage: } \boldsymbol{X}_i = \boldsymbol{X}_l + \delta(\boldsymbol{X}_i - \boldsymbol{X}_l) \tag{5.4}$$

and these four operations are characterized by four coefficients subject to:

$$\alpha > 0,\ \gamma > 1,\ \gamma > \alpha,\ 0 < \beta < 1,\ 0 < \delta < 1$$

In this study, standard values as suggested in [104] are used:

$$\alpha = 1,\ \gamma = 2,\ \beta = \frac{1}{2},\ \delta = \frac{1}{2}$$

While for the conditions to exit the iteration, two criteria are considered:

- $\boldsymbol{Ct}_{ItNum}$: the iteration number reaches the limit of preset value, and 100 is used in this study;
- $\boldsymbol{Ct}_{\epsilon}$: the maximal discrepancy between outputs of simplex defined as $\Delta = \underset{i \neq j}{max} |2(y_i - y_j)/(y_i + y_j)|$ is smaller than a predetermined value ϵ, and $\epsilon = 10^{-4}$ is used in this study.

It is worth noting that the optimization process iterates without considering any constraint. In this study, if a new-created point reaches out of the boundaries, the intersection onto the boundaries is used. Furthermore, the phase-out strategies are not supposed in these adaptation scenarios, and thus missloads should be avoided. As suggested in [103], the output can be penalized by an additional value if the constraint is broken. Under different forms of penalty, the convergence can be faster or slower, and it is also possible that the final result falls in the zone breaking the constraints (with missloads). Here the form of penalty and optional choices of foregoing four coefficients are not discussed, in order to focus on the analysis of scenarios. Relevant sensitivity studies and convergence tests are analyzed in detail in [103, 104]. If the final result of optimization still have missloads, other initial guess of simplex for the step 0 will be tried.

Because the criterion Ct_{ϵ} used for the exit focuses on the discrepancy of the output of different trajectories, it is possible to find very distinct adaptive strategies for the final points of simplex if several minimums exist. However, this method does not guarantee the exploration of all minimums. The outputs of interest in these two adaptation scenarios provide actually the primary results of interest. Further demands on the additional constraints or exploration of other possible inputs under a given output level can be discussed based on this primary result.

5.2.3 Analysis of adaptation scenario SCN MIX2SFR

5.2.3.1 Optimal transition

The values of inputs and output are presented in Table 5.3, and the evolution of 6-year-average effective thermal power are shown in Figure 5.15. In fact, for each

of three t_{ad}, the optimization process converges to extremely similar input parameters for the final six strategies of simplex. The standard deviations of inputs relative to the respective length of variation are all smaller than 5%. In particular, the output is the minimal $t_{e,2SFR}$ under the optimization. The discrepancy on this quantity is extremely small. Given the small discrepancies of inputs, one of these optimal strategies in the final simplex is taken for each t_{ad} to be shown in Table 5.3.

t_{ad}	$t_{e,MIX}$	$t_{s,2SFR}$	$t_{e,2SFR}$	BU_{UOX}	BU_{MIX}	Output ($t_{e,2SFR}$)
2065	2078	2114	2120	31.9	41.7	2120
2085	2088	2113	2120	33.8	43.4	2120
2100	2101	2118	2140	48.6	54.4	2140
(Unit)	year	year	year	GWd/t	GWd/t	year

Table 5.3: Values of inputs and output of optimal adaptation (by clustering) for the minimization of $t_{e,2SFR}$ in **SCN MIX2SFR** with respect to three t_{ad}

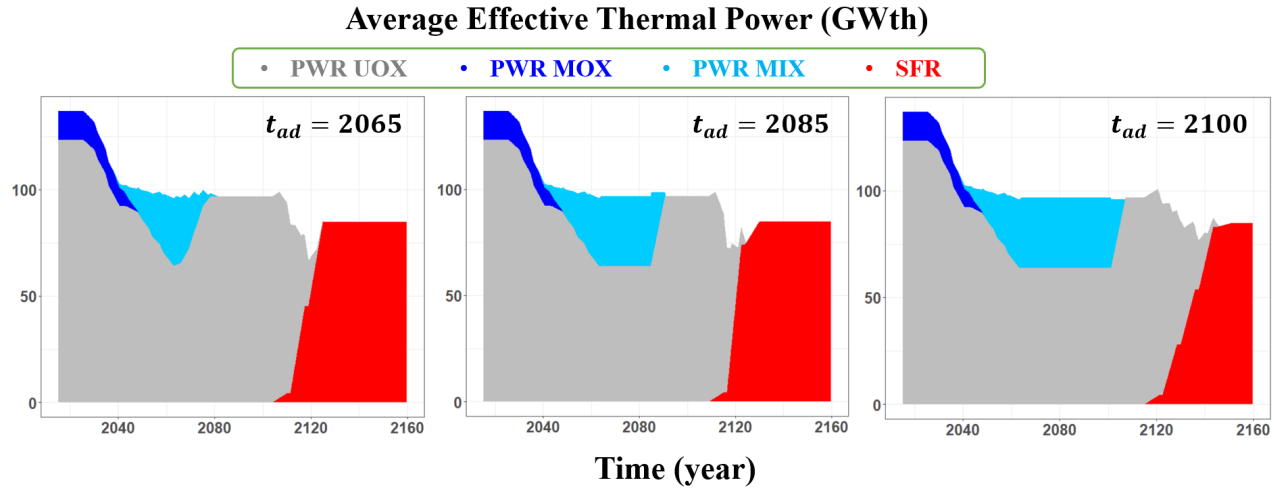

Figure 5.15: Effective thermal power evolution of optimal adaptation (by clustering) for the minimization of $t_{e,2SFR}$ in **SCN MIX2SFR** with respect to three t_{ad}

This optimization process indicates directly that the adaptation from 2065 and from 2085 can finish the substitution for EPR-fleet with SFRs by year 2120, as early as it does in **TRJ SFR** when the plutonium multi-recycling is not considered for PWR/EPR. Figure 5.15 may presents some delay after 2120 due to the respect of irradiation cycle and the average process. Even though $t_{e,2MIX}$ can be numerically determined, its uncertainty is indeed in the same magnitude of one SFR irradiation cycle and the exact value should not be over-interpreted. In contrast, the adaptation from 2100 leads to later completion of substitution. From the viewpoint of timeliness on the SFR deployment for 100% of fleet, the adaptation based on the prior trajectory **TRJ MIX** can be robust if necessary readjustments are taken before the end of century. This result relies on the assumption that the fleet can be as flexible as supposed on the ranges of input variation for the modification. To achieve these early $t_{e,2SFR}$, all optimal adaptive strategies suggest an early $t_{e,MIX}$, late $t_{s,2SFR}$ and low BU_{UOX} (except BU_{UOX} of $t_{ad} = 2100$), in order to accumulate more efficiently in-cycle plutonium inventory for SFR deployment. In fact, the production of plutonium by UOX irradiation is nearly compensated by the incineration by MIX irradiation, and thus the stop of MIX loading frees the fleet from plutonium incineration. Meanwhile, the plutonium production under

low BU_{UOX} of UOX is more efficient than in the SFR irradiation, implying the tendency of late $t_{s,2SFR}$.

The BU_{UOX} of $t_{ad} = 2100$ is measurably higher than the optimal strategies of other two t_{ad}. There can be two principal explanations. One is the use of different initial guess to start the iteration. In fact, the initial guess of inputs used for $t_{ad} = 2065$ and $t_{ad} = 2085$ are all at the low levels within the variation ranges. Because the minimum of output ($t_{e,2SFR}$) is achieved, no other guess is tested. But this initial guess for the optimization of $t_{ad} = 2100$ converges to an adaptation with missloads. Thus, another guess supposing high levels of all inputs is used. The second guess converges to the optimal adaptive strategy presented above, in a process where BU_{UOX} decreases progressively. As mentioned, this optimization algorithm does not guarantee with 100% certainty the achievement of global optimum, and an adaptive strategy of $t_{ad} = 2100$ resulting in $t_{e,2SFR} = 2120$ without missload may exist. But given the results of these two guesses, we can infer that such optimum suffers an extremely high risk of plutonium shortage over time if exists, and the biases of modelling and other uncertainties can break easily the validity of strategy. This will be further discussed in the following analyses of material evolution. Hence, no further effort is devoted to exploring other better-performing adaptation for $t_{ad} = 2100$.

The other reason involves the synchronization of macro reactor, similar to which is explained in Section 4.4. $t_{s,2SFR} = 2118$ is only 18 years after $t_{ad} = 2100$, equivalent to around five irradiation cycles of PWR. Because the demand of plutonium for SFRs rises significantly afterwards, it is crucial to provide sufficient plutonium in the good timing. Within the same number of cycles, the higher is BU_{UOX}, the larger available plutonium quantity is produced. In contrast, low BU_{UOX} only produces more plutonium than high BU_{UOX} with higher number of cycles under a period long enough, which is not necessarily the case here. Due to the respect of cycle length, low BU_{UOX} in this case may lead to a later time for the same or higher available plutonium inventory, which can result in possible missloads. Based on these two factors, a $BU_{UOX} = 48.6$ GWd/t for $t_{ad} = 2100$ is reached.

5.2.3.2 Reactor lifespan during the transition of fleet substitution with SFRs

Related to the fleet substitution for EPRs with SFR deployment, the estimation of EPR lifespan can be the first interest. An identical process as done in **TRJ SFR** illustrated in Section 5.1.2.1 is considered. There is a slight difference: 31 EPRs are installed by 2060 instead of 30, because no SFR is deployed. As a reminder, no lifespan limit is imposed for EPRs in this schema, in order to simplify the analysis. According to the fleet transition shown in Figure 5.15, the EPR lifespans in these three cases of t_{ad} are presented in Figure 5.16.

For all three cases in Figure 5.16a, the first decommissioning EPR seems singular, which requires a much longer life than others. This EPR is assumed to start operation in 2030. As the first EPR, it is old compared with others. If it starts decommissioning at the age of 40 by 2070, the new-built EPR that replaces it (before deploying any SFR) may be operated for more than 50 years after the decommissioning in 2120 (as the last built EPR, and thus being the last one to start decommissioning). Given the very short interval of decommissioning time of adjacent EPRs, the ages of other EPRs are not measurably influenced by the replacement with this new-built EPR in this case.

In the trajectories of $t_{ad} = 2065$ and $t_{ad} = 2085$, the ages of most of EPRs range from 65 to 70 years, slightly higher than the current estimation of acceptable life limit of nuclear power plant. A reasonably longer life of operation than the current

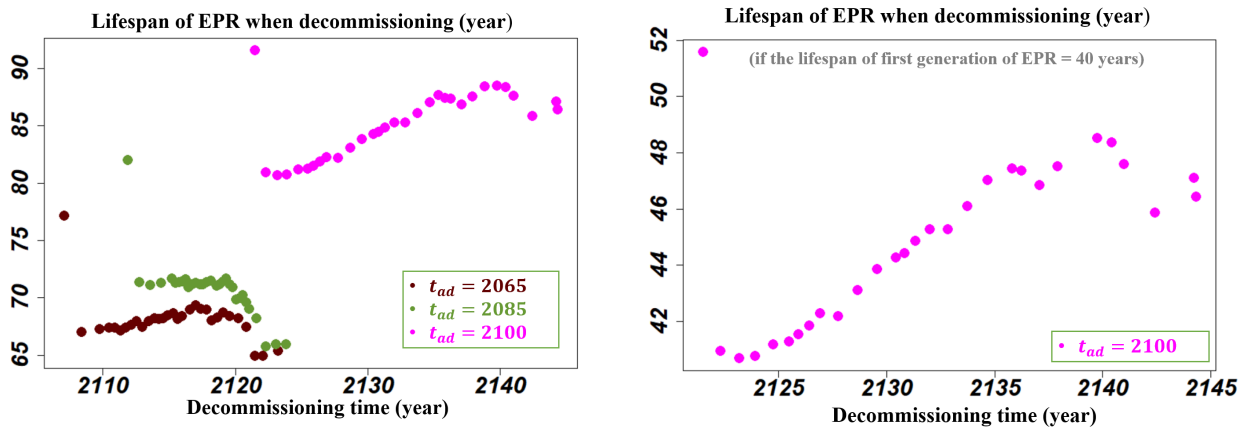

Figure 5.16: Estimation of EPRs lifespans during the transition towards SFR fleet, corresponding to the optimal adaptive strategies of three t_{ad}: (a) no limit is imposed for EPRs; (b) for $t_{ad} = 2100$, 40 years as lifespan limit is imposed for the first generation of EPRs.

estimation can be expected for EPRs. However, it can be somehow problematic for $t_{ad} = 2100$. If they are divided into two generations, each of them share only 40 years of operation as shown in Figure 5.16b. This is more coherent with the current estimation of reactor lifespan, while the industry may expect a longer life of EPRs to be more profitable. In fact, in the trajectory of adaptation from 2100, SFRs start replacing EPRs from 2118 till 2140. If a life limit of 40 years is imposed for the first generation of EPRs (constructed between 2030 and 2060), a large part of them are still young when the replacement with SFRs begins. It implies that the beginning of next century is not necessarily a good timing for massive SFR deployment.

5.2.3.3 Material evolution

Similar to the analysis of prior trajectories, material evolution help assess the performance of adaptive strategies from different angles. Total-cycle plutonium, idle plutonium in interim stocks, cumulative consumption of natural uranium and total-cycle MA of optimal adaptive strategies are shown in Figure 5.17, in comparison with that of **TRJ SFR** which does not consider a-priori the plutonium multi-recycling in PWRs.

Figure 5.17a shows the evolution of total-cycle plutonium, mainly accounted by in-cycle plutonium that is valorizable for SFR fuel fabrication. Due to the adaptation of quick stop of MIX fuels and low burn-up of UOX, the accumulation of plutonium is much faster than that in **TRJ SFR**. In the macro-SFR producing approximately 46.5 GWe, around 350 tons of plutonium is needed for each irradiation cycle. In consideration of the temporality of recycling, about 700 tons of plutonium in cycle is essential for a 100% fleet of SFRs. This figure shows the dynamic change of how this availability of plutonium can be achieved with adaptation. The multi-recycling of plutonium in PWRs stops or even slightly reduces the accumulation of plutonium. It is therefore evident that the longer is the period for the use of MIX in PWRs, the later will the EPR-fleet be substituted with SFRs.

These three optimal adaptations share indeed a very similar slope of plutonium accumulation. For $t_{ad} = 2100$, the plutonium inventory in the cycle (excluding the plutonium in the wastes, and it is very close to the total-cycle quantity) seems extremely difficult to reach 700 tons before 2120 with this production rate. The estimation of 700 tons for 100% fleet of SFRs is actually approximate.

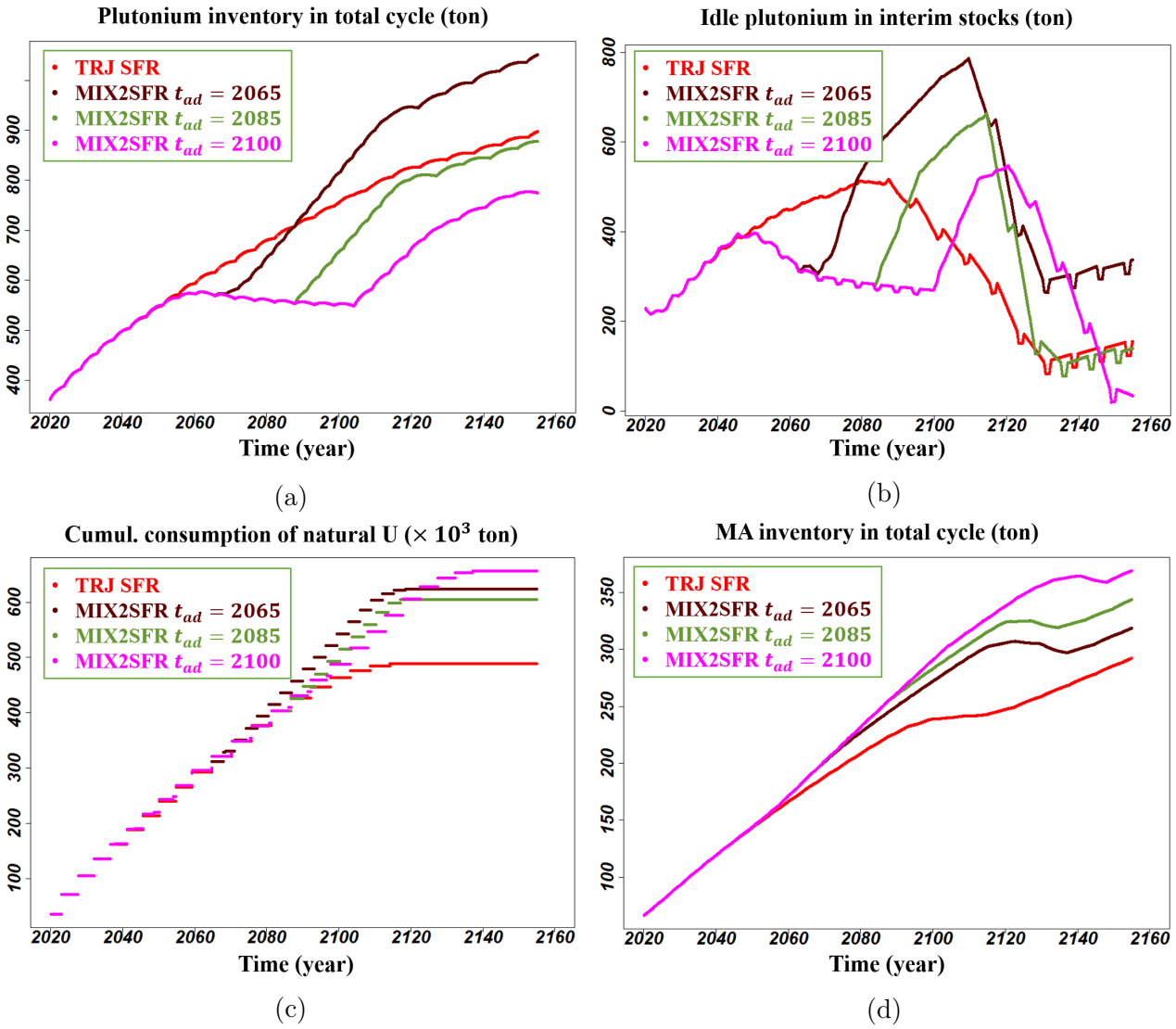

Figure 5.17: Evolution of materials in the optimal adaptive strategies in **SCN MIX2SFR** and the comparison with the trajectory **TRJ SFR**: (a) plutonium inventory in total cycle; (b) idle plutonium inventory in interim stocks; (c) cumulative consumption of natural uranium; (d) MA inventory in total cycle

Even though the adaptation of $t_{ad} = 2100$ can replace the fleet by 2140 when in-cycle plutonium reaches 700 tons, Figure 5.17b shows the high risk of miss-load. Intuitively, even if a robust adaptation suggesting $t_{e,2SFR} = 2120$ may exist for $t_{ad} = 2100$, the risk of plutonium shortage can be more severe.

Figure 5.17c shows the cumulative consumption of natural uranium resources. The stabilized level is generally much higher than **TRJ SFR**, because all of them consider very late deployment of SFR. This implies a much higher consumption of uranium resources in the 100% PWR UOX fleet. In case of the re-estimation of uranium scarcity, this larger need of uranium resource than that in **TRJ SFR** should be anticipated.

As for the accumulation of total-cycle MA, trajectories with optimal adaptations lead generally to a higher inventory than that in **TRJ SFR**, as shown in Figure 5.17d. It can be explained by the rapid increase under the use of MIX fuels. After the fleet substitution with SFRs, the MA inventory in total cycle of all these trajectories share approximately the same slope of increase. Thus, the regrets from the adaptation time on MA accumulated in total cycle can be measured by the discrepancies between these parallel evolution.

5.2.3.4 Capacity of related facility

Requirements on the capacity of front-end and back-end facilities should be also investigated for these adaptive strategies. Due to the fact that CLASS transports instantly the materials in responding to the demand of associated facility, the normalized by the duration between two adjacent demands is performed as suggested in Section 5.1.

For the fabrication capacities, only the annual fabrication of fresh SFR fuels for the active core (the SFR MOX, without the consideration of blanket) is shown in Figure 5.18, in comparison with the level in **TRJ SFR**. But it is also important to realize that the use of MIX is rapidly stopped, implying a relatively short period of the operation of fabrication plant for MIX, and a requirement of increasing capacity for fresh UOX fabrication.

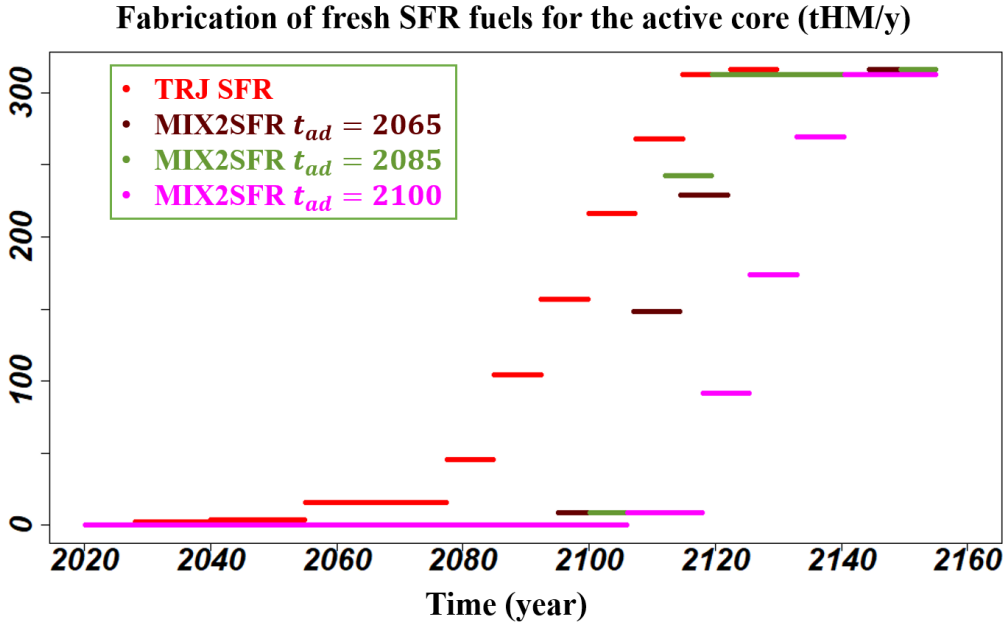

Figure 5.18: Annual fabrication of fresh SFR MOX fuels for the active core of optimal adaptive strategies in **SCN MIX2SFR**, in comparison with **TRJ SFR**

The final levels of fabrication capacities shown in Figure 5.18 are similar when the fleet transition finishes for all cases. For $t_{ad} = 2065$ and $t_{ad} = 2085$, the transition is short, and thus the fabrication capacity has to rise rapidly.

For the reprocessing capacities, because CLASS is not able to mix the spent fuels from different stocks in given fractions and because it responds to instant demands, unrealistic peaks of spent UOX reprocessing appear and are not presented here. These peaks can reach several thousands tHM/y, due to the reprocessing of spent UOX fuels with low plutonium content for the fabrication of high-plutonium-content fresh SFR fuels. The peaks may be smoothed by anticipation in advance or mixture of spent fuels. Nevertheless, these peaks are even one time higher than that of **TRJ SFR**, which means stricter constraints on the reprocessing of spent fuels than **TRJ SFR** should be anticipated.

5.2.3.5 Possible robust strategies with softer readjustments

In comparison to the timeliness of SFR deployment for 100% fleet in **TRJ SFR**, the adaptation on prior **TRJ MIX** in 2065 and in 2085 can be robust, which means the fleet substitution with SFRs is able to finish by 2120 ($t_{e,2SFR} = 2120$). But the optimal strategies previously identified suggest a relatively short transition of deployment, lasting about two cycles of SFR irradiation. This rapid modification

of fleet may be unrealistic or difficult from the economic and engineering point of view.

One may be interested in softer conditions of fleet transition for $t_{ad} = 2065$ and $t_{ad} = 2085$, subject to robust adaptation, i.e. $t_{e,2SFR} = 2120$. For instance, the starting time of SFR deployment $t_{s,2SFR}$ can be brought forward. Based on the physical analysis above, such robust adaptive strategies exist due to the rapid accumulation of in-cycle plutonium over the inventory needed for total fleet of SFRs.

Because the previous output $t_{e,2SFR}$ is also an input variable, the optimization algorithm can still be used to search for other inputs by presetting $t_{e,2SFR} = 2120$. Here the minimization of $t_{s,2SFR}$ can be supposed for a slower transition to lighten the burden of fleet replacement. Using the Nelder-Mead optimization, $t_{s,2SFR}$ is regarded as the new output, and robust adaptive strategies (thus subject to $t_{e,2SFR} = 2120$) that minimize $t_{s,2SFR}$ for $t_{ad} = 2065$ and $t_{ad} = 2085$ are identified. The final simplex of optimization converge to very similar strategies, and the mean values of inputs (and outputs) are presented in Table 5.4. The transition can be viewed in Figure 5.19.

t_{ad}	$t_{e,MIX}$	$t_{s,2SFR}$	$t_{e,2SFR}$	BU_{UOX}	BU_{MIX}	Output ($t_{s,2SFR}$)
2065	2066	2077	2120	47.7	59.2	2077
2085	2088	2087	2120	31.8	42.1	2087
(Unit)	year	year	year	GWd/t	GWd/t	year

Table 5.4: Mean values of inputs and output of robust adaptations ($t_{e,2SFR} = 2120$) that minimize $t_{s,2SFR}$ in **SCN MIX2SFR** with respect to $t_{ad} = 2065$ and $t_{ad} = 2085$

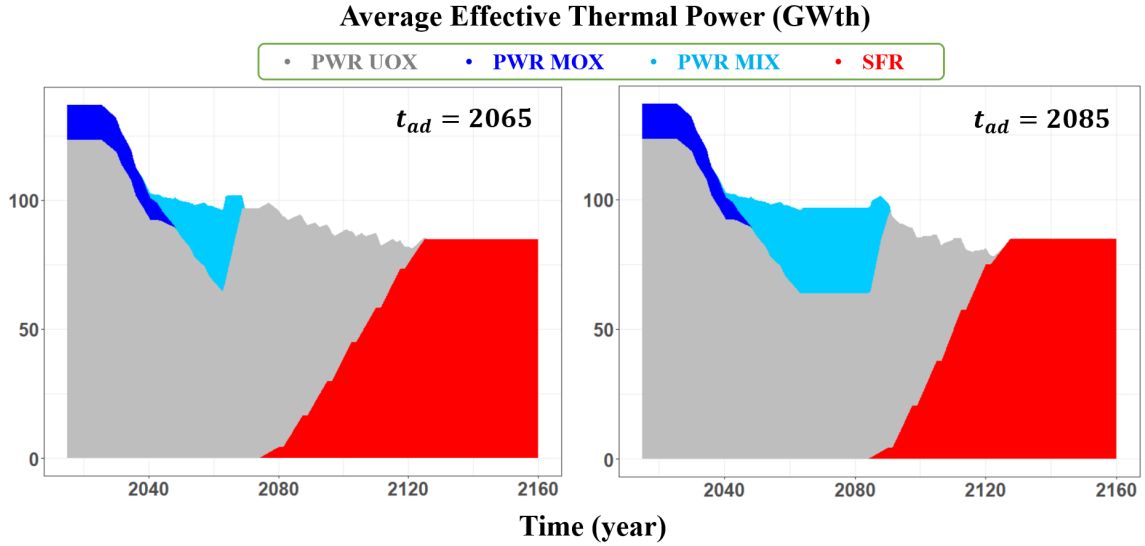

Figure 5.19: Fleet transition of robust adaptations ($t_{e,2SFR} = 2120$) that minimize $t_{s,2SFR}$ in **SCN MIX2SFR** with respect to $t_{ad} = 2065$ and $t_{ad} = 2085$

The existence of robust adaptive strategies allowing slower transition paces is verified. Compared with the previous robust adaptations identified in Table 5.3, these trajectories of robust adaptations can deploy SFRs within several irradiation cycles instead of a quick replacement, allowing sufficient engineering and industrial feed-backs and improvements. But the smoothness of transition is traded with an immediate stop of the use of MIX, in order to accumulate sufficient plutonium in the cycle.

Due to an earlier starting of SFR deployment, the first few decommissioning EPRs may be younger than that shown in Figure 5.16. The compromise between the lifespan for the maximization of economic profits of EPRs and the reasonable paces of transition depends on the interest and estimations of stakeholders.

5.2.3.6 Summary of adaptive robustness assessment of strategy in SCN MIX2SFR

In this adaptation scenario study, robust strategies adapting the prior trajectory **TRJ MIX** can be identified for the adaptation time of year 2065 and 2085, but not for 2100. In other words, if the adaptive actions are taken from the time before 2085, the substitution of EPR-fleet with SFRs can be achieved by 2120. But as shown by the analyses of these trajectories, rapid and large modifications of fleet are required, because the prior use of MIX fuels stopped the accumulation of in-cycle plutonium for SFR. In the transition phase of these adaptations, the EPRs have generally an age higher than the current estimation of life limit for nuclear power plants; in particular, during the optimal adaptation of $t_{ad} = 2100$ (but not robust), it is not evident about how to optimize the fleet update regarding the age of EPRs. These options of adaptation also lead to larger consumption of natural uranium resources and higher accumulation of MA inventory in total cycle.

Other alternative robust adaptations are also identified for $t_{ad} = 2065$ and $t_{ad} = 2085$, suggesting earlier start of SFR deployment and thus a smoother transition. To allow this, the use of MIX in EPRs are stopped right after t_{ad} in order to accumulate efficiently the plutonium for SFR deployment.

5.2.4 Analysis of adaptation scenario SCN SFR2MOXEUS

This adaptation scenario study adapts the prior trajectory **TRJ SFR** to the plutonium multi-recycling in PWRs/EPRs, halting the start of new SFRs. The optimization aims to identify the adaptations that maximizes the use of idle plutonium among all possible adaptive strategies. In practise, the maximum between year 2140 and 2160 of 6-year-average inventory of plutonium in all interim stocks is considered, denoted as $Pu_{idle,max}$. The minimization of this maximal level implies that the plutonium inventory outside the core waiting for the reuse can be guaranteed under a certain level. In particular, it is useful to compare with the prior trajectory **TRJ MIX**, in which the plutonium is always multi-recycled in PWRs/EPRs instead of being accumulated for SFR deployment. Based on this comparison, the adaptive strategy that leads to lower $Pu_{idle,max}$ than that of **TRJ MIX** can be considered robust.

MOXEUS is used for the plutonium multi-cycling in EPRs, allowing the variation of plutonium content in the fresh fuels. Instead of using MIX as in **TRJ MIX**, the use of MOXEUS model aims to adapt to the possibly large variability of plutonium quality when different types of spent fuels involve in the recycling.

5.2.4.1 Optimal transition

The Nelder-Mead optimization is used for the minimization of $Pu_{idle,max}$ in the exploration space as described in Table 5.2. For each of three t_{ad}, the optimization process converges to the identical optimal adaptation for the final simplex. The values of inputs and outputs of these are presented in Table 5.5, and their fleet transition are shown in Figure 5.20.

The optimal adaptive strategy for $t_{ad} = 2065$ suggests a EPR-fleet with more than 50% loaded by MOXEUS fuels, while the others are loaded by UOX. The duration to reach this fraction lasts around 20 years.

t_{ad}	$FrMXE_{inPWR,f}$	$t_{e,2MIX}$	BU_{UOX}	BU_{MXE}	Output ($Pu_{idle,max}$)
2065	52.8	2087	40.2	37.5	17
2085	34.3	2096	40.1	36.8	174
2100	33.4	2105	38.9	40.0	332
(Unit)	%	year	GWd/t	GWd/t	ton

Table 5.5: Mean values of inputs and output of optimal adaptive strategies in **SCN SFR2MOXEUS** with respect to three t_{ad}

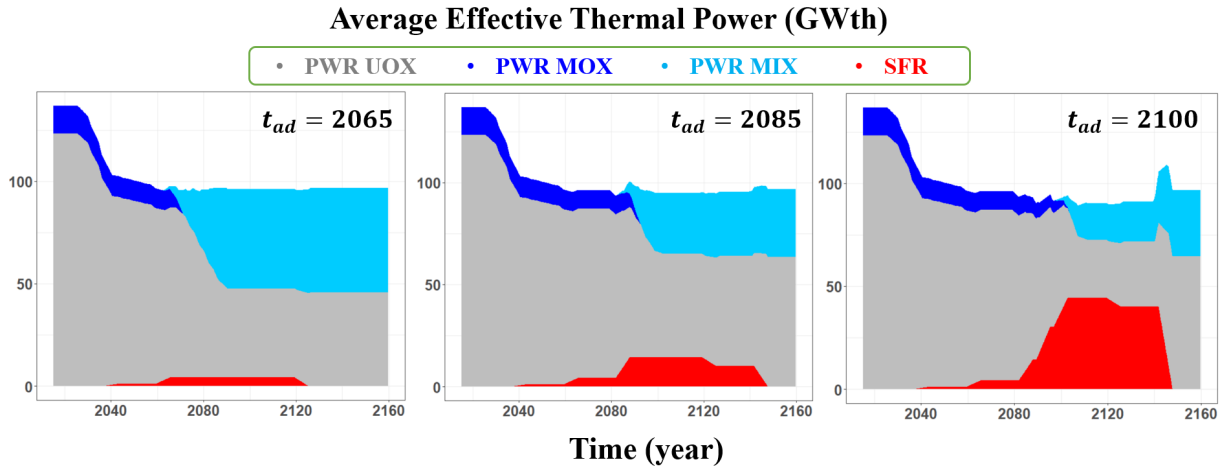

Figure 5.20: Effective thermal power evolution of optimal adaptation for the minimization of Pu_{idle} in **SCN SFR2MOXEUS** with respect to three t_{ad}

For the adaptations of other two t_{ad}, the configuration of EPR-fleet is similar to that in **TRJ MIX**, in which 34% of EPRs are loaded with MOXEUS/MIX. Moreover, the transition to reach this fraction is much shorter than the case of $t_{ad} = 2065$.

One may note that the burn-ups of two fuels are relatively low. Even though the production of plutonium by UOX irradiation under this low BU_{UOX} can be at an globally fast level, the low BU_{MXE} with this sufficiently high fraction $FrMXE_{inPWR,f}$ is able to absorb in time the plutonium produced and incinerate them efficiently.

For the performance regarding the output $Pu_{idle,max}$, the optimal adaptive strategies of three t_{ad} lead to respectively 17, 174 and 332 tons of plutonium as the maximal level in interim stocks between 2140 and 2160. Actually, due to the use of MOXEUS in such fraction, the total idle plutonium reaches or almost reaches the stabilization. In comparison, in the prior trajectory **TRJ MIX** without the accumulation of plutonium for SFR deployment, the idle plutonium is stabilized at around 250 tons. From the viewpoint of maximizing the use of plutonium, the optimal adaptive strategy of $t_{ad} = 2065$ and $t_{ad} = 2085$ are robust. But the extremely low $Pu_{idle,max}$ of $t_{ad} = 2065$ indicates a high risk of plutonium shortage if all parameters remain the same afterwards. In practise, the fleet can be further adapted with progressive adjustments on the share of two fuel types or the enrichment of ^{235}U in MOXEUS to avoid the missload. The one of $t_{ad} = 2100$ leads to higher inventory of idle plutonium out of use at a given time after 2140, and it is thus less performing and not robust. In fact, if the adaptive strategy is implemented from 2100, a measurable part of fleet is composed of SFRs. When all SFRs start decommissioning in 2140, the discharge of spent SFR fuels can be significant, accounting for a considerable part of idle plutonium when they are moved to interim stocks for subsequent reprocessing.

5.2.4.2 Material evolution

For the material evolution of these three optimal adaptive strategies, the plutonium inventory in total cycle and in interim stocks (idle plutonium), the cumulative consumption of natural uranium and the MA inventory in total cycle are studied. Their evolution are compared with the prior trajectory **TRJ MIX**, shown in Figure 5.21.

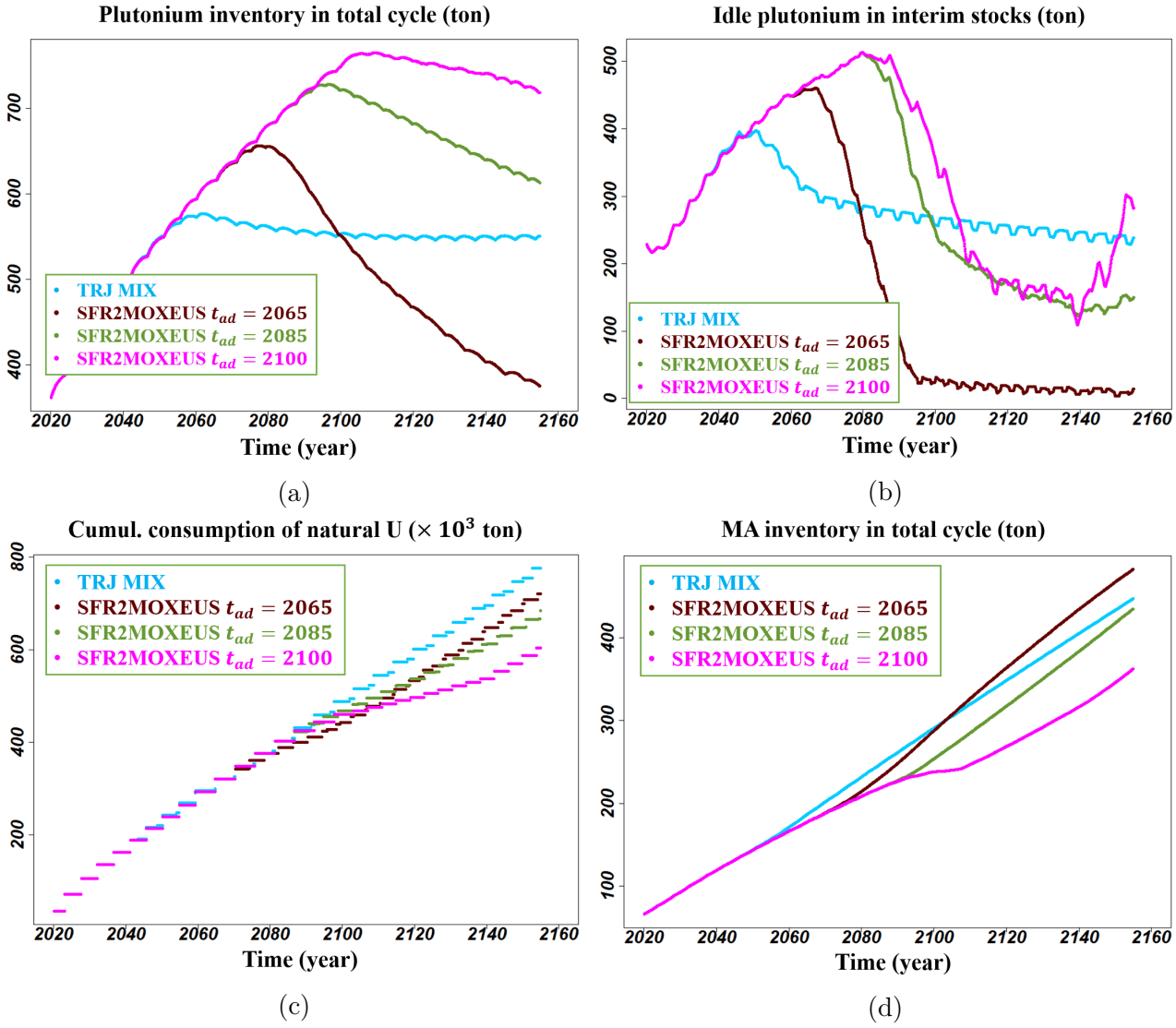

Figure 5.21: Evolution of materials in the optimal adaptive strategies in **SCN SFR2MOXEUS** and the comparison with the trajectory **TRJ MIX**: (a) plutonium inventory in total cycle; (b) idle plutonium inventory in interim stocks; (c) cumulative consumption of natural uranium; (d) MA inventory in total cycle

For the plutonium inventory in total cycle in Figure 5.21a, three optimal adaptive strategies are able to incinerate it when the fraction of MOXEUS in EPR-system reaches $FrMXE_{inPWR,f}$. It is much different from the use of MIX fuels in **TRJ MIX**, in which the plutonium in total cycle is stabilized. The adaptation from 2065 incinerates the plutonium much more efficiently than other two cases due to the higher fraction of MOXEUS. By the end of scenario, the total-cycle plutonium in this trajectory decreases to the current level.

The incineration of plutonium implies a considerable consumption of available plutonium in the stockpiles, verified in Figure 5.21b. During the transition when the fraction of MOXEUS in EPR-system increases, the inventory of idle plutonium decreases rapidly. When the final fraction is achieved, this inventory seems near

to the stabilization. As verified, the idle plutonium of adaptation from 2065 is kept at a very low level. In this trajectory, $^{235}\mathrm{U}$ in MOXEUS fuels should be enriched up to several percents, because there is not enough plutonium to reach the given burn-up. For the adaptation from 2100, the idle plutonium meet two abrupt increments between 2140 and 2160. They can be explained by the discharges of spent SFR fuels from the prior two irradiation cycle to 2140, when SFRs still accounted for nearly a half of electricity production from nuclear power, as shown in Figure 5.20. These two discharges release nearly 200 tons of plutonium in total for the later use, without recycling into SFRs. It is particularly the second discharge that leads to a higher idle plutonium inventory than that of **TRJ MIX**. In fact, the plutonium content in SFR fuels is higher than that in MOXEUS fuels. More importantly, the MOXEUS fraction in this trajectory is much lower than the SFR share in 2100. Therefore, it is not surprising that these two discharges without the recycling in SFRs lead to considerable increase of idle plutonium for $t_{ad} = 2100$ in this time interval. Nevertheless, this scenario is simplified for the simulation, like simultaneous decommissioning of a large number of SFRs by 2140. In the real application, a successive decommissioning plan may absorb somehow these increment peaks and probably avoid the unacceptable accumulation of idle plutonium.

The cumulative consumption of natural uranium resources in Figure 5.21c in these three trajectories of **SCN SFR2MOXEUS** and in the prior **TRJ MIX** have a similar evolution pattern. It is the longer phase of SFR deployment in the trajectory of adaptation from 2100 that mitigates the consumption of uranium; but after the adaptation, the evolution of consumption rises with a larger slope.

The evolution of MA in total cycle in Figure 5.21d in these four trajectories also share a similar tendency. Due to a higher fraction of MOXEUS, the trajectory of adaptation from 2065 produces faster MA than other trajectories. It is worth noting that in this trajectory, the inventory of MA is even higher than plutonium in total cycle from the middle of next century. In case of this disruption, this higher production of MA should be anticipated.

The cumulative consumption of natural uranium and the production of MA in total cycle highlight the difference of using MOXEUS and MIX. Because it is variable in MOXEUS, the plutonium content increases first before enriching $^{235}\mathrm{U}$ for the target burn-up, which can be higher than the 9.54% in the MIX design considered in this chapter. In other words, MOXEUS fuels tend to prioritize the use of plutonium over the enriched $^{235}\mathrm{U}$. Thus, the consumption of natural uranium by using MOXEUS seems never faster, whereas the slope of MA accumulation in total cycle can be measurably larger than that in **TRJ MIX**.

5.2.4.3 Capacity of related facility

Similar to the analysis in **SCN MIX2SFR**, only the fabrication concerning the MOXEUS fuels for the trajectories of adaptation and the MIX fuels for **TRJ MIX** are analyzed, as shown in Figure 5.22. The requirements on the annual fabrication capacity in the trajectories of these three optimal adaptive strategies are generally higher than that in **TRJ MIX**. For the adaptation from 2065, it is principally due to the higher fraction of MOXEUS than 34% of MIX in **TRJ MIX**. Furthermore, a lower burn-up of MOXEUS implies shorter irradiation cycle. Therefore, for a similar demand of total quantity, shorter irradiation cycle for the adaptation requires averagely a higher capacity of annual fabrication.

In terms of the reprocessing capacity, similar remarks can be noted. The reprocessing of spent UOX fuels for large demand of plutonium requires very high reprocessing capacity, and the peak can reach one time higher than the peak

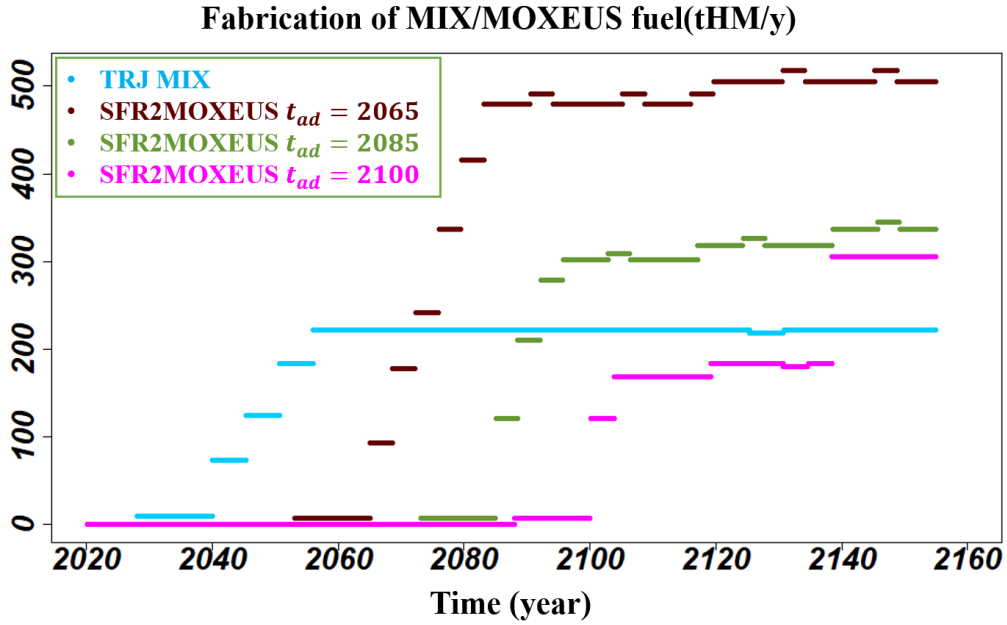

Figure 5.22: Annual fabrication of fresh MOXEUS fuels for the trajectories of optimal adaptive strategies in **SCN SFR2MOXEUS**, in comparison with the MIX fabrication in **TRJ MIX**

identified in **TRJ MIX**. Mixture of plutonium from different types of spent fuels and keeping relatively high reprocessing in advance may smooth these peaks.

5.2.4.4 Summary of adaptive robustness assessment in SCN SFR2MOXEUS

This adaptation supposes the disruption to SFR deployment, halting the start of new SFRs. To minimize the idle plutonium inventory, the multi-cycling by PWR MOXEUS is considered. The Nelder-Mead optimization is used to identify the fraction of MOXEUS, the time to reach this fraction and the burn-ups of UOX and MOXEUS that minimize the maximal-idle-plutonium during the last 20 years. The results are compared with the stabilization level of idle plutonium in **TRJ MIX**, in which plutonium is not accumulated for SFR. It shows that the optimal adaptations before year 2085 can keep always a lower level of idle plutonium than in **TRJ MIX**, and thus they are considered robust. In the trajectory of adaptation from 2100, the idle plutonium is accumulated over the comparison level, due to the discharge of a large number of decommissioning SFRs.

The optimal adaptive strategy of $t_{ad} = 2065$ suggests more than 50% of EPRs loaded with MOXEUS, a fraction much higher than other cases. This high fraction leads to a rapid drop of plutonium in total cycle and keeps interim stocks nearly empty. For the optimal adaptations of other two t_{ad}, the plutonium in total cycle decreases progressively, but it is still higher than the stabilization level achieved in **TRJ MIX**. Due to the delay of multi-recycling plutonium in EPRs (and potentially a priority of adding plutonium in MOXEUS), the cumulative consumption of natural uranium in the trajectories of MOXEUS adaptation is always lower than in **TRJ MIX**. However, the MA in total cycle may rise faster than the use of MIX, over or close to the plutonium inventory depending on t_{ad}.

Last but not least, a fabrication capacity higher than **TRJ MIX** for the adaptation may be required. It can be explained by the shorter MOXEUS irradiation cycle suggested by the optimal adaptive strategies identified. Similarly, the peaks of reprocessing should be anticipated, and this can be smoothed by adaptable reprocessing planning by mixing the plutonium from different types of spent fuels in advance.

5.3 Conclusion of this chapter

This chapter applies the methodology of robustness assessment to strategies that may be compared to the French national ones. A set of outputs are analyzed in order to provide a comprehensive assessment of strategy.

Based on the historical trajectory and current strategy, two prior trajectories for the pre-disruption scenario are considered: one focuses on the plutonium multi-recycling by using MIX fuels in PWRs/EPRs, denoted as **TRJ MIX**; while the other considers an accelerated planning of SFR deployment, denoted as **TRJ SFR**.

For **TRJ MIX**, a disruption to the use of MIX fuels is supposed, reconsidering the SFR deployment. The following adaptation aims to substitute the EPR-fleet with SFRs by year 2120, as fast as the trajectory **TRJ SFR** which never uses MIX fuels. Using the Nelder-Mead optimization, optimal adaptive strategies that minimizes the time $t_{e,2SFR}$ when SFRs are deployed in the whole fleet are identified for three adaptation times: year 2065, 2085 and 2100. Ultimately, the regret of using MIX fuels relative to the reconsideration of SFR deployment is principally presented on the plutonium availability. Within necessarily fast modification of the fuel cycle, the delay of plutonium accumulation can be well offset and absorbed, and the substitution may finish if it is adapted before year 2085. From the viewpoint of SFR deployment timeliness, the French national strategy of plutonium multi-recycling in PWRs by MIX fuels can be robust if an appropriate adaptation plan can be carried out before 2085. Otherwise, more time is needed to replace all EPRs if the adaptation begins from 2100. The lifespans of EPRs are slightly longer than the current estimations if **TRJ MIX** is adapted before 2085 but still adaptable. For the later adaptation, however, it is difficult to respect the appropriate lifespan interval.

Regardless of the adaptive robustness of early adaptation, there is definitively a higher demand of natural uranium resource and more MA is produced in total cycle in all trajectories of adaptation than that of **TRJ SFR**. It can be explained by the need of $^{235}\mathrm{U}$ enrichment and a higher MA production from the use of MIX fuels. Moreover, a similar fabrication capacity for SFR fuels is demanded as that in **TRJ SFR**, except that the transition is shorter. But a much higher mass flow of reprocessing may be needed if the SFR deployment is not anticipated sufficiently in advance.

Another prior trajectory **TRJ SFR** is also disrupted. After the disruption, the start of new SFR is halted, and the plutonium multi-recycling in EPRs using MOXEUS fuels aims to maximize the use of plutonium. To achieve this, adaptive strategies are explored to minimize the maximal level of idle plutonium during the last 20 years of scenario. To determine the adaptive robustness, this level is compared with the approximately stable level in **TRJ MIX**, in which the plutonium is not accumulated for SFR. From this angle, the prior strategy of SFR deployment is robust if necessary adaptations are taken from 2085 or earlier. Particularly, the optimal adaptation from year 2065 suggests more than 50% of EPRs loaded with MOXEUS, resulting in a rapid decrease of plutonium in total cycle and keeps the idle plutonium stocks almost empty. In case of a late adaptation like from year 2100, a large amount of plutonium will be discharged when SFRs start decommissioning, and it leads to a high inventory of plutonium out of use.

Due to a later deployment of MOXEUS than the use of MIX in **TRJ MIX**, the trajectories of adapting **TRJ SFR** consumes always fewer natural uranium cumulatively. Meanwhile, the use of MOXEUS may produce faster MA than MIX. As a result, the MA in total cycle of adaptation from 2085 or earlier increases faster than in **TRJ MIX**.

Chapter 6

Conclusion and Outlooks

The nuclear transition is an important part of national energy policy for the countries which depend on nuclear energy. After decades of nuclear power exploitation, several technologies can be considered for the future transition. The deployment of nuclear facilities and new technologies during the transition may last decades, having huge impacts on social, economic, temporal and spatial aspects: the investments for R&D and construction, decades of operation and maintenance, the management of significant radioactive materials and possible consequences on the environment, etc. To have a primary estimation of these impacts, national nuclear strategy decisions require detailed assessments by scenario studies.

As presented in a large number of electro-nuclear scenario studies, a broad spectrum of objectives leads to a diversity of pathways towards the undetermined futures. Under different objectives for nuclear future, some outcomes resulting from a given strategy simulation considered in one assessment study may be neglected or interpreted in different ways in another one. This may lead to contradictory criteria used in different assessments for the same strategy. One may lack a sufficiently clear vision about which objective is the most pertinent as it is deeply uncertain.

The ASTRID project in France and corresponding studies show such uncertainty for instance. In fact, the abortion of the ASTRID project illustrates the perspective change of nuclear technology for the next decades. From the physics point of view, the prospects of radioactive materials inventories and relevant management met considerable changes as well. But after these changes, no guarantee can be given yet to keep all constant for near terms.

Instead of staying on the deadlock considering only one single future, uncertainties should be well integrated in electro-nuclear scenario studies concerning the strategy assessments, keeping options open for future uncertain changes and possible adaptations. In this context, a methodology of strategy robustness assessment in electro-nuclear scenario studies under uncertainties of objectives has been developed inspired from the French nuclear fuel cycle, which is one of the countries having the highest electricity share on nuclear power.

Before any concrete assessment analysis, the framework and tools for analyses have been characterized, and relevant hypotheses and limits have been clarified. Notably, the modelling assumptions of CLASS used for dynamic simulations of fuel cycle in this work have been detailed. A preliminary scenario inspired from possible French fleet transitions have been studied, giving a basic understanding of the fuel cycle behaviors based on GSA. The fleet is always composed of PWR UOX and MOX in this scenario, while the total power, the MOX fraction, the timing of transition and other operational parameters are variable in large ranges. Morris method has been used to investigate the importance of

these variable parameters on several outputs. Some limits of the Morris method applied in electro-nuclear scenario studies have been revealed, principally due to the plutonium shortages in some trajectories defined in the DoE. Nevertheless, this preliminary analysis was able to rank the input parameters and to explain the fuel cycle responses to parameter variations.

Based on this paradigm, the disruption of objective has been regarded as an approach to take into account the objective uncertainties in electro-nuclear scenario studies. The framework of robustness assessment has been applied to the context where the objective of future SFR deployment was pre-selected (objective A), while a possibility of abrupt change of objective is considered. In case of disruption, nuclear wastes should be minimized without SFR (objective B). In this framework, two types of strategy robustness have been evaluated: the static robustness and the adaptive robustness.

The static robustness has been defined within a pre-disruption scenario study. A set of possible transition strategies have been explored in this scenario. They are called static strategies because the corresponding transitions are determined before any disruption, and thus lead to the outcomes without any strategy readjustment even if the disruption is considered. The static robustness of strategies indicates then their performance on both possible objectives, no matter which one is finally adopted in the future. For the adaptive robustness, a prior strategy before any disruption has been supposed; and in case of disruption, adaptive strategies have been considered from this prior trajectory. Based on this assumption, the adaptive robustness has been defined for the combination of two strategies, the prior one to be adapted, and the subsequent adaptation. A comparison threshold should be considered to indicate the adaptive robustness in this methodology. Conceptually, such threshold comes from the performance of a strategy that satisfies these following conditions:

- It was available in the pre-disruption scenario;
- It was consistent with the pre-selected objective (future SFR deployment here);
- If no readjustment is considered, it was supposed to be optimal for the objective after disruption, among all available strategies satisfying the foregoing two conditions.

In other words, this strategy indicated the best historical choice in case of disruption. The difference between the outcomes of the prior trajectory without adaptation and this threshold represents the regrets of implementing this prior strategy, regarding the new objective after disruption. Meanwhile, the difference between the outcomes after a specific adaptation and this threshold can be quantified as the performance of adaptive robustness, for such implemented prior strategy and the corresponding adaptive strategy. If the regrets aforementioned can be offset, such adaptation has been defined as robust adaptive strategy (based on a given prior trajectory), and its combination with the prior strategy has been considered adaptively robust.

This general framework is designed to be applicable in electro-nuclear scenario studies in order to build the solid methodology of robustness assessment. However, it still requires some adjustments in order to adapt to various features and assumptions in practical scenarios studies.

The methodology has been first developed in Chapter 3 within a family of scenarios that evaluated the strategies in year 2090. Inspired from possible transitions of the French fuel cycle, a pre-disruption scenario was designed from year

2015 to year 2090, in which the fleet transition strategies are explored. For the pre-selected objective A, the substitution ratio of fleet with SFRs, denoted as R_{Subs}, was evaluated in 2090 for the explored strategies. This quantity considers the available plutonium inventory in the cycle for a certain number of SFRs, and is normalized by the final fleet power level. Strategies dedicated to this objective should achieve $R_{Subs}(2090) \geq 1$. Meanwhile, regarding objective B in case of the disruption which is deeply uncertain, the transuranic inventory in total cycle and in the wastes, denoted as TRU_{tot}, should be minimized without SFR. This quantity in 2090 was regarded as the output of interest for this objective.

Corresponding to these two objectives, the performances of strategies in this pre-disruption scenario have been evaluated. PCA has been used to investigate the importance of input variable parameters on the number of missload as well as the two outputs of interest. The dominance of final total power $P_{tot,f}$, and the measurable effects of final MOX fraction $FrMOX_f$ and burn-up BU_{UOX} on R_{Subs} and TRU_{tot} in 2090 have been revealed. Graphical techniques such as pairs plots of inputs and outputs have also been used to complement the analyses. For the static robustness assessment, the Pareto front has been identified, presenting the optimal strategies with trade-offs on the maximization of R_{Subs} and the minimization of TRU_{tot} in 2090, subject to the condition $R_{Subs}(2090) \geq 1$. Due to the strong impacts of $P_{tot,f}$ on the two outputs, the Pareto front is achieved by a low but nearly constant $P_{tot,f}$, while the trade-offs vary over the choices of $FrMOX_f$ and BU_{UOX}. Strategies in this set were considered robust, depending on the compromises made for R_{Subs} and TRU_{tot} by 2090. Two extreme strategies on the Pareto front were chosen for their specific interest. One was the reference strategy that maximized R_{Subs}, the optimal strategy for the single pre-selected objective. It suggested a long transition towards a fleet of low $P_{tot,f}$, low $FrMOX_f$ and low BU_{UOX}, in order to accumulate rapidly plutonium in the cycle. The other one, called robust static optimum, minimized TRU_{tot} by 2090 under the condition $R_{Subs}(2090) \geq 1$. It suggested a short transition towards a fleet of low $P_{tot,f}$ but relatively high $FrMOX_f$ and high BU_{UOX}. In this trajectory, the available plutonium for MOX fabrication, which accounted for the major part of TRU_{tot}, was consumed as much as possible, presenting a risk of missload by 2090.

The adaptation scenarios supposed then the disruption and objective B was pursued. The TRU_{tot} in 2090 of the robust static optimum has been used as the comparison threshold relevant to the adaptive robustness in this scenario. The prior reference trajectory supposed to be optimal for the pre-selected objective before disruption has been adapted. Year 2040, 2050, 2060 and 2070 have been considered different adaptations times t_{ad}, accounting for the deep uncertainty of objective disruption. Extremely short transition towards phase-out or 100% MOX for all PWRs has been considered acceptable for future adaptations. In this studies, the duration of transition D, and $P_{tot,f}$ and $FrMOX_f$ were identified as the most important parameters for the TRU_{tot} minimization by 2090. The robust adaptations from this prior reference trajectory have been identified with $t_{ad} \leq 2060$, while no adaptive strategy was robust if $t_{ad} = 2070$. Equivalently, the combinations of the prior reference strategy with the appropriate adaptations have been assessed adaptively robust, and a time between year 2060 and 2070 have been determined as the time limit of robust adaptation. The temporality of adaptive robustness, defined as the duration between this time limit and the predetermined time for evaluation, was between 20 and 30 years.

To highlight the effect of the formulation and criterion uncertainty on the assessments, the objective B linked to the disruption has then been reformulated. In this study, the TRU inventory normalized by the cumulative electricity production, denoted as TRU_{tot}^{norm}, should be minimized in case of disruption. Compared

with TRU_{tot}, the use of TRU_{tot}^{norm} could be interpreted as an option to reduce the impact of the fleet power uncertainty, which has been considered uncontrollable but have a strong dominance on the extensive quantities like TRU_{tot}. As a direct result, the physical analyses revealed that $P_{tot,f}$ had little influence on TRU_{tot}^{norm}. Instead, $FrMOX_f$ and BU_{UOX} became the impactful ones. In regards to the output TRU_{tot}^{norm}, a different robust static optimum from that regarding TRU_{tot} has been identified. The robustness assessments then showed that in case of the disruption, it was very hard to reduce TRU_{tot}^{norm} from the prior reference trajectory by adaptations to a level lower than the one of the robust static optimum by 2090. Very few combinations of prior reference strategy and relevant adaptations could be adaptively robust. However, the low level from the robust static optimum has still been considered approachable by adaptations regardless t_{ad}. It was explained that TRU_{tot}^{norm} was strongly dependent on the use of plutonium, mainly characterized by $FrMOX_f$; and thus it could be approached by appropriately high $FrMOX_f$ after adaptation.

The comparison between two different formulations for the new objective after disruption has shown a measurable difference on the assessment results, and might potentially lead to divergent choices of strategy. The importance of the precision on scenario assumptions has therefore been highlighted.

In these scenario studies, the methodology of strategy robustness assessment assumed a connection between the strategy evaluation and a pre-determined time. The strategy evaluation at a pre-determined time used to be a common assumption in lots of project studies. Regardless, the relevant discussion showed that this might lead to assessment inconsistencies with different scenario time horizons.

The methodology has therefore evolved under new scenario studies, in order to disconnect strategy assessments from pre-determined time. This has guaranteed the inter-temporal consistency of analysis, as studied in Chapter 4. To achieve this, new outputs of strategies for the two objectives have been studied in the pre-disruption scenario: t_R standing for the time when R_{Subs} becomes higher than a given threshold, and t_{TRU} when TRU_{tot} gets higher than the relevant threshold. In this scenario, a strategy for objective A should achieve $t_R \leq 2090$, while taking precautionary measures for the disruption should yield $t_{TRU} \geq 2090$ (even though this value was not quantifiable in this scenario).

A statistical study using PCA has first investigated the consistency of input importance on t_R and t_{TRU}, over the choices of TRU_{tot} threshold to determine t_{TRU}, and over the choices of subsets regarding the quantification of t_R and t_{TRU}. In this study, two TRU_{tot} thresholds have been determined, and for each output studied (t_R or t_{TRU}), three subsets of valid strategies have been considered. The principal importance of $P_{tot,f}$ and the measurable effects of $FrMOX_f$ and BU_{UOX} on t_R and on t_{TRU} have been verified stable over all possible combinations of these two uncertain factors. Based on this statistical study, the strategy that minimizes t_R has been considered the reference strategy for the pre-selected objective A. But the determination of robust static strategies depended on the choice of TRU_{tot} threshold.

For the adaptation scenarios studies, the definition of strategy validity has also been adapted to the independence from pre-determined time. In fact, the time of the first missload has been defined as the time horizon of the corresponding trajectory. The first missload of valid adaptive strategies should then happen after the end of the new adaptive transition (or never had missload). We assumed that the low TRU_{tot} could be kept by phase-out after this missload. Moreover, the lowest TRU_{tot} by t_{ad} among those pre-disruption strategies achieving $t_R \leq 2090$

has been regarded as the threshold for adaptive robustness assessment. The time t'_{TRU}, when TRU_{tot} from the prior reference trajectory was led to be lower than this threshold, has been considered the output of interest. The combination of this prior strategy and those valid adaptation allowing t'_{TRU} achieved before the time horizon could then be considered adaptively robust.

Under these assumptions, adaptations from the prior reference trajectory have been first explored for year 2040. According to the definition of adaptive robustness in this study, only TRU-incineration adaptations could be of interest. For the valid adaptations, the lowest TRU_{tot} before the time horizon, denoted as TRU_{min}, and the time when it was achieved, denoted as t_{min}, have been investigated to help explain the fuel cycle behaviors and the results of t'_{TRU}. Due to the limited capability of TRU incineration of plutonium mono-recycling, extremely short transitions towards a fleet of relatively high $P_{tot,f}$ and high $FrMOX_f$ have been a necessary condition to be robust. To be simple, most of them suggested incinerating as much plutonium as possible by MOX during short term and then phase out.

Inspired from this analysis, the adaptability of pre-disruption strategies has been defined, standing for the fraction of robust adaptations in the adaptation space. Two indicators of adaptability have been deduced from the trajectories of pre-disruption strategies. The first one was $TRU_{eff}(t_{ad})$, the effective TRU inventory in total cycle by t_{ad} which considered the TRU_{tot} and the change of TRU during the irradiation cycles around t_{ad} before any adaptation. The second one was $Pu_{toMOX}(t_{ad})$, the available plutonium in spent UOX fuels for MOX fabrication. These two indicators helped indicate the potential of pre-disruption strategies to be adaptively robust, and complement the adaptation scenario studies based on a set of prior trajectories for $t_{ad} = 2070$.

Furthermore, this methodology of robustness assessment has been applied to the use of PWR MOXEUS for adaptation scenarios, which allowed plutonium multi-recycling. From the prior reference trajectory, the use of MOXEUS allows a longer transition and more sustainable reactor operation for those robust adaptations, and especially a deeper incineration of TRU than the use of MOX. As a result, the adaptability of pre-disruption strategies regarding the uncertain objective disruption has been increased a lot by the use of MOXEUS fuels.

Finally, the methodology has been applied to a more realistic scenario study based on the French national strategies. Two prior trajectories have been considered. The first one called **TRJ MIX** supposed the use of MIX fuel for plutonium multi-recycling. The other one called **TRJ SFR** supposed the massive SFR deployment between 2080 and 2120, without plutonium multi-recyling in PWRs. They have been inspired from expert scenarios and official documents, representing two nuclear futures in France. Several outputs have been taken into account in order to assess the strategies comprehensively.

As emphasized in this work, the deep uncertainties concerning these two trajectories should be taken into account. In case of disruption and adaptation were looked for, Nelder-Mead optimization algorithm has been used for the subsequent adaptation scenario studies.

From the prior trajectory **TRJ MIX**, the SFR deployment was reconsidered after disruption, and the end of fleet substitution with SFRs as early as in **TRJ SFR** has been viewed as the interest. Therefore, this adaptation scenario is called **SCN MIX2SFR**. The adaptations that minimized the end time of SFR deployment have been identified by the optimization approach. Appropriate adaptations that finished the fleet substitution with SFR deployment by 2120 were identified for year 2065 and 2085 as t_{ad}. In these trajectories, the SFR deployment could finish as

early as if the plutonium had never been supposed to be multi-recycled in PWRs. Thus, **TRJ MIX** combined with these two adaptations were considered adaptively robust for the respective t_{ad}. In contrast, the optimal adaptive strategy identified for late adaptation of $t_{ad} = 2100$ suggested finishing the fleet substitution by 2140. This temporal difference was regarded as the regret of using MIX fuels before disruption, and it was explained by the plutonium inventory availability for SFRs. Its accumulation needs the stop of the use of MIX fuels, and $t_{ad} = 2100$ seemed too late for such accumulation.

From the prior trajectory **TRJ SFR**, the new SFR commissioning has been halted after disruption, and the maximization of the use of idle plutonium has been regarded as the new objective. In this context, the adaptations using MOXEUS fuels in PWRs that minimized the plutonium in interim stocks during last 20 years of scenario have been identified by optimization. The MOXEUS has been used instead of MIX in order to adapt to the large variability of plutonium quality in different stocks. This adaptation scenario was then called **SCN SFR2MOXEUS**. The idle plutonium stabilized by the use of MIX fuels in **TRJ MIX** has been regarded as the comparison level to assess the adaptive strategy performances in **SCN SFR2MOXEUS**. By the optimization approach, the optimal strategies for year 2065 and 2085 as t_{ad} led to lower idle plutonium inventory than the comparison level. The combination of prior SFR-deployment strategy and these appropriate adaptations have been considered adaptively robust. For the optimal adaptation from 2100, a higher plutonium inventory in interim stocks than the comparison level has been identified at the end of scenario. This has been explained by the discharges of spent fuels from the last two irradiation cycles of decommissioning SFRs, which accounted for a significant part of nuclear electricity generation by 2100.

To summarize, the methodology of strategy robustness assessment under the deep uncertainty of objective disruption has been built through a series of exploratory scenario studies. It has also been applied to more realistic cases concerning the French national strategies.

To conclude, we must highlight the fact that this work is only a first step for robustness studies in electro-nuclear scenarios. Several choices made in work would deserve to be explored more in detail to assess their implications. First, we use the disruption as an important approach to integrate the uncertainty of objective. It splits these innumerable possibilities into two objectives and connects them by an abrupt switch. In each possible mono-objective future studied in this work, the valorization of the quantity of interest is approximately constant. For instance, for the pre-selected objective A, the same value of R_{Subs} is identically valued whenever it is evaluated: a $R_{Subs} = 1.5$ in 2070 means the same as that in 2090, 50% of the margin on the plutonium availability for the fleet substitution with SFRs. In reality, the status as well as the valorization of plutonium may evolve in a regular way rather than an abrupt change as the disruption supposes, leading to the time-dependent estimation on the need of plutonium. The quantity R_{Subs} does have to some extent captured the changes in plutonium needs by the normalization of time-dependent power. To generalize in a broader application, the same value of R_{Subs} may be also valued differently for different times. It may be especially useful for the nuclear wastes, which are not looked into in this work. For such time-dependant valuation, one could take inspiration from economic concepts and methods designed for this purposes and, this way, creates another approach to handle time-dependent uncertainties in electro-nuclear scenario studies in the future [105]. To achieve this, a solid inter-disciplinary base is

required to build the framework and methodology.

Also, the Nelder-Mead optimization introduced in this work is for mono-objective problem, and the constraint of rejecting missloads is imposed by the customized penalization on the relevant optimized output. It is not able to reveal the space of robust adaptation space, nor the trade-offs on several inputs and outputs if more than one quantities have to be optimized. Some advanced optimization techniques under constraints for multi-objective can be then applied to these realistic scenario studies, in order to provide a comprehensive assessment. It can be also compared with statistical analyses which may provide more information on a large space of strategies of interest.

Appendix A

Summary of the dissertation in French / Résumé de la thèse en français

Contexte et Introduction du sujet

La transition nucléaire joue un rôle important dans la politique énergétique nationale des pays utilisant l'énergie nucléaire. Après des décennies d'exploitation, plusieurs axes de technologie peut être considérés pour le futur du nucléaire. Avec le déploiement de nouvelles installations et de nouvelles technologies, la transition peut durer plusieurs décennies, imposant des grands impacts sur des aspects sociaux, économiques, temporels et spatiaux : des investissements de R&D et de grande chantier de construction, la gestion de grandes quantités matières radioactives, les impacts environnementaux, etc. Pour obtenir une estimation a priori de ces impacts, il faut des évaluations détaillées par les études de scénario pour la prise de décision des stratégies nucléaire nationaux.

Comme présenté dans de nombreuses études de scénario électro-nucléaire, un large spectre d'objectifs conduit à des futurs non-déterminés très diversifiés. Sous des objectifs différents de ces futurs possibles, certaines sorties issues de la simulation d'une stratégie pour une étude d'évaluation ne sont pas forcément utiles ou peuvent être interprétées d'une manière différente dans une autre étude, menant à l'utilisation de critères différents dans des évaluations différentes d'une même stratégie dans des contextes différents. De plus, il est très difficile d'avoir une vision claire du quel objectif est le plus pertinent, ou sera le plus pertinent dans le futur, car il est profondément incertain.

Le projet ASTRID en France et les études associées montrent ce type d'incertitude profonde. En effet, l'annulation du projet ASTRID illustre le changement des perspectives vis à vis du déploiement de technologie nucléaire pour les décennies suivantes. D'un point de vue physique, les prospectives a propos des inventaires de matières radioactives et des gestions associées ont fortement changés. Mais rien ne garanti que ces changements soit la dernière remise en question de ces status et personne ne peut garantir qu'un autre changement n'aura pas lieu dans le futur.

Au lieu de rester bloqué en considérant seulement un futur, il vaut mieux intégrer ce type d'incertitudes dans les évaluations de stratégie en gardant les options ouvertes pour des changements incertains et des addaptations possibles dans le futur. Dans ce contexte, une méthodologie d'évaluation de la robustesse d'une stratégie a été développé afin d'effectuer ces études de scénario électro-nucléaire sous les incertitudes profondes d'objectif. Elle a été appliqués dans des scénarios inspirés du cycle de combustible nucléaire en France qui est l'un des pays ayant la part la plus élevée d'énergie nucléaire dans son mix énergétique.

Simulations et analyse de scénarios électro-nucléaires

Avant de réaliser des analyses ou des évaluations, le cadre et l'outil de l'étude sont d'abord caractérisés, et les hypothèses et les limites de méthode sont clarifiées. En particulier, les hypothèses de la modélisation par CLASS, l'outil pour la simulation dynamique du cycle, sont bien détaillées. Une étude préliminaire de scénario inspiré du cycle français est réalisée pour offrir une compréhension basique des propriétés de la dynamique du cycle basée sur GSA. Par hypothèse, le parc français est toujours composé de REP (Réacteur à Eau Préssurisée) UOX et MOX dans cette étude, et la puissance totale du parc, la fraction globale de MOX dans le parc, le timing de la transition et d'autres paramètres opérationels sont variables dans une gamme large pour engendrer l'espace de stratégie à explorer. La méthode de Morris est utilisée pour étudier l'importance de ces paramètres sur plusieurs sorties. Cette étude montre des limites de cette méthode de Morris, principalement à cause de manque de plutonium pour certaines trajectoires dans le DoE. Malgré cela, cette étude préliminaire permet de classer ces paramètres d'entrée et d'expliquer les réponses du cycle vis-à-vis des variations des paramètres.

Basée sur cette méthode d'analyse du cycle, la disruption de l'objectif est prise comme une approche pour considérer l'incertitude de l'objectif dans les études de scénario électro-nucléaire. Une étude est alors entreprise dans le cadre où l'objectif primaire est de deployer des Réacteur à Neutrons Rapides refroidi au sodium (RNR-Na) dans le futur (objectif A), tout en considérant une possibilité de disrupter cet objectif et de viser alors la minimisation des déchets nucléaires sans RNR-Na (objectif B). Dans ce cadre, deux types de robustesse sont évalués : la robustesse statique et la robustesse adaptative.

La robustesse statique est définie dans un scénario sans disruption (nommé "scénario pré-disruption" pour le distinguer de celui supposant la mise en place de la disruption présenté par la suite). Les stratégies explorées dans ce scénario sont considérées statiques puisque leurs sorties de transition correspondent aux futurs sans aucun réajustement et elles sont déterminées avant toute disruption. La robustesse statique de ces stratégies indique la performance sur les deux objectifs à la fois, leur permettant d'être performantes quelque soit l'objectif final.

Pour la robustesse adaptative, on suppose qu'une stratégie primaire déterminée avant toute disruption a été mise en place. En cas de disruption, des stratégies adaptatives sont considérées à partir de la trajectoire primaire. De ce principe, la robustesse adaptative est définie pour la combinaison des deux stratégies, l'une primaire pour adapter, et l'autre indiquant l'adaptation suivante. Dans ce cas, il faut choisir un seuil de comparaison pour qualifier/quantifier la robustesse adaptative. Dans cette étude, ce seuil est, par hypothèse, issu d'une stratégie satisfaisant ces conditions :

- La stratégie peut être déterminé dans le scénario pré-disruption ;
- La stratégie est consistent avec l'objectif pré-sélectionné (ici c'est le déploiement de RNR-Na) ;
- Si aucun réajustment peut être autorisé au cas de la disruption, la stratégie est optimal pour l'objectif après la disruption parmi toutes les stratégies qui satisfont les deux conditions précédentes.

Autrement dit, cette stratégie représent peut être vue comme le meilleur choix historique au cas de la disrutpion. La différence entre le résultat de la stratégie

primaire et ce seuil représente les regrets d'avoir implémenté la stratégie primaire au regard de l'objectif après la disruption. Si l'adaptation de cette trajectoire primaire peut compenser ces regrets, une telle adaptation est considérée robuste, et la stratégie primaire est considérée adaptativement robuste avec cette stratégie adaptative. Dans ce cas, l'écart entre le résultat après l'adpatation sur la trajectoire primaire et le seuil peut être quantifié comme la performance de la robustesse adaptative.

Ce cadre général est dédié à développer une méthodologie solide d'évaluation de robustesse pour les études de scénario électro-nucléaire. Cependant, il faut encore des ajustements pour adapter aux caractéristiques et aux hypothèses variées pour des scénarios différents.

Robustesse évaluée avec un horizon temporel fixé

La méthodologie est premièrement développée dans le Chapitre 3, dans une famille de scénario où les stratégies sont évaluées en l'an 2090.

Inspiré des transitions possibles du cycle français, le scénario pré-disruption commence en 2015 et se termine en 2090. Dans ce scénario, les stratégies de transition avant toute disruption sont explorées dans un espace large concernant des variations des paramètres opérationnels. Pour quantifier la performance d'une stratégie vis-à-vis l'objectif A qui est pré-sélectionné, le taux de substitution du parc par des RNR-Na, exprimé par R_{Subs}, est calculé en 2090 pour chaque stratégie explorée. Cette grandeur considère l'inventaire de plutonium disponible dans le cycle pour deployer un certain nombre de RNR-Na, et elle est normalisée par la puissance finale du parc après la transition. Les stratégies remplissant l'objectif A doit avoir un $R_{Subs}(2090) \geq 1$. Pour prendre en compte les marges nécessaire sur la disponibilité de plutonium, la stratégie optimale pour cet objectif A doit maximiser $R_{Subs}(2090)$. S'il faut prendre en compte l'incertitude profonde de la disruption vers l'objectif B, l'inventaire transuranien dans le cycle total, incluant ceux dans les installations nucléaires et dans les déchets, noté comme TRU_{tot}, doit être minimisé sans RNR-Na. TRU_{tot} en 2090 est pris comme la sortie d'intérêt pour ce nouvel objectif en cas de disruption.

Concernant ces deux objectifs, les performances des stratégies dans ce scénario pré-disruption sont quantifiées. La PCA est utilisée pour étudier l'importance des variables entrées sur le nombre de fois ou le plutonium a manqué pour le chargement du combustible MOX, noté comme *missload*, et aussi sur les deux sorties d'intérêt correspondant aux deux objectifs possibles, $R_{Subs}(2090)$ et $TRU_{tot}(2090)$. La dominance de la puissance totale finale du parc, $P_{tot,f}$, et les effets mesurables issus de la fraction finale de MOX, $FrMOX_f$, et le taux de combustion de UOX, BU_{UOX}, sont bien révélés par PCA. Les techniques graphiques comme le *pairs plots* des variables entrées et sorties sont utilisées pour complémenter les analyses.

Les valeurs des deux sorties d'intérêt des stratégies explorées sont présentées dans la Figure A.1, colorées par la valeur de $P_{tot,f}$ correspondante. Selon la PCA précédente, $P_{tot,f}$ est la plus importante variable entrée pour les deux sorties, et cette importance est visible dans cette figure. Au regard de la robustesse statique, le front Pareto correspondant à ces deux objectifs est identifié, comprenant les stratégies optimaux vis-à-vis des deux objectifs contraditoires, la maximisation de $R_{Subs}(2090)$ et la minimisation de $TRU_{tot}(2090)$ sous condition $R_{Subs}(2090) \geq 1$; et elles sont entourées par des carrés dans la Figure A.1. Ces stratégies présentent des $P_{tot,f}$ similaires. Les compromis de performance entre ces deux objectifs

sont bien montrés dans cette figure. La compétition entre ces deux objectifs sont guidé par les valeurs de $FrMOX_f$ et de BU_{UOX}. Dans cette étude, on considère que ces stratégies optimales dans ce front Pareto sont robustes dépendant des compromis entre les deux objectifs.

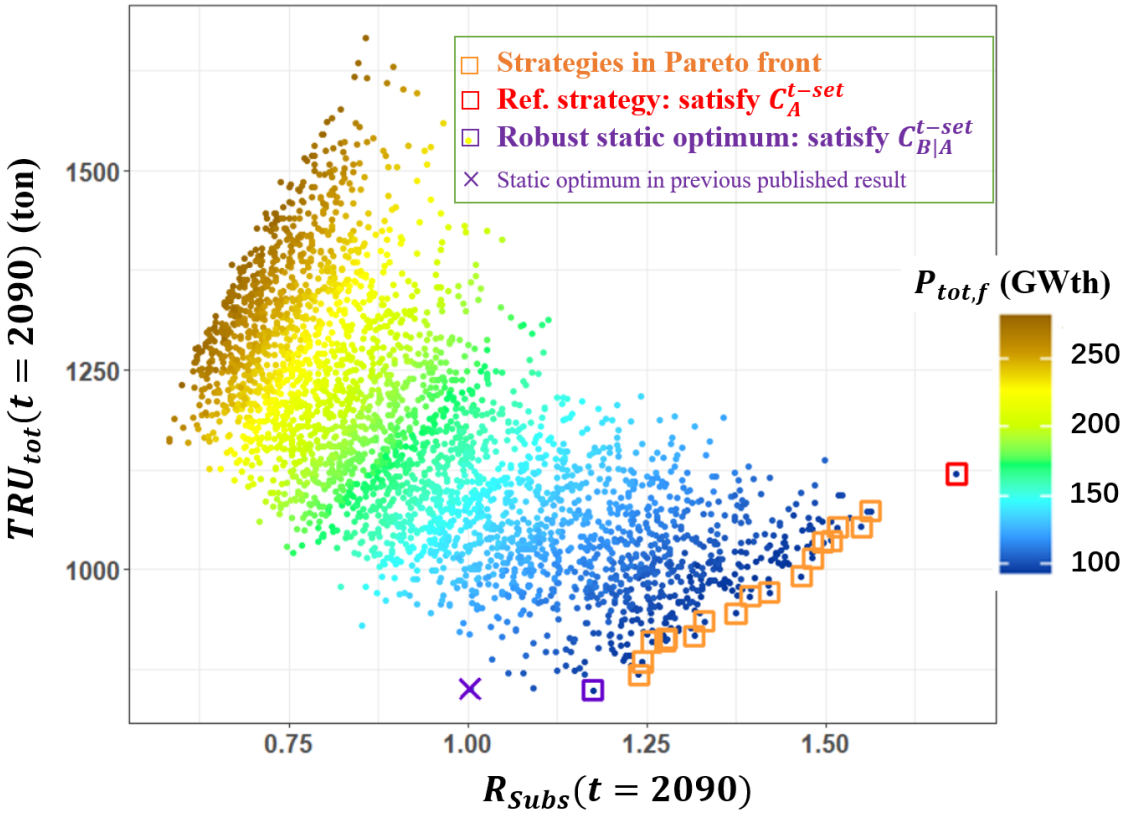

Figure A.1: TRU_{tot} vs R_{Subs} by 2090 of valid static strategies, colored by input $P_{tot,f}$

Deux cas extrêmes sur le front sont identifiés. L'un est entouré par le carré rouge dans la figure, la stratégie optimale pour l'objectif A qui maximise $R_{Subs}(2090)$. Cette stratégie, appelé la stratégie de référence dans le Chapitre 3, suppose une longue transition vers un parc de $P_{tot,f}$ bas, de $FrMOX_f$ bas et de BU_{UOX} bas, permettant d'accumuler rapidement l'inventaire de plutonium dans le cycle. L'autre, appelée l'optimum statique robuste, minimise $TRU_{tot}(2090)$ sous la condition $R_{Subs}(2090) \geq 1$. Cet optimum suppose une courte transition vers un parc de $P_{tot,f}$ bas, de $FrMOX_f$ élevée et de BU_{UOX} élevé. Dans cette trajectoire, le plutonium qui occupe la plupart de TRU_{tot} est incinéré le plus possible, et un risque de *missload* présente à la fin.

Après l'analyse dans le scénario pré-disruption, le scénario d'adaptation suppose l'occurence de la disruption, et ainsi l'adoption de l'objectif B. Le $TRU_{tot}(2090)$ de l'optimum statique robuste est pris comme le seuil de comparaison pour quantifier la robustesse adaptative pour les adaptations possibles. Dans ce scénario, la trajectoire primaire de la stratégie de référence est prise comme base pour l'adaptation, car elle est optimale pour l'objectif pré-sélectionné avant la disruption. Pour prendre en compte l'incertitude profonde de la disruption, quatre temps différent sont considérés pour commencer l'adaptation, noté t_{ad} : l'année 2040, 2050, 2060, et 2070. Une nouvelle transition du parc après la disruption est supposée pour l'adaptation. Pour cette transition, une durée extrêmement courte (jusqu'à un an) et des stratégies phase-out sont considérées acceptables ; les REP chargés de MOX dans 100% de coeur est considéré possible pour les adaptations futures.

Dans cette étude d'adaptation, la durée de transition noté D, la nouvelle $P_{tot,f}$

et la nouvelle $FrMOX_f$ sont identifiées comme les variables entrées les plus importantes pour la sortie d'intérêt $TRU_{tot}(2090)$ correspondant à l'objectif B après la disruption. Les évolutions de TRU_{tot} lors des adaptations à partir de la trajectoire primaire de la stratégie de référence sont illustrées dans la Figure A.2. Des adaptations robustes, i.e. qui mènent à un $TRU_{tot}(2090)$ plus bas que le seuil issu du $TRU_{tot}(2090)$ de l'optimum statique robuste, sont identifiées si $t_{ad} \leq 2060$, alors qu'aucune adaptation robuste est observée pour $t_{ad} = 2070$. D'une manière équivalente, les combinaisons de la stratégie de référence primaire et des adaptations appropriées peuvent être considérées adaptatives robustes, avec un temps limite entre 2060 et 2070. La temporalité de la robustesse adaptative, qui peut être définie comme la durée entre ce temps limite et le temps fixe pour l'évaluation de la stratégie (2090), est ainsi entre 20 et 30 ans.

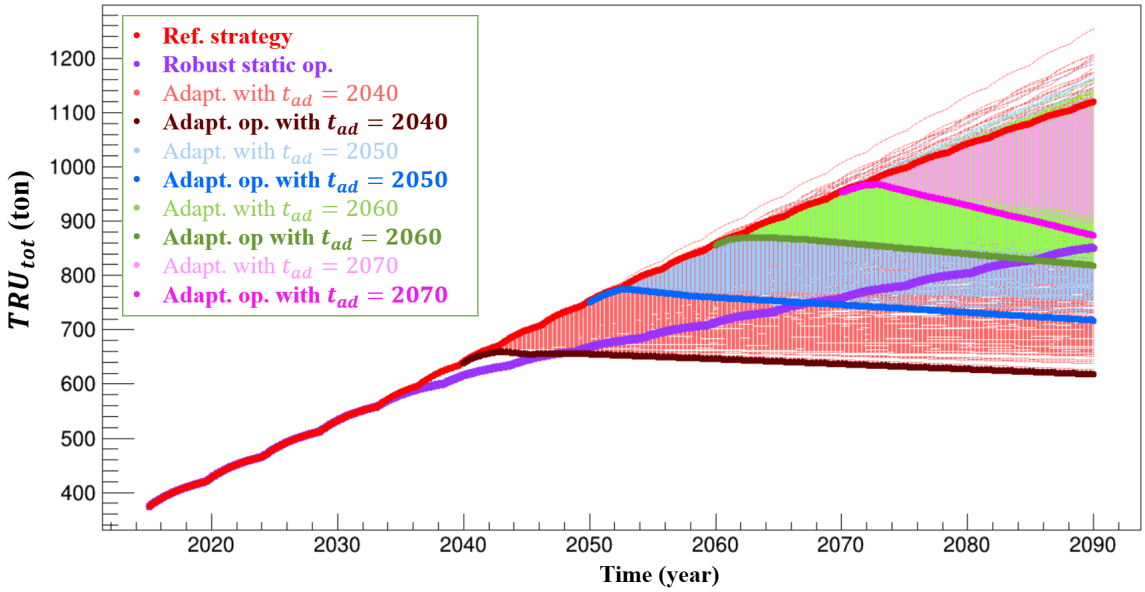

Figure A.2: Evolutions of TRU inventories in total cycle from valid strategies over t_{ad} as well as two particular pre-disruption strategies: the reference strategy and the robust static optimum

Il faut souligner que la formulation du problème et le critère utilisé pour l'évaluation de stratégie introduit une incertitude. Pour avoir une première évaluation de l'effet de cette incertitude, le critère pour l'objectif B lié à la disruption est reformulé dans un nouvel exercice à la fin du Chapitre 3. Dans cette étude, l'objectif B se traduit par la minimisation des inventaires transuraniens normalisés par la production cumulée d'électricité, noté par TRU_{tot}^{norm}. Comparé avec la formulation en TRU_{tot}, le critère en TRU_{tot}^{norm} peut être interprété comme un moyen de réduire l'effet de l'incertitude sur la puissance du parc. Une grandeure qui peut être aussi profondément incertaine et non-contrôlable sous contrainte des décisions politiques, alors que comme montré dans les analyses précédente, sa variation dans une large gamme a un grand impact sur des grandeurs extensives comme TRU_{tot}.

Avec ce nouveau critère utilisé pour l'objectif B, les études de scénario pré-disruption et d'adaptation sont relancées. Dans cette étude de scénario pré-disruption, PCA prouve que $P_{tot,f}$ a un effet négligeable sur TRU_{tot}^{norm}, ce qui confirme bien l'interprétation précédente. Dans ce cas, $FrMOX_f$ et BU_{UOX} sont les variable les plus impactantes sur TRU_{tot}^{norm}. A cause du nouveau critère, l'optimum statique robuste est différent de celui précédent. En considérant la stratégie de référence pour l'adaptation et ce nouvel optimum, l'évaluation de robustesse adaptative montre qu'il est difficile de réduire le TRU_{tot}^{norm} vers un niveau plus bas que celui de l'optimum statique robuste, comme présenté par l'évolution de

TRU_{tot}^{norm} après des adpatations dans la Figure A.3 : il y a peu de combinaisons de la stratégie de référence primaire et des adaptations réliées qui peuvent être adaptativement robuste. Cependant, pour n'importe quel temps d'adaptation t_{ad}., il n'est pas difficile de s'approcher du niveau de seuil donné par l'optimum statique robuste. Pour l'expliquer, TRU_{tot}^{norm} est fortement dépendant de l'utilisation de plutonium, principalement caractérisé par la fraction de MOX du parc. Le niveau de l'optimum peut être approché par une $FrMOX_f$ élevée pour l'adaptation.

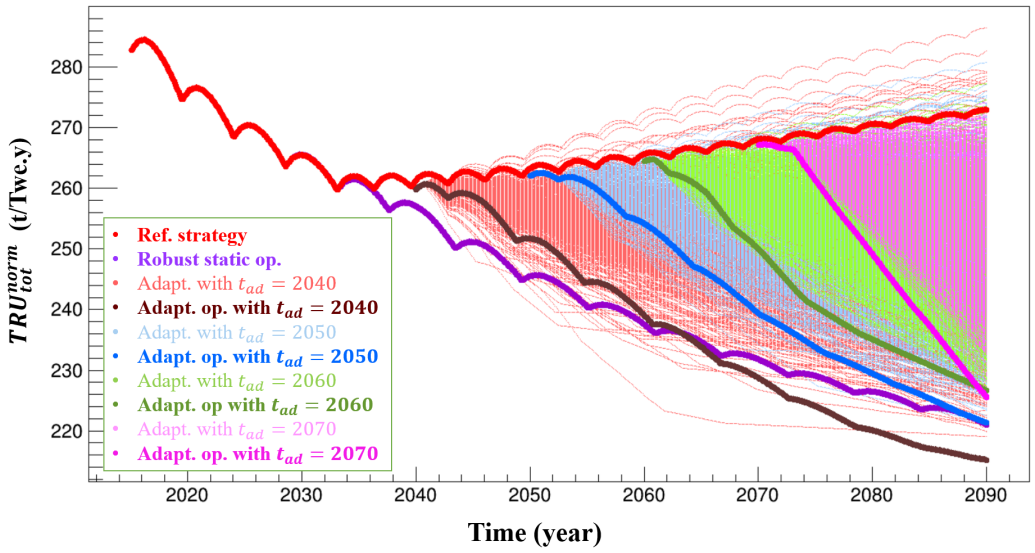

Figure A.3: Evolution of TRU_{tot}^{norm} of adaptive strategies, and the prior trajectories of reference strategy and robust static optimum

La comparaison des deux formulations pour l'objectif B présente une différence mesurable de l'évaluation des stratégies, qui peut potentiellement faire diverger les choix de stratégie. Il faut donc mettre l'accent sur l'importance de la précision sur l'hypothèse de l'analyse et des critères utilisés.

Ces études de scénarios nous permettent de développer une méthodologie d'évaluation de la robustesse des stratégies, en regardant les résultats à l'horizon fixé. Cette évaluation à l'horizon temporel fixé est une hypothèse commune dans de nombreuses études. Par contre, l'évaluation avec cette méthode d'une stratégie peut conduire à des conclusions très différentes si l'horizon temporel change.

Robustesse déconnectée de l'horizon donné

Pour garantir la consistence inter-temporelle de l'évaluation de robustesse, la méthodologie est réétablie dans les nouvelles études de scénario dans le chapitre 4. De nouvelles sorties sont définies pour le nouveau scénario pré-disruption : le t_R représente le temps quand la valeur de R_{Subs} d'une trajectoire est plus élevée qu'un seuil donné, et le t_{TRU} représente le temps quand la valeur de TRU_{tot} devient plus élevée qu'un seuil associé. Les déterminations de t_R et de t_{TRU}, dépendant de l'évolution de R_{Subs} et de TRU_{tot} respectivement, sont graphiquement représentées dans la Figure A.4. Dans ce scénario, une stratégie remplissant l'objectif A pour le déploiement de RNR-Na au futur implique $t_R \leq 2090$; alors que la prise de précaution au regard de la disruption doit décaler t_{TRU} le plus tard possible, comme $t_{TRU} \geq 2090$ par exemple (même si la valeur correspondante n'est pas quantifiable dans ce scénario car la simulation se termine en 2090).

PCA est utilisée pour étudier l'importance des variables entrées sur t_R et t_{TRU}, en prenant 1 comme le seuil de R_{Subs} pour déterminer t_R ; alors que deux choix

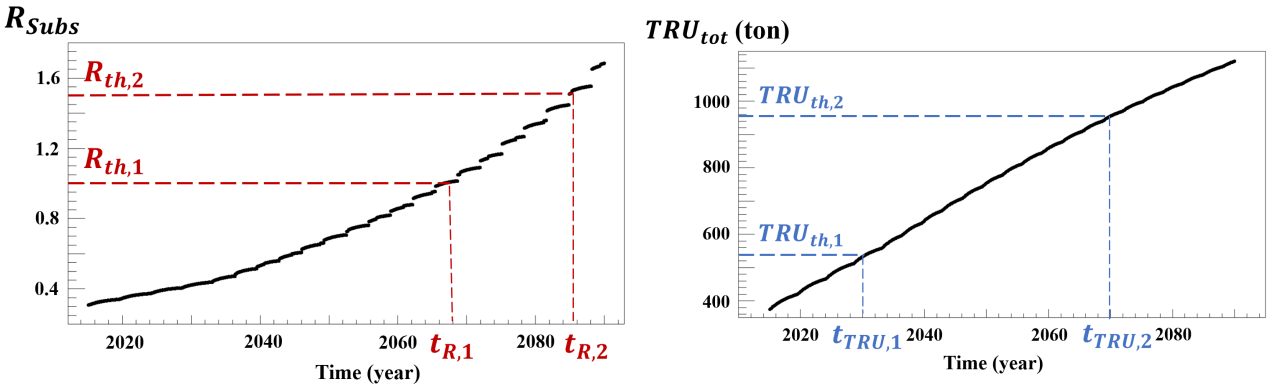

Figure A.4: Determination of t_R and t_{TRU} of a trajectory from a given strategy, according to the choices of thresholds R_{th} and TRU_{th}

différents du seuil de TRU_{tot} pour déterminer t_{TRU} des stratégies, et des choix de la prise en compte des ensembles différents des stratégies pour cette analyse statistique, sont intérogés. Dans chaque analyse respective (t_R ou t_{TRU}), trois sous-ensembles des stratégies valides sont considérés. La comparaison systematique vérifie que l'importance principale de $P_{tot,f}$ et les effets measurables de $FrMOX_f$ et de BU_{UOX} sur t_R et sur t_{TRU} sont bien stables pour des hypothèses différentes des choix du seuil de TRU_{tot} et de l'ensemble de trajectoire considéré. La stratégie de référence dans cette étude peut être déterminée de façon unique par le critère de la minimisation de t_R (essentiellement parce que le seuil de R_{Subs} est fixé dans cette étude), mais la détermination des stratégies statiques robustes dépend du choix du seuil de TRU_{tot}.

Pour l'étude de scénario d'adaptation, la definition de la validité des stratégies est aussi adaptée afin de permettre la déconnection de l'horizon fixé. En effet, le temps du premier missload est défini comme l'horizon temporel pour la trajectoire correspondante. Pour qu'une stratégie adaptative soit valide, le premier missload doit arriver après la nouvelle transition planifiée par l'adaptation (ou qu'il n'y ait jamais de missload). On suppose que le niveau bas de TRU_{tot} peut être maintenu par phase-out en cas de missload. En regardant toutes les stratégies impiquant $t_R \leq 2090$ dans le scénario pré-disruption, TRU_{tot} minimal au temps d'adaptation, i.e. la valeur minimale de $TRU_{tot}(t_{ad})$, est utilisée comme le seuil pour l'évaluation de la robustesse adaptative, noté $TRU_{th,ad}$. Une nouvelle grandeur t'_{TRU} est définie comme la sortie d'intérêt dans ce scénario, qui indique le temps quand le TRU_{tot} à partir de la trajectoire de référence primaire est mené vers un niveau en dessous du seuil par une adaptation associée. Pour être robuste, l'adaptation doit être capable de mener t'_{TRU} plus tôt que l'horizon temporel en respectant le critère de validité dans ce scénario d'adaptation.

Sous ces hypothèses, la trajectoire de référence est prise pour l'adaptation en 2040. Selon la définition de la robustesse adaptative dans cette étude, seulement des adaptations permettant l'incinération nette de TRU_{tot} sont d'intérêt. Pour ces adaptations valides, le plus bas TRU_{tot} atteint dans l'horizon, noté TRU_{min}, et le moment où il est atteint, noté t_{min}, sont étudiés pour aider à expliquer le comportement du cycle sous transitions et les résultats associés de t'_{TRU}. A cause de la capacité limitée d'incinération de TRU par mono-recyclage de plutonium, les transitions extrêment courtes vers un parc de haut $P_{tot,f}$ et haute $FrMOX_f$ sont nécessaires pour des adaptations robustes, comme présentées par les évolutions de TRU_{tot} issues des adaptations permettant l'incinération nette de TRU_{tot} dans la Figure A.5. Dans la plupart de ces cas, l'inventaire de plutonium disponible pour le combustible MOX est consommé le plus vite possible, suivi par un missload tôt,

qui sous-entend un phase-out.

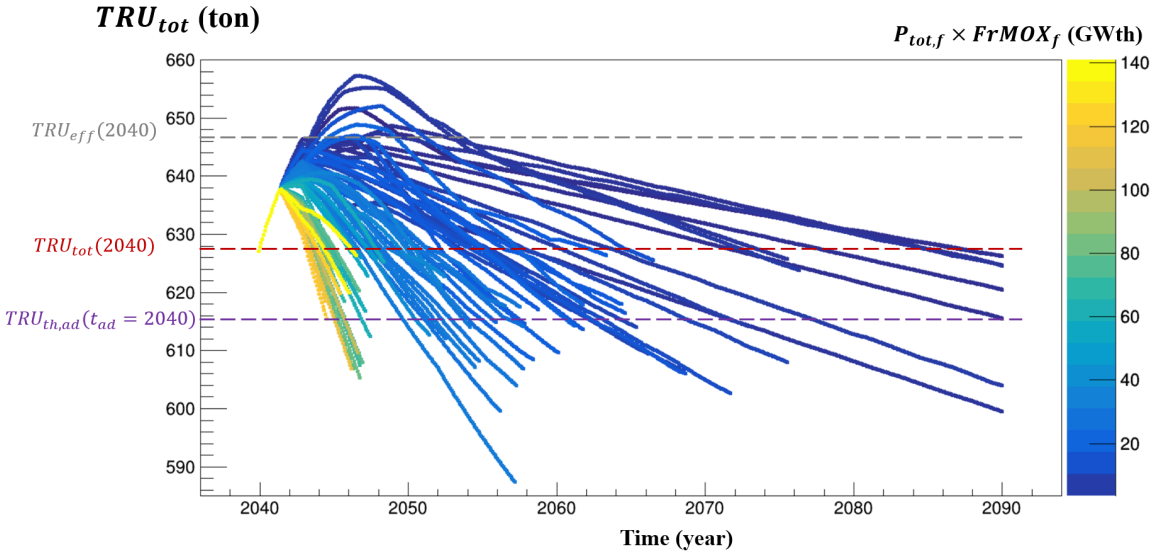

Figure A.5: Evolution of TRU_{tot} of S_{burn} adaptations, colored by final MOX power level $P_{tot,f} \times FrMOX_f$

Inspiré de cette analyse, l'adaptabilité d'une stratégie pré-disruption est définie comme la fraction d'adaptations robustes dans l'espace d'exploration. Dans ce parc d'intérêt, deux indicateurs d'adaptabilité sont déduits dans les résultats des stratégies pré-disruption. Le premier est l'inventaire TRU effectif au temps d'adaptation, noté $TRU_{eff}(t_{ad})$, considérant $TRU_{tot}(t_{ad})$ ainsi que le changement des transuraniens pendant les cycles d'irradiation des réacteurs traversant t_{ad}. Le second est l'inventaire de plutonium disponible dans les combustibles UOX usés pour la fabrication de MOX, noté $Pu_{toMOX}(t_{ad})$. Ces deux grandeurs indiquent approximativement le potentiel d'être adaptativement robuste pour une stratégie pré-disruption, graphiquement expliqué par la Figure A.6. Grâce à ces deux indicateurs, l'étude de scénario d'adaptation se généralise sur un grand ensemble de trajectoires primaires associées aux stratégies pré-disruption dans le Chapitre 4, correspondante à l'année 2040 et 2070 pour t_{ad}.

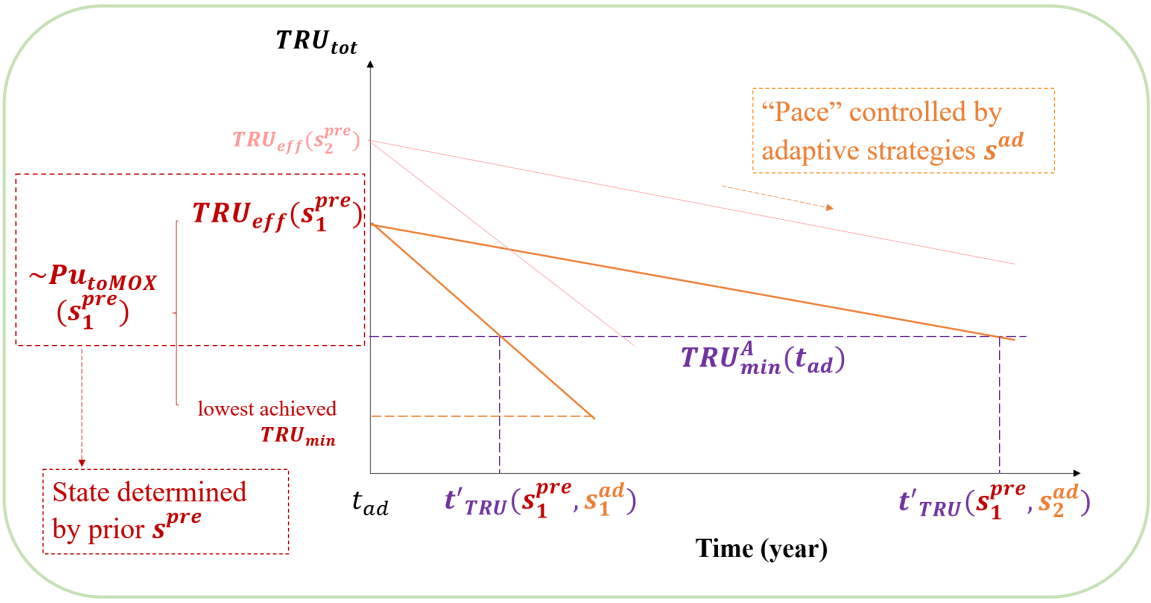

Figure A.6: Graphical representation of the influence of prior pre-disruption strategy and adaptive strategy on TRU_{tot} evolution, in the fleet of PWR UOX and MOX

Une étude d'ouverture applique ensuite cette méthodologie en autorisant l'utilisation de combustible avancé MOXEUS qui représente un chemin de multi-recyclage de plutonium dans les REP lors des adaptations futures. Basée sur la trajectoire de référence primaire, l'utilisation de MOXEUS permet d'être robuste en prenant des transitions moins tendues que le mono-recyclage : des durées plus longues de transition et d'exploitation. Dans le même temps, et plus important, l'incinération des transuraniens est plus profonde, comme présenté par les évolutions de TRU_{tot} des adaptations d'intérêt dans la Figure A.7. Par conséquent, l'adaptabilité de la stratégie de référence augmente si l'utilisation de MOXEUS sera autorisée sous l'incertitude profonde de la disruption.

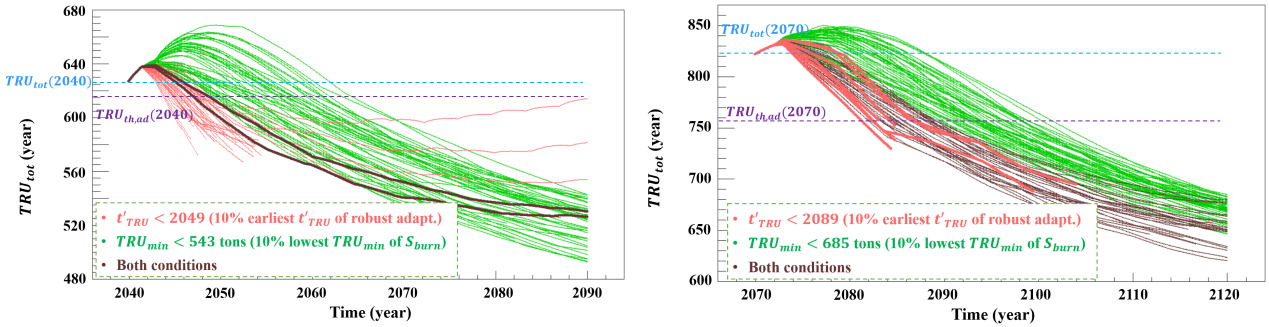

(a) $t_{ad} = 2040$ (b) $t_{ad} = 2070$

Figure A.7: Contrast of trajectories on the minimization of t'_{TRU} and the minimization of TRU_{min}. Some strategies are overlapped in two example groups

Scénarios applicatifs sur le choix incertain de multi-recyclage de plutonium : en REP ou en RNR-Na

Pour finir, la méthodologie est appliquée dans une étude de scénario plus réaliste que ceux précédents, se focusant sur les choix de multi-recyclage de plutonium envisagés par les stratégies nationales françaises. De la première étape, deux stratégies représentatives sont prises pour présenter deux chemins possibles pre-disrution. La première trajectoire, notée **TRJ MIX**, suppose l'utilisation du combustible MIX pour le multi-recyclage dans les REP, inspiré du rapport officiel PPE. La seconde, notée **TRJ SFR**, suppose le déploiement massif de RNR-Na à partir de 2080 et le parc est complètement remplacé par les RNR-Na en 2120. Les RNR sont simulés dans cette trajectoire. Les évolutions du parc dans ces deux trajectoires sont illustrées dans la Figure A.8. Plusieurs sorties sont étudiées pour évaluer ces deux stratégies selon des angles différents.

La contradiction entre ces deux trajectoires peut être observée : dans **TRJ SFR**, une grande quantité de plutonium est demandé pour déployer des RNR-Na, alors que l'utilisation de MIX dans **TRJ MIX** empêche l'accumulation de plutonium. Même si la stratégie de **TRJ MIX** peut être vue comme une stratégie référence correspondante à la perspective nationale, elle n'est pas robuste vis-à-vis une demande possible de la ré-considération du déploiement de RNR-Na à cause d'une ré-estimation de la disponibilité des ressources d'uranium.

C'est face à cette problématique que la robustesse adaptative de la stratégie de **TRJ MIX** doit être considérée. Le scénario d'adaptation associé, noté **SCN MIX2SFR**, suppose qu'il y aura une demande forte du déploiement de RNR-Na au milieu de la trajectoire de **TRJ MIX**. Après la disruption de la stratégie de **TRJ MIX**, on vise donc à minimiser le temps pour lequel le parc peut être remplacé

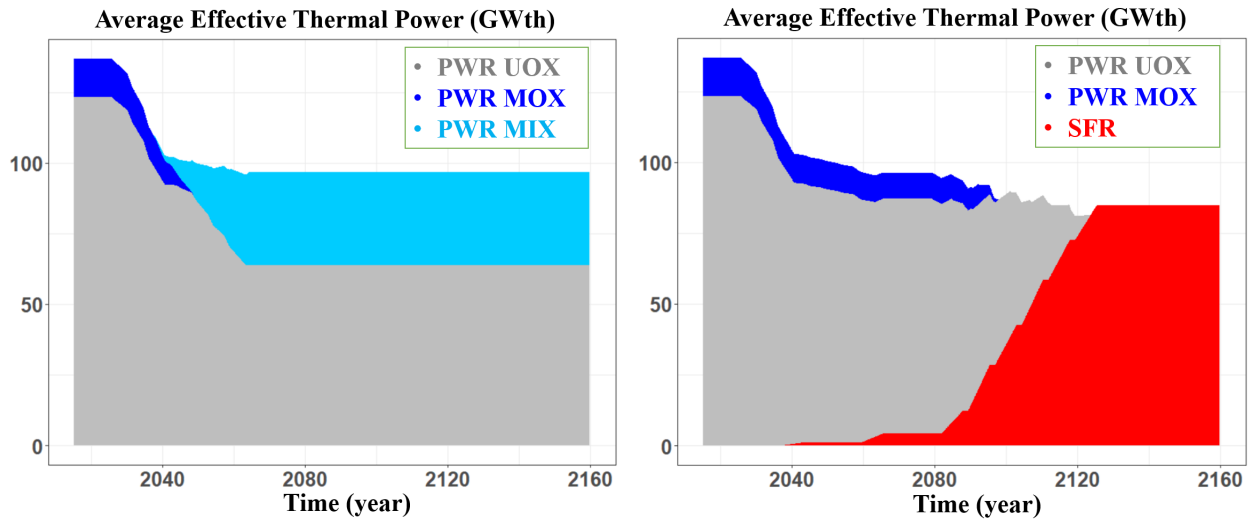

(a) **TRJ MIX** (b) **TRJ SFR**

Figure A.8: Evolution of effective thermal power in two trajectories of interest **TRJ MIX** and **TRJ SFR**

complètement par des RNR-Na d'un point de vue de la disponibilité de plutonium. Si cette transition de déploiement peut être finie en 2120 comme dans **TRJ SFR**, la stratégie primaire de **TRJ MIX** peut être considérée adaptativement robuste pour ce nouvel objectif. Pour identifier les adaptations optimales qui minimisent ce temps de la fin du déploiement de RNR-Na, l'algorithme d'optimisation de Nelder-Mead est utilisé pour interroger les trois temps possibles d'adaptation t_{ad} : 2065, 2085, et 2100. Sous ces hypothèses, des adaptations optimales de $t_{ad} = 2065$ et de $t_{ad} = 2085$ sont robustes, alors que l'adaptation en 2100 ne peut accumuler suffisant de plutonium pour un parc de RNR-Na que trop tard, et la transition se termine en 2140. Cet écart de 20 ans peut être vu comme le regret d'utiliser le combustible MIX dans les REP précédemment vis-à-vis cette disruption avec une l'adaptation tardive.

Pour completer, la stratégie de **TRJ SFR** est aussi disruptée dans un scénario d'adaptation noté **SCN SFR2MOXEUS**. Ce scénario suppose l'arrêt de mise en place de nouveaux RNR-Na au milieu de **TRJ SFR**, potentiellement à cause de nouvelles estimations économiques des RNR-Na. Pour être le plus rentable possible, des RNR-Na en opération continuent leurs services jusqu'à leurs fins de vie. En effet, le déploiement de RNR-Na implique une accumulation considérable de plutonium ; une fois des projets de RNR-Na doit être arrêtés, un inventaire significatif de plutonium est possiblement inoccupé, qui est le cas contraire dans **TRJ MIX** où le plutonium dans le stock est quasiment constant. Autrement dit, la stratégie de **TRJ SFR** n'est pas forcément statiquement robuste concernant cette disruption. Dans cette situation, on cherche des adaptations visant à minimiser l'inventaire de plutonium disponible dans les stocks pendant les 20 dernières années du scénario. Pour évaluer la robustesse adaptative, le niveau stable de plutonium disponible présenté dans **TRJ MIX** est pris comme un seuil de comparaison.

Dans ces adapataions, au lieu du MIX, le combustible MOXEUS est utilisé pour le multi-recyclage de plutonium dans les REP. Comme pour le **SCN MIX2SFR**, des adaptations optimales au vue de la minimisation du plutonium dans les stocks sont identifiées par l'optimisation de Nelder-Mead en consiérant les trois t_{ad}. Les adaptations optimales de $t_{ad} = 2065$ et de $t_{ad} = 2085$ sont robustes, alors que celle de $t_{ad} = 2100$ provoque des augmentations mesurables de plutonium dans les stocks pendant les 20 dernières années. Pour expliquer ces sauts, il faut noter

que la part de RNR-Na en 2100 occupe plus d'une moitié du parc, contenant une quantité significative de plutonium dans les coeurs. Si cette part de RNR-Na sont démissionnée et le plutonium n'est plus recyclé par de nouveaux RNR-Na, les inventaires de plutonium issus des deux derniers cycles d'irradiation deviennent disponibles dans les stocks. Même si l'utilisation de MOXEUS recycle une certaine partie de ces inventaires, la teneur de plutonium dans MOXEUS est plus basse que celle dans les combustibles de RNR-Na et la fraction de MOXEUS est plus basse da la part de RNR-Na en 2100. Ces facteurs mènent à l'accumulation rapide et significative de plutonium dans les stocks.

Conclusion et perspectives

Pour résumer, la méthodologie de l'évaluation de la robustesse des stratégies sous l'incertitude profonde de l'objectif est développée dans une famille d'études de scénarios électro-nucléaires. Cette méthodologie est appliquée dans une étude se focalisant sur des cas concrets qui sont inspirés des stratégies nationales françaises.

Cependant, les travaux réalisés dans cette thèse ne constituent que la première étape des évaluations concernant la robustesse des stratégies. La disruption dans ces travaux est utilisée comme une approche pour intégrér l'incertitude de l'objectif, mais ce changement brutal est réalisé une fois pour toute. En réalité, la trajectoire peut changer de direction plusieurs fois pendant une durée raisonnable, ou d'une manière progressive.

De plus, le choix d'une stratégie peut être influencée par plus qu'un critère, non seulement physique, mais aussi économique. Il est important d'introduire d'autres mesures pour intégrer les facteurs économiques dans le futur. Cette integration avec des concepts économiques est aussi un bon point de départ pour tester de nouvelles idées sur la façon de comment considérer la temporalité des actions dans les études de scénarios et leurs impacts sur les résultats.

Bibliography

[1] Office parlementaire d'évaluation des choix scientifiques et technologiques. The 2006 Programme Act on the Sustainable Management of Radioactive Materials and Wastes, 2006. [Cited on page 11.]

[2] CEA/DEN. *CEA report 2012 – Tome 3: 4th-Generation Sodium-cooled Fast Reactors: the ASTRID Technological Demonstrator*, chapter 5.1 Requirements to be Complied with and Basic Choices for ASTRID. Publications of Commissariat à l'énergie atomique et aux énergies alternatives (CEA), 2012. [Cited on page 11.]

[3] Stéphanie Tillement and Frédéric Garcias. ASTRID, Back to the Future: Bridging Scales in the Development of Nuclear Infrastructures. *Nuclear Technology*, 2021. [Cited on page 11.]

[4] V. Alexeeva, V. Anastasov, M. Cometto, S. Dardour, E. English, B. Magne, D. Subbotnitskiy, H. Turton, and A. Van Heek. *Climate Change and Nuclear Power 2020*. International Atomic Energy Agency (IAEA), 2020. [Cited on page 15.]

[5] V. [Masson-Delmotte, P. Zhai, H.-O. Pörtner, D. Roberts, J. Skea, P.R. Shukla, A. Pirani, W. Moufouma-Okia, C. Péan, R. Pidcock, S. Connors, J.B.R. Matthews, Y. Chen, X. Zhou, M.I. Gomis, E. Lonnoy, T. Maycock, M. Tignor, and T. Waterfield. Global Warming of 1.5°C.An IPCC Special Report on the impacts of global warming of 1.5°C above pre-industrial levels and related global greenhouse gas emission pathways, in the context of strengthening the global response to the threat of climate change, sustainable development, and efforts to eradicate poverty. Technical report, IPCC 2018. [Cited on page 15.]

[6] International Atomic Energy Agency (IAEA). Nuclear Power's Changing Future, 2014. [Cited on page 15.]

[7] P.K. Dey, M. Giroux, A. Khaperskaya, J. Laidler, A. Machiels, M. Masson, F. Storrer, and G. Uchiyama. Spent Fuel Reprocessing Options. Technical report, International Atomic Energy Agency (IAEA), 2008. [Cited on page 16.]

[8] Xavier Doligez, Sandra Bouneau, Stella David, Marc Ernoult, Abdoul-Aziz Zakari-Issoufou, Nicolas Thiollière, Adrien Bidaud, Olivier Meplan, Alexis Nuttin, and Nicolas Capellan. Fundamentals of reactor physics with a view to the (possible) futures of nuclear energy. *Comptes Rendus Physique*, 18, 10 2017. [Cited on pages 16 and 31.]

[9] Marc Ernoult. *Gestion avancée du plutonium en REP — Complémentarité des cycles thorium et uranium*. PhD thesis, Université Paris-Sud XI, 2014. [Cited on pages 16, 161, and 182.]

[10] Nicolas Thiollière. Les études de scénarios nucléaires à l'IN2P3, 2019. Journée Annuelle de GDR SciNEE. [Cited on pages 16, 21, and 56.]

[11] Frank Carré and Jean-Michel Delbecq. Overview on the French Nuclear Fuel Cycle Strategy and Transition Scenario Studies. *Revue Générale Nucléaire*, pages 95–101, 11 2014. [Cited on page 16.]

[12] R. Araujo da Silva, M. Dunn, D. Deroubaix, P.C. Florido, A. Grigoriev, J. Hatter, Y. Hosokawa, K. Kawabata, K. Koyama, D.S. Shukla, M.J. Smith, J.H. Yoo, and Fubao Zhang. Country Nuclear Fuel Cycle Profile - Second Edition. Technical report, International Atomic Energy Agency (IAEA), 2005. [Cited on page 16.]

[13] Institut de Radioprotection et de Sûreté Nucléaire (IRSN). Cycle du combustible nucléaire en France - Dossier « Impact Cycle 2016», 2018. Rapport IRSN - Réunion du Groupe permanent d'experts pour les laboratoires et les usines du 25 mai 2018. [Cited on pages 16, 97, 138, and 182.]

[14] IAEA-PRIS. Country Statistics - France. [Cited on pages 16 and 42.]

[15] Sophie Missirian, Patrick Devin, and Jean-Michel Hoorelbeke. French C̈ycle Impactäpproach, 2018. Technical Meeting IAEA — Integrated approaches to the back end of the fuel cycle. [Cited on pages 16, 17, and 235.]

[16] CEA/DEN/DISN/ACF. Inventaire prospectif entre 2016 et 2100 des matières et des déchets radioactifs produits par le parc français selon différents scénarios d'évolution. Technical report, Commissariat à l'énergie atomique et aux énergies alternatives (CEA), 2018. [Cited on pages 18, 170, 173, and 175.]

[17] S. Aniel, J. Bergeron, and A. Puill. Evaluation of the Maximum Plutonium Content of a MOX-Fuelled Pressurized Water Reactor Versus Isotopic Composition with Respect to the Void Coefficient. Technical Report IAEA-TECDOC–941, International Atomic Energy Agency (IAEA), 1997. [Cited on page 18.]

[18] Ministère de la transition écologique et solidaire. Programmation Pluriannuelle de l'Energie: 2019-2023, 2024-2028, 2020. [Cited on pages 18, 20, 23, 68, 156, 170, 171, 184, and 185.]

[19] N.E. Stauff, T.K. Kim, T.A. Taiwo, L. Buiron, G. Rimpault, E. Brun, Y.K. Lee, I. Pataki, A. Kereszturi, A. Tota, C. Parisi, and E. Fridman. Benchmark for Neutronic Analysis of Sodium-cooled Fast Reactor Cores with Various Fuel Types and Core Sizes. Technical report, OECD/NEA, 2016. [Cited on pages 18, 45, and 46.]

[20] Julie Brizi. *Cycles uranium et thorium en réacteurs à neutrons rapides refroidis au sodium. Aspects neutroniques et déchets associés.* PhD thesis, Université Paris Sud - Paris XI, 2010. [Cited on pages 18 and 19.]

[21] M. Tiphine, C. Coquelet-Pascal, G. Krivtchik, R. Eschbach, C. Chabert, B. Carlier, M. Caron-Charles, G. Senentz, L. Durpel, C. Garzenne, and F. Laugier. Simulations of Progressive Potential Scenarios of Pu Multirecycling in SFR and Associated Phase-out in the French Nuclear Power Fleet. In *GLOBAL 2015 - 21st International Conference and Exhibition "Nuclear Fuel Cycle for a Low-Carbon Future"*, 2015. [Cited on pages 18, 23, 65, 170, 174, and 175.]

[22] V. Romanello, M. Salvatores, A. Schwenk-Ferrero, F. Gabrielli, W. Maschek, and B. Vezzoni. Comparative study of fast critical burner reactors and subcritical accelerator driven systems and the impact on transuranics inventory in a regional fuel cycle. *Nuclear Engineering and Design*, 241:433–443, 2011. [Cited on page 19.]

[23] Benjamin A. Lindley, Carlo Fiorina, Robert Gregg, Fausto Franceschini, and Geoffrey T. Parks. The effectiveness of full actinide recycle as a nuclear waste management strategy when implemented over a limited timeframe – Part I: Uranium fuel cycle. *Progress in Nuclear Energy*, 85:498–510, 2015. [Cited on page 19.]

[24] CEA/DEN. *Avancées des recherches sur la séparation-transmutation et le multi-recyclage du plutonium dans les réacteurs à flux de neutrons rapides*. Publications of Commissariat à l'énergie atomique et aux énergies alternatives (CEA), 2015. [Cited on page 19.]

[25] Edouard Mbala Malambu, Bronwyn Hyland, Lionel Boucher, Bertrand Carlier, Jean-Paul Grouiller, Massimo Salvatores, Vincenzo Romanello, Aleksandra Schwenk-Ferrero, Stefano Monti, Kiyoshi Ono, Francisco Alvarez-Velarde, Enrique Miguel Gonzalez, Kathryn A. McCarthy, Kemal O. Pasamehmetoglu, Simone Massara, Yong-Joon Choi, and Gary Dyck. Transition Towards a Sustainable Nuclear Fuel Cycle. Technical report, OECD/NEA, 2013. [Cited on pages 19, 23, and 45.]

[26] D. Lutz, W. Bernnat, K. Hesketh, E. Sartori, H. Küsters, G. Schlosser, J. Vergnes, H.W. Wiese, S. Cathalau, A. Puill, H. Takano, E. Saji, and P. Jewkes. Physics of Plutonium Recycling. Volume II: Plutonium Recycling in Pressurized-water Reactors. Technical report, OECD/NEA, 1995. [Cited on page 19.]

[27] K. Hesketh, E. Sartori, M. Delpech, D. Lutz, G. Schlosser, I. Champtiaux, M. Goutefarde, M. Juanola, S. Cathalau, W. Bernnat, M. Mattes, T.T.J.M. Peeters, Y. Peneliau, A. Puill, H. Takano, A. McWhorter, and H. Déry. Physics of Plutonium Recycling. Volume VI: Multiple Pu Recycling in Advanced PWRs. Technical report, OECD/NEA, 2002. [Cited on page 19.]

[28] J.P. Grouiller, J.Y. Doriath, A. Vasile, A. Zaetta, J.L. Guillet, and D. Greneche. Different Possible Scenarios for Plutonium Recycling in PWRs. Paris, France, 2001. [Cited on page 19.]

[29] Gilles Youinou and Alfredo Vasile. Plutonium Multirecycling in Standard PWRs Loaded with Evoutionary Fuels. *Nuclear Science and Engineering*, 151:25–45, 2005. [Cited on page 19.]

[30] A. Vasile, Ph. Dufour, H. Golfier, J.P. Grouiller, J.L. Guillet, Ch. Poinot, G. Youinou, and A. Zaetta. Advanced fuels for plutonium management in pressurized water reactors. *Journal of Nuclear Materials*, 319:173–179, 2003. [Cited on page 19.]

[31] Guillaume Martin, Maxime Guyot, Frédéric Laugier, Gérald Senentz, Guillaume Krivtchik, et al. French Scenarios Towards Fast Plutonium Multirecycling in PWR. Charlotte, United States, 2018. [Cited on pages 19, 170, and 173.]

[32] C. Chabert, A. Touron, A. Saturnin, G. Krivtchik, J.-L. Girotto, et al. Prospective inventory of radioactive materials and waste produced by the French nuclear fleet according to various options. Seattle, United States, September 2019. [Cited on pages 19 and 170.]

[33] Y. Rugama, S. Zheng, and V. Garat. Multi-recycling of MOX Fuel on LWRs. Juan-les-pins, France, May 2019. [Cited on pages 19 and 170.]

[34] *Classification of Radioactive Waste – General Safety Guide No. GSG-1*. International Atomic Energy Agency (IAEA), 2009. [Cited on page 20.]

[35] Hannah Kosow and Robert Gaßner. Methods of future and scenario analysis: overview, assessment, and selection criteria. Studies 39, Bonn, 2008. [Cited on page 21.]

[36] Liviu Andreescu, Radu Gheorghiu, Marian Zulean, and Adrian Curaj. Understanding normative foresight outcomes: Scenario devleopment and the 'veil of ignorance' effect. *Technological Forecasting & Social Change*, 80:711–722, 2013. [Cited on page 21.]

[37] C. Golinelli and Guillet J.L. MOX in France: Status and Prospects. Vienna, Austria, 1997. [Cited on page 22.]

[38] Connaissance des Energies. Réacteur nucléaire EPR , 2020. https://www.connaissancedesenergies.org/fiche-pedagogique/reacteur-nucleaire-epr. [Cited on page 22.]

[39] Institut de Radioprotection et de Sûreté Nucléaire (IRSN). Réacteur EPR, 2017. https://www.irsn.fr/FR/connaissances/Installations_nucleaires/Les-centrales-nucleaires/reacteur-epr/Pages/sommaire.aspx#.YGV-27DitPY. [Cited on pages 22 and 64.]

[40] World Nuclear Association. Nuclear Power in France, 2021. https://www.world-nuclear.org/information-library/country-profiles/countries-a-f/france.aspx. [Cited on page 22.]

[41] Xavier Clément, Aude Ganier, Amélie Lorec, Patrick Philippon, Vahé Ter Minassian, Alexandra Bender, Coralie Godfroid, Brigitte Raffray, Micheline Bayard, Fabrice Mathé, and David Torondel. Les Défis du CEA : Innover pour un Nucléaire Durable, 2016. Publication of Commissariat à l'énergie atomique et aux énergies alternatives, R. C. S. Paris B77568019. [Cited on page 22.]

[42] Léa Tillard. *Impact du déploiement de réacteurs de type ASTRID sur la gestion dynamique du plutonium dans des scénarios de transitions électronucléaires*. PhD thesis, Université Paris-Saclay, France, 2019. [Cited on pages 22, 23, 32, 34, 38, 42, 67, and 180.]

[43] D. Freynet, C. Coquelet-Pascal, R. Eschbach, G. Krivtchik, and E. Merle-Lucotte. Multiobjective optimization for nuclear fleet evolution scenarios using COSI. *EPJ N - Nuclear Sciences & Technologies*, 2:9, 2016. [Cited on pages 23 and 65.]

[44] T. Kooyman. On the use of plutonium burning fast reactors to reduce PWR irradiated assemblies' stockpile. Juan-les-pins, France, May 2019. [Cited on page 23.]

[45] OECD/NEA. Impacts of the Fukushima Daiichi Accident on Nuclear Development Policies. Technical report, OECD/NEA, 2017. [Cited on page 23.]

[46] Mark Hibbs. *The Future of Nuclear Power in China*. Carnegie Scholar, 2018. [Cited on page 23.]

[47] Warren Walker, Robert Lempert, and Jan Kwakkel. *Deep Uncertainty*, pages 395–402. Springer, 01 2013. [Cited on pages 23, 58, and 80.]

[48] Guillaume Krivtchik. *Analysis of uncertainty propagation in nuclear fuel cycle scenarios*. PhD thesis, 2014. [Cited on pages 23 and 24.]

[49] Weifeng Zhou. *Resilience analysis of nuclear fuel cycle scenarios*. PhD thesis, Université Grenoble Alpes, France, 2020. [Cited on pages 23, 43, 57, 59, 61, 98, and 170.]

[50] Fanny Courtin. *Etude de l'incinération du plutonium en REP MOX sur support d'uranium enrichi avec le code de simulation dynamique du cycle CLASS*. PhD thesis, Ecole nationale supérieure Mines-Télécom Atlantique, France, 2017. [Cited on pages 24, 34, 42, 112, 156, 161, and 164.]

[51] Warren E. Walker, S. Adnan Rahman, and Jonathan Cave. Adaptive policies, policy analysis, and policy-making. *European Journal of Operational Research*, 128:282–289, 2001. [Cited on pages 24 and 58.]

[52] S.O. Funtowicz and J.R. Ravetz. *Uncertainty and Quality in Science for Policy*. Kluwer Academic Publishers, Netherlands, 1990. [Cited on page 24.]

[53] Max D. Morris. Factorial Sampling Plans for Preliminary Computational Experiments. *Technometrics*, 33(2):161–174, 1991. [Cited on pages 26, 30, 47, 51, 53, and 61.]

[54] B. Mouginot, B. Leniau, N. Thiollière, M. Ernoult, S. David, X. Doligez, A. Bidaud, O. Méplan, R. Montesanto, G. Bellot, J.B. Clavel, I. Duhamel, E. Letang, and J. Miss. CORE LIBRARY FOR ADVANCED SCENARIO SIMULATION, C.L.A.S.S.: PRINCIPLE & APPLICATION. In *PHYSOR 2014 - The Role of Reactor Physics toward a Sustainable Future*, Kyoto, Japan, October 2014. [Cited on pages 29 and 34.]

[55] B. Leniau, B. Mouginot, N. Thiollière, X. Doligez, A. Bidaud, F. Courtin, M. Ernoult, and S. David. A neural network approach for burn-up calculation and its application to the dynamic fuel cycle code CLASS. *Annals of Nuclear Energy*, 81:125–133, July 2015. [Cited on pages 29, 33, 34, 36, 37, and 66.]

[56] Martin Guillet, Xavier Doligez, Guy Marleau, Maxime Paradis, Marc Ernoult, and Nicolas Thiollière. Coupled CLASS and DONJON5 3D full-core calculations and comparison with the neural network approach for fuel cycles involving MOX fueled PWRs. *Annals of Nuclear Energy*, 152:107971, 2021. [Cited on pages 31, 32, 37, and 66.]

[57] Léa Tillard, Jean-Baptiste Clavel, Xavier Doligez, Éric Dumonteil, Marc Ernoult, Jiali Liang, and Nicolas Thiollière. Analysis of Transition Scenario from a PWR to a SFR Fleet Simulated with the CLASS code. In *International Nuclear Fuel Cycle Conference (GLOBAL 2019)*, Seattle, Washington, USA, 2019. [Cited on pages 32 and 67.]

[58] CEA/DEN. *La neutronique*. Publications of Commissariat à l'énergie atomique et aux énergies alternatives (CEA), 2015. [Cited on page 32.]

[59] O. Méplan, A. Nuttin, O. Laulan, S. David, F. Michel-Sendis, and J. Wilson. MURE : MCNP Utility for Reactor Evolution - Description of the methods, first applications and results. In *ENC 2005 - European Nuclear Conference. Nuclear Power for the XXIst Century : From basic research to high-tech industry*, December 2005. [Cited on page 32.]

[60] Marc Ernoult, Jiali Liang, Xavier Doligez, Olivier Méplan, Sandra Bouneau, and Sylvain David. Automated selection of nuclides and reactions of interest in a depletion simulation. Precision loss estimation for multiple outputs. *Progress in Nuclear Energy*, 2021. [Cited on page 32.]

[61] N. Capellan, J. Wilson, S. David, O. Meplan, J. Brizi, A. Bidaud, A. Nuttin, and P. Guillemin. 3D coupling of Monte Carlo neutronics and thermal-hydraulics calculations as a simulation tool for innovative reactor concepts. In *Proceedings of the GLOBAL 2009 congress - The Nuclear Fuel Cycle: Sustainable Options and Industrial Perspectives*, Paris, France, September 2009. [Cited on page 32.]

[62] L. Boucher, K.A. McCarthy, Y.J. Choi, K. Ono, F. Álvarez Velarde, E.M. González, B. Dixon, and B. Hyland. Benchmark Study on Nuclear Fuel Cycle Transition Scenarios Analysis Codes. Technical report, OECD/NEA, 2012. [Cited on page 33.]

[63] Christine Coquelet-Pascal, Marion Tiphine, Guillaume Krivtchik, David Freynet, Camille Cany, Romain Eschbach, and Christine Chabert. COSI6: A TOOL FOR NUCLEAR TRANSITION SCENARIO STUDIES AND APPLICATION TO SFR DEPLOYMENT SCENARIOS WITH MINOR ACTINIDE TRANSMUTATION. *Nuclear technology*, 192:91–110, November 2015. [Cited on page 33.]

[64] V. Tsibulskiy, S. Subbotin, M. Khoroshev, and F. Depisch. DESAE (Dynamic Energy System- Atomic Energy): Integrated Computer Model for Performing Global Analysis in INPRO Assessment Studies. In *International Conference on Nuclear Engineering "ICONE 14"*, Miami, Florida, USA, July 2006. [Cited on page 33.]

[65] F. Álvarez Velarde, E.M. González-Romero, and I. Merino Rodríguez. Validation of the burn-up code EVOLCODE 2.0 with PWR experimental data and with a Sensitivity/Uncertainty analysis. *Annals of Nuclear Energy*, 73:175 – 188, 2014. [Cited on page 33.]

[66] J.J. Jacobson, A.M. Yacout, G.E. Matthern, S.J. Piet, D.E. Shropshire, R.F. Jeffers, and T. Schweitzer. Verifiable Fuel Cycle Simulation Model (VISION): A Tool for Analyzing Nuclear Fuel Cycle Futures. *Nuclear Technology*, 172(2):157–178, 2010. [Cited on page 33.]

[67] G. EDWARDS, B. HYLAND, D. WOJTASZEK, S. HÄKKINEN, T. VIITANEN, B. CARLIER, C. COQUELET-PASCAL, R. ESCHBACH, D. FREYNET, M. TIPHINE, F. GABRIELLI, B. VEZZONI, A. BROLLY, K. ONO, A. OTHAKI, F. ÁLVAREZ-VELARDE, B. DIXON, and S. CORNET. The Effects of the Uncertainty of Input Parameters on Nuclear Fuel Cycle Scenario Studies. Technical report, OECD/NEA, 2017. [Cited on pages 33 and 55.]

[68] Áron Brolly, Máté Szieberthb, Máté Halászb, Lajos Nagyb, and Sándor Fehér. Development and application of SITON, a new fuel cycle simulation code. In *Actinide and Fission Product Partitioning and Transmutation - Thirteenth Information Exchange Meeting*, Seoul, Republic of Korea, September 2014. [Cited on page 33.]

[69] Nicolas Thiollière, Xavier Doligez, Maté Halasz, Guillaume Krivtchik, Baptiste Mouginot, Ivan Merino, Aris villacorta Skarbeli, Augusto Hernandez Solis, Fransisco Álvarez Velarde, Fanny Courtin, Hubert Druenne, Marc Ernoult, Katy Huff, Mate Szieberth, Bart Vermeeren, and Paul Wilson. Impact of Fresh Fuel Loading Management in Fuel Cycle Simulators: A Functionality Isolation Test. *Nuclear Engineering and Design*, 2021. [Cited on pages 33, 35, and 153.]

[70] I. Merino Rodríguez, A. Hernández-Solís, N. Messaoudi, and G. Van den Eynde. The nuclear fuel cycle code anicca: Verification and a case study for the phase out of belgian nuclear power with minor actinide transmutation. *Nuclear Engineering and Technology*, 52(10):2274 – 2284, 2020. [Cited on page 33.]

[71] Kathryn D. Huff, Matthew J. Gidden, Robert W. Carlsen, Robert R. Flanagan, Meghan B. McGarry, Arrielle C. Opotowsky, Erich A. Schneider, Anthony M. Scopatz, and Paul P.H. Wilson. Fundamental concepts in the Cyclus nuclear fuel cycle simulation framework. *Advances in Engineering Software*, 94:46 – 59, 2016. [Cited on page 33.]

[72] Máté Gergely Halász. *Development of a fast burn-up method and investigation of transmutation in Generation IV fast reactors*. PhD thesis, Budapest University of Technology and Economics Institute of Nuclear Techniques, Hungary, 2018. [Cited on page 33.]

[73] F. Courtin, B. Leniau, B. Mouginot, N. Thiollière, X. Doligez, A. Somaini, and A. Bidaud. PWR MOX Fuel Physics Models for the Dynamic Fuel Cycle Simulation Tool CLASS. In *Physics of Reactors 2016 (PHYSOR 2016): Unifying Theory and Experiments in the 21st Century*, Sun Valley, Idaho, USA, May 2016. [Cited on page 34.]

[74] Fanny Courtin, Baptiste Leniau, Nicolas Thiollière, Baptiste Mouginot, Xavier Doligez, Alice Somaini, Abdoul-Aziz Zakari-Issoufou, Stella David, Adrien Bidaud, and Jean-Baptiste Clavel. Neutronic predictors for pwr fuelled with multi-recycled plutonium and applications with the fuel cycle simulation tool class. *Progress in Nuclear Energy*, 100:33–47, 09 2017. [Cited on pages 34, 37, and 156.]

[75] Abdoul-Aziz Zakari-Issoufou, Xavier Doligez, Alice Somaini, Quentin Hoarau, Stella David, Sandra Bouneau, Fanny Courtin, Baptiste Leniau, Nicolas Thiollière, Baptiste Mouginot, Adrien Bidaud, Nicolas Capellan, Olivier Meplan, and Alexis Nuttin. Americium mono-recycling in PWR: A step towards transmutation. *Annals of Nuclear Energy*, 102, April 2017. [Cited on page 34.]

[76] B. Leniau, F. Courtin, B. Mouginot, N. Thiollière, X. Doligez, and A. Bidaud. Generation of SFR Physics Models for the Nuclear Fuel Cycle Code CLASS. In *Physics of Reactors 2016 (PHYSOR 2016): Unifying Theory and Experiments in the 21st Century*, Sun Valley, Idaho, USA, May 2016. [Cited on pages 34, 36, and 37.]

[77] M. Ernoult, X. Doligez, N. Thiollière, A.A. Zakari-Issoufou, A. Bidaud, S. Bouneau, J.B. Clavel, F. Courtin, S. David, and A. Somaini. Global and Flexible Models for Sodium-cooled Fast Reactors in Fuel Cycle Simulations. In *PHYSOR 2018: Reactor Physics paving the way towards more efficient systems*, Cancun, Mexico, April 2018. [Cited on pages 34, 37, 175, and 180.]

[78] Léa Tillard, Jean-Baptiste Clavel, Xavier Doligez, Eric Dumonteil, Marc Ernoult, Florian Mang, and Abdoul-Aziz Zakari-Issoufou. Development of a multi-zone irradiation model for scenario studies involving ASTRID-like SFRs. In *the International Congress on Advances in Nuclear Power Plants (ICAPP): Advances in nuclear power plants*, May 2019. [Cited on pages 34, 37, and 38.]

[79] Nicolas Thiollière, Fanny Courtin, Baptiste Leniau, Baptiste Mouginot, Xavier Doligez, and Adrien Bidaud. Prediction of MgO volume fraction in an ADS fresh fuel for the scenario code CLASS. *Progress in Nuclear Energy*, 85:518–524, August 2015. [Cited on page 34.]

[80] J.C. Butcher. Coefficients for the study of Runge-Kutta integration processes. *Journal of the Australian Mathematical Society*, 3(2):185–201, 1963. [Cited on page 36.]

[81] Weifeng Zhou, Guillaume Krivtchik, and Patrick Blaise. Resilience of nuclear fuel cycle scenarios: Definition, method and application to a fleet with uncertain power decrease. *International Journal of Energy Research*, 12 2020. [Cited on pages 43 and 57.]

[82] Abdoul-Aziz Zakari-Issoufou, Marc Ernoult, and Xavier Doligez. Consequences on Using Macro Power Reactors in Nuclear Scenarios, 2018. 3rd Technical Workshop On Fuel Cycle Simulation. [Cited on page 43.]

[83] AREVA. Livraison à EDF du 4 000ème assemblage de combustible MOX, 2014. [Cited on page 43.]

[84] I.M. Sobol'. Sensitivity analysis for non-linear mathematical models. *Mathematical Modelling and Computational Experiments*, pages 407–414, 1993. [Cited on page 46.]

[85] I.M Sobol'. Global sensitivity indices for nonlinear mathematical models and their Monte Carlo estimates. *Mathematics and Computers in Simulation*, 55(1):271 – 280, 2001. The Second IMACS Seminar on Monte Carlo Methods. [Cited on page 46.]

[86] Nicolas Thiollière, Jean-Baptiste Clavel, Fanny Courtin, Xavier Doligez, Marc Ernoult, Zakari Issoufou, Guillaume Krivtchik, Baptiste Leniau, Baptiste Mouginot, Adrien Bidaud, Sylvain David, Victor Lebrin, Carole Perigois, Yann Richet, and Alice Somaini. A methodology for performing sensitivity analysis in dynamic fuel cycle simulation studies applied to a PWR fleet simulated with the CLASS tool. *EPJ Nuclear Sci. Technol.*, 2018. [Cited on pages 47, 50, and 82.]

[87] A.V. Skarbeli and F. Álvarez Velarde. Uncertainty quantification on advanced fuel cycle scenario simulations applying local and global methods. *Annals of Nuclear Energy*, 124:349–356, 2019. [Cited on page 47.]

[88] F. Courtin, N. Thiollière, X. Doligez, M. Ernoult, B. Leniau, J. Liang, B. Mouginot, and A.-A. Zakari-Issoufou. Assessment of plutonium inventory management in the French nuclear fleet with the fuel cycle simulator CLASS. *Nuclear Engineering and Design*, page 111042, 2021. [Cited on page 47.]

[89] Qiao Ge and Monica Menendez. Extending Morris method for qualitative global sensitivity analysis of models with dependent inputs. *Reliability Engineering and System Safety*, 162:28–39, 2017. [Cited on page 55.]

[90] Robert J. Lempert, David G. Groves, Steven W. Popper, and Steve C. Bankes. A General, Analytic Method for Generating Robust Strategies and Narrative Scenarios. *Management Science*, 52(4):514–528, 2006. [Cited on page 58.]

[91] Robert J. Lempert and Myles T. Collins. Managing the Risk of Uncertain Threshold Responses: Comparison of Robust, Optimum, and Precautionary Approaches. *Risk Analysis*, 27(4), 2007. [Cited on pages 58 and 61.]

[92] C. McPhail, H.R. Maier, J.H. Kwakkel, M. Giuliani, A. Castelletti, and S. Westra. . Robustness Metrics: How Are They Calculated, When Should They Be Used and Why Do They Give Different Results? *Earth's Future*, 6:169–191, 2018. [Cited on pages 58, 61, and 80.]

[93] Guillaume Martin and C. Coquelet-Pascal. Symbiotic equilibrium between Sodium Fast Reactors and Pressurized Water Reactors supplied with MOX fuel. *Annals of Nuclear Energy*, 103:356–362, 2017. [Cited on page 65.]

[94] Jiali Liang, Marc Ernoult, Xavier Doligez, Sylvain David, Léa Tillard, and Nicolas Thiollière. Robustness Study of Electro-Nuclear Scenario under Disruption. *Journal of Nuclear Engineering*, 2, 2021. [Cited on page 65.]

[95] Marc Ernoult, Sylvain David, Xavier Doligez, Jiali Liang, Nicolas Thiollière, and Léa Tillard. Systematic Analysis of Multivariate Scenarios Using Advanced Clustering Methods. In *PHYSOR 2020: Transition to a Scalable Nuclear Future*, Cambridge, United Kingdom, March 2020. [Cited on pages 65 and 93.]

[96] M.D. McKay, R.J. Beckman, and W.J. Conover. Comparison of Three Methods for Selecting Values of Input Variables in the Analysis of Output from a Computer Code. *Technometrics*, 21(2):239–245, 1979. [Cited on pages 69 and 87.]

[97] V. Eglajs and P. Audze. New approach to the design of multifactor experiments. *Problems of Dynamics and Strengths*, 35, 1977. [Cited on pages 69 and 87.]

[98] R.L. Iman, J.C. Helton, and J.E. Campbell. An approach to sensitivity analysis of computer models, Part 1. Introduction, input variable selection and preliminary variable assessment. *Journal of Quality Technology*, 13(3):174–183, 1981. [Cited on pages 69 and 87.]

[99] R Core Team. R: A Language and Environment for Statistical Computing, 2013. R Foundation for Statistical Computing. [Cited on page 69.]

[100] K.V. Mardia, J.T. Kent, and J.M. Bibby. *Multivariate Analysis*. Academic Press, 1979. [Cited on pages 69 and 70.]

[101] R.A. Johnson and D.W. Wichern. *Applied Multivariate Statistical Analysis*. Pearson Prentice Hall, 2007. [Cited on pages 69 and 70.]

[102] Jiali Liang, Marc Ernoult, Xavier Doligez, Sylvain David, Sandra Bouneau, Nicolas Thiollière, Guillaume Krivtchik, Fanny Courtin, Weifeng Zhou, and Stéphanie Tillement. Assessment of Strategy Robustness Under Disruption of Objective in Dynamic Fuel Cycle Studies. *Annals of Nuclear Energy*, 154, 2021. [Cited on pages 81, 82, 83, and 241.]

[103] J.A. Nelder and R. Mead. A Simplex Method for Function Minimization. *The Computer Journal*, 7:308–313, 1965. [Cited on pages 170, 185, and 190.]

[104] Saša Singer and Sanja Singer. Efficient Implementation of the Nelder-Mead Search Algorithm. *Applied Numerical Analysis & Computational Mathematics*, 1, 2004. [Cited on page 190.]

[105] Nicolas Thiollière. Arbitrage temporel: L'actualisation dans le calcul économique. Projet NEEDS / CINEASTE – Workshop Temporalité #2. [Cited on page 208.]

Acronyms

ANN Artificial Neural Network.

APA Advanced Plutonium Assembly.

ASTRID Advanced Sodium Technological Reactor for Industrial Demonstration.

BOC Beginning Of Cycle.

CLASS Core Library for Advance Scenario Simulation.

CNRS Centre National de la Recherche Scientifique ([EN.] French National Center for Scientific Research).

CORAIL COmbustible Recycling A ILot.

DoE Design of Experiment.

EOC End Of Cycle.

EPR European Pressurized Reactor.

ESFR European Sodium Fast Reactor.

FiFo First in First out.

FIT Functionality Isolation Test.

FLM Fuel Loading Model.

FP Fission Product.

GSA Global Sensitivity Analysis.

IRSN Institut de Radioprotection et de Sûreté Nucléaire ([EN.] Institute for Radiological Protection and Nuclear Safety).

LHS Latin Hypercube Sampling.

LiFo Last in First out.

MA Minor Actinide.

MOX Mixed OXide.

MOXEUS MOX on Enriched Uranium Support.

OAT One At a Time.

PC Principal Component.

PCA Principal Component Analysis.

PPE Programmations Pluriannuelles de l'Energie.

PWR Pressurized Water Reactor.

SFR Sodium-cooled Fast Reactor.

TRU transuranium.

UOX Uranium OXide.

WPS Wide Parametric Sweeping.

List of Figures

List of Tables

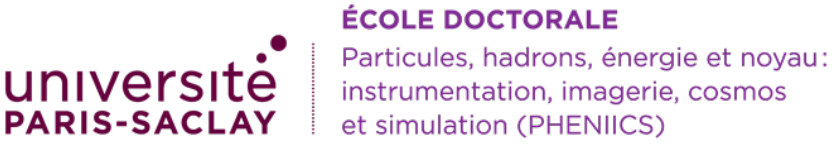
université
PARIS-SACLAY
ÉCOLE DOCTORALE
Particules, hadrons, énergie et noyau:
instrumentation, imagerie, cosmos
et simulation (PHENIICS)